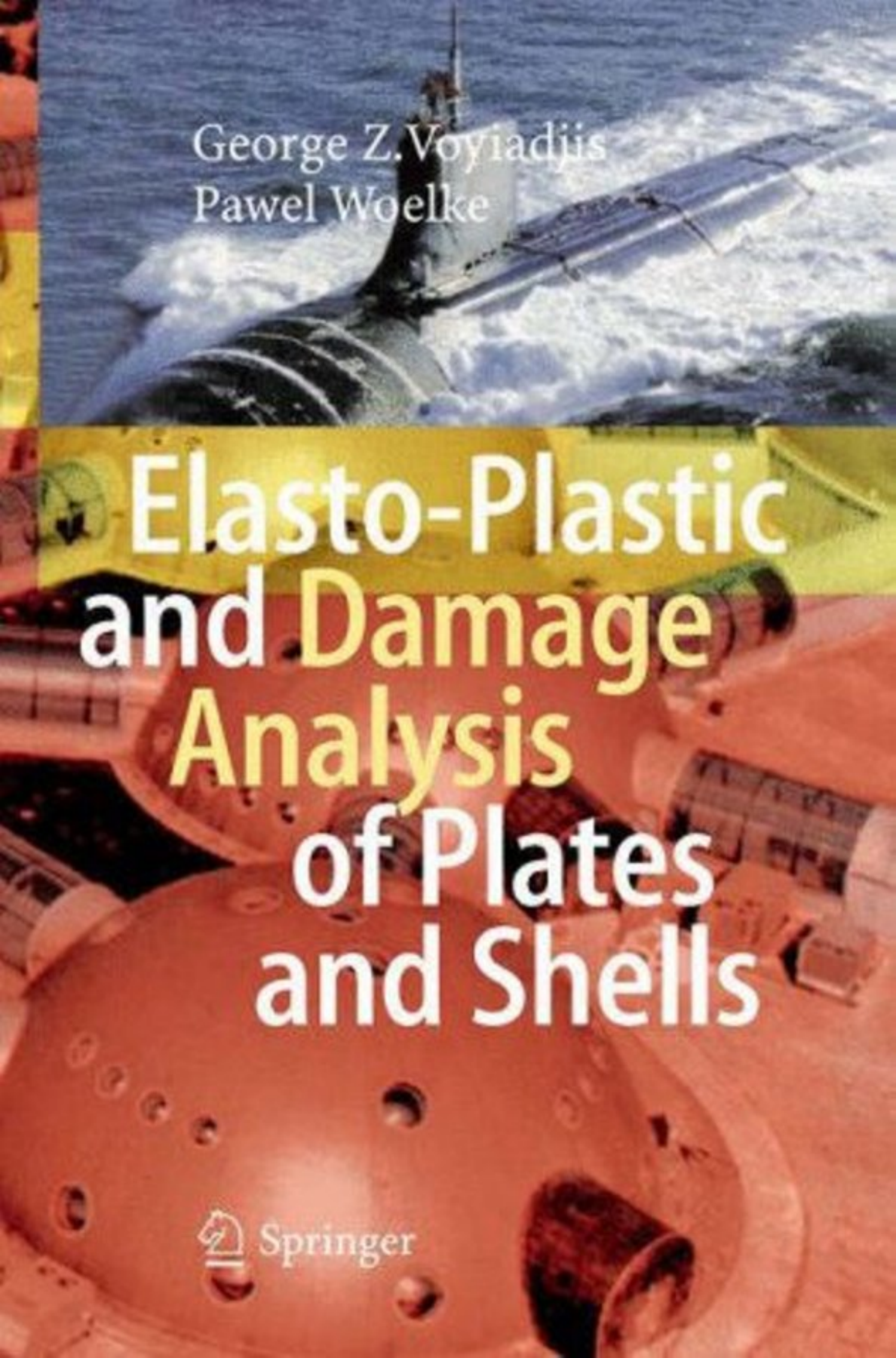
George Z. Voyiadjis
Pawel Woelke
Elasto-Plastic and Damage Analysis of Plates and Shells
Springer

Elasto-Plastic and Damage Analysis of Plates and Shells

George Z. Voyiadjis · Pawel Woelke

Elasto-Plastic and Damage Analysis of Plates and Shells

With 82 Figures and 14 Tables

Springer

Dr. George Z. Voyiadjis
Department of Civil and Environmental Engineering
CEBA Building, Taylor Hall
Room 3508-B
Louisiana State University
Baton Rouge, LA 70803-6405
USA
voyiadjis@eng.lsu.edu

Dr. Pawel Woelke
Applied Science Dept.
Weidlinger Associates, Inc.
375 Hudson Street, 12 FL
New York, NY 10014-3656
USA
woelke@wai.com

ISBN: 978-3-540-79350-2 e-ISBN: 978-3-540-79351-9

Library of Congress Control Number: 2008929594

© 2008 Springer-Verlag Berlin Heidelberg

This work is subject to copyright. All rights are reserved, whether the whole or part of the material is concerned, specifically the rights of translation, reprinting, reuse of illustrations, recitation, broadcasting, reproduction on microfilm or in any other way, and storage in data banks. Duplication of this publication or parts thereof is permitted only under the provisions of the German Copyright Law of September 9, 1965, in its current version, and permission for use must always be obtained from Springer. Violations are liable to prosecution under the German Copyright Law.

The use of general descriptive names, registered names, trademarks, etc. in this publication does not imply, even in the absence of a specific statement, that such names are exempt from the relevant protective laws and regulations and therefore free for general use.

Cover design: Kirchner, Erich

Printed on acid-free paper

9 8 7 6 5 4 3 2 1

springer.com

In Memory of Professor Maciej Bieniek

Professor Maciej Bieniek

The subject of shell mechanics was extensively studied by the senior author's advisor and friend, Professor Maciej Bieniek, to whom this book is dedicated. Maciej P. Bieniek was born in Wilno, Poland, in 1927. His academic and professional career began in June 1945, at Cracow Polytechnic, the first technical university to open in Poland after the war. He later transferred to Gdansk University of Technology, from which he graduated in 1948 with the equivalent of an M.Sc. degree in civil engineering, majoring in Structures and Transportation. He remained in Gdansk, where and upon completion of his research on viscoelastic wave propagation, he received his Ph.D. degree in Applied Mechanics in 1951.

In 1958, Bieniek was appointed a Visiting Scholar in the Department of Civil Engineering and Engineering Mechanics at Columbia University and the following year, Visiting Associate Professor. In 1960, he was named an Associate Professor of Civil Engineering. Three years later, Bieniek became a Professor of Civil Engineering at the University of Southern California. His research interests at that time were in the areas of structural dynamics, mechanics of shells, random vibrations, and elasto-plastic wave propagation. Bieniek returned to Columbia in 1969 as a Professor of Civil Engineering. In 1979, he received the Great Teacher Award of the Society of Columbia Graduates. He chaired the department from 1979 to 1981. In 1989, he was named Renwick Professor and, upon his retirement in 1993, Renwick Professor Emeritus.

Bieniek supervised 33 doctoral students, including the senior author of this book. He also authored and co-authored numerous scientific publications in refereed technical journals. His achievements cover highly advanced areas in continuum mechanics, vibrations, structural dynamics, shell mechanics, and reliability of structures. He was known for his innovative approach to research with an emphasis on applicability to engineering practice.

Throughout his career, Bieniek was active as a consultant. At Weidlinger Associates, he was responsible for development of the two dynamic finite element codes: TRANAL, for buried structures, and EPSA, for submerged shells. Both are widely used by Weidlinger Associates as well as various government agencies.

He also served as a consultant to the Port Authority of New York and New Jersey and to the Triborough Bridge and Tunnel Authority on New York City's major suspension bridges. His significant contributions were recognized in 1991, by the

Roebling Award of the Metropolitan Section of the American Society of Civil Engineers (ASCE). In 1995, Bieniek was named an Honorary Member of the ASCE, one of the highest honors an engineer can receive.

Maciej P. Bieniek died on January 23, 2006, in Atlanta, GA.

Baton Rouge, Louisiana — George Z. Voyiadjis
New York — Pawel Woelke

Preface

Shells and plates are critical structures in numerous engineering applications. Analysis and design of these structures is of continuing interest to the scientific and engineering communities. Accurate and conservative assessments of the maximum load carried by a structure, as well as the equilibrium path in both the elastic and inelastic range, are of paramount importance to the engineer.

The elastic behavior of shells has been closely investigated, mostly by means of the finite element method. Inelastic analysis however, especially accounting for damage effects, has received much less attention from researchers.

In this book, we present a computational model for finite element, elasto-plastic, and damage analysis of thin and thick shells. Formulation of the model proceeds in several stages. First, we develop a theory for thick spherical shells, providing a set of shell constitutive equations. These equations incorporate the effects of transverse shear deformation, initial curvature, and radial stresses.

The proposed shell equations are conveniently used in finite element analysis. A simple C^0 quadrilateral, doubly curved shell element is developed. By means of a quasi-conforming technique, shear and membrane locking are prevented. The element stiffness matrix is given explicitly, making the formulation computationally efficient.

We represent the elasto-plastic behavior of thick shells and plates by means of the non-layered model, using an Updated Lagrangian method to describe a small-strain geometric non-linearity. For the treatment of material non-linearities, we adopt an Iliushin's yield function expressed in terms of stress resultants, with isotropic and kinematic hardening rules.

Finally, we incorporate the damage effects modeled through the evolution of porosity into the yield function, giving a generalized and convenient yield surface expressed in terms of the stress resultants. As the elastic stiffness matrix is derived explicitly, and a non-layered model in which integration through the thickness is unnecessary is used, the current stiffness matrix is also given explicitly and numerical integration is not performed at any stage of the analysis. This makes the model mathematically consistent, accurate for a variety of applications, and economical in terms of computational power. We would like to acknowledge the editing assistance of Ann Rae Jonas.

Contents

Chapter 1
Introduction

1.1 Shell Structures

In this book, we present a comprehensive analysis of homogenous and isotropic shells. We also consider plates and beams, but only as a special case of shells. The constitutive equations are developed for shells, and can be easily reduced to plate or beam equations.

A beam is a structural element in which the length is substantially larger than the width and thickness. A plate is a flat surface in which the thickness is small compared to the other two dimensions. A shell is a curved surface in which the thickness is much smaller than the other dimensions. The geometrical properties of shells, e.g. single or double curvature, give these lightweight structures a tremendous advantage over plates. Plates and beams are usually loaded in the direction normal to the plane, or longitudinal axis in the case of the latter, and they carry the loads primarily through bending. The load-carrying efficiency of shells is based on their curvature, which allows multiple stress paths and an optimum form of transmission of different load types.

Shells support the loads in two main ways. If subjected to uniform pressures, shells usually can resist the loads by membrane (in-plane) action. The most desirable situation is when a shell is subjected to a uniform load causing tensile stresses, because the material can be used to its full strength (Wadee, 2005). Concentrated loads, however, introduce local bending stresses, which are much more likely to cause yielding or ultimately failure of the shell. The eggshell is a good illustration of these actions. If you try to squash an egg using a uniform or approximately uniform external pressure, you will notice that it can resist a very high pressure considering its small thickness. If you press a finger against the egg's surface, applying a "point load", the shell fractures under a much smaller force. As with the eggshell, structural shells are best utilized when subjected to uniform loading.

Local reinforcement of certain critical regions of shell structures is often necessary. A possible location of these areas is at the transition from one basic surface to another. The connection between the main cylindrical vessel and its spherical ends is a good example of the critical region, where stiffening may be required (Wadee, 2005). Stiffened shells are beyond the scope of this work and will not be considered any further.

G.Z. Voyiadjis, P. Woelke, *Elasto-Plastic and Damage Analysis of Plates and Shells*,

© Springer-Verlag Berlin Heidelberg 2008

The analysis of shells often involves two distinct theories. A membrane theory is capable of describing only the membrane behavior, i.e., is performed under the assumption that a curved surface is incapable of conveying the shear forces or bending moments (Ugural, 1999). A bending theory includes the effects of bending in the analysis. Although for practical purposes, the membrane stresses are of far greater importance than the bending stresses, one needs a general or bending theory to account for the discontinuity effects in geometry, e.g. changes in thickness, or boundary conditions. These effects cannot be approximated by means of the membrane theory only.

Most, investigations of beams, plates and shells are performed under the assumption that the thickness is small relative to the other two dimensions. The shell or plate is considered thin if the effects of transverse shear deformations on the behavior of the structure are negligible. Normal strains and stresses in the out-of-plane (radial) direction are also considered negligible for thin shells. This is mostly the case for ratios of thickness h to radius of curvature R equal to or less than 1/50. This limit is not definite, however, and some of the results in the literature show that under certain boundary conditions, the shear deformation can be significant even for very thin shells or plates. With the increased use of thick shells in various engineering applications such as cooling towers, dams, and pressure vessels it is imperative to develop a simple and accurate theory for moderately thick to thick shells, accounting not only for transverse shears, but also for radial effects and initial curvature.

Shells are often considered to act globally as a member, e.g. a lighting column. In that case, a global behavior of the component can be approximated accurately using a simplistic model. The local behavior of the shell is, however, often critical in the analysis of the structure. Dimpling in domes, or development of the Yoshimura pattern (Fig. 1.1) due to buckling in compressed cylinders, are complex phenomena, that require an in-depth analysis with non-linear behavior taken into account. Although buckling, as an eigenvalue problem, is not considered here, the local behavior of shells is closely approximated.

All the aforementioned structural elements are extensively used in various applications in many fields of engineering. Different types of shells have often been used for industrial purposes. Examples of single curvature shells are storage tanks and silos, pressure vessels, submarines, airplanes, chimneys, oilrigs or even lighting columns. A double curvature form of a shell can be used to construct spherical tanks and reservoirs, roofs, stadiums, vehicles, water towers and many other structures. Examples of the shell structures are shown in Fig. 1.2.

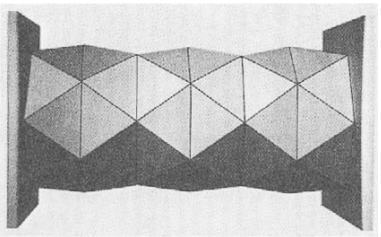

Fig. 1.1 Yoshimura pattern in a compressed cylinder (Thompson and Hunt, 1984) with kind permission from John Wiley & Sons

(a)

(b)

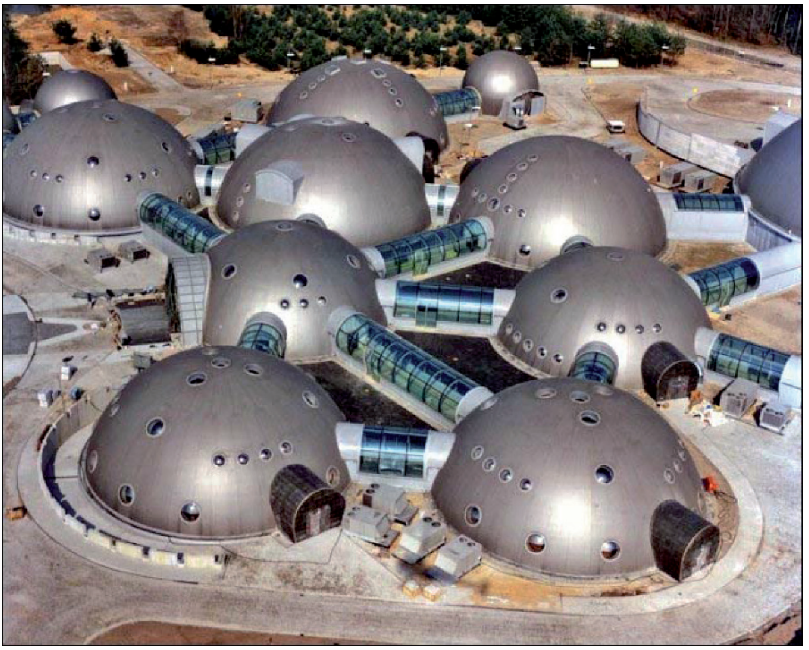

Fig. 1.2 Examples of shell structures: (**a**) Submarine Seawolf, US Navy (1996); (**b**) Headquarters of a radio station (RFM-FM) in Poland, Monolithic Dome Institute (2005)

1.2 Motivation and Scope

Shells are important for various engineering applications. Analysis and design of these structures is therefore of continuing interest to the scientific and engineering communities. Accurate and conservative assessments of the maximum load carried by the structure, as well as the equilibrium path in both elastic and inelastic range are therefore of paramount importance in understanding the integrity of the structure.

Determination of the equilibrium path in the elastic and inelastic range usually involves a complex analysis. Manual calculations provide valuable information about the behaviour of shells. They are, however, mostly performed under simplifying assumptions and for a specific problem. Universal algorithms based on manual calculations and accurately approximating the load-displacement response for a variety of shell problems are virtually unobtainable. At the same time, recent developments in computer technology allow us to formulate relatively simple computational models capable of delivering accurate results. By means of the finite element method (FEM), it is possible to carry out elasto-plastic and damage analyses for both thick and thin shells of general shape. Finite elements offer tremendous flexibility and the ability to account for nearly every effect observed in the experimental or "real life" tests of the material or structural behavior. Attempting to investigate every experimentally observable phenomenon is, however, neither necessary nor feasible. Constitutive modeling is understood as a reasonable choice of effects, which are the most important for explanation of the phenomenon described (Perzyna, 2005). The model formulated and presented here is addressed to the scientific and engineering communities. Thus, it considers the most important issues from the structural analysis point of view. Our objective is to develop a computational model for non-linear elasto-plastic large displacements damage analysis for isotropic shells.

One difficult of non-linear calculations is that they are based on incremental and/or iterative algorithms, which may require prohibitively large storage of computer memory. Computational efficiency needs special attention in non-linear modeling of shells. To formulate a simple and efficient algorithm that delivers close approximations to the equilibrium path in both the elastic and inelastic range, it is necessary to proceed in several stages.

A refined shell theory, providing a set of shell constitutive equations, is given first. The theory is universal and general, i.e. it accounts for both membrane and bending behavior and is formulated for thick shells, accounting for the effects of the transverse shear deformations, radial stresses and initial curvature. The assumptions used to derive the shell equations are described in the following section, and detailed derivations are given in Chap. 2.

The constitutive equations generated by the theory are conveniently used in finite element analysis. A simple C^0 quadrilateral, doubly curved shell element is developed. To overcome membrane and shear locking as well as other numerical deficiencies, we adopt quasi-conforming technique that features an explicit form of the stiffness matrix. Chapter 3 focuses on the formulation of the developed finite element.

Shelled structures are often subjected to loading conditions that cause very large displacements. Geometrical non-linearities are crucial in the elasto-plastic and

damage modeling of shells. Thus, to achieve a desired accuracy, geometric non-linearities must be accounted for. We consider small strain problems, studied by means of the Updated Lagrangian method. Details of the geometrically non-linear calculations are given in Chap. 4.

We adopt a "non-layered" plastic model in the treatment of the material non-linearities for both its efficiency and its convenient applicability to engineering problems. The yield function is defined in the stress resultant space; integration of the stresses over the thickness of the shell is not necessary. Isotropic and kinematic hardening rules are developed, with the latter aimed at representing the Bauschinger effect. The definitions of the yield surface, flow, and hardening rules, with the derivation of the stiffness matrix, are given in Chap. 5.

The final stage of the formulation is the description of the influence of damage on the behavior of shells. The experimental results show that the degradation of material properties of ductile metals in the elastic range due to damage effects is negligible. Hence, the damage is considered here as a phenomenon induced by the plastic strain and is represented by the scalar porosity parameter introduced into the yield function. Static loading conditions are considered here, with both plasticity and damage treated as rate independent processes. The description of the effects of damage is introduced into the model in Chap. 6.

Chapter 7 describes a the computational issues. The numerical algorithms used here are outlined, along with the developed software and hardware information.

Each component of the formulation, namely the theory, finite element analysis, non-linear analysis and damage description, are integral parts of the model. Nevertheless, they are universal and introduce original ideas on every level of the algorithm. This leads to the ability of the finite elements introduced within this framework also to be used separately, as "stand-alone" concepts.

1.3 Basic Assumptions

The main assumptions of the computational model we develop are:

- Material is homogenous and isotropic;
- We consider shells of general shape, both thick and thin, with both membrane and bending actions;
- Buckling as an eigenvalue problem is not considered;
- Loading conditions are static;
- We adopt a non-layered approach in plastic analysis;
- Plasticity and damage are treated as rate-independent processes;
- Damage variable is isotropic and induced by the plastic strain

Additional assumptions, pertinent to the particular components of the model will be explained in detail in the following chapters.

References

Flugge, W. (1960). Stresses in Shells. Springer, New York.
Monolithic Dome Institute (2005). RMF Radio Station in Poland Occupies 21st Century Facility, April 2005, http://www.monolithicdome.com/domenews/2005/rmf.html
Perzyna, P. (2005) The thermodynamical theory of elasto-viscoplasticity. Eng. Trans., 53, 3, 235–316, Warszawa 2005.
Thompson, J.M.T. and Hunt, G.W. (1984). Elastic Instability Phenomena. Wiley, New York.
Ugural, A.C. (1999). Stresses in Plates and Shells. McGraw-Hill Inc., New York.
Ugural, A.C. and Fenster, S.K. (1975). Advanced Strength and Applied Elasticity. Elsevier, New York.
US Navy (1996). Seawolf completes initial sea trials; Navy Wire Service – A −1915; www.chinfo.navy.mil/navpalib/ships/submarines/seawolf/seawolf1.html
Wadee, K. (2005). "Khurram Wadee's home page"; University of Exeter, Exeter, Devon, UK EX4 4QJ, www.ex.ac.uk/∼mkwadee/mkwadee.html

Chapter 2
Shell Constitutive Equations

2.1 Introduction

A simple theory of plates was originally developed by Sophie Germain. The corrected version by Kirchhoff (1850) is widely used in the analysis of thin plates. Using Kirchhoff's concept Love developed the complete two-dimensional theory of thin shells more than 100 years ago, and numerous. Contributions to this subject have been made since then. Any two-dimensional theory of shells approximates the real three-dimensional problem. Researchers have been seeking better approximations for the exact three-dimensional elasticity solutions for shells. In the last three decades, the developed refined two-dimensional linear theories of thin shells include important contributions Sanders (1959), Flugge (1960), and Niordson (1978). In these refined shell theories, the initial curvature effect is taken into consideration. Nevertheless, the deformation is based on the Love–Kirchhoff assumption, and the radial stress effect is neglected. We will refer to all the theories built on the Kirchhoff–Love assumption, as *the classical theory*. The refined theories by Sanders (1959), Flugge (1960), and Niordson (1978) provide very good results for the analysis of thin shells. The theory of Sanders-Koiter has been widely used in the finite element analysis of shells (Ashwell and Gallagher, 1976). Niordson (1971) showed, however, that Love's strain energy expression has inherent errors of relative order $[h/R + (h/L)^2]$, where h is the thickness of the shell, R is the magnitude of the smallest principal radius of curvature, and L is a characteristic wave length of the deformation pattern of the middle surface. Consequently, when the refined theories of thin shells are applied to thick shells, with h/R not small compared to unity, the error can be quite large. Unlike the theory of thin shells, the comprehensive theory of thick shells, with not only transverse shear strains considered but also initial curvature and radial stresses, has received limited attention from researchers. Voyiadjis and Shi (1991) developed a refined shell theory for thick cylindrical shells that is very accurate and convenient for finite element analysis. We present here a refined shell theory for thick spherical shells, with the shell equations based on similar assumptions as those of Voyiadjis and Shi (1991). The work of Voyiadjis and Woelke (2004) can be considered a more general formulation of the Voyiadjis and Shi theory (1991).

G.Z. Voyiadjis, P. Woelke, *Elasto-Plastic and Damage Analysis of Plates and Shells*,

© Springer-Verlag Berlin Heidelberg 2008

In the following sections of this chapter we present detailed derivations of the shell constitutive equations. The general form of these expressions is complicated; they can, however, easily be reduced to commonly used shell equations, as shown below. At every stage of the formulation, we make references to the classical shell theory.

2.1.1 Thickness of the Shell

Thick shells have a number of distinctly different features from thin shells. For thick shells, the Kirchhoff–Love assumption is no longer valid. According to this assumption, plane sections remain plane after the deformation, as well as perpendicular to the middle surface. The angle of rotation of the cross-section ϕ is therefore equal to the first derivative of the vertical displacement $\partial w/\partial x$, and transverse shear deformation γ_{xz} can be neglected (Fig. 2.1).

If the thickness of the shell becomes significant, the transverse shear strains γ_{xz} are not negligible and the angle of rotation of the cross-section is altered, as shown in Fig. 2.1. Our formulation is unified for both thick and thin shells and thus, the influence of the transverse shear strains is considered in the analysis.

In our theory, we use the following hypothesis: plane sections originally perpendicular to the middle surface remain plane after the deformation but not perpendicular to the middle surface (Fig. 2.1). From this hypothesis, we deduce that the displacements u and v along x and y directions are:

$$u = -z\phi_x \text{ and } v = -z\phi_y \tag{2.1}$$

where ϕ_x and ϕ_y are the angles of rotation of the sections originally perpendicular to the middle section, in the xz and yz planes respectively, given by:

$$\phi_x = \frac{\partial w}{\partial x} - \gamma_{xz} \text{ and } \phi_y = \frac{\partial w}{\partial y} - \gamma_{yz} \tag{2.2}$$

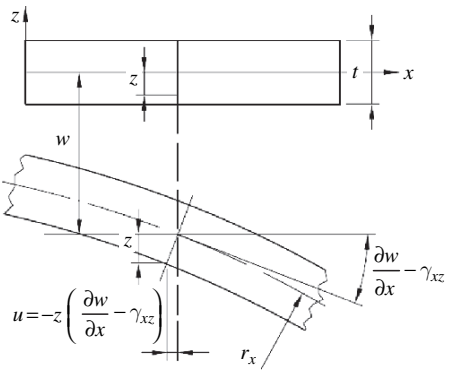

Fig. 2.1 Transverse shear deformations (Voyiadjis and Woelke, 2006)

where w is the vertical displacement in the z direction and γ_{xz}, γ_{yz} are the transverse shear strains in the xz and yz planes, respectively. Shells in which the ratio of the thickness to the radius of curvature is equal or less than 1/50 are most often considered thin. In the case of thin shells, transverse shear strains are negligible. This is true for most of the types of analyses and boundary conditions. Some types of loading conditions however, cause significant shear forces, regardless of the thickness of the structure. An example of such a loading condition would be a concentrated bending moment M applied at mid-span of the beam of length L (Fig. 2.2).

We recognize that there are two ways to apply the concentrated bending moment. It can be formed by the vertical force couple P (Fig. 2.2a), or by the horizontal force couple P (Fig. 2.2b). With the former, a very large shear force is generated at midspan of the beam. This force increases as the distance of the force couple s decreases. For the correct representation of the deformation of the beam here, transverse shear strains need to be considered, regardless of the thickness of the beam. We encounter the same situation when such loading conditions are applied to plates and shells.

For dynamic and wave propagation problems, shear forces can be very important, especially at higher modes of vibration in both thin and thick shells. In composite laminates, addressing the delamination process requires detailed analysis with the influence of shear accounted for. Dynamic and wave propagation problems are, however, beyond the scope of this book, and will not be discussed further.

It is not difficult to incorporate transverse shear deformations in shells. This can be accomplished following the work of Reissner (1945) for the plate theory. Many other authors have directed their attention to the transverse shear strains, which are important for analysis of the bending of thick isotropic structures (Basar et al., 1992, 1993; Bathe, 1982; Bathe and Brezzi, 1985; Bathe and Dvorkin, 1984; Dennis and Palazotto, 1989; Palazotto and Linnemann, 1991; Niordson 1978, 1985; Noor and Burton, 1989; Reissner, 1945, 1975; Mindlin, 1951; Reddy, 1984, 1989; Kratzig, 1992; Kratzig and Jun, 2003; Voyiadjis and Kattan, 1986, 1991; Voyiadjis and Baluch, 1981, and many others).

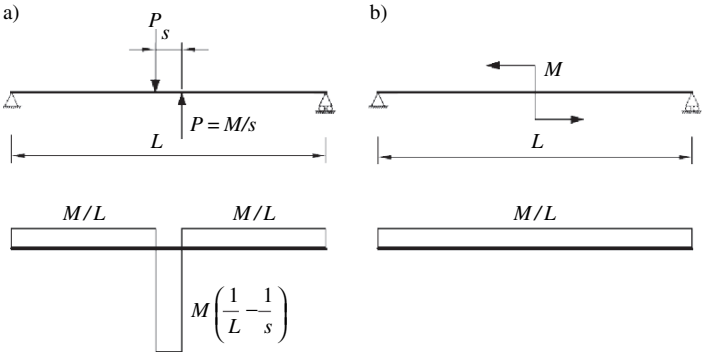

Fig. 2.2 Concentrated couples formed by: (**a**) The vertical forces P causing significant shear forces and (**b**) The horizontal forces P - no significant shear forces (Hu, 1984 see also Woelke et al. 2006)

2.1.2 Initial Curvature and Radial (Transverse Normal) Stresses

Another important distinction between thick and thin shell analyses is that in thick shells the initial curvatures not only contribute to the stress resultants and stress couples, but also result in a nonlinear distribution of the in-plane stresses across the thickness of the shell. This is because the length of the surface at a distance z from the middle surface – ds_1 (Fig. 2.3) is different from that of the middle surface – ds (Fig. 2.3). We also account for this effect in our formulation of the shell equations.

The parameter R – in Fig. 2.3 is a radius of curvature of the middle surface of the shell, and ϕ is the angle between two meridians creating a middle surface of the shell.

Earlier shell theories focused on the two-dimensional shell equations and on maintaining a linear stress distribution through the shell thickness (Flugge, 1960; Niordson, 1985). Refinement of the stress distribution in thick shells has not been extensively studied in terms of the inclusion of radial stresses. The theory of thin shells may provide a good estimate of the strain energy for some problems in thick shells. It cannot, however, provide an accurate distribution of the stresses through the thickness (Gupta and Khatua, 1978). This accuracy is imperative from an engineering point of view.

Our theory is based on the assumed out, of, plane stress components that satisfy given traction boundary conditions. These stress components are established by means of the analytical investigation of the distribution of the radial stresses in thick spherical containers subjected to internal and external pressure, performed by Lame (1852). Thus, the distribution of the radial stresses is the starting point for the derivation.

In our shell theory, all the in-plane stresses exhibit a non-linear distribution through the thickness. This is primarily a result of the incorporation of the initial curvature effect in the theoretical formulation of the proposed shell theory (Fig. 2.3). Using specific examples, we compare the nonlinear stress expressions with those obtained through the three-dimensional theory of elasticity.

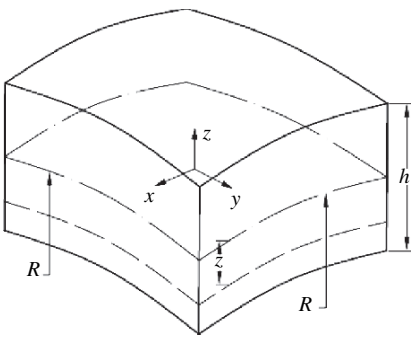

$$ds = Rd\phi$$

$$ds_1 = (R+z)\,d\phi$$

$$ds_1 = \left(1+\frac{z}{R}\right)ds$$

Fig. 2.3 Initial curvature effect

2.2 Plate Constitutive Equations

In this section we derive widely known stress components in a plate. Any shell theory can be considered a generalization of the plate theory; it is therefore useful to present the plate equations first, before addressing the shell problem. For completeness, we present stresses and stress resultants in a plate loaded out-of-plane, as well as the governing differential equation of the plate (Sects. 2.2.1, 2.2.2, 2.2.3).

2.2.1 Stresses and Stress Resultants in a Thin Plate

We follow the Kirchhoff–Love assumption, i.e., plane sections remain plane and perpendicular to the middle section after the deformation. This assumption leads to the following equations:

$$\gamma_{xz} = \gamma_{yz} = \varepsilon_z = 0 \tag{2.3}$$

We consider out of plane loading at this stage; thus the normal strains arise as a result of bending action only. To obtain the strains, we need to determine the extension (Δs) of the surface of the plate that is at a distance z from the middle surface (Fig. 2.4).

The term ε is the strain caused by the bending action in the plate and κ is the curvature of the deformed plate given by:

$$\kappa = \frac{\partial}{\partial s}\left(\frac{\partial w}{\partial s} - \gamma_{sz}\right) \tag{2.4}$$

s - direction tangential to the middle surface.

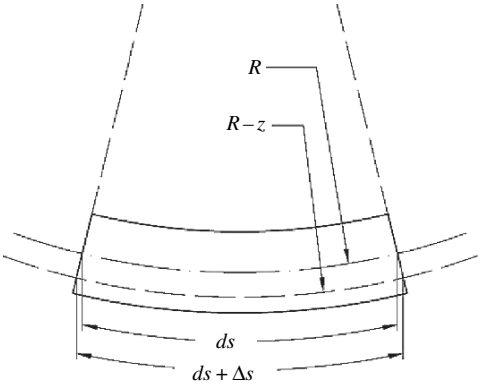

$$\frac{ds + \Delta s}{ds} = \frac{R - z}{R}$$

$$\frac{\Delta s}{ds} = -\frac{z}{R} = \varepsilon$$

$$\varepsilon = -z\kappa$$

Fig. 2.4 Normal strains caused by bending

Substituting (2.3) into the above yields:

$$\kappa = \frac{\partial^2 w}{\partial s^2} \tag{2.5}$$

or:

$$\kappa_x = \frac{\partial^2 w}{\partial x^2};\ \kappa_y = \frac{\partial^2 w}{\partial y^2} \text{ and } \kappa_{xy} = \frac{\partial^2 w}{\partial x \partial y} \tag{2.6}$$

Thus we can write the flowing relations:

$$\varepsilon_x = -z\frac{\partial^2 w}{\partial x^2};\ \varepsilon_y = -z\frac{\partial^2 w}{\partial y^2} \text{ and } \varepsilon_{xy} = -z\frac{\partial^2 w}{\partial x \partial y} \tag{2.7}$$

The stress-strain relationships for a flat thin plate can be written as follows:

$$\sigma_x = \frac{E}{1-\nu^2}\left(\varepsilon_x + \nu\varepsilon_y\right) = -\frac{Ez}{1-\nu^2}\left(\frac{\partial^2 w}{\partial x^2} + \nu\frac{\partial^2 w}{\partial y^2}\right) \tag{2.8}$$

$$\sigma_y = \frac{E}{1-\nu^2}\left(\varepsilon_y + \nu\varepsilon_x\right) = -\frac{Ez}{1-\nu^2}\left(\frac{\partial^2 w}{\partial y^2} + \nu\frac{\partial^2 w}{\partial x^2}\right) \tag{2.9}$$

$$\tau_{xy} = \frac{E}{2(1+\nu)}\gamma_{xy} = -\frac{Ez}{1+\nu}\frac{\partial^2 w}{\partial x \partial y} \tag{2.10}$$

Following (2.3) the remaining components of the stress tensor are zero, i.e.:

$$\sigma_z = \tau_{xz} = \tau_{yz} = 0 \tag{2.11}$$

In (2.8), (2.9), (2.10), E is the Young's modulus and ν is the Poisson's ratio.

To obtain the stress resultants in a plate we integrate the stresses over the thickness of the plate, as follows:

$$M_x = \int_{-t/2}^{t/2} \sigma_x z dz = -D\left(\frac{\partial^2 w}{\partial x^2} + \nu\frac{\partial^2 w}{\partial y^2}\right) \tag{2.12}$$

$$M_y = \int_{-t/2}^{t/2} \sigma_y z dz = -D\left(\frac{\partial^2 w}{\partial y^2} + \nu\frac{\partial^2 w}{\partial x^2}\right) \tag{2.13}$$

$$M_{xy} = \int_{-t/2}^{t/2} \tau_{xy} z dz = -D(1-\nu)\frac{\partial^2 w}{\partial x \partial y} \tag{2.14}$$

where D is the flexural rigidity of the plate given by:

$$D = \frac{Eh^3}{12\left(1-\nu^2\right)} \tag{2.15}$$

and h is the thickness of the plate.

Comparing (2.8), (2.9), (2.10) with (2.12), (2.13), (2.14) we express the stresses in terms of stress resultants, as follows:

$$\sigma_x = \frac{M_x z}{I} \tag{2.16}$$

$$\sigma_y = \frac{M_y z}{I} \tag{2.17}$$

$$\tau_{xy} = \frac{M_{xy} z}{I} \tag{2.18}$$

where I is a second moment of area (per unit width) given by:

$$I = \frac{h^3}{12} \tag{2.19}$$

and h is the thickness of the plate.

Assuming the plate to be thin and loaded out-of-plane, the bending moments given by (2.12), (2.13), (2.14) are the only non-zero stress resultants.

2.2.2 Equilibrium Equations and Governing Differential Equation of Plate

The equilibrium conditions govern the variations of the stress resultants in a plate. To derive the equilibrium equations, we study a differential plate element of area $dxdy$ subjected to a uniform vertical (negative z direction) load per unit area p (Fig. 2.5; for clarity p is not depicted).

The differential plate element in Fig. 2.5 is considered very small; thus, the stress resultants can be assumed constant over the face of the element. The variations of the forces and moments acting on different surfaces of the plate are expressed by the Taylor's expansion:

$$M_{xy} + \frac{\partial M_{xy}}{\partial x} dx \tag{2.20}$$

The summation of the forces in the z direction leads to the following equation:

$$\left(Q_x + \frac{\partial Q_x}{\partial x} dx\right) dy - Q_x dy + \left(Q_y + \frac{\partial Q_y}{\partial y} dy\right) dx - Q_y dx - p dx dy = 0 \tag{2.21}$$

which can be reduced to:

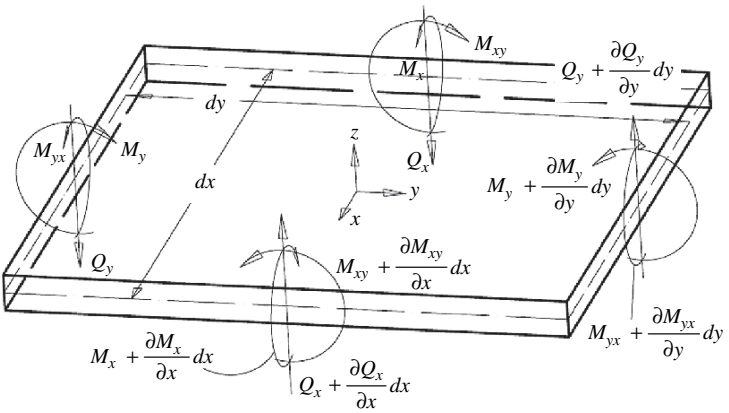

Fig. 2.5 Positive stress resultants (per unit length) on a plate element

$$\frac{\partial Q_x}{\partial x} + \frac{\partial Q_y}{\partial y} - p = 0 \tag{2.22}$$

The summation of moments around the x axis leads to:

$$\begin{aligned} &-\left(M_{xy} + \frac{\partial M_{xy}}{\partial x} dx\right) dy + M_{xy} dy + M_y dx - \left(M_y + \frac{\partial M_y}{\partial y} dy\right) dx \\ &-\left(Q_y + \frac{\partial Q_y}{\partial y} dy\right) dx \frac{dy}{2} - Q_y dx \frac{dy}{2} = 0 \end{aligned} \tag{2.23}$$

Reducing the above equation and neglecting the infinitesimal terms, we obtain:

$$\frac{\partial M_{xy}}{\partial x} + \frac{\partial M_y}{\partial y} + Q_y = 0 \tag{2.24}$$

Similarly the summation of moments around the y axis gives:

$$\begin{aligned} &\left(M_x + \frac{\partial M_x}{\partial x} dx\right) dy - M_x dy - M_{yx} dx + \left(M_{yx} + \frac{\partial M_{yx}}{\partial y} dy\right) dx \\ &+\left(Q_x + \frac{\partial Q_x}{\partial x} dx\right) dy \frac{dx}{2} + Q_x dy \frac{dx}{2} = 0 \end{aligned} \tag{2.25}$$

which can be simplified to:

$$\frac{\partial M_x}{\partial x} + \frac{\partial M_{yx}}{\partial y} + Q_x = 0 \tag{2.26}$$

Substituting (2.12), (2.13), (2.14) into (2.24) and (2.26) respectively, we obtain the expression for the shear forces:

$$Q_y = D\frac{\partial}{\partial y}\left(\nabla^2 w\right) \tag{2.27}$$

$$Q_x = D\frac{\partial}{\partial x}\left(\nabla^2 w\right) \tag{2.28}$$

where ∇ is the Laplace operator, given by

$$\nabla^2 = \frac{\partial^2}{\partial x^2} + \frac{\partial^2}{\partial y^2} \tag{2.29}$$

Substituting (2.27) and (2.28) into (2.22) yields:

$$D\left[\frac{\partial^2}{\partial x^2}\left(\frac{\partial^2 w}{\partial x^2} + \frac{\partial^2 w}{\partial y^2}\right) + \frac{\partial^2}{\partial y^2}\left(\frac{\partial^2 w}{\partial x^2} + \frac{\partial^2 w}{\partial y^2}\right)\right] = p \tag{2.30}$$

or:

$$\nabla^4 w = \frac{p}{D} \tag{2.31}$$

where:

$$\nabla^4 = \frac{\partial^4}{\partial x^4} + 2\frac{\partial^4}{\partial x^2 \partial y^2} + \frac{\partial^4}{\partial y^4} \tag{2.32}$$

Equation (2.31) is the governing differential equation for the deflection of plates. With the exceptions of the simple problems, solution of (2.31) is cumbersome. The most common approach involves finding a displacement function w that satisfies the governing differential equations of plates, as well as static and kinematic boundary conditions. Such a method is often referred to as the inverse method (Ugural, 1999). In most practically important cases of the analysis, the choice of the displacement function satisfying the boundary conditions and the governing plate equation requires a systematic approach. One of the most common such methods is application of the Fourier series. Methods of solutions of (2.31) are beyond the scope of this book and will not be discussed further.

2.2.3 Transverse Shear and Transverse Normal Stresses in a Plate

In Sect. 2.2.1 the derivation of the plate equations was performed under the Kirchhoff–Love assumption, i.e., transverse shear strains and stresses were neglected. These stresses are important for various engineering problems, as discussed in Sect. 2.1.1. A general theory of shells should take the shear deformation into account.

Transverse shear stresses can easily be determined by means of the equations of equilibrium of stresses given by:

$$\begin{aligned}
\frac{\partial \sigma_x}{\partial x} + \frac{\partial \tau_{xy}}{\partial y} + \frac{\partial \tau_{xz}}{\partial z} + F_X = 0 \\
\frac{\partial \tau_{xy}}{\partial x} + \frac{\partial \sigma_y}{\partial y} + \frac{\partial \tau_{yz}}{\partial z} + F_y = 0 \\
\frac{\partial \tau_{xz}}{\partial x} + \frac{\partial \tau_{yz}}{\partial y} + \frac{\partial \sigma_z}{\partial z} + F_z = 0
\end{aligned} \tag{2.33}$$

where F_x, F_y, F_z are the body forces in *x, y, z* directions respectively.

Neglecting the body forces in the first of (2.33) and solving for τ_{xz} gives:

$$\tau_{xz} = -\int_z^{h/2} \left(\frac{\partial \sigma_x}{\partial x} + \frac{\partial \tau_{xy}}{\partial y} \right) dz \tag{2.34}$$

Substitution of (2.16), (2.17), (2.18) into the above yields:

$$\tau_{xz} = -\left(\frac{\partial M_x}{\partial x} + \frac{\partial M_{xy}}{\partial y} \right) \int_z^{h/2} \frac{z}{I} dz = -\left(\frac{\partial M_x}{\partial x} + \frac{\partial M_{xy}}{\partial y} \right) \frac{6}{h^3} \left(\frac{h^2}{4} - z^2 \right) \tag{2.35}$$

Using (2.26) we can rewrite the above relation as:

$$\tau_{xz} = \frac{3Q_x}{2h} \left[1 - \left(\frac{2z}{h} \right)^2 \right] \tag{2.36}$$

Following the same procedure for τ_{yz} we obtain:

$$\tau_{yz} = \frac{3Q_y}{2h} \left[1 - \left(\frac{2z}{h} \right)^2 \right] \tag{2.37}$$

The transverse normal stresses can be determined in a similar manner, using the above shear stresses along with the equations of equilibrium given by relations (2.33):

$$\sigma_z = -\int_z^{h/2} \left(\frac{\partial \tau_{xz}}{\partial x} + \frac{\partial \tau_{yz}}{\partial y} \right) dz = -\frac{3}{2} \left(\frac{\partial Q_x}{\partial x} + \frac{\partial Q_y}{\partial y} \right) \left(\frac{1}{3} - \frac{z}{h} + \frac{4z^3}{3h^3} \right) \tag{2.38}$$

Using (2.22), the above expression can be rewritten as:

$$\sigma_z = -\frac{3p}{4} \left[\frac{2}{3} - \frac{2z}{h} + \frac{1}{3} \left(\frac{2z}{h} \right)^3 \right] \tag{2.39}$$

2.3 Coordinate Transformation – Strains in Spherical Coordinates

In the following sections, we derive the constitutive equations for spherical shells. It is natural to use spherical coordinates to do so, as they relate better physically to the geometry of the structure. Fig. 2.6 shows the coordinate system.

We define $\mathbf{r}$ as a vector connecting the origin O of the rectangular coordinate system (x, y, z) to point P (Fig. 2.6). Noe $\theta \in [0, \pi]$ is a latitude angle measured from the positive z-axis and vector $\mathbf{r}$, and $\phi \in [0, 2\pi]$ is a longitude angle measured counterclockwise from the positive x-axis to the orthogonal projection of OP onto the xy-plane (Schenck, 1999). The vectors $\mathbf{e}_r, \mathbf{e}_\theta, \mathbf{e}_\phi$ are the unit vectors in r, θ, ϕ directions, respectively. The following are the relations between the rectangular coordinates (x, y, z) and the spherical coordinates (r, θ, ϕ) are:

$$\begin{aligned} x &= r\sin\theta\cos\phi \qquad r^2 = x^2 + y^2 + z^2 \\ y &= r\sin\theta\sin\phi \qquad \tan\phi = y/x \\ z &= r\cos\theta \qquad\qquad \cos\theta = z/r \end{aligned} \tag{2.40}$$

The objective is to determine the strain tensor ε in spherical coordinates:

$$\varepsilon = \begin{bmatrix} \varepsilon_r & \varepsilon_{r\theta} & \varepsilon_{r\phi} \\ \varepsilon_{\theta r} & \varepsilon_\theta & \varepsilon_{\theta\phi} \\ \varepsilon_{\phi r} & \varepsilon_{\phi\theta} & \varepsilon_\phi \end{bmatrix} \tag{2.41}$$

To compute components of the above tensor, we need to relate partial derivatives with respect to rectangular and spherical coordinates. Using the chain rule we obtain the following relations:

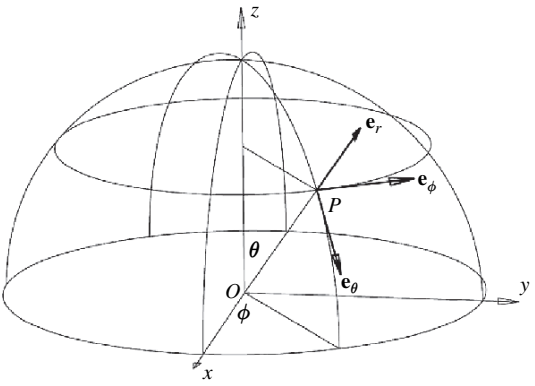

Fig. 2.6 Spherical coordinate system

$$\begin{aligned}\frac{\partial}{\partial x} &= \frac{\partial}{\partial r}\frac{\partial r}{\partial x} + \frac{\partial}{\partial \theta}\frac{\partial \theta}{\partial x} + \frac{\partial}{\partial \phi}\frac{\partial \phi}{\partial x} \\ \frac{\partial}{\partial y} &= \frac{\partial}{\partial r}\frac{\partial r}{\partial y} + \frac{\partial}{\partial \theta}\frac{\partial \theta}{\partial y} + \frac{\partial}{\partial \phi}\frac{\partial \phi}{\partial y} \\ \frac{\partial}{\partial z} &= \frac{\partial}{\partial r}\frac{\partial r}{\partial z} + \frac{\partial}{\partial \theta}\frac{\partial \theta}{\partial z} + \frac{\partial}{\partial \phi}\frac{\partial \phi}{\partial z}\end{aligned} \tag{2.42}$$

Using (2.40) the above relations can be written in a matrix form as:

$$\begin{bmatrix} \frac{\partial}{\partial x} \\ \frac{\partial}{\partial y} \\ \frac{\partial}{\partial z} \end{bmatrix} = \begin{bmatrix} \sin\theta\cos\phi & \cos\theta\cos\phi & -\sin\phi \\ \sin\theta\sin\phi & \cos\theta\sin\phi & \cos\phi \\ \cos\theta & -\sin\theta & 0 \end{bmatrix} \begin{bmatrix} \frac{\partial}{\partial x} \\ \frac{1}{r}\frac{\partial}{\partial \theta} \\ \frac{1}{r\sin\theta}\frac{\partial}{\partial \phi} \end{bmatrix} = \mathbf{R} \begin{bmatrix} \frac{\partial}{\partial x} \\ \frac{1}{r}\frac{\partial}{\partial \theta} \\ \frac{1}{r\sin\theta}\frac{\partial}{\partial \phi} \end{bmatrix} \tag{2.43}$$

Spherical components of the displacements also need to be computed before the strain tensor is determined. The rectangular displacement vector $\mathbf{u}(x, y, z)$ is given by:

$$\mathbf{u}(x, y, z) = u_x(x, y, z)\,\mathbf{i} + u_y(x, y, z)\,\mathbf{j} + u_z(x, y, z)\,\mathbf{k} \tag{2.44}$$

where **i, j, k** are unit vectors in the direction *x, y, z*, respectively (Fig. 2.6). The spherical displacement vector $\mathbf{u}_s(r, \theta, \phi)$ is given by:

$$\mathbf{u}_s(r, \theta, \phi) = u_r(r, \theta, \phi)\,\mathbf{e}_r + u_\theta(r, \theta, \phi)\,\mathbf{e}_\theta + u_\phi(r, \theta, \phi)\,\mathbf{e}_\phi \tag{2.45}$$

The unit vectors $\mathbf{e}_r, \mathbf{e}_\theta, \mathbf{e}_\phi$ can be computed using vector **r**, giving a parametric representation of the sphere:

$$\mathbf{r} = r\sin\theta\cos\phi\;\mathbf{i} + r\sin\theta\sin\phi\;\mathbf{j} + r\cos\theta\;\mathbf{k} \tag{2.46}$$

Vectors tangential to the surface of the sphere in θ and ϕ directions are obtained through differentiation of **r** with respect to θ and ϕ:

$$\frac{\partial \mathbf{r}}{\partial \theta} = \mathbf{r}_\theta = r\cos\theta\cos\phi\;\mathbf{i} + r\cos\theta\sin\phi\;\mathbf{j} - r\sin\theta\;\mathbf{k} \tag{2.47}$$

$$\frac{\partial \mathbf{r}}{\partial \phi} = \mathbf{r}_\phi = -r\sin\theta\sin\phi\;\mathbf{i} + r\sin\theta\cos\phi\;\mathbf{j} \tag{2.48}$$

By dividing the above vectors by their respective lengths, we find the unit tangential vectors $\mathbf{e}_\theta, \mathbf{e}_\phi$:

$$\mathbf{e}_\theta = \frac{\mathbf{r}_\theta}{|\mathbf{r}_\theta|} = \cos\theta\cos\phi\;\mathbf{i} + \cos\theta\sin\phi\;\mathbf{j} - \sin\theta\;\mathbf{k} \tag{2.49}$$

$$\mathbf{e}_\phi = \frac{\mathbf{r}_\phi}{|\mathbf{r}_\phi|} = -\sin\phi\,\mathbf{i} + \cos\phi\,\mathbf{j} \tag{2.50}$$

The unit vector $\mathbf{e}_r$, which is normal to the surface is a cross product of $\mathbf{e}_\theta$ and $\mathbf{e}_\phi$:

$$\mathbf{e}_r = \mathbf{e}_\theta \times \mathbf{e}_\phi = \sin\theta\cos\phi\,\mathbf{i} + \sin\theta\sin\phi\,\mathbf{j} + \cos\theta\,\mathbf{k} \tag{2.51}$$

Because we are using a right-handed coordinate system, the above calculated vector is normal to the surface and pointing outward, as shown in Fig. 2.6. If the cross product of $\mathbf{e}_\phi \times \mathbf{e}_\theta$ were computed instead, the resulting would be a unit vector normal to the surface, but pointing inwards.

Substituting (2.49), (2.50), (2.51) into (2.45) results in:

$$\begin{aligned}\mathbf{u}_s(r,\theta,\phi) &= u_r(r,\theta,\phi)(\sin\theta\cos\phi\,\mathbf{i} + \sin\theta\sin\phi\,\mathbf{j} + \cos\theta\,\mathbf{k}) \\ &+ u_\theta(r,\theta,\phi)(\cos\theta\cos\phi\,\mathbf{i} + \cos\theta\sin\phi\,\mathbf{j} - \sin\theta\,\mathbf{k}) \\ &+ u_\phi(r,\theta,\phi)(-\sin\phi\,\mathbf{i} + \cos\phi\,\mathbf{j}) = u_x\mathbf{i} + u_y\mathbf{j} + u_z\mathbf{k}\end{aligned} \tag{2.52}$$

which yields:

$$\begin{aligned}u_x &= u_r\sin\theta\cos\phi + u_\theta\cos\theta\cos\phi - u_\phi\sin\phi \\ u_y &= u_r\sin\theta\sin\phi + u_\theta\cos\theta\sin\phi - u_\phi\cos\phi \\ u_z &= u_r\cos\theta - u_\theta\sin\theta\end{aligned} \tag{2.53}$$

Equation (2.53) can be written in a matrix form as:

$$\begin{bmatrix}u_x\\u_y\\u_z\end{bmatrix} = \begin{bmatrix}\sin\theta\cos\phi & \cos\theta\cos\phi & -\sin\phi\\ \sin\theta\sin\phi & \cos\theta\sin\phi & \cos\phi\\ \cos\theta & -\sin\theta & 0\end{bmatrix}\begin{bmatrix}u_r\\u_\theta\\u_\phi\end{bmatrix} = \mathbf{R}\begin{bmatrix}u_r\\u_\theta\\u_\phi\end{bmatrix} \tag{2.54}$$

As expected, the transformation matrix $\mathbf{R}$ in the above equation is the same as the matrix relating partial differentiation with respect to rectangular and spherical coordinates in (2.43).

We now proceed to the derivation of the strain tensor in spherical coordinates. The following differential operators are defined:

$$\nabla = \begin{bmatrix}\dfrac{\partial}{\partial x}\\[2mm] \dfrac{\partial}{\partial y}\\[2mm] \dfrac{\partial}{\partial z}\end{bmatrix}; \qquad \nabla_s = \begin{bmatrix}\dfrac{\partial}{\partial x}\\[2mm] \dfrac{1}{r}\dfrac{\partial}{\partial\theta}\\[2mm] \dfrac{1}{r\sin\theta}\dfrac{\partial}{\partial\phi}\end{bmatrix}; \qquad \nabla = \mathbf{R}\nabla_s \tag{2.55}$$

The strain tensor in rectangular coordinates is given by:

$$\varepsilon = \frac{1}{2}\left(\frac{\partial \mathbf{u}}{\partial \mathbf{x}} + \frac{\partial \mathbf{u}}{\partial \mathbf{x}}^T\right) \tag{2.56}$$

where $\mathbf{u}$ is a rectangular displacement vector given by (2.44). We first consider a transpose to $\partial\mathbf{u}/\partial\mathbf{x}$:

$$\frac{\partial \mathbf{u}}{\partial \mathbf{x}}^T = \nabla \begin{pmatrix} u_x & u_y & u_z \end{pmatrix} \tag{2.57}$$

substituting (2.54) and (2.55) into the above gives (Schenck, 1999):

$$\begin{aligned} \frac{\partial \mathbf{u}}{\partial \mathbf{x}}^T &= \mathbf{R}\nabla_s\left[\begin{pmatrix} u_x & u_y & u_z \end{pmatrix}\mathbf{R}^{-1}\right] = \mathrm{R}\nabla_s\left[\begin{pmatrix} u_x & u_y & u_z \end{pmatrix}\right]\mathbf{R}^{-1} + \mathbf{R}\left\{\begin{pmatrix} u_x \\ u_y \\ u_z \end{pmatrix}\nabla_s{}^T\right\}^T\mathbf{R}^{-1} \\ &= \mathbf{R}\begin{bmatrix} \dfrac{\partial u_r}{\partial r} & \dfrac{\partial u_\theta}{\partial r} & \dfrac{\partial u_\phi}{\partial r} \\ \dfrac{1}{r}\dfrac{\partial u_r}{\partial \theta} & \dfrac{1}{r}\dfrac{\partial u_\theta}{\partial \theta} & \dfrac{1}{r}\dfrac{\partial u_\phi}{\partial \theta} \\ \dfrac{1}{r\sin\theta}\dfrac{\partial u_r}{\partial \phi} & \dfrac{1}{r\sin\theta}\dfrac{\partial u_\theta}{\partial \phi} & \dfrac{1}{r\sin\theta}\dfrac{\partial u_\phi}{\partial \phi} \end{bmatrix}\mathbf{R}^{-1} + \mathbf{R}\mathbf{A} \end{aligned} \tag{2.58}$$

where $\mathbf{A}$ is:

$$\begin{aligned} \mathbf{A} &= \begin{bmatrix} u_r\dfrac{\partial}{\partial r} & u_\theta\dfrac{\partial}{\partial r} & u_\phi\dfrac{\partial}{\partial r} \\ \dfrac{u_r}{r}\dfrac{\partial}{\partial \theta} & \dfrac{u_\theta}{r}\dfrac{\partial}{\partial \theta} & \dfrac{u_\phi}{r}\dfrac{\partial}{\partial \theta} \\ \dfrac{u_r}{r\sin\theta}\dfrac{\partial}{\partial \phi} & \dfrac{u_\theta}{r\sin\theta}\dfrac{\partial}{\partial \phi} & \dfrac{u_\phi}{r\sin\theta}\dfrac{\partial}{\partial \phi} \end{bmatrix}\mathbf{R}^{-1} = \\ &= \begin{bmatrix} u_r\dfrac{\partial}{\partial r} & u_\theta\dfrac{\partial}{\partial r} & u_\phi\dfrac{\partial}{\partial r} \\ \dfrac{u_r}{r}\dfrac{\partial}{\partial \theta} & \dfrac{u_\theta}{r}\dfrac{\partial}{\partial \theta} & \dfrac{u_\phi}{r}\dfrac{\partial}{\partial \theta} \\ \dfrac{u_r}{r\sin\theta}\dfrac{\partial}{\partial \phi} & \dfrac{u_\theta}{r\sin\theta}\dfrac{\partial}{\partial \phi} & \dfrac{u_\phi}{r\sin\theta}\dfrac{\partial}{\partial \phi} \end{bmatrix}\begin{bmatrix} \sin\theta\cos\phi & \sin\theta\sin\phi & \cos\theta \\ \cos\theta\cos\phi & \cos\theta\sin\phi & -\sin\theta \\ -\sin\phi & \cos\phi & 0 \end{bmatrix} \end{aligned} \tag{2.59}$$

After differentiation we obtain:

$$\mathbf{A} = \begin{bmatrix} 0 & 0 & 0 \\ \dfrac{c\phi\,(u_r c\theta - u_\theta s\theta)}{r} & \dfrac{s\phi\,(u_r c\theta - u_\theta s\theta)}{r} & \dfrac{-u_r s\theta - u_\theta c\theta}{r} \\ \dfrac{-s\phi\,(u_r s\theta - u_\theta c\theta) - u_\phi c\phi}{rs\theta} & \dfrac{c\phi\,(u_r s\theta + u_\theta c\theta) - u_\phi s\phi}{rs\theta} & 0 \end{bmatrix} =$$

$$= \begin{bmatrix} 0 & 0 & 0 \\ -\dfrac{u_\theta}{r} & \dfrac{u_r}{r} & 0 \\ -\dfrac{u_\phi}{r} & -\dfrac{c\theta}{s\theta}\dfrac{u_\phi}{r} & \dfrac{u_r}{r} + \dfrac{c\theta}{s\theta}\dfrac{u_\phi}{r} \end{bmatrix} \mathbf{R}^{-1} \tag{2.60}$$

where s denotes sin and c denotes cos.

Using the above expression in (2.58) yields:

$$\frac{\partial \mathbf{u}^T}{\partial \mathbf{x}} = \mathbf{R} \begin{bmatrix} \dfrac{\partial u_r}{\partial r} & \dfrac{\partial u_\theta}{\partial r} & \dfrac{\partial u_\phi}{\partial r} \\ \dfrac{1}{r}\dfrac{\partial u_r}{\partial \theta} - \dfrac{u_\theta}{r} & \dfrac{1}{r}\dfrac{\partial u_\theta}{\partial \theta} + \dfrac{u_r}{r} & \dfrac{1}{r}\dfrac{\partial u_\phi}{\partial \theta} \\ \dfrac{1}{r\sin\theta}\dfrac{\partial u_r}{\partial \phi} - \dfrac{u_\phi}{r} & \dfrac{1}{r\sin\theta}\dfrac{\partial u_\theta}{\partial \phi} - \cot\theta\dfrac{u_\phi}{r} & \dfrac{1}{r\sin\theta}\dfrac{\partial u_\phi}{\partial \phi} + cot\theta\dfrac{u_\theta}{r} + \dfrac{u_r}{r} \end{bmatrix} \mathbf{R}^{-1} \tag{2.61}$$

$$= \mathbf{R}\mathbf{U}_s{}^T\mathbf{R}^{-1}$$

Substituting (2.61) into (2.56) results in:

$$\boldsymbol{\varepsilon} = \frac{1}{2}\left(\frac{\partial \mathbf{u}}{\partial \mathbf{x}} + \frac{\partial \mathbf{u}}{\partial \mathbf{x}}^T\right) = \frac{1}{2}\left(\mathbf{R}\mathbf{U}_s\mathbf{R}^{-1} + \mathbf{R}\mathbf{U}_s{}^T\mathbf{R}^{-1}\right) = \mathbf{R}\frac{1}{2}\left(\mathbf{U}_s + \mathbf{U}_s{}^T\right)\mathbf{R}^{-1} \tag{2.62}$$

where the strain tensor in spherical coordinates is given by (Love, 1944; Schenck, 1999):

$$\boldsymbol{\varepsilon}_s = \frac{1}{2}\left(\mathbf{U}_s + \mathbf{U}_s^T\right) \tag{2.63}$$

From (2.61) and (2.63) we find the spherical components of the strain as follows:

$$\varepsilon_r = \frac{\partial u_r}{\partial r} \tag{2.64}$$

$$\varepsilon_\theta = \frac{1}{r}\frac{\partial u_\theta}{\partial \theta} + \frac{u_r}{r} \tag{2.65}$$

$$\varepsilon_\phi = \frac{1}{r\sin\theta}\frac{\partial u_\phi}{\partial \phi} + \cot\theta\frac{u_\theta}{r} + \frac{u_r}{r} \tag{2.66}$$

$$\varepsilon_{r\theta} = \frac{1}{2}\left(\frac{1}{r}\frac{\partial u_r}{\partial \theta} - \frac{u_\theta}{r} + \frac{\partial u_\theta}{\partial r}\right) \tag{2.67}$$

$$\varepsilon_{\phi r} = \frac{1}{2}\left(\frac{1}{r\sin\theta}\frac{\partial u_r}{\partial \phi} - \frac{u_\phi}{r} + \frac{\partial u_\phi}{\partial r}\right) \tag{2.68}$$

$$\varepsilon_{\theta\phi} = \frac{1}{2}\left(\frac{1}{r\sin\theta}\frac{\partial u_\theta}{\partial \phi} - \cot\theta\frac{u_\phi}{r} + \frac{1}{r}\frac{\partial u_\phi}{\partial \theta}\right) \tag{2.69}$$

2.4 Theoretical Formulation of the Shell Equations

Our shell theory is based on the following:

- Assumed out-of-plane stress components that satisfy given traction boundary conditions;
- Three-dimensional elasticity equations with an integral form of the equilibrium equations; and
- Stress resultants and stress couples acting on the middle surface of the shell together with average displacements along a normal of the middle surface of the shell and the average rotations of the normal (Voyiadjis and Baluch, 1981).

The resulting constitutive equations of shells reduce to those given by Flugge (1960) when the shear deformation and radial effects are neglected. In this case, the average displacement's are replaced by the middle surface displacements.

The shell equations derived in this chapter are presented in several stages. The solution of the thick spherical container subjected to uniform pressure, which along with the assumed out-of-plane stress components provides a basis for the formulation, is given first. Using the stress-strain and strain-displacement relationships, we determine the displacement field. By means of displacements, we obtain the remaining components of the strain and stress tensors. From the stresses, we calculate the stress resultant and stress couples, accounting for the initial curvature effect. In Sect. 2.5, the average displacements of the shell are defined in order to identify the boundary conditions. The stress resultants and stress couples are then expressed in terms of the average displacements of the shell.

Our theory can easily be reduced to the equivalent plate theory, which is given in Sect. 2.3. Finally, the numerical examples verifying the reliability of the proposed shell constitutive equations are presented.

2.4.1 Assumed Out-of-Plane Stress Components

We consider a thick spherical container subjected to uniform external and internal pressures. This problem was analyzed by Lame (1852), who through analytical calculations obtained an expression for the radial stresses in the spherical vessel shown in Fig. 2.7. The radial stress distribution for thick spheres subjected to constant radial loads at both surfaces $z = -h/2$ and $z = -h/2$ (Fig. 2.7) is given by (2.70):

$$\sigma_z = \frac{(r_2/r)^3 - 1}{c_1} p_i + \frac{(r_1/r)^3 - 1}{c_2} p_o \tag{2.70}$$

where:

$$c_1 = 1 - \left(\frac{r_2}{r_1}\right)^3 \text{ and } c_2 = \left(\frac{r_1}{r_2}\right)^3 - 1 \tag{2.71}$$

$$r = R + z \tag{2.72}$$

and:

σ_z – radial stresses;
p_i, p_o – distributed radial loads on the inner and outer surfaces respectively ($z = -h/2$ and $z = h/2$);
r_1, r_2 – radius of curvature of the inner and outer surfaces respectively (Fig. 2.7);
r – radius of curvature of the plane away from the middle plane; and
R – radius of curvature of the mid-plane (Fig. 2.7).

The stress field in a spherical container given in Fig. 2.7 needs to satisfy the following boundary conditions (Fig. 2.8):

$$\begin{aligned}
\sigma_z &= p_o \quad at \quad z = h/2 \\
\tau_{z\phi} &= p_{\phi o} \quad at \quad z = h/2 \\
\tau_{z\theta} &= p_{\theta o} \quad at \quad z = h/2 \\
\sigma_z &= -p_i \quad at \quad z = -h/2 \\
\tau_{z\phi} &= -p_{\phi i} \quad at \quad z = -h/2 \\
\tau_{z\theta} &= -p_{\theta i} \quad at \quad z = -h/2
\end{aligned} \tag{2.73}$$

Based on the solution given by (2.70) and (2.71), the above given boundary conditions, and the transverse shear stresses given by (2.36) and (2.37), and accounting for the initial curvature effect, the following out-of-plane stress components are assumed:

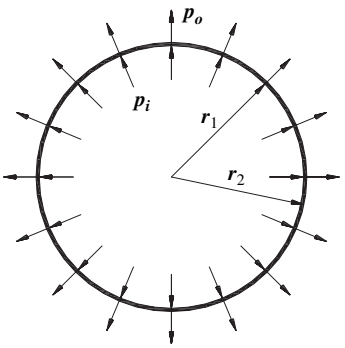

Fig. 2.7 A spherical container under uniform pressures **(Voyiadjis and Woelke, 2004)**

$$\tau_{\theta z} = \left(1 + \frac{z}{R}\right) \frac{3Q_\theta}{2h} \left[1 - \left(\frac{2z}{h}\right)^2\right] + \frac{(r_2/r)^3 - 1}{c_1} p_{\theta i} + \frac{(r_1/r)^3 - 1}{c_2} p_{\theta o} \quad (2.74)$$

$$\tau_{\phi z} = \left(1 + \frac{z}{R}\right) \frac{3Q_\phi}{2h} \left[1 - \left(\frac{2z}{h}\right)^2\right] + \frac{(r_2/r)^3 - 1}{c_1} p_{\phi i} + \frac{(r_1/r)^3 - 1}{c_2} p_{\phi o} \quad (2.75)$$

where:

$\tau_{\theta z}$, $\tau_{\phi z}$ – transverse shear stresses (first subscripts – θ and ϕ denote the direction of the normal to the plane on which stresses are acting; second subscripts – z denote the direction of the stresses);
$p_{\theta i}$, $p_{\theta o}$ – distributed loads along the θ direction, on the inner and outer surfaces respectively;
$p_{\phi i}$, $p_{\phi o}$ – distributed loads along the ϕ direction;
Q_θ, Q_ϕ – transverse shear forces; and
h – thickness of the shell.

Equations (2.74) and (2.75) express the assumed transverse shear stresses. The first term in both the equations depicts the transverse shear stresses calculated for the plate cross section, given by (2.36) and (2.37). The transverse shear stresses in curved shells are modified by the term $(1 + z/R)$, which accounts for the fact that the cross section is not rectangular, but exhibits a curvature. The last two terms from (2.74) and (2.75) are assumed such that the stresses satisfy the boundary conditions. This is achieved by using functions similar to those representing the distribution of the radial stresses in (2.70). The assumed stress field ((2.70), (2.74), (2.75)) satisfies the boundary conditions given by (2.73).

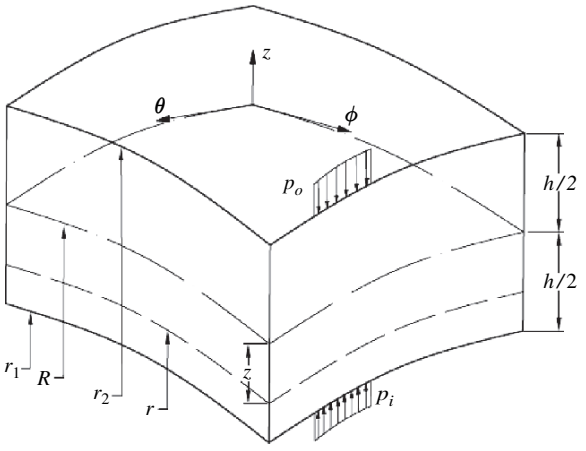

Fig. 2.8 A spherical shell element

2.4.2 Displacement Field

We use the three-dimensional elasticity constitutive equations to derive the displacement field. Using Hooke's law for a linear elastic material, we obtain the transverse normal strain ε_z in terms of the stresses as follows:

$$\varepsilon_z = \frac{1}{E}[\sigma_z - \nu(\sigma_\theta + \sigma_\phi)] \tag{2.76}$$

where σ_θ and σ_ϕ are normal stresses in the θ and ϕ directions, respectively.

Using (2.16) and (2.17) the sum of the normal stresses: $(\sigma_\theta + \sigma_\phi)$ can be written as:

$$\sigma_\theta + \sigma_\phi = \frac{12(M_\theta + M_\phi)z}{h^3} \tag{2.77}$$

Equation (2.77) was first used by Reissner (1975) to modify the expression for the transverse displacement w. Substituting expressions (2.70) and (2.77) into (2.76) we obtain:

$$\varepsilon_z = \frac{\partial w}{\partial z} = \frac{1}{E}\left[\frac{(r_2/r)^3 - 1}{c_1} p_i + \frac{(r_1/r)^3 - 1}{c_2} p_o - \frac{12\nu}{h^3}(M_\theta + M_\phi)z\right] \tag{2.78}$$

Integrating (2.78) with respect to z yields:

$$w(\theta, \phi, z) = w_0(\theta, \phi) + \frac{1}{E}\int\left[\frac{(r_2/r)^3 - 1}{c_1} p_i + \frac{(r_1/r)^3 - 1}{c_2} p_o - \frac{12\nu}{h^3}(M_\theta + M_\phi)z\right]dz \tag{2.79}$$

Denoting:

$$M = (M_\theta + M_\phi) \tag{2.80}$$

and representing $1/(R + z)$ as a power series:

$$\frac{1}{R+z} = \frac{1}{R} - \frac{z}{R^2} + \frac{z^2}{R^3} - \ldots\ldots \tag{2.81}$$

we have:

$$w(\theta, \phi, z) = w_0(\theta, \phi) + \frac{1}{E}\left\{\frac{p_i}{c_1}\left[-z + \frac{r_2^3}{R^3}\left(z - \frac{3}{2}\frac{z^2}{R}\right)\right]\right.$$

$$\left. + \frac{p_o}{c_2}\left[-z + \frac{r_1^3}{R^3}\left(z - \frac{3}{2}\frac{z^2}{R}\right)\right] - \nu\frac{6z^2}{h^3}M\right\} \tag{2.82}$$

In the classical theory of bending of thin shells, the term z/R and its higher order terms are neglected. In the term z/R while neglecting all higher order terms. Equation (2.82) is the resulting expression for $w(\theta, \phi, z)$.

To determine the remaining components of the displacement field, i.e. $u(\theta, \phi, z)$ and $v(\theta, \phi, z)$, we use the following strain-displacement relations in spherical coordinates:

$$\frac{\partial v}{\partial z} + \frac{1}{(R+z)}\frac{\partial w}{\partial \phi} - \frac{v}{(R+z)} = \gamma_{\phi z} = \frac{\tau_{\phi z}}{G} \tag{2.83}$$

$$\frac{1}{(R+z)\sin\phi}\frac{\partial w}{\partial \theta} + \frac{\partial u}{\partial z} - \frac{u}{(R+z)} = \gamma_{\theta z} = \frac{\tau_{\theta z}}{G} \tag{2.84}$$

where u, v, w are the displacements along the θ, ϕ, z axes, respectively. Multiplying both sides of the (2.83) and (2.84) by $1/(R+z)$, we obtain:

$$\frac{1}{(R+z)}\frac{\partial v}{\partial z} - \frac{1}{(R+z)}\frac{v}{(R+z)} = \frac{1}{(R+z)}\left(\frac{\tau_{\phi z}}{G} - \frac{1}{R+z}\frac{\partial w}{\partial \phi}\right) \tag{2.85}$$

$$\frac{1}{(R+z)}\frac{\partial u}{\partial z} - \frac{1}{(R+z)}\frac{u}{(R+z)} = \frac{1}{(R+z)}\left(\frac{\tau_{\theta z}}{G} - \frac{1}{(R+z)\sin\phi}\frac{\partial w}{\partial \theta}\right) \tag{2.86}$$

The left side of both of the above equations can be rewritten as:

$$\frac{\partial}{\partial z}\left(\frac{v}{R+z}\right) = \frac{1}{(R+z)}\left(\frac{\tau_{\phi z}}{G} - \frac{1}{R+z}\frac{\partial w}{\partial \phi}\right) \tag{2.87}$$

$$\frac{\partial u}{\partial z}\left(\frac{u}{R+z}\right) = \frac{1}{(R+z)}\left(\frac{\tau_{\theta z}}{G} - \frac{1}{(R+z)\sin\phi}\frac{\partial w}{\partial \theta}\right) \tag{2.88}$$

as

$$v = (R+z)\int_{-h/2}^{h/2} \frac{1}{(R+z)}\left(\frac{\tau_{\phi z}}{G} - \frac{1}{R+z}\frac{\partial w}{\partial \phi}\right) dz \tag{2.89}$$

$$u = (R+z)\int_{-h/2}^{h/2} \frac{1}{(R+z)}\left(\frac{\tau_{\theta z}}{G} - \frac{1}{(R+z)\sin\phi}\frac{\partial w}{\partial \theta}\right) dz \tag{2.90}$$

Solution of the above equations in their current form produces cumbersome logarithmic terms. To avoid such terms, we replace the term $1/(R+z)$ in the (2.89) and (2.90) with the power series given by (2.81). Substituting for the appropriate shearing stress from expressions (2.83) and (2.84) into (2.89) and (2.90), and integrating both expressions with respect to z, we obtain the remaining components of the displacement field:

$$
\begin{aligned}
u(\theta,\phi,z) = (1+z/R)\Bigg\{ & u_0(\theta,\phi) + \frac{Q_\theta}{2Gh} z\left[3-\frac{4z^2}{h^2}\right] \\
& - \frac{1}{R\sin\phi}\frac{\partial w_0}{\partial\theta}\left(z-\frac{z^2}{R}\right) + \frac{2\nu}{Eh^3}\frac{1}{R\sin\phi}\frac{\partial M}{\partial\theta} z^3\left(1-\frac{3z}{2R}\right) \\
& - \frac{1}{Ec_1}\frac{1}{R\sin\phi}\frac{\partial p_i}{\partial\theta}\left[-\frac{z^2}{2}+\frac{2z^3}{3R}+\frac{r_2^3}{R^3}\left(\frac{z^2}{2}-\frac{7z^3}{6R}\right)\right] \\
& - \frac{1}{Ec_2}\frac{1}{R\sin\phi}\frac{\partial p_o}{\partial\theta}\left[-\frac{z^2}{2}+\frac{2z^3}{3R}+\frac{r_1^3}{R^3}\left(\frac{z^2}{2}-\frac{7z^3}{6R}\right)\right] \\
& + \frac{p_{\theta i}}{Gc_1}\left[-z+\frac{z^2}{2R}+\frac{r_2^3}{R^3}\left(z-\frac{2z^2}{R}\right)\right] \\
& + \frac{p_{\theta o}}{Gc_2}\left[-z+\frac{z^2}{2R}+\frac{r_1^3}{R^3}\left(z-\frac{2z^2}{R}\right)\right]\Bigg\}
\end{aligned}
\tag{2.91}
$$

$$
\begin{aligned}
v(\theta,\phi,z) = (1+z/R)\Bigg\{ & v_0(\theta,\phi) + \frac{Q_\phi}{2Gh} z\left[3-\frac{4z^2}{h^2}\right] \\
& - \frac{1}{R}\frac{\partial w_0}{\partial\phi}\left(z-\frac{z^2}{R}\right) + \frac{2\nu}{Eh^3}\frac{1}{R}\frac{\partial M}{\partial\phi} z^3\left(1-\frac{3z}{2R}\right) \\
& - \frac{1}{Ec_1}\frac{1}{R}\frac{\partial p_i}{\partial\phi}\left[-\frac{z^2}{2}+\frac{2z^3}{3R}+\frac{r_2^3}{R^3}\left(\frac{z^2}{2}-\frac{7z^3}{6R}\right)\right] \\
& - \frac{1}{Ec_2}\frac{1}{R}\frac{\partial p_o}{\partial\phi}\left[-\frac{z^2}{2}+\frac{2z^3}{3R}+\frac{r_1^3}{R^3}\left(\frac{z^2}{2}-\frac{7z^3}{6R}\right)\right] \\
& + \frac{p_{\phi i}}{Gc_1}\left[-z+\frac{z^2}{2R}+\frac{r_2^3}{R^3}\left(z-\frac{2z^2}{R}\right)\right] \\
& + \frac{p_{\phi o}}{Gc_2}\left[-z+\frac{z^2}{2R}+\frac{r_1^3}{R^3}\left(z-\frac{2z^2}{R}\right)\right]\Bigg\}
\end{aligned}
\tag{2.92}
$$

In our shell theory, we omit the variations of the distributed loads $p_{\phi i}$, $p_{\phi o}$, $p_{\theta i}$, $p_{\theta o}$ for simplicity and conciseness. The reader may choose to include them by following the procedure outlined below.

2.4.3 Stress Components

To obtain the remaining stress components, the following three-dimensional stress–strain relationships are used:

$$\sigma_\theta = \frac{E}{\left(1-\nu^2\right)}\left[\varepsilon_\theta + \nu\varepsilon_\phi\right] + \frac{\nu}{1-\nu}\sigma_z \tag{2.93}$$

$$\sigma_\phi = \frac{E}{\left(1-\nu^2\right)}\left[\varepsilon_\phi + \nu\varepsilon_\theta\right] + \frac{\nu}{1-\nu}\sigma_z \tag{2.94}$$

$$\tau_{\theta\phi} = G\gamma_{\theta\phi} \tag{2.95}$$

together with the following strain–displacement relations in spherical coordinates:

$$\varepsilon_\theta = \frac{1}{(R+z)\sin\phi}\frac{\partial u}{\partial\theta} + \frac{v}{(R+z)}ctg\phi + \frac{w}{R+z} \tag{2.96}$$

$$\varepsilon_\phi = \frac{1}{(R+z)}\frac{\partial v}{\partial\phi} + \frac{w}{R+z} \tag{2.97}$$

$$\gamma_{\theta\phi} = \frac{1}{(R+z)\sin\phi}\frac{\partial v}{\partial\theta} + \frac{1}{(R+z)}\frac{\partial u}{\partial\phi} - \frac{u}{(R+z)}ctg\phi \tag{2.98}$$

Substituting for the displacements u, v and w from (2.91), (2.92), (2.82) respectively, into expressions (2.96), (2.97), (2.98), and substituting the resulting strains into equations (2.93), (2.94), (2.95) we obtain the following expression for the normal stresses in the θ and ϕ directions respectively:

$$\begin{aligned}\sigma_\theta = \frac{E}{1-\nu^2} + \Bigg\{ & \frac{1}{R\sin\phi}\frac{\partial u_0}{\partial\theta} + \frac{\cos\phi}{R\sin\phi}v_0 + \frac{\nu}{R}\frac{\partial v_0}{\partial\phi} \\ & + \frac{z}{2Gh}\left[3 - \frac{4z^2}{h^2}\right]\left[\frac{1}{R\sin\phi}\frac{\partial Q_\theta}{\partial\theta} + \frac{\cos\phi}{R\sin\phi}Q_\phi + \frac{\nu}{R}\frac{\partial Q_\phi}{\partial\phi}\right] \\ & + \Delta_1^2\left[-\frac{1}{R}\left(z - \frac{z^2}{R}\right)w_0 + \frac{2\nu}{Eh^3}\frac{1}{R}z^3\left(1 - \frac{3z}{2R}\right)M\right. \\ & - \frac{1}{Ec_1}\frac{1}{R}\left[-\frac{z^2}{2} + \frac{2z^3}{3R} + \frac{r_2^3}{R^3}\left(\frac{z^2}{2} - \frac{7z^3}{6R}\right)\right]p_i \\ & \left. - \frac{1}{Ec_2}\frac{1}{R}\left[-\frac{z^2}{2} + \frac{2z^3}{3R} + \frac{r_1^3}{R^3}\left(\frac{z^2}{2} - \frac{7z^3}{6R}\right)\right]p_o\right]\end{aligned}$$

$$+\frac{p_{\phi i}\cos\phi}{Gc_1R\sin\phi}\left[-z+\frac{z^2}{2R}+\frac{{r_2}^3}{R^3}\left(z-\frac{2z^2}{R}\right)\right] \tag{2.99}$$

$$+\frac{p_{\phi o}\cos\phi}{Gc_2R\sin\phi}\left[-z+\frac{z^2}{2R}+\frac{{r_1}^3}{R^3}\left(z-\frac{2z^2}{R}\right)\right]$$

$$+\frac{1+\nu}{R\left(1+\frac{z}{R}\right)}\left[w_0+\frac{p_i}{Ec_1}\left[-z+\frac{{r_2}^3}{R^3}\left(z-\frac{3}{2}\frac{z^2}{R}\right)\right]\right.$$

$$\left.+\frac{p_o}{Ec_2}\left[-z+\frac{{r_1}^3}{R^3}\left(z-\frac{3}{2}\frac{z^2}{R}\right)\right]-\nu\frac{6z^2}{Eh^3}M\right]\Bigg\}$$

$$+\frac{\nu}{1+\nu}\left[\frac{p_i}{c_1}\left(\frac{{r_2}^3}{(R+z)^3}-1\right)+\frac{p_o}{c_2}\left(\frac{{r_1}^3}{(R+z)^3}-1\right)\right]$$

where:

$$\Delta_1^2=\frac{1}{R\sin^2\phi}\frac{\partial^2}{\partial\theta^2}+\frac{\cos\phi}{R\sin\phi}\frac{\partial}{\partial\phi}+\frac{\nu}{R}\frac{\partial^2}{\partial\phi^2} \tag{2.100}$$

$$\sigma_\phi=\frac{E}{1-\nu^2}\left\{\frac{1}{R\sin\phi}\frac{\partial u_0}{\partial\theta}+\frac{\nu\cos\phi}{R\sin\phi}v_0+\frac{1}{R}\frac{\partial v_0}{\partial\phi}\right.$$

$$+\frac{z}{2Gh}\left[3-\frac{4z^2}{h^2}\right]\left[\frac{\nu}{R\sin\phi}\frac{\partial Q_\theta}{\partial\theta}+\frac{\nu\cos\phi}{R\sin\phi}Q_\phi+\frac{1}{R}\frac{\partial Q_\phi}{\partial\phi}\right]$$

$$+\Delta_2^2\left[-\frac{1}{R}\left(z-\frac{z^2}{R}\right)w_0+\frac{2\nu}{Eh^3}\frac{1}{R}z^3\left(1-\frac{3z}{2R}\right)M\right.$$

$$-\frac{1}{Ec_1}\frac{1}{R}\left[-\frac{z^2}{2}+\frac{2z^3}{3R}+\frac{r_2^3}{R^3}\left(\frac{z^2}{2}-\frac{7z^3}{6R}\right)\right]p_i$$

$$\left.-\frac{1}{Ec_2}\frac{1}{R}\left[-\frac{z^2}{2}+\frac{2z^3}{3R}+\frac{r_1^3}{R^3}\left(\frac{z^2}{2}-\frac{7z^3}{6R}\right)\right]p_o\right]$$

$$+\frac{\nu p_{\phi i}\cos\phi}{Gc_1R\sin\phi}\left[-z+\frac{z^2}{2R}+\frac{r_2^3}{R^3}\left(z-\frac{2z^2}{R}\right)\right] \tag{2.101}$$

$$+\frac{\nu p_{\phi o}\cos\phi}{Gc_2R\sin\phi}\left[-z+\frac{z^2}{2R}+\frac{r_1^3}{R^3}\left(z-\frac{2z^2}{R}\right)\right]$$

$$+\frac{1+\nu}{R\left(1+\frac{z}{R}\right)}\left[w_0+\frac{p_i}{Ec_1}\left[-z+\frac{r_2^3}{R^3}\left(z-\frac{3}{2}\frac{z^2}{R}\right)\right]\right.$$

$$+\frac{p_o}{Ec_2}\left[-z+\frac{r_1^3}{R^3}\left(z-\frac{3}{2}\frac{z^2}{R}\right)\right]-\nu\frac{6z^2}{Eh^3}M\Bigg]\Bigg\}$$
$$+\frac{\nu}{1+\nu}\left[\frac{p_i}{c_1}\left(\frac{r_2^3}{(R+z)^3}-1\right)+\frac{p_o}{c_2}\left(\frac{r_1^3}{(R+z)^3}-1\right)\right]$$

where:

$$\Delta_2^2=\frac{\nu}{R\sin^2\phi}\frac{\partial^2}{\partial\theta^2}+\frac{\nu\cos\phi}{R\sin\phi}\frac{\partial}{\partial\phi}+\frac{1}{R}\frac{\partial^2}{\partial\phi^2} \tag{2.102}$$

The shear stresses in the $\theta\phi$-plane are:

$$\begin{aligned}\tau_{\theta\phi}=G\Bigg\{&\frac{1}{R\sin\phi}\frac{\partial v_0}{\partial\theta}+\frac{1}{R}\frac{\partial u_0}{\partial\phi}-\frac{u_0\cos\phi}{R\sin\phi}v_0\\&+\frac{z}{2Gh}\left[3-\frac{4z^2}{h^2}\right]\left[\frac{1}{R\sin\phi}\frac{\partial Q_\phi}{\partial\theta}+\frac{1}{R}\frac{\partial Q_\theta}{\partial\phi}\frac{\cos\phi}{R\sin\phi}Q_\theta\right]\\&+\Delta_3{}^2\Bigg[-\frac{1}{R}\left(z-\frac{z^2}{R}\right)w_0+\frac{2\nu}{Eh^3}\frac{1}{R}z^3\left(1-\frac{3z}{2R}\right)M\\&-\frac{1}{Ec_1}\frac{1}{R}\left[-\frac{z^2}{2}+\frac{2z^3}{3R}+\frac{r_2^3}{R^3}\left(\frac{z^2}{2}-\frac{7z^3}{6R}\right)\right]p_i\\&-\frac{1}{Ec_2}\frac{1}{R}\left[-\frac{z^2}{2}+\frac{2z^3}{3R}+\frac{r_1^3}{R^3}\left(\frac{z^2}{2}-\frac{7z^3}{6R}\right)\right]p_o\Bigg]\\&+\frac{p_{\phi i}\cos\phi}{Gc_1R\sin\phi}\left[-z+\frac{z^2}{2R}+\frac{r_2^3}{R^3}\left(z-\frac{2z^2}{R}\right)\right]\\&+\frac{p_{\phi o}\cos\phi}{Gc_2R\sin\phi}\left[-z+\frac{z^2}{2R}+\frac{r_1^3}{R^3}\left(z-\frac{2z^2}{R}\right)\right]\Bigg\}\end{aligned} \tag{2.103}$$

where:

$$\Delta_3^2=\frac{2}{R\sin\phi}\frac{\partial^2}{\partial\theta\partial\phi}+\frac{2\cos\phi}{R\sin^2\phi}\frac{\partial}{\partial\theta} \tag{2.104}$$

2.4.4 Stress Couples and Stress Resultants on the Middle Surface

The definitions of the stress couples with the initial curvature effect taken into account are:

$$M_\theta = -\int_{-h/2}^{h/2} \sigma_\theta z \left(1 + \frac{z}{R}\right) dz \tag{2.105}$$

$$M_\phi = -\int_{-h/2}^{h/2} \sigma_\phi z \left(1 + \frac{z}{R}\right) dz \tag{2.106}$$

$$M_{\theta\phi} = -\int_{-h/2}^{h/2} \tau_{\theta\phi} z \left(1 + \frac{z}{R}\right) dz \tag{2.107}$$

The positive bending moment is the one that results in positive stresses in the bottom part of the shell (Fig. 2.5). We now substitute the stresses given by (2.100), (2.102), (2.104) into the respective relations for the stress couples to obtain:

$$\begin{aligned}
M_\theta = D \Bigg\{ & -\frac{1}{R^2 \sin\phi} \frac{\partial u_0}{\partial \theta} - \frac{\cos\phi}{R^2 \sin\phi} v_0 - \frac{\nu}{R^2} \frac{\partial v_0}{\partial \phi} \\
& - \frac{6}{5Gh} \left[\frac{1}{R \sin\phi} \frac{\partial Q_\theta}{\partial \theta} + \frac{\cos\phi}{R \sin\phi} Q_\phi + \frac{\nu}{R} \frac{\partial Q_\phi}{\partial \phi} \right] \\
& + \frac{1}{R} \Delta_1^2 w_0 + \left(\frac{9\nu h}{112 E R^3} - \frac{3\nu}{10 E R h} \right) \Delta_1^2 M \\
& - \frac{1}{E R^2 c_1} \left[\frac{h^2}{24} \left(1 + \frac{12}{5} \frac{r_2^3}{R^2} - \frac{r_2^3}{R^3} \right) \right] \Delta_1^2 p_i \\
& - \frac{1}{E R^2 c_2} \left[\frac{h^2}{24} \left(1 + \frac{12}{5} \frac{r_1^3}{R^2} - \frac{r_1^3}{R^3} \right) \right] \Delta_1^2 p_o \\
& + \frac{p_{\phi i} \cos\phi}{R \sin\phi} \frac{1}{G c_1} \left[1 - \frac{r_2^3}{R^3} - \frac{3h^2}{40 R^2} \right] + \frac{p_{\phi o} \cos\phi}{R \sin\phi} \frac{1}{G c_2} \left[1 - \frac{r_1^3}{R^3} - \frac{3h^2}{40 R^2} \right] \\
& + \frac{1+\nu}{E R} \left[\frac{p_i}{c_1} \left[1 + \nu - \frac{r_2^3}{R^3} (1 - 2\nu) \right] + \frac{p_o}{c_2} \left[1 + \nu - \frac{r_1^3}{R^3} (1 - 2\nu) \right] \right] \Bigg\}
\end{aligned} \tag{2.108}$$

$$\begin{aligned}
M_\phi = D \Bigg\{ & -\frac{\nu}{R^2 \sin\phi} \frac{\partial u_0}{\partial \theta} - \frac{\nu \cos\phi}{R^2 \sin\phi} v_0 - \frac{1}{R^2} \frac{\partial v_0}{\partial \phi} \\
& - \frac{6}{5Gh} \left[\frac{\nu}{R \sin\phi} \frac{\partial Q_\theta}{\partial \theta} + \frac{\nu \cos\phi}{R \sin\phi} Q_\phi + \frac{1}{R} \frac{\partial Q_\phi}{\partial \phi} \right] \\
& + \frac{1}{R} \Delta_2^2 w_0 + \left(\frac{9\nu h}{112 E R^3} - \frac{3\nu}{10 E R h} \right) \Delta_2^2 M
\end{aligned}$$

$$
\begin{aligned}
&-\frac{1}{ER^2c_1}\left[\frac{h^2}{24}\left(1+\frac{12}{5}\frac{r_2^{\,3}}{R^2}-\frac{r_2^{\,3}}{R^{\,3}}\right)\right]\Delta_2^2 p_i \\
&-\frac{1}{ER^2c_2}\left[\frac{h^2}{24}\left(1+\frac{12}{5}\frac{r_1^{\,3}}{R^2}-\frac{r_1^{\,3}}{R^{\,3}}\right)\right]\Delta_2^2 p_o \\
&+\frac{\nu p_{\phi i}\cos\phi}{R\sin\phi}\frac{1}{Gc_1}\left[1-\frac{r_2^{\,3}}{R^{\,3}}-\frac{3h^2}{40R^2}\right]+\frac{\nu p_{\phi o}\cos\phi}{R\sin\phi}\frac{1}{Gc_2}\left[1-\frac{r_1^{\,3}}{R^{\,3}}-\frac{3h^2}{40R^2}\right] \\
&+\frac{1+\nu}{ER}\left[\frac{p_i}{c_1}\left[1+\nu-\frac{r_2^{\,3}}{R^{\,3}}(1-2\nu)\right]+\frac{p_o}{c_2}\left[1+\nu-\frac{r_1^{\,3}}{R^{\,3}}(1-2\nu)\right]\right]\Bigg\}
\end{aligned}
\tag{2.109}
$$

$$
\begin{aligned}
M_{\theta\phi} = D\frac{1-\nu}{2}\Bigg\{&-\frac{1}{R^2\sin\phi}\frac{\partial v_0}{\partial\theta}-\frac{1}{R^2}\frac{\partial u_0}{\partial\phi}-\frac{\cos\phi}{R^2\sin\phi}u_0 \\
&-\frac{6}{5Gh}\left[\frac{1}{R\sin\phi}\frac{\partial Q_\phi}{\partial\theta}+\frac{1}{R}\frac{\partial Q_\theta}{\partial\phi}-\frac{\cos\phi}{R\sin\phi}Q_\theta\right] \\
&+\frac{1}{R}\Delta_3^2 w_0+\left(\frac{9\nu h}{112ER^{\,3}}-\frac{3\nu}{10ERh}\right)\Delta_3^2 M \\
&-\frac{1}{ER^2c_1}\left[\frac{h^2}{24}\left(1+\frac{12}{5}\frac{r_2^{\,3}}{R^2}-\frac{r_2^{\,3}}{R^{\,3}}\right)\right]\Delta_3^2 p_i \\
&-\frac{1}{ER^2c_2}\left[\frac{h^2}{24}\left(1+\frac{12}{5}\frac{r_1^{\,3}}{R^2}-\frac{r_1^{\,3}}{R^{\,3}}\right)\right]\Delta_3^2 p_o \\
&+\frac{p_{\theta i}\cos\phi}{R\sin\phi}\frac{1}{Gc_1}\left[1-\frac{r_2^{\,3}}{R^{\,3}}-\frac{3h^2}{40R^2}\right]+\frac{p_{\theta o}\cos\phi}{R\sin\phi}\frac{1}{Gc_2}\left[1-\frac{r_1^{\,3}}{R^{\,3}}-\frac{3h^2}{40R^2}\right]\Bigg\}
\end{aligned}
\tag{2.110}
$$

Substituting for the stresses σ_θ, σ_ϕ, $\tau_{\theta\phi}$ from (2.100), (2.102), and 2.104) into the definitions of the stress resultants:

$$
N_\theta = \int_{-h/2}^{h/2}\sigma_\theta\left(1+\frac{z}{R}\right)dz \tag{2.111}
$$

$$
N_\phi = \int_{-h/2}^{h/2}\sigma_\phi\left(1+\frac{z}{R}\right)dz \tag{2.112}
$$

$$
N_{\theta\phi} = \int_{-h/2}^{h/2}\tau_{\theta\phi}\left(1+\frac{z}{R}\right)dz \tag{2.113}
$$

we obtain the following expression for the normal force in the θ direction:

$$
\begin{aligned}
N_\theta = \frac{Eh}{1-\nu^2}\Bigg\{ & \frac{1}{R\sin\phi}\frac{\partial u_0}{\partial\theta} + \frac{\cos\phi}{R\sin\phi}v_0 + \frac{\nu}{R}\frac{\partial v_0}{\partial\phi} \\
& + \frac{h}{10GR}\left[\frac{1}{R\sin\phi}\frac{\partial Q_\theta}{\partial\theta} + \frac{\cos\phi}{R\sin\phi}Q_\phi + \frac{\nu}{R}\frac{\partial Q_\phi}{\partial\phi}\right] \\
& + \frac{1}{Ec_1}\left[\frac{h^2}{24R}\left(1-\frac{r_2^3}{R^3}\right)\right]\Delta_1^2 p_i + \frac{1}{Ec_2}\left[\frac{h^2}{24R}\left(1-\frac{r_1^3}{R^3}\right)\right]\Delta_1^2 p_o \\
& - \frac{p_{\phi i}\cos\phi}{\sin\phi}\frac{1}{Gc_1}\left[\frac{h^2}{24R^2}\left(1+2\frac{r_2^3}{R^3}\right)\right] - \frac{p_{\phi o}\cos\phi}{\sin\phi}\frac{1}{Gc_2}\left[\frac{h^2}{24R^2}\left(1+2\frac{r_1^3}{R^3}\right)\right] \\
& + \frac{1+\nu}{R}w_0 + \left(\frac{9\nu h}{112ER^3} - \frac{3\nu}{10ERh}\right)(1+\nu)M \\
& + \frac{(1+\nu)h^2}{ER}\left[\frac{p_i}{c_1}\left(1-\frac{r_2^3}{10R^3}\right) + \frac{p_o}{c_2}\left(1-\frac{r_1^3}{10R^3}\right)\right]\Bigg\}
\end{aligned}
\tag{2.114}
$$

The normal force in the ϕ direction is:

$$
\begin{aligned}
N_\phi = \frac{Eh}{1-\nu^2}\Bigg\{ & \frac{\nu}{R\sin\phi}\frac{\partial u_0}{\partial\theta} + \frac{\nu\cos\phi}{R\sin\phi}v_0 + \frac{1}{R}\frac{\partial v_0}{\partial\phi} \\
& + \frac{h}{10GR}\left[\frac{\nu}{R\sin\phi}\frac{\partial Q_\theta}{\partial\theta} + \frac{\nu\cos\phi}{R\sin\phi}Q_\phi + \frac{1}{R}\frac{\partial Q_\phi}{\partial\phi}\right] \\
& + \frac{1}{Ec_1}\left[\frac{h^2}{24R}\left(1-\frac{r_2^3}{R^3}\right)\right]\Delta_2^2 p_i + \frac{1}{Ec_2}\left[\frac{h^2}{24R}\left(1-\frac{r_1^3}{R^3}\right)\right]\Delta_2^2 p_o \\
& - \frac{p_{\phi i}\nu\cos\phi}{\sin\phi}\frac{1}{Gc_1}\left[\frac{h^2}{24R^2}\left(1+2\frac{r_2^3}{R^3}\right)\right] - \frac{p_{\phi o}\nu\cos\phi}{\sin\phi}\frac{1}{Gc_2}\left[\frac{h^2}{24R^2}\left(1+2\frac{r_1^3}{R^3}\right)\right] \\
& + \frac{1+\nu}{R}w_0 + \left(\frac{9\nu h}{112ER^3} - \frac{3\nu}{10ERh}\right)(1+\nu)M \\
& + \frac{(1+\nu)h^2}{ER}\left[\frac{p_i}{c_1}\left(1-\frac{r_2^3}{10R^3}\right) + \frac{p_o}{c_2}\left(1-\frac{r_1^3}{10R^3}\right)\right]\Bigg\}
\end{aligned}
\tag{2.115}
$$

The normal force in the $\theta\phi$-plane is:

$$N_{\theta\phi} = \frac{Eh}{1-\nu^2}\left(\frac{1-\nu}{2}\right)\left\{\frac{1}{R\sin\phi}\frac{\partial v_0}{\partial\theta} + \frac{1}{R}\frac{\partial u_0}{\partial\phi} - \frac{\cos\phi}{R\sin\phi}u_0\right.$$
$$+ \frac{h}{10GR}\left[\frac{1}{R\sin\phi}\frac{\partial Q_\phi}{\partial\theta} + \frac{1}{R}\frac{\partial Q_\theta}{\partial\phi} - \frac{\cos\phi}{R\sin\phi}Q_\theta\right]$$
$$+ \frac{1}{Ec_1}\left[\frac{h^2}{24R}\left(1-\frac{r_2^3}{R^3}\right)\right]\Delta_3^2 p_i + \frac{1}{Ec_2}\left[\frac{h^2}{24R}\left(1-\frac{r_1^3}{R^3}\right)\right]\Delta_3^2 p_o$$
$$\left. - \frac{p_{\phi i}\cos\phi}{\sin\phi}\frac{1}{Gc_1}\left[\frac{h^2}{24R^2}\left(1+2\frac{r_2^3}{R^3}\right)\right] - \frac{p_{\phi o}\cos\phi}{\sin\phi}\frac{1}{Gc_2}\left[\frac{h^2}{24R^2}\left(1+2\frac{r_1^3}{R^3}\right)\right]\right\} \tag{2.116}$$

2.4.5 Average Displacements $\bar{u}$, $\bar{v}$, $\bar{w}$ and Rotations ϕ_θ, ϕ_ϕ

To identify the appropriate boundary conditions for the derived shell theory, we introduce average displacements $\bar{u}$, $\bar{v}$, $\bar{w}$, and rotations ϕ_θ, ϕ_ϕ. The rotations are for sections $\theta = const$ and $\phi = const$, respectively. We first define the transverse shear resultants as:

$$Q_\theta = T\gamma_{\theta z} \tag{2.117}$$
$$Q_\phi = T\gamma_{\phi z} \tag{2.118}$$

where T is given by:

$$T = \frac{5}{6}Gh \tag{2.119}$$

and $\gamma_{\theta z}$, $\gamma_{\phi z}$ are expressed similarly to (2.83) and (2.84):

$$\gamma_{\theta z} = \frac{1}{(R+z)\sin\phi}\frac{\partial\bar{w}}{\partial\theta} + \frac{\partial\bar{u}}{\partial z} - \frac{\bar{u}}{(R+z)} \tag{2.120}$$

$$\gamma_{\phi z} = \frac{\partial\bar{v}}{\partial z} + \frac{1}{(R+z)}\frac{\partial\bar{w}}{\partial\phi} - \frac{\bar{v}}{(R+z)} \tag{2.121}$$

We obtain the average transverse displacement $\bar{w}$ by equating the work of the transverse shear stress $\tau_{\phi z}$ due to the displacement w to the work of the transverse shear resultant Q_ϕ due to the average displacement $\bar{w}$ (Voyiadjis and Baluch, 1981; Hu, 1984).

$$\int_{-h/2}^{h/2} \tau_{\phi z} w \left(1 + \frac{z}{R}\right) dz = Q_\phi \bar{w} \tag{2.122}$$

One could choose to equate the work of the transverse shear stress $\tau_{\theta z}$ due to the displacement w to the work of the transverse shear resultant Q_θ due to the average displacement $\bar{w}$ instead, which yields the same expression for $\bar{w}$, given by:

$$\bar{w} = w_0 - M\left(\frac{3\nu}{10Eh} - \frac{9\nu h}{112ER^2}\right) - \frac{1}{10}\frac{h^2}{REc_1}\frac{r_2^3}{R^3}p_i - \frac{1}{10}\frac{h^2}{REc_2}\frac{r_1^3}{R^3}p_o \tag{2.123}$$

Similarly, to obtain $\bar{u}$, $\bar{v}$ ϕ_θ, ϕ_ϕ we use the following equations:

$$\int_{-h/2}^{h/2} \sigma_\theta u \left(1 + \frac{z}{R}\right) dz = N_\theta \bar{u} + M_\theta \phi_\theta \tag{2.124}$$

$$\int_{-h/2}^{h/2} \sigma_\phi v \left(1 + \frac{z}{R}\right) dz = N_\phi \bar{v} + M_\phi \phi_\phi \tag{2.125}$$

The resulting expressions for $\bar{u}$, $\bar{v}$, ϕ_θ, ϕ_ϕ are given by:

$$\bar{u} = u_0 + \frac{1}{ER\sin\phi}\frac{h^2}{24}\left[\frac{1}{c_1}\frac{\partial p_i}{\partial\theta}\left(1 - \frac{r_2^3}{R^3}\right) + \frac{1}{c_2}\frac{\partial p_o}{\partial\theta}\left(1 - \frac{r_1^3}{R^3}\right)\right] \tag{2.126}$$

$$\bar{v} = v_0 + \frac{1}{ER}\frac{h^2}{24}\left[\frac{1}{c_1}\frac{\partial p_i}{\partial\phi}\left(1 - \frac{r_2^3}{R^3}\right) + \frac{1}{c_2}\frac{\partial p_o}{\partial\phi}\left(1 - \frac{r_1^3}{R^3}\right)\right] \tag{2.127}$$

$$\phi_\theta = \frac{1}{R\sin\phi}\frac{\partial\bar{w}}{\partial\theta} - \frac{6}{5Gh}Q_\theta - \frac{\bar{u}}{R} \tag{2.128}$$

$$\phi_\phi = \frac{1}{R}\frac{\partial\bar{w}}{\partial\phi} - \frac{6}{5Gh}Q_\phi - \frac{\bar{v}}{R} \tag{2.129}$$

Using equations (2.117) and (2.118) we can rewrite (2.128) and (2.129):

$$\phi_\theta = \frac{1}{R\sin\phi}\frac{\partial\bar{w}}{\partial\theta} - \gamma_{\theta z} - \frac{\bar{u}}{R} \tag{2.130}$$

$$\phi_\phi = \frac{1}{R}\frac{\partial\bar{w}}{\partial\phi} - \gamma_{\phi z} - \frac{\bar{v}}{R} \tag{2.131}$$

The remaining stress resultants and stress couples may be expressed more concisely in terms of $\bar{u}$, $\bar{v}$, $\bar{w}$, $\gamma_{\theta z}$, $\gamma_{\phi z}$:

$$M_\theta = D\left[\frac{1}{R\sin\phi}\frac{\partial}{\partial\theta}\left(\frac{1}{R\sin\phi}\frac{\partial\bar{w}}{\partial\theta}-\gamma_{\theta z}-\frac{\bar{u}}{R}\right)+\frac{ctg\phi}{R}\left(\frac{1}{R}\frac{\partial\bar{w}}{\partial\phi}-\gamma_{\phi z}-\frac{\bar{v}}{R}\right)\right.$$
$$\left.+\frac{\nu}{R}\frac{\partial}{\partial\phi}\left(\frac{1}{R}\frac{\partial\bar{w}}{\partial\phi}-\gamma_{\phi z}-\frac{\bar{v}}{R}\right)\right]+k_1p_i+k_2p_o+k_3p_{\phi i}+k_4p_{\phi o} \tag{2.132}$$

$$M_\phi = D\left[\frac{\nu}{R\sin\phi}\frac{\partial}{\partial\theta}\left(\frac{1}{R\sin\phi}\frac{\partial\bar{w}}{\partial\theta}-\gamma_{\theta z}-\frac{\bar{u}}{R}\right)+\frac{\nu ctg\phi}{R}\left(\frac{1}{R}\frac{\partial\bar{w}}{\partial\phi}-\gamma_{\phi z}-\frac{\bar{v}}{R}\right)\right.$$
$$\left.+\frac{1}{R}\frac{\partial}{\partial\phi}\left(\frac{1}{R}\frac{\partial\bar{w}}{\partial\phi}-\gamma_{\phi z}-\frac{\bar{v}}{R}\right)\right]+k_1p_i+k_2p_o+\nu k_3p_{\phi i}+\nu k_4p_{\phi o} \tag{2.133}$$

$$M_{\theta\phi} = D\frac{1-\nu}{2}\left[\frac{1}{R}\frac{\partial}{\partial\phi}\left(\frac{1}{R\sin\phi}\frac{\partial\bar{w}}{\partial\theta}-\gamma_{\theta z}-\frac{\bar{u}}{R}\right)-\frac{ctg\phi}{R}\left(\frac{2}{R\sin\phi}\frac{\partial\bar{w}}{\partial\theta}-\gamma_{\theta z}+\frac{\bar{u}}{R}\right)\right.$$
$$\left.+\frac{1}{R\sin\phi}\frac{\partial}{\partial\theta}\left(\frac{1}{R}\frac{\partial\bar{w}}{\partial\phi}-\gamma_{\phi z}-\frac{\bar{v}}{R}\right)\right]+k_3\frac{1-\nu}{2}p_{\phi i}+k_4\frac{1-\nu}{2}p_{\phi o} \tag{2.134}$$

$$N_\theta = \frac{Eh}{1-\nu^2}\left[\frac{1}{R\sin\phi}\frac{\partial\bar{u}}{\partial\theta}+\frac{ctg\phi}{R}\bar{v}+\frac{\nu}{R}\frac{\partial\bar{v}}{\partial\phi}+\frac{1+\nu}{R}\bar{w}\right]$$
$$+\frac{D}{R}\left[\frac{1}{R\sin\phi}\frac{\partial\gamma_{\theta z}}{\partial\theta}+\frac{ctg\phi}{R}\gamma_{\phi z}+\frac{\nu}{R}\frac{\partial\gamma_{\phi z}}{\partial\phi}\right]+k_5p_i+k_6p_o+k_7p_{\phi i}+k_8p_{\phi o} \tag{2.135}$$

$$N_\phi = \frac{Eh}{1-\nu^2}\left[\frac{\nu}{R\sin\phi}\frac{\partial\bar{u}}{\partial\theta}+\frac{\nu ctg\phi}{R}\bar{v}+\frac{1}{R}\frac{\partial\bar{v}}{\partial\phi}+\frac{1+\nu}{R}\bar{w}\right]$$
$$+\frac{D}{R}\left[\frac{\nu}{R\sin\phi}\frac{\partial\gamma_{\theta z}}{\partial\theta}+\frac{\nu ctg\phi}{R}\gamma_{\phi z}+\frac{1}{R}\frac{\partial\gamma_{\phi z}}{\partial\phi}\right]+k_5p_i+k_6p_o+\nu k_7p_{\phi i}+\nu k_8p_{\phi o} \tag{2.136}$$

$$N_{\theta\phi} = \frac{Eh}{1-\nu^2}\left(\frac{1-\nu}{2}\right)\left[\frac{1}{R\sin\phi}\frac{\partial\bar{v}}{\partial\theta}+\frac{1}{R}\frac{\partial\bar{u}}{\partial\phi}-\frac{ctg\phi}{R}\bar{u}\right]$$
$$+\frac{D}{R}\left(\frac{1-\nu}{2}\right)\left[\frac{1}{R\sin\phi}\frac{\partial\gamma_{\phi z}}{\partial\theta}-\frac{ctg\phi}{R}\gamma_{\theta z}+\frac{1}{R}\frac{\partial\gamma_{\theta z}}{\partial\phi}\right] \tag{2.137}$$
$$+\left(\frac{1-\nu}{2}\right)k_7p_{\theta i}+\left(\frac{1-\nu}{2}\right)k_8p_{\theta o}$$

where:

$$k_1 = D\frac{1+\nu}{ERc_1}\left[1+\nu-\frac{r_2^3}{R^3}(1-2\nu)\right] \tag{2.138}$$

$$k_2 = D\frac{1+\nu}{ERc_2}\left[1+\nu-\frac{r_1^3}{R^3}(1-2\nu)\right] \tag{2.139}$$

$$k_3 = D\frac{ctg\phi}{RGc_1}\left(1-\frac{r_2^3}{R^3}\right) \tag{2.140}$$

$$k_4 = D\frac{ctg\phi}{RGc_2}\left(1-\frac{r_1^3}{R^3}\right) \tag{2.141}$$

$$k_5 = \frac{h^3}{Rc_1(1-\nu)} \tag{2.142}$$

$$k_6 = \frac{h^3}{Rc_2(1-\nu)} \tag{2.143}$$

$$k_7 = -\frac{Eh}{1-\nu^2}\left[\frac{ctg\phi}{Gc_1}\frac{h^2}{24R^2}\left(1+2\frac{r_2^3}{R^3}\right)\right] \tag{2.144}$$

$$k_8 = -\frac{Eh}{1-\nu^2}\left[\frac{ctg\phi}{Gc_2}\frac{h^2}{24R^2}\left(1+2\frac{r_1^3}{R^3}\right)\right] \tag{2.145}$$

These constitutive equations reduce to those given by Flugge (1960) when the shear deformation and radial effects are neglected. In this case, the average displacements are replaced by the middle surface displacements and we obtain the transverse shear forces Q_θ, Q_ϕ from the equilibrium equations in terms of the stress couples.

An alternative set of expressions for the normal forces and bending moments can be obtained in terms of the strains ε_θ, ε_ϕ, $\gamma_{\theta z}$, $\gamma_{\phi z}$ and corresponding rotations ϕ_θ, ϕ_ϕ. These relations (Voyiadjis and Woelke, 2004) are:

$$M_\theta = D\left[\frac{1}{R\sin\phi}\frac{\partial\phi_\theta}{\partial\theta}+\frac{\nu}{R}\frac{\partial\phi_\phi}{\partial\phi}+\frac{ctg\phi}{R}\phi_\phi\right]+k_1p_i+k_2p_o+k_3p_{\phi i}+k_4p_{\phi o} \tag{2.146}$$

$$M_\phi = D\left[\frac{\nu}{R\sin\phi}\frac{\partial\phi_\theta}{\partial\theta}+\frac{1}{R}\frac{\partial\phi_\phi}{\partial\phi}+\frac{\nu ctg\phi}{R}\phi_\phi\right]+k_1p_i+k_2p_o+\nu k_3p_{\phi i}+\nu k_4p_{\phi o} \tag{2.147}$$

$$\begin{aligned} M_{\theta\phi} = {} & D\frac{1-\nu}{2}\left[\frac{1}{R}\frac{\partial\phi_\theta}{\partial\phi}+\frac{1}{R\sin\phi}\frac{\partial\phi_\phi}{\partial\theta}-\frac{ctg\phi}{R}\left(\frac{2}{R\sin\phi}\frac{\partial\bar{w}}{\partial\theta}-\gamma_{\theta z}+\frac{\bar{u}}{R}\right)\right] \\ & +k_3\frac{1-\nu}{2}p_{\phi i}+k_4\frac{1-\nu}{2}p_{\phi o} \end{aligned} \tag{2.148}$$

$$N_\theta = \frac{Eh}{1-\nu^2}\left[\varepsilon_\theta + \nu\varepsilon_\phi\right] + \frac{D}{R}\left[\frac{1}{R\sin\phi}\frac{\partial\gamma_{\theta z}}{\partial\theta} + \frac{ctg\phi}{R}\gamma_{\phi z} + \frac{\nu}{R}\frac{\partial\gamma_{\phi z}}{\partial\phi}\right] + k_5 p_i + k_6 p_o + k_7 p_{\phi i} + k_8 p_{\phi o} \tag{2.149}$$

$$N_\phi = \frac{Eh}{1-\nu^2}\left[\varepsilon_\phi + \nu\varepsilon_\theta\right] + \frac{D}{R}\left[\frac{\nu}{R\sin\phi}\frac{\partial\gamma_{\theta z}}{\partial\theta} + \frac{\nu ctg\phi}{R}\gamma_{\phi z} + \frac{1}{R}\frac{\partial\gamma_{\phi z}}{\partial\phi}\right] + k_5 p_i + k_6 p_o + \nu k_7 p_{\phi i} + \nu k_8 p_{\phi o} \tag{2.150}$$

$$N_{\theta\phi} = \frac{Eh}{1-\nu^2}(1-\nu)\varepsilon_{\theta\phi} + \frac{D}{R}\left(\frac{1-\nu}{2}\right)\left[\frac{1}{R\sin\phi}\frac{\partial\gamma_{\phi z}}{\partial\theta} - \frac{ctg\phi}{R}\gamma_{\theta z} + \frac{1}{R}\frac{\partial\gamma_{\theta z}}{\partial\phi}\right] + \left(\frac{1-\nu}{2}\right)k_7 p_{\theta i} + \left(\frac{1-\nu}{2}\right)k_8 p_{\theta o} \tag{2.151}$$

2.4.6 Equilibrium Equations and Boundary Conditions

To derive the small deformation equilibrium equation, we consider the small shell element shown in Fig. 2.9. The externally applied forces per unit area are given by p_θ, p_ϕ, p_z in θ, ϕ, z directions, respectively (not shown in Fig. 2.9 for clarity).

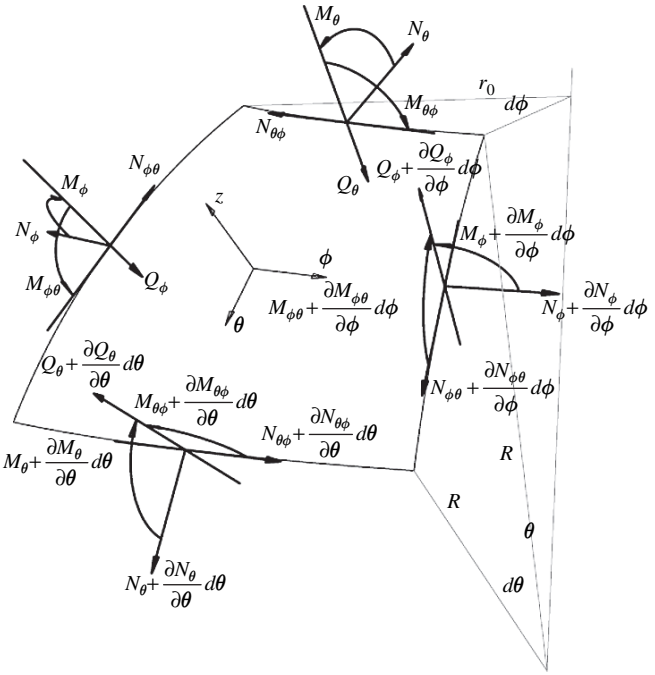

Fig. 2.9 Stress resultants on a shell element

The equilibrium requirements for forces in θ, ϕ, z directions and moments around θ, ϕ, z axes require that the following equations be satisfied:

$$\frac{\partial}{\partial\theta}\left(N_\theta \sin\theta\right) + \frac{\partial N_{\theta\phi}}{\partial\phi} - N_\phi \cos\theta + Q_\theta \sin\theta + p_\theta R \sin\theta = 0 \tag{2.152}$$

$$\frac{\partial}{\partial\theta}\left(N_{\phi\theta} \sin\theta\right) + \frac{\partial N_\phi}{\partial\phi} + N_{\theta\phi} \cos\theta + Q_\phi \sin\theta + p_\phi R \sin\theta = 0 \tag{2.153}$$

$$N_\phi \sin\theta + N_\theta \sin\theta - \frac{\partial Q_\phi}{\partial\phi} - \frac{\partial}{\partial\theta}\left(Q_\theta \sin\theta\right) - p_z R \sin\theta = 0 \tag{2.154}$$

$$\frac{\partial}{\partial\theta}\left(M_\theta \sin\theta\right) + \frac{\partial M_{\theta\phi}}{\partial\phi} - M_\phi \cos\theta + Q_\theta R \sin\theta = 0 \tag{2.155}$$

$$\frac{\partial}{\partial\theta}\left(M_{\phi\theta} \sin\theta\right) + \frac{\partial M_\phi}{\partial\phi} - M_{\theta\phi} \cos\theta - Q_\phi R \sin\theta = 0 \tag{2.156}$$

$$\frac{M_{\theta\phi}}{R} - \frac{M_{\theta\phi}}{R} = N_{\theta\phi} - N_{\phi\theta} \tag{2.157}$$

In the above expressions p_ϕ, p_θ, p_z are the equivalent distributed loads acting on the middle surface of the shell. Equation (2.157) is identically satisfied, reducing the number of equilibrium equations to five. The stress resultants and couples can be expressed in terms of either $\bar{u}$, $\bar{v}$, $\bar{w}$, γ_θ, γ_ϕ or $\bar{u}$, $\bar{v}$, $\bar{w}$, ϕ_θ, ϕ_ϕ. We therefore have five unknowns to solve from the conditions (2.152), (2.153), (2.154), (2.155), (2.156).

The static and kinematic boundary conditions can be expressed in terms of either $\bar{u}$, $\bar{v}$, $\bar{w}$, γ_θ, γ_ϕ or $\bar{u}$, $\bar{v}$, $\bar{w}$, ϕ_θ, ϕ_ϕ, together with the use of the constitutive (2.132), (2.133), (2.134), (2.135). The boundary conditions (BCs) are given as follows:

- if the edge $(0, \phi)$ is simply supported the BCs may be written as: $\bar{w}(0, \phi) = 0$; $\phi_\phi(0, \phi) = 0$; $M_\theta(0, \phi) = 0$
- if the edge $(0, \phi)$ is clamped the BCs may be written as: $\bar{w}(0, \phi) = 0$; $\phi_\phi(0, \phi) = 0$; $\phi_\theta = (0, \phi)$; $\bar{u}(0, \phi) = 0$
- if on the edge $(0, \phi)$ stretching of the mid-plane is prevented, BCs may be written as: $u_0(0, \phi) = 0$; $v_0(0, \phi) = 0$ and if additionally the pressures p_z are uniformly distributed, i.e. $\frac{\partial p_z}{\partial\theta} = \frac{\partial p_z}{\partial\phi} = 0$ then $\bar{u}(0, \phi) = 0$; $\bar{v}(0, \phi) = 0$
- if the edge $(0, \phi)$ is free to stretch in the θ direction, then: $v_0(0, \phi) = 0$; $N_\theta(0, \phi) = 0$
- if the edge $(0, \phi)$ is free the BCs may be written as follows: $M_\theta(0, \phi) = 0$; $Q_\theta(0, \phi) = 0$; $M_{\theta\phi}(0, \phi) = 0$; $N_\theta(0, \phi) = 0$; $N_{\theta\phi}(0, \phi) = 0$

2.4.7 The Non-Linear Nature of the Stress Distribution

The nonlinear distribution of the in-plane stresses through the thickness in our theory is due to the incorporation of the initial curvature of the shell and the three-dimensional constitutive equations obtained from relations (2.93), (2.94), (2.95).

This effect becomes highly pronounced in thick shells when the magnitude of the maximum stress is changed significantly compared to the linear stress variation theory.

In the expressions for in-plane stress components $\sigma_\theta, \sigma_\phi, \tau_{\theta\phi}$ given by (2.100), (2.100), (2.102), (2.102), (2.103), (2.104), nonlinear terms such as $1/(R+z)$ and z^2/R are incorporated. Consequently, the stresses given by our theory have a nonlinear distribution along the thickness of the shell. Let us consider the simple case of a constant normal pressure and investigate the corresponding stress distribution of σ_ϕ through the thickness. Here we have:

$$\begin{aligned}
\sigma_\phi = \frac{E}{1-\nu^2}\Bigg\{ & \frac{1}{R\sin\phi}\frac{\partial u_0}{\partial\theta} + \frac{\nu\cos\phi}{R\sin\phi}v_0 + \frac{1}{R}\frac{\partial v_0}{\partial\phi} + \\
& + \frac{z}{2Gh}\left[3 - \frac{4z^2}{h^2} - \frac{3z}{R}\left(1 - \frac{2z}{3R} - \frac{2z^2}{h^2}\right)\right] \\
& \left[\frac{\nu}{R\sin\phi}\frac{\partial Q_\theta}{\partial\theta} + \frac{\nu\cos\phi}{R\sin\phi}Q_\phi + \frac{1}{R}\frac{\partial Q_\phi}{\partial\phi}\right] \\
& + \Delta_2^2\left[-\frac{1}{R}\left(z - \frac{z^2}{R}\right)w_0 + \frac{2\nu}{Eh^3}\frac{1}{R}z^3\left(1 - \frac{3z}{2R}\right)M\right] \\
& + \frac{\nu p_{\phi i}\cos\phi}{Gc_1 R\sin\phi}\left[-z + \frac{z^2}{2R} + \frac{r_2^3}{R^3}\left(z - \frac{2z^2}{R}\right)\right] \\
& + \frac{\nu p_{\phi o}\cos\phi}{Gc_2 R\sin\phi}\left[-z + \frac{z^2}{2R} + \frac{r_1^3}{R^3}\left(z - \frac{2z^2}{R}\right)\right] \\
& + \frac{1+\nu}{R\left(1+\frac{z}{R}\right)}\left[w_0 + \frac{p_i}{Ec_1}\left[-z + \frac{r_2^3}{R^3}\left(z - \frac{3}{2}\frac{z^2}{R}\right)\right]\right. \\
& \left. + \frac{p_o}{Ec_2}\left[-z + \frac{r_1^3}{R^3}\left(z - \frac{3}{2}\frac{z^2}{R}\right)\right] - \nu\frac{6z^2}{Eh^3}M\right]\Bigg\} \\
& + \frac{\nu}{1+\nu}\left[\frac{p_i}{c_1}\left(\frac{r_2^3}{(R+z)^3} - 1\right) + \frac{p_o}{c_2}\left(\frac{r_1^3}{(R+z)^3} - 1\right)\right]
\end{aligned} \tag{2.158}$$

In equation (2.158) all the terms are nonlinear in z except for those associated with: $\dfrac{1}{R\sin\phi}\dfrac{\partial u_0}{\partial\theta}, \dfrac{\partial v_0}{\partial\phi}, \dfrac{\partial^2 w_0}{\partial\theta^2}$.

The stress distribution obtained using our theory will be compared with the elasticity theory.

2.4.8 The Equivalent Formulation for Thick Plates

It is relatively simple to reduce our theory to a thick plate theory. As R approaches infinity the stress resultants and stress couples reduce to:

$$N_x = \frac{Eh}{1-\nu^2}\left(\frac{\partial \bar{u}}{\partial x} + \nu\frac{\partial \bar{v}}{\partial y}\right) + k_1\,(p_i + p_o) \tag{2.159}$$

$$N_y = \frac{Eh}{1-\nu^2}\left(\frac{\partial \bar{v}}{\partial y} + \nu\frac{\partial \bar{u}}{\partial x}\right) + k_1\,(p_i + p_o) \tag{2.160}$$

$$N_x = N_y = Gh\left(\frac{\partial \bar{u}}{\partial y} + \frac{\partial \bar{v}}{\partial x}\right) \tag{2.161}$$

$$Q_x = T\left(\frac{\partial \bar{w}}{\partial x} - \phi_x\right) \tag{2.162}$$

$$Q_y = T\left(\frac{\partial \bar{w}}{\partial y} - \phi_y\right) \tag{2.163}$$

$$M_x = D\left(\frac{\partial \phi_x}{\partial x} + \nu\frac{\partial \phi_y}{\partial y}\right) + k_2\,(p_i + p_o) \tag{2.164}$$

$$M_y = D\left(\frac{\partial \phi_y}{\partial y} + \nu\frac{\partial \phi_x}{\partial x}\right) + k_2\,(p_i + p_o) \tag{2.165}$$

$$M_{xy} = M_{yx} = D\frac{1-\nu}{2}\left(\frac{\partial \phi_x}{\partial y} + \frac{\partial \phi_y}{\partial x}\right) \tag{2.166}$$

where:

$$k_1 = \frac{\nu h}{2\,(1-\nu)} \tag{2.167}$$

$$k_2 = -D\frac{6\nu\,(1+\nu)}{5Eh} \tag{2.168}$$

Note that our shell theory reduces to exactly the same equivalent thick plate theory as that of Voyiadjis and Shi (1991). The Voyiadjis and Shi theory (1991) can therefore be regarded as a the special case of our theory, as was indicated in Chap. 1.

2.5 Examples

We test the validity of these concepts through the following examples. The shell equations derived in this chapter are complicated, and obtaining analytical closed-form solutions can be tedious. This is because the formulation takes into account many important effects affecting the behavior of shells that are often neglected. Use of the finite element method based on the present shell equations would alleviate this difficulty. At this stage, however, the main objective is to verify our refined theory

of shells, not its finite element implementation. We therefore consider two problems: cylindrical and spherical tanks subjected to uniform pressures (Sects. 2.4.1 and 2.4.3) for which the analytical solutions can be obtained by means of rational simplifying assumptions and manual calculations. The problems of a hemispherical dome and an arch (Sects. 2.4.2 and 2.4.4), were solved with the aid of the numerical procedure, based on the constitutive equations formulated here. We compare the results of the analysis provided by our theory with those obtained from the theory of elasticity, as well as the classical theory of thin shells (Niordson, 1985).

2.5.1 Thick Sphere Subjected to Uniform Pressures

We investigate the stress distribution of σ_ϕ for a thick spherical container subjected to uniform pressures p_i, p_o as shown in Fig. 2.2 ($p_i = 5\,kPa,\ p_o = 4\,kPa$). In this case, we have:

$$v = Q_\phi = \frac{\partial M_\phi}{\partial \phi} = 0 \tag{2.169}$$

and

$$w = w(z) \tag{2.170}$$

The stress σ_ϕ using our theory is expressed in this case as follows:

$$\sigma_\phi = \frac{E}{R+z}\left\{w_0 + \frac{p_i}{Ec_1}\left[-z + \frac{r_2^3}{R^3}\left(z - \frac{3}{2}\frac{z^2}{R}\right)\right] + \frac{p_o}{Ec_2}\left[-z + \frac{r_1^3}{R^3}\left(z - \frac{3}{2}\frac{z^2}{R}\right)\right]\right\} \tag{2.171}$$

The corresponding exact elasticity solution for this problem is given by Lame (1852):

$$\sigma_\phi = -\frac{p_o}{2c_2}\left(2 + \frac{r_1^3}{(R+z)^3}\right) - \frac{p_i}{2c_1}\left(2 + \frac{r_2^3}{(R+z)^3}\right) \tag{2.172}$$

The distribution of σ_ϕ given by our theory is compared to the elasticity solution by Lame (1852) in Table 2.1:

Using the theory of elasticity, we have:

$$w_0 = \frac{R}{E}\sigma_\phi|_{z=0} \tag{2.173}$$

$$\sigma_\phi|_{z=0} = -\frac{p_o}{2c_2}\left(2 + \frac{r_1^3}{R^3}\right) - \frac{p_i}{2c_1}\left(2 + \frac{r_2^3}{R^3}\right) \tag{2.174}$$

Substituting for w_0 from (2.173) and (2.174) into (2.172), we obtain the following expression for σ_ϕ:

Table 2.1 σ_ϕ Distribution for spherical shell

r_1	$\mathbf{r_2}$	$\mathbf{r_2/r_1}$	$\mathbf{h = r_2 - r_1}$	$\mathbf{c_1}$	$\mathbf{c_2}$	Elasticity σ_ϕ [kPa]		Present theory σ_ϕ [kPa]	
						$\mathbf{r = r_1}$	$\mathbf{r = r_2}$	$\mathbf{R = r_1}$	$\mathbf{r = r_2}$
3	3.9	1.3	0.9	−1.2	−0.545	19.7782	15.2782	19.712	15.315
3	4.5	1.5	1.5	−2.4	−0.704	14.18421	9.68421	14.01	9.7539
3	5.1	1.7	2.1	−3.9	−0.796	11.95004	7.45004	11.633	7.5458
3	6	2	3	−7	−0.875	10.42857	5.92857	9.8571	6.0476
3	6.6	2.2	3.6	−9.6	−0.906	9.899254	5.39925	9.1463	5.5253

$$\sigma_\phi = \frac{R}{R+z}\left[-\frac{p_o}{2c_2}\left(2+\frac{r_1^3}{R^3}\right)-\frac{p_i}{2c_1}\left(2+\frac{r_2^3}{R^3}\right)\right] + \frac{1}{R+z}\left[\frac{p_i}{Ec_1}\left(-z+\frac{r_2^3}{R^3}\left(z-\frac{3}{2}\frac{z^2}{R}\right)\right)+\frac{p_o}{Ec_2}\left(-z+\frac{r_1^3}{R^3}\left(z-\frac{3}{2}\frac{z^2}{R}\right)\right)\right] \tag{2.175}$$

It can easily be shown that σ_ϕ obtained from (2.175) for the case of $z = 0$ is identical to σ_ϕ obtained from the elasticity solution expressed by (2.172), for the same case. As expected, in the case of a sphere, $\sigma_\phi = \sigma_\theta$.

Gupta and Khatua (1978), in their derivation of a thick shell superparametric finite element, proposed a modification in the expression for the circumferential stress σ_ϕ, given by:

$$\sigma_\phi = \frac{R}{R+z}\sigma_0 \tag{2.176}$$

where σ_0 is the average hoop stress. We note that Gupta and Khatua's scheme, however, cannot distinguish between the internal and external pressures.

As shown in Table 2.1, our theory is very close to the exact elasticity solution for thick spherical containers. To show the advantages of our theory our the classical, thin shell theory, we analyze the problem of a spherical container subject to a uniform internal pressure $p_i = 5kPa$. Figure 2.10 shows a comparison of the solution obtained with the classical theory by Niordson (1985), and that obtained with our theory.

As expected, the results deviate from the exact solution as the thickness of the shell increases (Fig. 2.11). There is a significant improvement, however, in the results obtained using our theory over those obtained with the classical theory, which yields large errors for thick shells.

A close investigation of the relative errors shows that the error in our result is much smaller than that in the results obtained using the classical thin shell theory (Fig. 2.11). The latter is built on the Kirchhoff–Love assumption, which, as shown by Niordson (1971), has a relative error on the order of $[h/R+(h/L)^2]$. We therefore expect the error of the classical theory to be very close to the expression given by Niordson: $[h/R + (h/L)^2]$. As shown in Fig. 2.11, the classical theory has an error equal approximately to the Niordson error. Our theory also shows some loss of

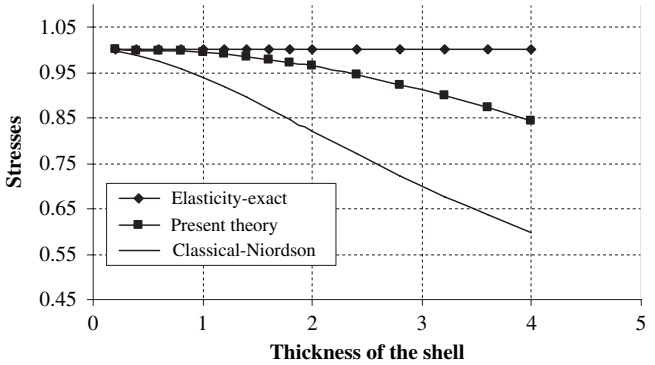

Fig. 2.10 Normalized σ_ϕ for spherical container subjected to internal pressure Voyiadjis and Woelke 2004

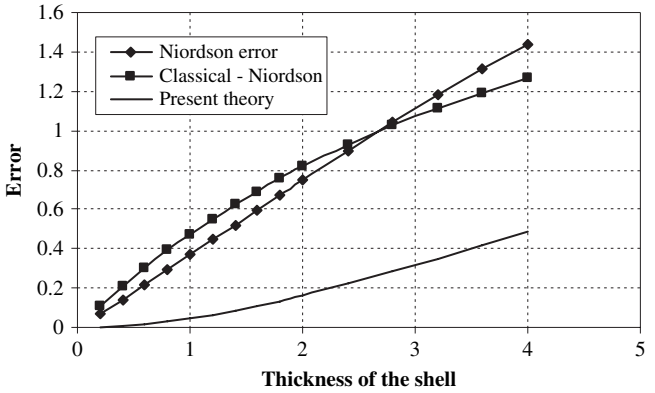

Fig. 2.11 Relative errors Voyiadjis and Woelke 2004

accuracy as the thickness of the shell increases. This loss, however, is significantly smaller than the Niordson error.

2.5.2 Thick Cylinder Subjected to Uniform Pressures

Our theory can be reduced to the case of cylindrical shells, as given by Voyiadjis and Shi (1991). Therefore, the Voyiadjis and Shi (1991) formulation may be regarded as a special case of our theory. To show this, we now investigate the stress distribution of σ_ϕ for a thick cylinder subjected to uniform pressures p_i and p_o. As in the previous example, we have:

$$v = Q_\phi = \frac{\partial M_\phi}{\partial \phi} = 0 \tag{2.177}$$

and

$$w = w(z) \tag{2.178}$$

To reduce our theory to the case of cylindrical shells, we need to adopt two distinct radii of curvatures $R_\theta = R_x$ and R_ϕ in the θ and ϕ directions, respectively. In cylindrical shells we have $R_\theta = R_x = \infty$, and therefore we may write:

$$R_\theta \sin\phi \partial\theta = \partial x \text{ and } \frac{u}{R_\theta} = \frac{v}{R_\theta} = \frac{w}{R_\theta} = 0 \tag{2.179}$$

Considering also Lame's solution for thick cylinders, we obtain the stress distribution for σ_ϕ as given by Voyiadjis and Shi for the case of cylindrical shells:

$$\sigma_\phi = \frac{E}{R+z}\left\{w_0 + \frac{p_i}{Ec_1}\left[-z + \frac{r_2^2}{R^2}\left(z - \frac{z^2}{R}\right)\right] + \frac{p_o}{Ec_2}\left[-z + \frac{r_1^2}{R^2}\left(z - \frac{z^2}{R}\right)\right]\right\} \tag{2.180}$$

The corresponding exact elasticity solution for this problem is given by:

$$\sigma_\phi = -\frac{p_o}{c_2}\left(1 + \frac{r_1^2}{(R+z)^2}\right) - \frac{p_i}{c_1}\left(1 + \frac{r_2^2}{(R+z)^2}\right) \tag{2.181}$$

Table 2.2 compares the results of the given problem obtained by various other theories with those obtained here. Our theory shows excellent agreement with the closed-form solution of the cylindrical shell problem provided by Lame (1852). This verifies the applicability of the our work not only to spherical shells but also to shells with different radii of curvature in two directions. Our theory may therefore be applied to shells of general shapes.

Table 2.2 σ_ϕ Distribution for the cylindrical shell

	Winkler's theory		Elasticity-exact		Present theory	
r_2/r_1	$r = r_1$	$r = r_2$	$r = r_2$	$r = r_2$	$r = r_2$	$r = r_2$
1.5	−26.971	20.607	−27.858	21.275	−27.971	20.029
2	−7.725	4.863	−7.755	4.917	−7.642	4.358
3	−2.285	1.095	−2.292	1.130	−2.105	0.925

2.6 Summary

The examples in this chapter show that the proposed equations are accurate and in good agreement with the exact solutions and with other theories. The classical theory of shells based on the Kirchhoff–Love assumption, yields errors that could become large in the case of thick shells. Our theory shows a significant reduction

in error. This is evident in the first example (Sect. 2.5.1). The results we present are accurate for very thick as well as very thin shells.

A limitation of our shell equations is use of the spherical strains in the derivation. This restrains their direct use from problems in which the radius of the shell is different in two distinct directions, e.g., cylinders. We showed, however, that the theory could be easily reduced to the cylindrical case with no substantial loss of accuracy. Furthermore, through the finite element method, the constitutive equations derived here may be used to model shells of arbitrary shape, as well as arches, beams, and plates. Thus, our theory is general and universal and gives excellent results for all of the above-discussed cases.

Although numerous shell theories are available in the published literature, it is difficult to find one that takes into account the transverse shears, initial curvature and radial stresses. Our objective is to present a computational model for the non-linear analysis of plates, and shells and a refined shell theory is necessary to achieve that objective. Instead of using an existing formulation as a base for the algorithm, we opted to develope a new and original theory of thick shells, which for certain applications is more accurate than other theories.

The motivation for including all of the effects considered in our shell equations is the higher demands imposed nowadays on the accuracy of structural analysis. Unfortunately, higher accuracy usually means increased complexity, which is the case here. Complicated equations are frequently solved with the aid of simplifying assumptions, which inherently lead to loss of accuracy. Application of the average displacements is an example of such an assumption. Nevertheless, it is useful to incorporate more and more phenomena observed physically and experimentally in modeling of materials and structures, as such an approach ultimately drives scientific developments and technology.

References

Ashwell, D.G. and Gallagher, R.H. (Eds) (1976). Finite Elements for Thin Shells and Curved Membranes. Wiley, New York.

Basar, Y., Ding, Y., Schultz, R. (1992). Shear-deformation models for the finite-rotation analysis of multilayered shell structures. Modeling of Shells with Non-linear behaviour, Euromech Colloquium 292, 2–4 Sept. 1992, Munich, Germany.

Basar, Y., Ding, Y., Schultz, R. (1993). Refined shear-deformation models for composite laminates with finite rotations. Int. J. Solids Struct., 30, 19, 2611–2638.

Bathe, K.J. (1982). Finite Element Procedures in Engineering Analysis. Prentice-Hall, Englewood Cliffs, NJ.

Bathe, K.J. and Brezzi, F. (1985). On the convergence of the four-node plate bending element based on Mindlin-Reissner plate theory and a mixed interpolation. Proceedings Conference on Mathematics of Finite Elements and Applications, Academic Press, New York.

Bathe, K.J. and Dvorkin, E.N. (1984). A continuum mechanics based four-node shell element for general non-linear analysis. Int. J. Comp. Aided Eng. Software, 1, 1, 77–88.

Dennis, S.T., Palazotto, A.N. (1989). Transverse shear deformation in orthotropic cylindrical pressure vessels using a higher-order shear theory. AIAA J., 27, 10, 1441–1447.

Dvorkin, E.N. and Bathe, K.J. (1984) A continuum mechanics based four-node shell element for general non-linear analysis. Eng. Computation. 1, 1, 77–88.

Flugge, W. (1960). Stresses in Shells, 2nd edition, Springer, Berlin.

Gupta, A.K. and Khatua, T.P. (1978). On thick superparametric shell element. Int. J. Numer. Meths Eng., 12, 1883–1889.
Hu, H-C. (1984). The Variational Principles in Elasticity and its Application. Scientific Publisher, Beijing.
Kirchhoff, G, (1850). Uber das Gleichgewicht und die Bewegung einer elastischen Scheibe. J. Reine Angew. Math., 40, 51–58.
Kratzig, W.B. (1992). 'Best' transverse shearing and stretching shell theory for nonlinear finite element simulations. Comp. Meth. Appl. Mech. Eng., 103, 135–160.
Kratzig, W.B., Jun, D. (2003). On 'best' shell models-from classical shells, degenerated and multi-layered concepts to 3D. Arch. Appl. Mech., 73, 1–25.
Lame, G. (1852). *Lecons sur la theorie mathematique d'elasticite des corps solides*, Bachelier, Paris, France., Reprint: 2006, ISBN: 2-87647-261-9.
Love, A.E.H., (1944). A Treatise on the Mathematical Theory of Elasticity. Dover (reprinted), New York.
Mindlin, R.D. (1951). Thickness-Shear and Flexural Vibrations of Crystal Plates. J. Appl. Phys., 22, 316–323.
Niordson, F.I. (1971). A note on the strain energy of elastic shells. Int. J. Solids Struct., 7, 1573–1579.
Niordson, F.I. (1978). A consistent refined shell theory. Complete Analysis and its Applications, Vekua Anniversary Volume, 421–429. Nauka, Moscow.
Niordson, F.I. (1985). Shell Theory. North-Holland, Amsterdam.
Noor, A.K. and Burton, W.S. (1989). Assessment of shear deformation theory for multilayered composite plates. Appl. Mech. Rev., 42(1), 1–13.
Palazotto, A.N. and Linnemann, P.E. (1991). Vibration and buckling characteristics of composite cylindrical panels incorporating the effects of a higher order shear theory. Int. J. Solids Struct., 28, 3, 341–361.
Reddy, J.N. (1984). A simple high-order theory for laminated composite plates. J. Appl. Mech., 51, 745–752.
Reddy, J.N. (1989). On refined computational models composite laminates. Int. J. Num. Meths. Eng. 27, 361–382.
Reissner, E. (1945). The effects of transverse shear deformation on the bending of elastic plates. J. Appl. Mech. ASME, 12, 66–77.
Reissner, E. (1975). On transverse bending of plates, including the effects of transverse shear deformation. Int. J. Solids Struct., 11, 569–576.
Sanders, J.L. (1959). An improved first approximation theory of thin shells. NASA Report 24.
Schenck, D.R. (1999). Some Formation Problems for Linear Elastic Materials. Doctoral Dissertation, Virginia Polytechnic Institute, Blacksburg, Virginia.
Ugural, A.C. (1999). Stresses in Plates and Shells. McGraw-Hill, Inc., New York.
Voyiadjis, G.Z. and Baluch, H.M. (1981). Refined theory for flexural motions of isotropic plates. J.Sound Vib., 76, 57–64.
Voyiadjis, G.Z., and Kattan, P.I.. (1986). Thick rectangular plates on an elastic foundation. J. Eng. Mech., ASCE, 112, 11, 1218–1240.
Voyiadjis, G.Z. and Kattan, P.I. (1991). Effect of transverse normal strain on the bending of thick circular plates on the elastic foundation subjected to surface loads. Int. J. Mech. Sci., 33, 6, 413–433.
Voyiadjis, G.Z. and Shi, G. (1991). Refined two-dimensional theory for thick cylindrical shells. Int. J. Solids Struct.. 27, 261–282.
Voyiadjis, G.Z. and Woelke, P. (2004). A refined theory for thick spherical shells. Int. J. Solids Struct. 41, 3747–3769.
Voyiadjis, G.Z. and Woelke, P. (2006). General non-linear finite element analysis of thick plates and shells. Int. J. Solids Struct., 43, 2209–2242.
Woelke, P., Chan, K.K., Daddazio, R. and Abboud, N. (2006) Stress resultant based elastoviscoplastic thick shell model. 77th Shock and Vibration Symposium Proceedings, Monterrey, CA.

Chapter 3
Shell Element Based on the Refined Theory of Thick Spherical Shells

3.1 Introduction

Formulation of a computational model for thick shells presents many problems, as briefly described in Sect. 1.3.2. In the following sections, we discuss the most important of these problems-shear and membrane locking and mesh instabilities along with the remedies we adopted to overcome them.

After the introducing the details of the finite element procedure, which lead, to the formulation of the stiffness matrix of the element, we verify the reliability of the numerical algorithm through a series of discriminating examples.

3.1.1 Shear Locking

Shear locking is a numerical deficiency experienced in thick shell finite elements that account for the transverse shear deformation. For conciseness, we examine the problem using a thick beam, as the phenomenon is the same. Consider a typical thick beam element with four degrees of freedom, as shown in Fig. 3.1.

This finite element algorithm is founded on the refined shell theory discussed in Chap. 2. The main assumption of the theory was that the plane sections remain plane after the deformation, but not perpendicular to the middle surface. The transverse shear strains are therefore not negligible, as they are with thin plates or shells. For a thick beam the shear strain γ_{xz} is given by the (3.1):

$$\gamma_{xz} = \frac{\partial w}{\partial x} - \phi_x \tag{3.1}$$

where ϕ_x is the angle of rotation of the section originally perpendicular to the middle surface and w is a vertical displacement (Fig. 1.3). The strain energy density of the thick beam element is:

$$U = U_b + U_s \tag{3.2}$$

G.Z. Voyiadjis, P. Woelke, *Elasto-Plastic and Damage Analysis of Plates and Shells*,

© Springer-Verlag Berlin Heidelberg 2008

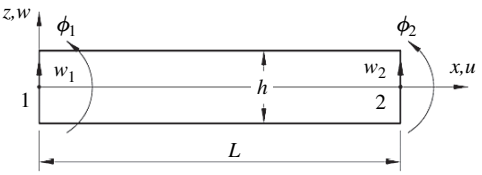

Fig. 3.1 Thick beam element

where U_b and U_s are bending and shear strain energy densities respectively, given by:

$$U_b = \frac{1}{2}\int_V \frac{{\sigma_x}^2}{E} dV = \frac{1}{2}\int_V E{\varepsilon_x}^2 dV = \frac{1}{2}\frac{Ebh^3}{12}\int_0^L \frac{d\phi_x}{dx} dx \tag{3.3}$$

$$U_s = \frac{1}{2}\int_V \frac{{\tau_{zx}}^2}{G} dV = \frac{1}{2}\int_V G{\gamma_{zx}}^2 dV = \frac{5}{2}\frac{Gbh}{6}\int_0^L \left(\frac{dw}{dx} - \phi_x\right)^2 dx \tag{3.4}$$

The constants E and G are the elastic and shear moduli, respectively; b is the width of the beam and h is the thickness. The term 5/6 in the shear strain energy expression is the "form factor", which accounts for the parabolic distribution of the shear stress τ_{zx} over a rectangular cross section (Cook et al., 1989). From the strain energy given by (3.3) and (3.4) we may obtain the stiffness matrix:

$$[\mathbf{k}] = [\mathbf{k}_b] + [\mathbf{k}_s] \tag{3.5}$$

where $[\mathbf{k}_b]$ resists bending strain ε_x and $[\mathbf{k}_s]$ resists shear strain γ_{xz}. For a given beam we can write:

$$([\mathbf{k}_b] + [\mathbf{k}_s])\{\mathbf{D}\} = \{\mathbf{R}\} \tag{3.6}$$

where $\{\mathbf{D}\}$ and $\{\mathbf{R}\}$ are the vectors of the nodal displacements and nodal external forces respectively. The displacements of the thin beam $\{\mathbf{D}\}$ should be governed only by $[\mathbf{k}_b]$ as, the transverse shear deformation γ_{xz} is negligible. In other words, if the shear rigidity $5Gbt/12$ becomes much larger than $Ebt^3/12$ in (3.5) and (3.6), then $[\mathbf{k}_s]$ should enforce the constraint $\gamma_{xz} = 0$. Instead, when the thickness of the beam decreases, $[\mathbf{k}_s]$ grows in relation to $[\mathbf{k}_b]$. Thus, $[\mathbf{k}_s]$ acts as a penalty matrix causing (3.6) to yield $\{\mathbf{D}\} = \{\mathbf{0}\}$, unless $[\mathbf{k}_s]$ is singular, (Cook et al., 1989). A singular $[\mathbf{k}_s]$ can be achieved through a variety of methods described in Sect. 1.3.2. The most popular method to overcome locking is selective reduced integration. This approach has been examined extensively by Zienkiewicz (1971), Stolarski and Belytschko (1981, 1982), Belytschko et al. (1984a,b,c) Hughes (1987), and many others. Determination of the components of the stiffness matrix, given in (3.6) usually involves numerical integration of the strain energy density expression given by (3.2). Numerical integration requires a certain number of sampling or Gauss integration points, at which the values of the integrated functions are determined. If the number of the sampling points is the same for all of the strain energy components, the integration is uniform; otherwise it is selective. The integration is also called full if there are

enough sampling points to ensure the exact integration of all stiffness coefficients. If the number of Gauss points is smaller than needed to perform the exact integration the scheme is called reduced integration. Through selective reduced integration, one can integrate a bending mode of the strain energy (which should be dominant for thin shells) with sufficient number of sampling points to ensure the exactness of the solution and underintegrate the shear mode of the strain energy causing $[\mathbf{k}_s]$ to become singular, which prevents shear locking. This method, although very effective, as reported by many authors, is mathematically inconsistent.

As discussed above, to overcome shear locking we use the quasi-conforming technique, along with the appropriate interpolation formulas of the displacement fields. We directly interpolate the strain fields rather than obtain them from the assumed displacements. The element strains can be expressed in terms of the element nodal displacement vector by explicit integration along the element boundaries. The strain energy terms are integrated analytically, and the stiffness matrix is computed by multiplication of the already integrated matrices. The numerical integration is not performed, effectively preventing the shear stiffness form "suppressing" the bending modes.

The mesh of the finite elements may also lock as a result of inadequate representation of the displacement field on the element boundaries. Widely used bilinear elements are characterized by the linear displacement functions. Although these elements are attractive because of their simplicity, they are too stiff in bending. Take, for example the rectangular, bilinear element subjected to bending moments as shown in Fig. 3.2.

The correct deformation, shown in Fig. 3.2c gives rise to storage of the energy caused by the normal strains only, while the bilinear element shown in Fig. 3.2b stores the energy caused by the normal strain ε_x and a spurious shear strain γ_{xz}. Thus, for the same deformation we have: $M_1 > M_2$. The unwanted shear strain that produces $M_1 > M_2$ is called "parasitic shear". This effect becomes decisive especially when the ratio of a/b is large. Here, we use Hu's (1981) cubic approximation formulas for the displacements avoiding the problem of parasitic shear. Moreover, the compatibility equations are enforced only in the weak sense, i.e., under the integral sign, which has the desirable effect of softening the structure of elements.

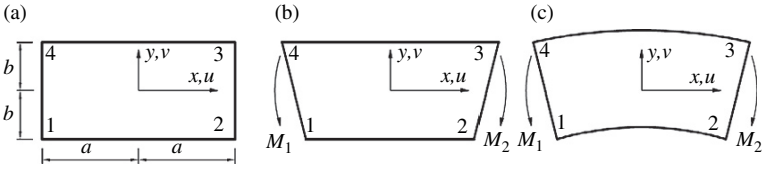

Fig. 3.2 **(a)** Rectangular bilinear element. **(b)** Deformed element-edges straight. **(c)** Correctly deformed element for pure bending

3.1.2 Membrane Locking

The term "membrane locking" refers to an excessive stiffness in bending of the curved elements; it is similar to shear locking. In the curved element in pure bending, the nodal displacements should be resisted only by the bending action. If an element suffers from membrane locking, the deformation is also resisted by the membrane action. Because the membrane stiffness is much greater than the bending stiffness in thin shells and arches, the desired bending mode is suppressed from the element response to load (Cook et al., 2002). For conciseness, we use the simple problem of a circular arch as an example of membrane locking in a curved element with a low-order displacement field (Fig. 3.3). This problem was presented by Cook et al. (2002).

The membrane strain ε_m and the curvature κ are given by:

$$\varepsilon_m = \frac{du}{ds} + \frac{w}{R} \text{ and } \kappa = \frac{1}{R}\frac{du}{ds} - \frac{d^2w}{ds^2} \tag{3.7}$$

where s is a tangential direction. The membrane strain ε_m is associated with the membrane force in the s direction. The curvature κ is associated with the bending moment. By analogy with the displacement fields used for a straight beam, we use the radial and axial displacement functions:

$$\begin{aligned} u &= a_1 + a_2 s \\ w &= a_3 + a_4 s + a_5 s^2 + a_6 s^3 \end{aligned} \tag{3.8}$$

where a_i are the generalized degrees of freedom. Substituting the above equations into (3.7) we have:

$$\begin{aligned} \varepsilon_m &= \left(a_2 + \frac{a_3}{R}\right) + \frac{a_4}{R}s + \frac{a_5}{R}s^2 + \frac{a_6}{R}s^3 \\ \kappa &= \frac{a_2}{R} - 2a_5 - 6a_6 s \end{aligned} \tag{3.9}$$

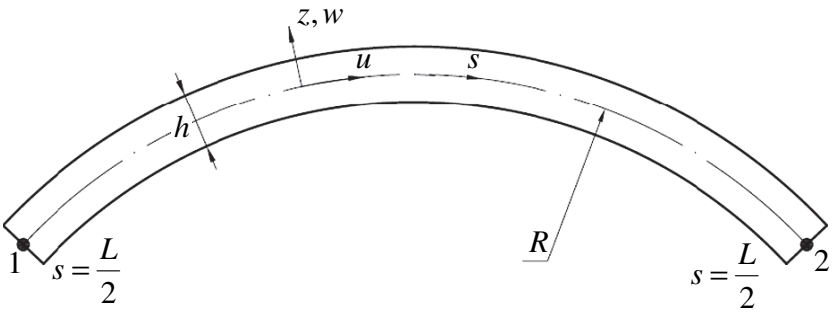

Fig. 3.3 Arch element

Under most loading conditions, a slender arch has little membrane strain, which implies the inextensibility condition:

$$\varepsilon_m = \frac{du}{ds} + \frac{w}{R} = 0 \tag{3.10}$$

For the infinitely slender arch, the above condition requires that:

$$\left(a_2 + \frac{a_3}{R}\right) = 0,\ a_4 = 0,\ a_5 = 0,\ a_6 = 0 \tag{3.11}$$

If the (3.11) are enforced, the only contribution to κ is from the membrane term, a_2. This is of course insufficient for the appropriate representation of the bending mode. If, however, equations (3.11) are not satisfied, the membrane strain ε_m is not zero. The nonzero membrane strain produces very large energy, leading to very large membrane stiffness. The bending modes are then suppressed and the bending deformation is "locked out", where the deformation should be governed by bending. The problem disappears when $R = \infty$.

As with shear locking, reduced selective integration is the most commonly used approach to overcoming membrane locking. The principle is the same as that discussed above. Here, the membrane modes must be underintegrated to enforce the inextensibility condition and free the formulation from membrane locking.

We use the linear interpolation functions for the membrane displacements and the third order polynomials given by Hu (1981), for the vertical displacement and angles of rotation. In the quasi-conforming technique, independently from the displacement approximations, the strains are assumed such that the compatibility equations are satisfied in a weak sense, i.e. under the integral sign. The appropriate choice of strain fields leads to satisfaction of the inextensibility condition. This method has reported to be a very effective way of overcoming the deficiency of membrane locking (Tang et al., 1980; Shi and Voyiadjis, 1991a; Lu and Liu, 1981). It is also mathematically more consistent than reduced selective integration, the integrations are performed analytically and exactly. The stiffness matrix in the quasi-conforming technique is given explicitly, making the algorithm computationally very efficient. We chose to use the quasi-conforming method to alleviate the numerical deficiencies discussed above and to deliver an explicit stiffness matrix.

3.1.3 Mesh Instabilities

Mesh instabilities in the shell finite elements arise from shortcomings in the element formulation process, such as inadequate integration scheme or inadequate approximation of strains or displacements. Here, an instability is not in no way related to buckling problems of structures (Cook et al., 2002). Various types of instabilities are often referred to as kinematic, hourglass, or zero energy modes. The zero energy

mode occurs when a nodal displacement vector {**D**} associated with straining of the element produces zero strain energy. A spurious energy mode is the reverse situation, i.e., when a non-zero energy mode is present, despite the element's moving as a rigid body, with no strains. These two modes, as well as the other types of mesh instabilities have been discussed in detail by Zienkiewicz (1978), Cook et al. (2002), and many others.

A computational procedure we present, relies again on the quasi-conforming technique and the direct interpolation of the strain fields to prevent spurious energy modes. The appropriate approximation of the strains results in a reliable algorithm free of common mesh instabilities.

3.2 Finite Element Formulation

3.2.1 Shell Constitutive Equations

In the previous chapter, we derived the refined shell theory of thick shells. The final set of constitutive equations defined in the spherical coordinates, is given by (2.133), (2.134), (2.135), (2.136), (2.137), (2.138), (2.139), (2.140), (2.141), (2.142), (2.143), (2.144), (2.145), (2.146). These expressions were given in terms of the average displacements: $\overline{u}, \overline{v}, \overline{w}, \phi_\theta, \phi_\phi$ given by (2.124), and (2.127), (2.128), (2.129), (2.130), (2.131), (2.132). To formulate a spherical shell finite element with the rectangular local coordinate system, it is necessary first to define the strains of the shell in the Cartesian coordinate system. We express the strains and curvatures in terms of the average displacements $\overline{u}, \overline{v}, \overline{w}, \phi_x, \phi_y$ as:

$$\varepsilon_x = \frac{\partial \overline{u}}{\partial x} + \frac{\overline{w}}{R} \tag{3.12}$$

$$\varepsilon_y = \frac{\partial \overline{v}}{\partial x} + \frac{\overline{w}}{R} \tag{3.13}$$

$$\varepsilon_{xy} = \frac{1}{2}\left(\frac{\partial \overline{u}}{\partial y} + \frac{\partial \overline{v}}{\partial x}\right) \tag{3.14}$$

$$\kappa_x = \frac{\partial \phi_x}{\partial x} = \frac{\partial}{\partial x}\left(\frac{\partial \overline{w}}{\partial x} - \gamma_{xz} - \frac{\overline{u}}{R}\right) \tag{3.15}$$

$$\kappa_y = \frac{\partial \phi_y}{\partial y} = \frac{\partial}{\partial y}\left(\frac{\partial \overline{w}}{\partial y} - \gamma_{yz} - \frac{\overline{v}}{R}\right) \tag{3.16}$$

$$\kappa_{xy} = \frac{1}{2}\left(\frac{\partial \phi_x}{\partial y} + \frac{\partial \phi_y}{\partial x}\right) \tag{3.17}$$

The stress resultants and couples can be now expressed in terms of the strains given above:

$$M_x = D\left[\kappa_x + \nu\kappa_y\right] \tag{3.18}$$

$$M_y = D\left[\kappa_y + \nu\kappa_x\right] \tag{3.19}$$

$$M_{xy} = D\,(1-\nu)\,\kappa_{xy} \tag{3.20}$$

$$N_x = S\left[\varepsilon_x + \nu\varepsilon_y\right] \tag{3.21}$$

$$N_y = S\left[\varepsilon_y + \nu\varepsilon_x\right] \tag{3.22}$$

$$N_{xy} = S\,(1-\nu)\,\varepsilon_{xy} \tag{3.23}$$

$$Q_x = T\gamma_{xz} \tag{3.24}$$

$$Q_y = T\gamma_{yz} \tag{3.25}$$

where:

$$D = \frac{Eh^3}{12\left(1-\nu^2\right)},\ S = \frac{Eh}{\left(1-\nu^2\right)},\ T = \frac{5}{12}\frac{Eh}{(1+\nu)} \tag{3.26}$$

In the expressions for membrane forces, given by (3.21), (3.22), (3.23), the variations of the transverse shear strains were neglected. The influence of the shear strains on the bending moments is significant in thick shells and plates, and therefore accounted for in the definition of the angles of rotations given by (3.15) and (3.16). The membrane forces derived in the previous chapter are functions of the membrane strains and of the variations of the shear strains. The effect of the latter is considered small and was therefore disregarded ((3.21), (3.22), (3.23)). We later confirmed that this approximation does not lead to substantial deterioration of the accuracy of our model. We use the above shell constitutive equations to formulate the coupled strain energy density and derive the stiffness matrix of the element.

3.2.2 Displacements and Boundary Conditions

We formulate a simple C^0 thick/thin shell element based on our refined spherical shell theory and quasi-conforming technique. It satisfies the Kirchhoff-Love hypothesis for the case of thin plates or shells.

The average displacements along a point on the middle surface and the average rotations of the normal given in Chap. 2, by (2.124) and (2.127), (2.128), (2.129), (2.130), (2.131), (2.132) are used instead of the usual middle surface displacement of the shell. In the case of thin shells, the average displacements are replaced by the middle surface displacement. In rectangular coordinates, we have:

$$\overline{u} = u_0 + \frac{1}{E}\frac{h^2}{24}\left[\frac{1}{c_1}\frac{\partial p_i}{\partial x}\left(1-\frac{{r_2}^3}{R^3}\right) + \frac{1}{c_2}\frac{\partial p_o}{\partial x}\left(1-\frac{{r_1}^3}{R^3}\right)\right] \tag{3.27}$$

$$\overline{v} = v_0 + \frac{1}{E}\frac{h^2}{24}\left[\frac{1}{c_1}\frac{\partial p_i}{\partial y}\left(1 - \frac{{r_2}^3}{R^3}\right) + \frac{1}{c_2}\frac{\partial p_o}{\partial y}\left(1 - \frac{{r_1}^3}{R^3}\right)\right] \tag{3.28}$$

$$\overline{w} = w_0 - M\left(\frac{3\nu}{10Eh} - \frac{9\nu h}{112ER^2}\right) - \frac{1}{10}\frac{h^2}{REc_1}\frac{{r_2}^3}{R^3}p_i - \frac{1}{10}\frac{h^2}{REc_2}\frac{{r_1}^3}{R^3}p_o \tag{3.29}$$

$$\phi_x = \frac{\partial \overline{w}}{\partial x} - \gamma_{xz} - \frac{\overline{u}}{R} \tag{3.30}$$

$$\phi_y = \frac{\partial \overline{w}}{\partial y} - \gamma_{yz} - \frac{\overline{v}}{R} \tag{3.31}$$

The static and kinematic boundary conditions, expressed in terms of $\overline{u}, \overline{v}, \overline{w}, \phi_x, \phi_y$, together with the use of the constitutive (3.18), (3.19), (3.20), (3.21), (3.22), (3.23), (3.24), (3.25) are similar to those given in Sect. 2.4.6. Boundary conditions (BC) are:

- if the edge $(0, y)$ is simply supported the BCs are given as:

$$\overline{w}(0, y) = 0;\ \phi_y(0, y) = 0;\ M_x(0, y) = 0$$

- if the edge $(0, y)$ is clamped the BCs are given as:

$$\overline{w}(0, y) = 0;\ \phi_y(0, y) = 0;\ \phi_x = (0, y);\ \overline{u}(0, y) = 0$$

- if on the edge $(0, y)$ stretching of the mid-plane is prevented, BCs are given as: $u_0(0, y) = 0;\ v_0(0, y) = 0$ and if additionally the pressures p_z are uniformly distributed, i.e. $\partial p_z/\partial x = \partial p_z/\partial y = 0$ then $\overline{u}(0, y) = 0;\ \overline{v}(0, y) = 0$
- if the edge $(0, y)$ is free to stretch in the x direction, then: $v_0(0, y) = 0; N_x(0, y) = 0$
- if the edge $(0, y)$ is free the BCs are given as:

$$M_x(0, y) = 0;\ Q_x(0, y) = 0;\ M_{xy}(0, y) = 0;\ N_x(0, y) = 0;\ N_{xy}(0, y) = 0$$

For simplicity and conciseness, we denote the average displacements $\overline{u}, \overline{v}, \overline{w}, \phi_x, \phi_y$ as u, v, w, ϕ_x, ϕ_y. We therefore have the quadrilateral, doubly curved finite element with five degrees of freedom per node: u, v, w, ϕ_x, ϕ_y and twenty degrees of freedom per element. The vector of the nodal displacements is:

$$\mathbf{q} = \left\{u_1, v_1, w_1, \phi_{x1}, \phi_{y1}, u_2, v_2, w_2, \phi_{x2}, \phi_{y2}, u_3, v_3, w_3, \phi_{x3}, \phi_{y3}, u_4, v_4, w_4, \phi_{x4}, \phi_{y4}\right\}^T \tag{3.32}$$

3.2.3 Element Displacement and Strain Fields – Quasi-Conforming Method

The finite element we present is a four-node quadrilateral, doubly curved element. The radius of curvature R is constant in both directions. We assume continuity of the displacement fields but not their derivatives. We therefore have a C^0 continuity problem with twenty degrees of freedom in each element. The quasi-conforming technique proposed by Tang et al. (1980, 1983) is used to compute the element stiffness matrix. In this case, the strain field is interpolated directly, rather than evaluated from the displacement field through differentiation. The functions describing the surface are defined only on the interelement boundaries, leaving the functions inside the elements undefined explicitly. This method is related to the so-called "generalized hybrid model", which can also be derived using Hu-Washizu principle (Tang et al., 1983, Hu, 1981, Shi and Voyiadjis (1990)). The quasi-conforming element technique gives an explicit form of the stiffness matrix, as integrations are carried out directly.

As stated above our objective is to develop an element applicable to both thick and thin shells. The challenge lies partly in determining how to assume the displacement distribution on the element boundary. Many authors adopt simple and convenient linear interpolation formulas on the boundary of the element. The results of such approximations may suffice when the shear rigidity is not very large. When the shear rigidity approaches infinity, however, the linear displacement interpolation leads to a contradiction with the Kirchhoff–Love assumption, which states that the shear deformation must vanish when the shell is thin. Thus, the linear displacement interpolations are unsuitable when the shear rigidity is very large (Hu, 1981). We discuss this shortcoming in Sect. 3.1.1. To formulate a reliable and universal model for both thick and thin shells, we need the three-generalized-displacement theory, on which the element is based, to degenerate to the classical theory satisfying the Kirchhoff–Love assumption for the case of thin shells. As the shear forces Q_x, Q_y are generally finite, the shear deformations γ_{xz} and γ_{yz} must vanish when the shear rigidity T approaches infinity (see (3.24), (3.25), (3.26)). This can be achieved through the interpolation functions within the element ensuring that w, ϕ_x, ϕ_y are in general three independent functions, but also ϕ_x, ϕ_y also depend on w according to the classical theory (Hu, 1981). Hu points out that such interpolation formulas must contain the ratio of the flexural and shear rigidities. We use the approximation of the displacement w and tangent rotation ϕ_s for the straight beam of length l given by Hu:

$$w = \frac{1}{2}\left[1 - \xi + \frac{\lambda}{2}\left(\xi^3 - \xi\right)\right] w_i + \frac{1}{4}\left[1 - \xi^2 + \lambda\left(\xi^3 - \xi\right)\right]\frac{l}{2}\phi_i$$
$$+\frac{1}{2}\left[1 + \xi - \frac{\lambda}{2}\left(\xi^3 - \xi\right)\right] w_j + \frac{1}{4}\left[-1 + \xi^2 + \lambda\left(\xi^3 - \xi\right)\right]\frac{l}{2}\phi_j \quad (3.33)$$

$$\phi_s = -\frac{3}{2l}\lambda\left[1-\xi^2\right]w_i + \frac{1}{4}\left[2-2\xi-3\lambda\left(1-\xi^2\right)\right]\phi_i$$
$$+\frac{3}{2l}\lambda\left[1-\xi^2\right]w_j + \frac{1}{4}\left[2+2\xi-3\lambda\left(1-\xi^2\right)\right]\phi_j \tag{3.34}$$

A subscript s in (3.34) refers to the tangent direction at the edge of the element, as shown in Fig. 3.4.

The linear approximation of the normal rotation is adopted here, similarly to Shi and Voyiadjis (1991b), (see Fig. 3.4):

$$\phi_n = \frac{1}{2}\left[1-\xi\right]\phi_{ni} + \frac{1}{2}\left[1+\xi\right]\phi_{nj} \tag{3.35}$$

where:

$$\xi = \frac{2x}{l} \quad -1 \le \xi \le 1 \tag{3.36}$$

The parameter λ in (3.33), (3.34) is given by:

$$\lambda = \frac{1}{\left(1+12\dfrac{D}{TL^2}\right)} \tag{3.37}$$

where D and T denote the flexural and shear rigidities of the shell, respectively. In (3.37) the parameter D/Tl^2 accounts for the shear deformation effect. When the shear rigidity is very large and $(h/l)^2 \to 0$, $\lambda \to 1$, w in (3.33) reduces to a Hermite function. When the shear rigidity is very small $\lambda = 0$, then (3.33) reduces to Cook's (1972) interpolation formula. The interpolation formulas given by (3.33), (3.34) are therefore suitable for both the classical theory of shells and the thick shell theory based on which the present element is formulated. For a two-dimensional

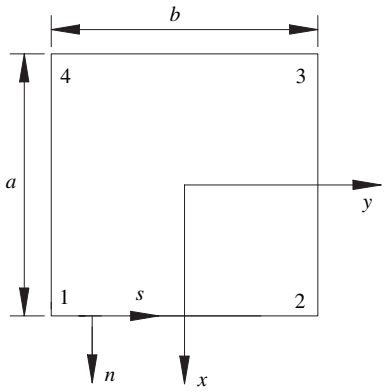

Fig. 3.4 Shell element on a plane, n-normal and s-tangential directions

problem we let L_x be the effective length in the x direction and L_y the corresponding effective length in the y direction. The two-dimensional expressions equivalent to (3.37) are (Woelke and Voyiadjis, 2006):

$$\lambda_x = \frac{1}{\left(1 + 12\dfrac{D}{T{L_x}^2}\right)} \text{ and } \lambda_y = \frac{1}{\left(1 + 12\dfrac{D}{T{L_y}^2}\right)} \tag{3.38}$$

Following the argument in Sect. 3.1.2, the linear approximations for the membrane displacements u, v are:

$$u = \frac{1}{4}[1 - \xi]\, u_i + \frac{1}{4}[1 + \xi]\, u_j \tag{3.39}$$

$$v = \frac{1}{4}[1 - \xi]\, v_i + \frac{1}{4}[1 + \xi]\, v_j \tag{3.40}$$

where ξ is given by (3.36).

The method we use in the linear elastic analysis of shells called is the "quasi-conforming technique" (Tang et al., 1983) because the compatibility equations are satisfied in a weak sense, i.e., under the integral sign and the displacement and, the strain fields are approximated independently. To determine the element strain fields using the quasi-conforming technique, we discretize the strains in the element as:

$$\boldsymbol{\varepsilon_b}^{\mathbf{T}} = \left\{ \frac{\partial \phi_x}{\partial x} \quad \frac{\partial \phi_y}{\partial y} \quad \frac{\partial \phi_x}{\partial y} + \frac{\partial \phi_y}{\partial x} \right\} \tag{3.41}$$

$$\boldsymbol{\varepsilon_m}^{\mathbf{T}} = \left\{ \frac{\partial u}{\partial x} + \frac{w}{R} \quad \frac{\partial v}{\partial y} + \frac{w}{R} \quad \frac{\partial u}{\partial y} + \frac{\partial v}{\partial x} \right\} \tag{3.42}$$

$$\boldsymbol{\varepsilon_s}^{\mathbf{T}} = \left\{ \frac{\partial w}{\partial x} - \phi_x - \frac{u}{R} \quad \frac{\partial w}{\partial y} - \phi_y - \frac{v}{R} \right\} \tag{3.43}$$

The derivatives may also be expressed by Taylor's expansion or approximately by a polynomial with n truncated terms:

$$\frac{\partial \phi_x}{\partial x} = \alpha_0 + \alpha_1 x + \alpha_2 y + \ldots = \sum_{i}^{n=1} P_i \alpha_i \tag{3.44}$$

We follow the same procedure for the remaining element strain fields. According to the given nodal variables, the compatibility equations, and the requirement for the proper rank of the element stiffness matrix (Liu et al., 1984), the strain fields are interpolated as:

- Linear bending strain field:

$$\boldsymbol{\varepsilon}_{\mathbf{b}} = \begin{Bmatrix} \dfrac{\partial \phi_x}{\partial x} \\ \dfrac{\partial \phi_y}{\partial y} \\ \dfrac{\partial \phi_x}{\partial y} + \dfrac{\partial \phi_y}{\partial x} \end{Bmatrix} = \begin{bmatrix} 1 & x & y & xy & 0 & 0 & 0 & 0 & 0 & 0 & 0 \\ 0 & 0 & 0 & 0 & 1 & x & y & xy & 0 & 0 & 0 \\ 0 & 0 & 0 & 0 & 0 & 0 & 0 & 0 & 1 & x & y \end{bmatrix} \begin{Bmatrix} \alpha_1 \\ \alpha_2 \\ \alpha_3 \\ \alpha_{10} \\ \alpha_{11} \end{Bmatrix} = \mathbf{P}_{\mathbf{b}} \boldsymbol{\alpha}_{\mathbf{b}} \quad (3.45)$$

- Stretch strain field:

$$\boldsymbol{\varepsilon}_{\mathbf{m}} = \begin{Bmatrix} \dfrac{\partial u}{\partial x} + \dfrac{w}{R} \\ \dfrac{\partial v}{\partial y} + \dfrac{w}{R} \\ \dfrac{\partial u}{\partial y} + \dfrac{\partial v}{\partial x} \end{Bmatrix} = \begin{bmatrix} 1 & y & 0 & 0 & 0 \\ 0 & 0 & 1 & x & 0 \\ 0 & 0 & 0 & 0 & 1 \end{bmatrix} \begin{Bmatrix} \alpha_{12} \\ \alpha_{13} \\ \alpha_{14} \\ \alpha_{15} \\ \alpha_{16} \end{Bmatrix} = \mathbf{P}_{\mathbf{m}} \boldsymbol{\alpha}_{\mathbf{m}} \quad (3.46)$$

- Constant transverse shear strain:

$$\boldsymbol{\varepsilon}_{\mathbf{s}} = \begin{Bmatrix} \dfrac{\partial w}{\partial x} - \phi_x - \dfrac{u}{R} \\ \dfrac{\partial w}{\partial y} - \phi_y - \dfrac{v}{R} \end{Bmatrix} = \begin{bmatrix} 1 & 0 \\ 0 & 1 \end{bmatrix} \begin{Bmatrix} \alpha_{17} \\ \alpha_{18} \end{Bmatrix} = \mathbf{P}_{\mathbf{s}} \boldsymbol{\alpha}_{\mathbf{s}} \quad (3.47)$$

where $\alpha_1, \alpha_2, \ldots, \alpha_{18}$, are the undetermined strain parameters.

The compatibility equations of the displacement field are not enforced *a priori* in the above strain interpolations.

Let $\mathbf{P}$ be the trial function for the assumed strain field ((3.45)–(3.47)):

$$\boldsymbol{\varepsilon} = \mathbf{P}\boldsymbol{\alpha} \quad (3.48)$$

and $\mathbf{N}$-the corresponding test function. We multiply both sides by the test function and integrate over the element domain:

$$\iint_{\Omega} \mathbf{N}^{\mathbf{T}} \boldsymbol{\varepsilon} d\Omega = \boldsymbol{\alpha} \iint_{\Omega} \mathbf{N}^{\mathbf{T}} \mathbf{P} d\Omega \quad (3.49)$$

The strain parameter $\boldsymbol{\alpha}$ is determined from the quasi-conforming technique as follows:

$$\boldsymbol{\alpha} = \mathbf{A}^{-1}\mathbf{C}\mathbf{q} \quad (3.50)$$

where $\mathbf{q}$ is the element nodal displacement vector given by (3.32), and:

$$\mathbf{A} = \iint_{\Omega} \mathbf{N}^{\mathbf{T}} \mathbf{P} d\Omega \tag{3.51}$$

$$\mathbf{Cq} = \iint_{\Omega} \mathbf{N}^{\mathbf{T}} \boldsymbol{\varepsilon} d\Omega \tag{3.52}$$

We may now express the strain field in terms of the nodal displacements as follows:

$$\boldsymbol{\varepsilon} = \mathbf{P}\boldsymbol{\alpha} = \mathbf{PA}^{-1}\mathbf{Cq} = \mathbf{Bq} \tag{3.53}$$

In most cases, including the present one, it is convenient to use $\mathbf{P} = \mathbf{N}$ to obtain a symmetric stiffness matrix. Both matrices $\mathbf{A}$ and $\mathbf{C}$ can easily be evaluated explicitly. To briefly illustrate this take, the transverse shear strain $\boldsymbol{\varepsilon}_{\mathbf{s}}$ as an example. Substituting $\mathbf{P}_{\mathbf{s}}$ from (3.47) into (3.51) and (3.52), setting $\mathbf{N} = \mathbf{P}$, and using Green's theorem, we now obtain:

$$\mathbf{A}_{\mathbf{s}} = \begin{bmatrix} 1 & 0 \\ 0 & 1 \end{bmatrix} \iint_{\Omega} d\Omega = \Omega \begin{bmatrix} 1 & 0 \\ 0 & 1 \end{bmatrix} \tag{3.54}$$

and:

$$\mathbf{C}_{\mathbf{s}}\mathbf{q} = \iint_{\Omega} \begin{Bmatrix} \dfrac{\partial w}{\partial x} - \phi_x - \dfrac{u}{R} \\ \dfrac{\partial w}{\partial y} - \phi_y - \dfrac{v}{R} \end{Bmatrix} d\Omega = \oint \begin{Bmatrix} w n_x ds \\ w n_y ds \end{Bmatrix} - \iint_{\Omega} \begin{Bmatrix} \phi_x - \frac{u}{R} \\ \phi_y - \frac{v}{R} \end{Bmatrix} d\Omega \tag{3.55}$$

where Ω is the element area, n_x, n_y are the direction cosines along the element boundaries, and ds is the differential arc-length along the element boundaries. To evaluate $\mathbf{C}_{\mathbf{s}}, \mathbf{A}_{\mathbf{s}}$, we use the displacement interpolations given by (3.33), (3.34) and (3.39), (3.40) respectively. Solving (3.55) and determining of $\mathbf{C}_{\mathbf{b}}, \mathbf{C}_{\mathbf{m}}$, however require that the interpolation functions for rotations ϕ_x, ϕ_y and membrane displacements u, v be two-dimensional. To evaluate the integrals, we can use the approximate methods given by Hu (1981) and Shi and Voyiadjis (1991b), which allow direct use of the displacement approximations given by (3.33), (3.34), and (3.39), (3.40). Alternatively, the two-dimensional interpolation formulas for all the necessary displacements can be constructed, such that they reduce to the one-dimensional cases of the string net functions. The two-dimensional rotation function that reduces to the string functions obtained by (3.34), (3.35) is given by:

$$\begin{aligned} \phi_x(\xi, \eta) = {} & \frac{3}{4a}\lambda_x \left[\left(1-\xi^2\right)(1-\eta)\right] w_1 + \frac{3}{4a}\lambda_x \left[\left(1-\xi^2\right)(1+\eta)\right] w_2 \\ & - \frac{3}{4a}\lambda_x \left[\left(1-\xi^2\right)(1+\eta)\right] w_3 - \frac{3}{4a}\lambda_x \left[\left(1-\xi^2\right)(1-\eta)\right] w_4 \end{aligned}$$

$$+\frac{1}{8}\left[2+2\xi-3\lambda_x\left(1-\xi^2\right)\right](1-\eta)\,\phi_{x1}+\frac{1}{8}\left[2+2\xi-3\lambda_x\left(1-\xi^2\right)\right](1+\eta)\,\phi_{x2}$$
$$+\frac{1}{8}\left[2-2\xi-3\lambda_x\left(1-\xi^2\right)\right](1+\eta)\,\phi_{x3}+\frac{1}{8}\left[2-2\xi-3\lambda_x\left(1-\xi^2\right)\right](1-\eta)\,\phi_{x4} \tag{3.56}$$

where:

$$\xi=\frac{2x}{a},\ \eta=\frac{2y}{b}\quad -1\le\xi,\eta\le 1 \tag{3.57}$$

In the same way we can construct the rotation interpolation $\phi_y(\xi,\eta)$, as well as all the other two-dimensional displacement functions, namely $w(\xi,\eta)$, $u(\xi,\eta)$ and $v(\xi,\eta)$. A complete set of the expressions, by means of which the matrices $\mathbf{A}$ and $\mathbf{C}$ can be evaluated appears in the Appendix.

Having determined the components of the strain displacement matrices $\mathbf{B_m}$, $\mathbf{B_b}$, $\mathbf{B_s}$, the strain fields can now be written in a form similar to (3.53):

$$\boldsymbol{\varepsilon}_\mathbf{b}=\mathbf{P_b}\mathbf{A_b}^{-1}\mathbf{C_b}\mathbf{q}=\mathbf{B_b}\mathbf{q} \tag{3.58}$$

$$\boldsymbol{\varepsilon}_\mathbf{m}=\mathbf{P_m}\mathbf{A_m}^{-1}\mathbf{C_m}\mathbf{q}=\mathbf{B_m}\mathbf{q} \tag{3.59}$$

$$\boldsymbol{\varepsilon}_\mathbf{s}=\frac{1}{\Omega}\mathbf{C_b}\mathbf{q}=\mathbf{B_s}\mathbf{q} \tag{3.60}$$

3.2.4 Strain Energy and Stiffness Matrix

To determine the stiffness matrix of the element, we use the strain energy density, expressed as:

$$U=\frac{1}{2}\left(M_x\kappa_x+M_y\kappa_y+2M_{xy}\kappa_{xy}+N_x\varepsilon_x+N_y\varepsilon_y+2N_{xy}\varepsilon_{xy}+Q_x\gamma_{xz}+Q_y\gamma_{yz}\right) \tag{3.61}$$

Substituting (3.12), (3.13), (3.14), (3.15), (3.16), (3.17), (3.18), (3.19), (3.20), (3.21), (3.22), (3.23), (3.24), (3.25) into the above expression we obtain the following:

$$U=U_b+U_m+U_s \tag{3.62}$$

where U_b, U_m, U_s are respectively: the bending component of the strain energy density function (quadratic function of curvatures), the membrane component (quadratic function of membrane strains) and the transverse shear component of the strain energy. We now define the following groups of strains, namely the bending, membrane and shear strains separately in the form of vectors:

$$\boldsymbol{\varepsilon_b} = \left\{\kappa_x, \kappa_y, 2\kappa_{xy}\right\}^T \tag{3.63}$$

$$\boldsymbol{\varepsilon_m} = \left\{\varepsilon_x, \varepsilon_y, 2\varepsilon_{xy}\right\}^T \tag{3.64}$$

and

$$\boldsymbol{\varepsilon_s} = \left\{\gamma_{xz}, \gamma_{yz}\right\}^T \tag{3.65}$$

We then write the strain energy densities U_b, U_m, U_s, U_{bm} in matrix form as:

$$U_b = \frac{1}{2}\boldsymbol{\varepsilon_b}^{\mathbf{T}} D \begin{bmatrix} 1 & \nu & 0 \\ \nu & 1 & 0 \\ 0 & 0 & 1-\nu/2 \end{bmatrix} \boldsymbol{\varepsilon_b} = \frac{1}{2}\boldsymbol{\varepsilon_b}^{\mathbf{T}}\mathbf{D}\boldsymbol{\varepsilon_b} \tag{3.66}$$

$$U_m = \frac{1}{2}\boldsymbol{\varepsilon_m}^{\mathbf{T}} S \begin{bmatrix} 1 & \nu & 0 \\ \nu & 1 & 0 \\ 0 & 0 & 1-\nu/2 \end{bmatrix} \boldsymbol{\varepsilon_m} = \frac{1}{2}\boldsymbol{\varepsilon_m}^{\mathbf{T}}\mathbf{S}\boldsymbol{\varepsilon_m} \tag{3.67}$$

$$U_s = \frac{1}{2}\boldsymbol{\varepsilon_s}^{\mathbf{T}} T \begin{bmatrix} 1 & 0 \\ 0 & 1 \end{bmatrix} \boldsymbol{\varepsilon_s} = \frac{1}{2}\boldsymbol{\varepsilon_s}^{\mathbf{T}}\mathbf{T}\boldsymbol{\varepsilon_s} \tag{3.68}$$

The total strain energy in the element domain Ω can be written as:

$$\Pi_e = \iint_{\Omega} U d\Omega s \tag{3.69}$$

or using (3.66), (3.67), (3.68) as follows:

$$\Pi_e = \frac{1}{2}\iint_{\Omega} \left(\boldsymbol{\varepsilon_b}^{\mathbf{T}}\mathbf{D}\boldsymbol{\varepsilon_b} + \boldsymbol{\varepsilon_m}^{\mathbf{T}}\mathbf{S}\boldsymbol{\varepsilon_m} + \boldsymbol{\varepsilon_s}^{\mathbf{T}}\mathbf{T}\boldsymbol{\varepsilon_s}\right) d\Omega \tag{3.70}$$

We express the strains $\boldsymbol{\varepsilon_b}, \boldsymbol{\varepsilon_m}, \boldsymbol{\varepsilon_s}$ in terms of the nodal displacement vector $\mathbf{q}$ as:

$$\boldsymbol{\varepsilon_b} = \mathbf{B_b}\mathbf{q} \tag{3.71}$$

$$\boldsymbol{\varepsilon_m} = \mathbf{B_m}\mathbf{q} \tag{3.72}$$

$$\boldsymbol{\varepsilon_s} = \mathbf{B_s}\mathbf{q} \tag{3.73}$$

where $\mathbf{q}$ is given by (3.32). Substituting expressions (3.71), (3.72), (3.73) into (3.70) we obtain:

$$\Pi_e = \frac{1}{2}\mathbf{q}^{\mathbf{T}}\iint_{\Omega} \left(\mathbf{B_b}^{\mathbf{T}}\mathbf{D}\mathbf{B_b} + \mathbf{B_m}^{\mathbf{T}}\mathbf{S}\mathbf{B_m} + \mathbf{B_s}^{\mathbf{T}}\mathbf{T}\mathbf{B}_s\right) d\Omega\mathbf{q} \tag{3.74}$$

or:

$$\Pi_e = \frac{1}{2}\mathbf{q}^{\mathbf{T}}\left[\mathbf{K_b} + \mathbf{K_m} + \mathbf{K_s}\right]\mathbf{q} \tag{3.75}$$

where $\mathbf{K_b}$, $\mathbf{K_m}$, $\mathbf{K_s}$ are the element stiffness matrices related to bending, membrane and transverse shear deformation, given by:

$$\mathbf{K_b} = \iint_{\Omega} \mathbf{B_b}^{\mathbf{T}}\mathbf{D}\mathbf{B}_b d\Omega \tag{3.76}$$

$$\mathbf{K_m} = \iint_{\Omega} \mathbf{B_m}^{\mathbf{T}}\mathbf{S}\mathbf{B_m} d\Omega \tag{3.77}$$

$$\mathbf{K_s} = \iint_{\Omega} \mathbf{B_s}^{\mathbf{T}}\mathbf{T}\mathbf{B}_s d\Omega \tag{3.78}$$

Substituting (3.58), (3.59), (3.60) into (3.76), (3.77), (3.78) we obtain:

$$\mathbf{K_b} = \mathbf{C_b}^{\mathbf{T}}\mathbf{A_b}^{-\mathbf{T}} \iint_{\Omega} \mathbf{P_b}^{\mathbf{T}}\mathbf{D}\mathbf{P_b} d\Omega \mathbf{A_b}^{-\mathbf{1}}\mathbf{C_b} \tag{3.79}$$

$$\mathbf{K_m} = \mathbf{C_m}^{\mathbf{T}}\mathbf{A_m}^{-\mathbf{T}} \iint_{\Omega} \mathbf{P_m}^{\mathbf{T}}\mathbf{S}\mathbf{P_m} d\Omega \mathbf{A_m}^{-\mathbf{1}}\mathbf{C_m} \tag{3.80}$$

$$\mathbf{K_s} = \mathbf{C_s}^{\mathbf{T}}\left(\frac{\mathbf{T}}{\Omega}\right)\mathbf{C_s} \tag{3.81}$$

Analysis of a problem by means of the finite elements formulated here involves solution of the system of linear algebraic equations:

$$\mathbf{K}\mathbf{q} = \mathbf{R} \tag{3.82}$$

where $\mathbf{K}$ is the element stiffness matrix given by:

$$\mathbf{K} = \mathbf{K_b} + \mathbf{K_m} + \mathbf{K_s} \tag{3.83}$$

$\mathbf{R}$ is the external load vector, and $\mathbf{q}$ is the vector of nodal displacements given by (3.32).

3.3 Numerical Examples

Several benchmark problems selected from the literature (MacNeal and Harder, 1985; Belytschko et al., 1985; Simo et al., 1989a,b) are used here to evaluate the performance of the proposed generalized shell element. Any set of problems for

Table 3.1 Standard Shell elements used here as reference

Name	Description
4-ABQ	Doubly curved shell element used by ABAQUS, built on Mindlin/Sanders Koiter theory with reduced integration and hourglass control (1959, 1960), Hibbit, Karlson & Sorensen, Inc. (2001)
4-DKQ	Discrete Kirchhoff quadrilateral element
9-GAMMA	Belytschko (1985), biquadratic degenerated shell element with uniform reduced integration
4-SRI	Bilinear degenerated shell element with selective, reduced integration, Hughes and Hinton (1986), Hughes (1987)
9-SRI	Biquadratic degenerated shell element with selective, reduced integration
MIXED	Simo (1989), bilinear shell element with mixed formulations and full 2×2 quadrature

shell elements should be discriminating. Inextensional bending modes of deformation must be tested, as well as rigid body modes, complex membrane state of stress, and shear deformation modes (Belytschko et al., 1985). We selected these problems to challenge the above mentioned capabilities of our formulation, as well as to examine its functioning for thick and very thick shells. We compare the convergence of the results with other formulations available in the literature. Table 3.1 gives the shell elements used here as reference, as well as the abbreviations used in the text.

3.3.1 The Patch Test

We consider a square plate problem is considered here, that is modeled by a single element, subjected to constant tension and bending, as shown in Fig. 3.5. The displacements obtained using the present element are exact as they match the analytical solution.

3.3.2 Cantilevered Beam

Another problem frequently used as a benchmark test is the evaluation of the performance of an proposed element in straight cantilever beams (Fig. 3.6). A point load applied to the free end of the beam evokes all of the principal deformation modes.

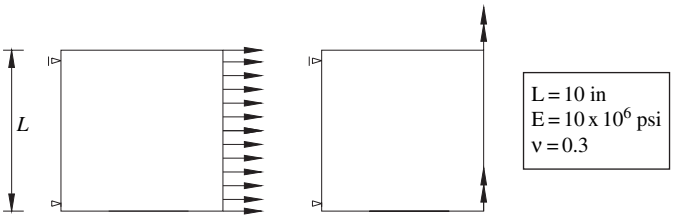

Fig. 3.5 Constant stress patch test: tension and bending (E-Young's modulus; ν-Poisson's ratio)

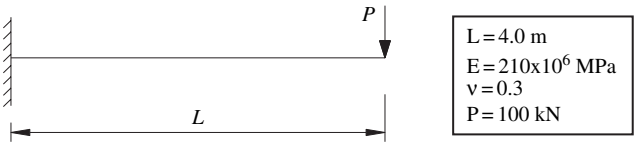

Fig. 3.6 Cantilevered beam problem (E-Young's modulus; ν-Poisson's ratio)

The height and thickness of the beam are, respectively, $h = 0.4$ m, and $b = 0.2$ m. We investigate the maximum displacement of the beam, which is modeled with four, eight, and ten elements and compare the results with those obtained using the engineering beam theory. Table 3.2 shows the comparison.

The results shown in Fig. 3.7 indicate that the current element is in very good agreement with the analytical solution. It shows a robust performance.

3.3.3 Morley's Hemispherical Shell (Morley and Moris, 1978)

The following example is used as a standard test to evaluate the performance of finite elements (MacNeal and Harder, 1985; Simon et al., 1989). The problem represents a hemisphere with four point loads alternating in sign at 90^0 intervals on the equator, which is a free edge (Fig. 3.8).

Table 3.2 Vertical displacement at the free end [m] (EBT*-Engineering Beam Theory)

Number of elements	Analytical $EBT^* \times 10^{-3}$	Present $FE \times 10^{-3}$	Normalized present FE
4	9.52	9.369	0.98
8	9.52	9.493	0.997
10	9.52	9.517	0.999

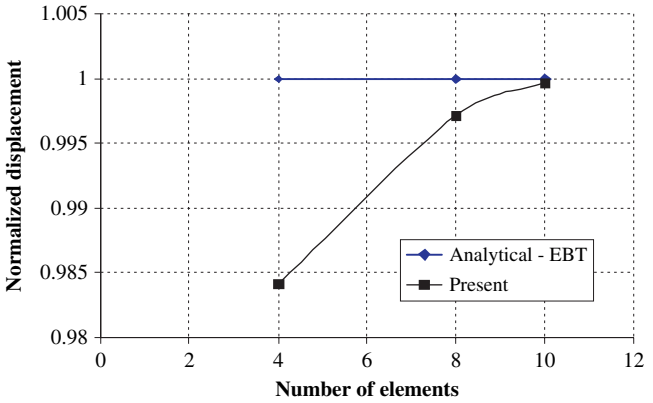

Fig. 3.7 Convergence of the present element for the cantilevered beam problem, displacement under the load

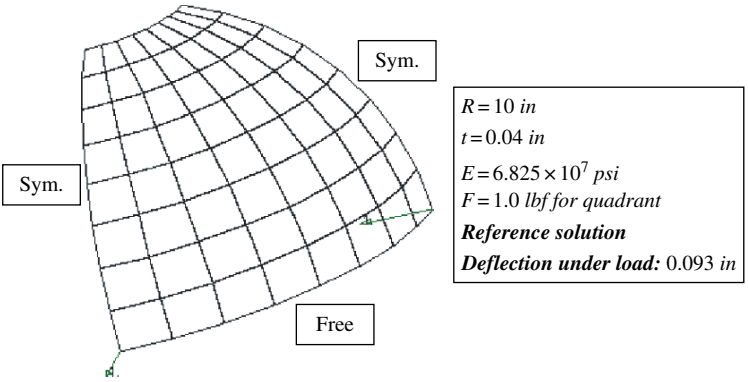

Fig. 3.8 Morley's Sphere (t-thickness, R-radius, E-Young's modulus, F-load)

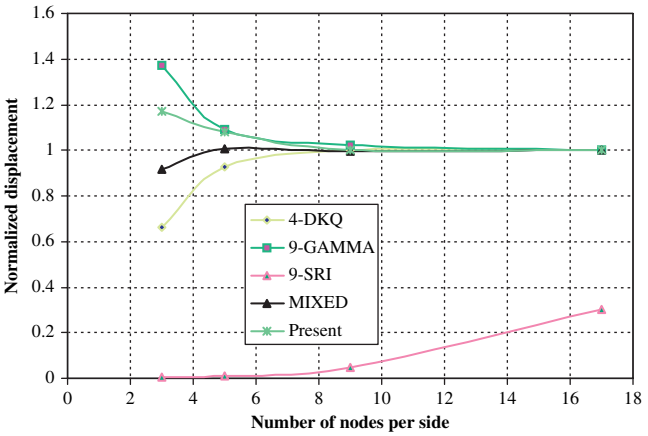

Fig. 3.9 Comparison of results by different shell formulations – Morley's Sphere, deflection under the load

In the hemispherical shell problem, the membrane strains are very small, making the problem a discriminating test of the element's ability to represent inextensional modes. Moreover, under these loading conditions, large sections of the model rotate as almost rigid bodies, which allows us to check the ability of the element to model rigid body motion (Belytschko et al., 1985).

Bending strains contribute significantly to the radial displacement at the point of the application of the load F. The value of the displacement under the concentrated load is 0.094 in, which was obtained by MacNeal and Harder (1985). Simon et al. (1989) found, however that the analytical solution of this problem yields a value of 0.093 in, which is used as a reference solution. The results are given in Table 3.3. Figure 3.10 compares the proposed element's performance with that of 4-DKQ, 9-SRI, 9-GAMMA, and MIXED elements.

Table 3.3 Normalized displacement under the load for the hemispherical shell

Nodes per side	Mixed	4-DKQ	9-GAMMA	9-SRI	Present
3	0.919	0.663	1.37	0.002	1.17
5	1.004	0.928	1.09	0.01	1.08
9	0.998	1.001	1.02	0.05	1.002
17	0.999	1.003	1.00	0.3	1.002

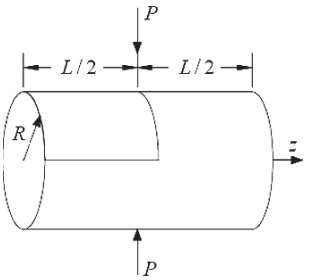

L = 600 in
R = 300 in
t = 3 in
$E = 3 \times 10^6$ psi
ν = 0.3
P = 1.0 lbf
Ends constrained: $u_x = u_y = \phi_z = 0$
Reference solution: 1.82488×10^{-5} in

Fig. 3.10 Pinched cylinder with diaphragms – geometry and material properties (t-thickness, E-Young's modulus, ν-Poisson's ratio)

As shown in Fig. 3.9, the proposed doubly curved finite element performs very well in this test. It converges quickly and produces accurate results, even for a very coarse mesh.

We also investigate the transverse shear stresses for the above problem with different shell thicknesses and compare the values obtained with those of the 4-ABQ element in Table 3.4. Normal stresses σ_x are used in Table 3.4 in order to compare the relative magnitudes of the normal and transverse shear stresses. The last column of the table gives the ratio of τ_{xz}/σ_x. It shows the increasing importance of the transverse shear stresses with the increase of the thickness of the shell. For the first shell analyzed, with thickness 0.04 in., τ_{xz} is only 0.0068 of the normal stresses σ_x, whereas for the thickness of 0.9 in. the ratio increases to 0.12. It demonstrates the expected pattern whereby the transverse shear stresses become much more significant for thick shells.

Table 3.4 Transverse shear and normal stresses for the hemispherical shell

Thickness t[in]	$\tau_{xz}[psi]$		$\tau_{yz}[psi]$		$\sigma_x[psi]$		Ratio τ_{xz}/σ_x
	4-ABQ	Present	4-ABQ	Present	4-ABQ	Present	
0.04	−38.71	−38.5	−22.38	−22.21	−5691	−5658	0.0068
0.1	−15.11	−14.98	−6.7	−6.62	−965.7	−954.6	0.0156
0.18	−8.131	−7.96	−3.596	−3.51	−305.4	−298.303	0.0266
0.28	−5.047	−4.97	−2.417	−2.37	−127.3	−125.6	0.0396
0.4	−3.41	−3.19	−1.804	−1.703	−62.34	−61.63	0.0547
0.54	−2.441	−2.3	−1.42	−1.33	−33.93	−33.26	0.0719
0.7	−1.824	−1.642	−1.152	−1.121	−19.92	−19.67	0.0915
0.9	−1.376	−1.27	−0.9376	−0.926	−11.82	−11.68	0.1164

Our formulation provides sound and reasonable predictions of the transverse stresses, which is particularly important in the case of thick shells. It emphasizes a main thrusts of our theory, on which the current element is built. The approximations given here are better than most of the reference models, except for the MIXED shell element by Simon et al. (1989), which confirms the validity of out theoretical concepts and numerical procedure.

3.3.4 Pinched Cylinder with Diaphragms

The pinched cylinder with a diaphragm is one of the most severe tests for both inextensional bending modes and complex membrane states. An element that passes this test will also perform well if the boundary conditions are simplified to free ends. It is therefore sufficient to present only the cylinder with diaphragms (Belytschko et al., 1985).

A short cylinder with two pinching vertical forces at the middle section and two rigid diaphragms at the ends is modeled here. Because of the symmetry we consider only one octant of the cylinder and apply the appropriate boundary conditions. We investigate the radial displacement under the load and normalize the results against the analytical solution of the problem: 1.82488×10^{-5} in. (Lindberg et al., 1969; Flugge, 1960). The geometry of the problem is shown in Fig. 3.10.

The normalized numerical results are shown in Table 3.5 and Fig. 3.11.

The above problem is one of the most demanding tests for shell elements. Most of the Mindlin elements, accounting for shear deformation do not converge efficiently in this problem, except for the discrete Kirchhoff formulations. The present element again offers a very good approximation, as well as fast convergence. It is known that for the pinched cylinder with diaphragms, the elements using the discrete Kirchhoff constraints are among the best performers. The new element is, however, no lesser in this case, providing results closer to the exact solution than any of the other elements considered, except for the above-mentioned 4-DKQ (Discrete Kirchhoff constraints).

Despite performing robustly in this test, the finite element developed here experiences mild membrane locking. When the series of cylinders with diaphragms, with a reduced radius of curvatures ($R = 200\,in,\ R = 100\,in,\ R = 50\,in$) were examined, the mesh of finite elements showed a tendency to be slightly too stiff, predicting about 80% of the reference solution for the case of $R = 50\,in$. The problem gradually disappears when the radius of curvature of the cylinder is increased.

Table 3.5 Normalized displacement – pinched cylinder with diaphragms

Nodes per side	Mixed	4-DKQ	4-SRI	Present
5	0.399	0.626	0.373	0.562
9	0.763	0.951	0.747	0.909
17	0.935	1.016	0.935	1.003

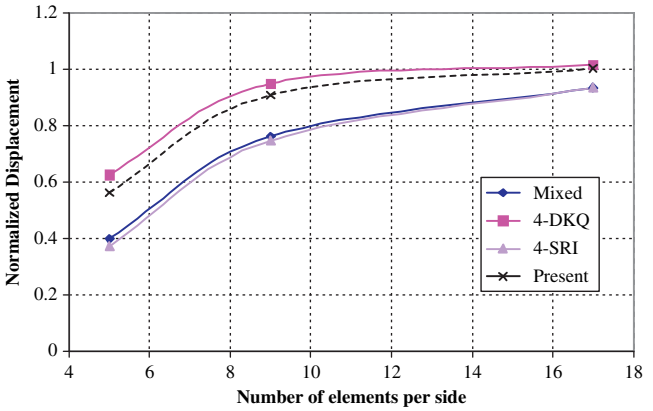

Fig. 3.11 Comparison of results by different shell formulations – pinched cylinder with diaphragms, displacement under the load

3.3.5 Scordellis-Lo Roof

The Scordellis-Lo Roof problem is one of the best tools for testing the accuracy of the elements in solving complex states of membrane strains. Representation of the inextensional modes is not crucial in this problem, as the membrane strain energy makes a large portion of the strain energy. Therefore, even the elements that experience severe membrane locking may converge in this test. Inaccuracies in the membrane stress representation, however, will hinder the convergence process.

The Scordellis-Lo Roof is a short cylindrical section, loaded by gravity forces (Scordelis and Lo, 1969). The geometry and material properties of the problem are shown in Fig. 3.12.

As with the pinched cylinder, because of the symmetry we consider only an octant. The vertical displacement at midpoint of the free edge was reported by Scordellis and Lo as 0.3024 in., which will serve here as a reference solution. Table 3.6 shows the results of the problem. Convergence of the element is shown in Fig. 3.13.

All of the elements considered here converge reasonably well. Our formulation is in good agreement with the analytical result, although, its performance is not better

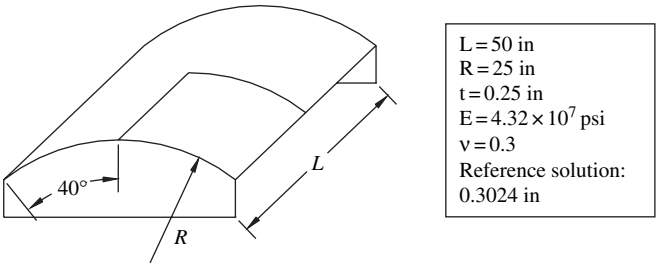

Fig. 3.12 Scordellis-Lo Roof (t-thickness, E-Young's modulus, ν-Poisson's ratio)

Table 3.6 Normalized displacement – Scordellis-Lo Roof

Nodes per side	Mixed	4-DKQ	4-SRI	Present
3	1.45	1.391	1.263	1.58
5	1.083	1.048	0.964	1.14
9	1.015	1.005	0.984	1.022
17	1.00	0.996	0.999	1.002

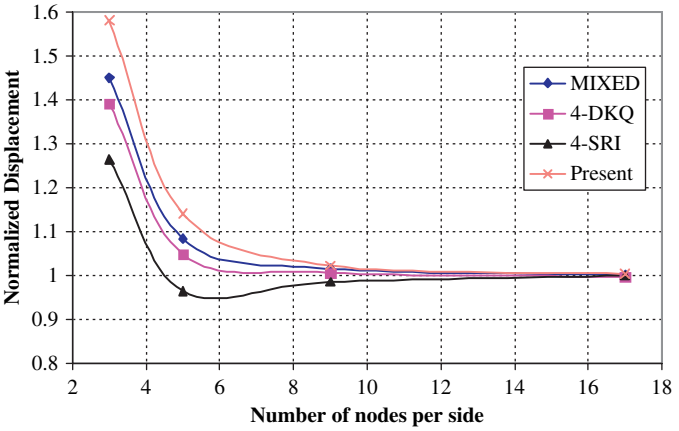

Fig. 3.13 Comparison of results by different shell formulations – Scordellis-Lo Roof, vertical displacement at midpoint

than that of the elements with which it is compared. It converges completely with a reasonable mesh of 16×16 elements (Fig. 3.13).

Although the vertical displacement at midpoint of the shell is very closely approximated, as seen in Fig. 3.13, the deflection pattern is less accurate. The value of the vertical displacement at a distance $L/4$ from the midpoint is about 10% larger than displacement at midpoint. As expected, this error is also observed in the pattern of the internal forces, which are calculated from the displacement. As Scordelis-Lo Roof is a very demanding test of the ability of the element to model complex states of membrane strains, the deficient interpolation of these strains is most likely the reason for the loss of accuracy of the displacement patterns.

3.3.6 Pinched Cylinder

We now consider a similar test to the pinched cylinder with diaphragms (Sect. 3.3.4), which serves however, a different purpose. The ends of the cylinder are free (no rigid diaphragms). As noted above an element that gives accurate results for the cylinder with diaphragms will also perform very well if the boundary conditions are simplified to free ends. We therefore use the present example to investigate the

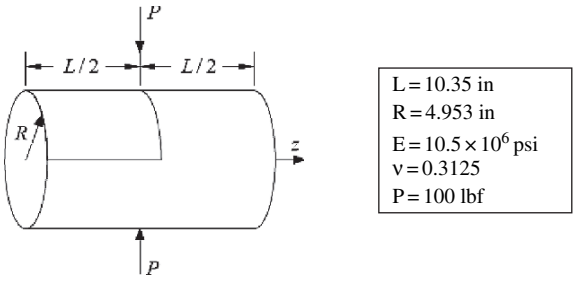

Fig. 3.14 Pinched cylinder without diaphragms (E-Young's modulus, ν-Poisson's ratio)

performance of out formulation for the case of very thick shells. The characteristics of the problem are shown in Fig. 3.14.

We vary the thickness of the cylinder and investigate the displacement under point loads. The results obtained with the present finite element are compared with those obtained using the 4-ABQ doubly curved shell element used by ABAQUS, built on Mindlin/Sanders Koiter (Sanders, 1959; Koiter, 1960) theory with reduced integration and hourglass control, as well as with an analytical solution of the problem by Timoshenko and Woinowsky-Krieger (1959). The latter treat the problem as an inextensional deformation of a circular cylinder, i.e., the membrane strains are zero and the deformation is governed only by the bending modes. The values of the displacements provided by the inextensional solution are therefore slightly too low. Nevertheless, they may still be regarded as accurate, especially for the case of thin shells. The correction factor increasing the displacement under the load by 0.4%, due to extensional bending, was estimated by Ashwell and Sabir (1971) for a thin shell ($t = R/320$). Although for very thick shells ($t = R/2$) this correction factor reaches 1.3%, it is still considered small. Thus, the results of the inextensional deformation of the cylindrical shell by Timoshenko and Woinowsky-Krieger (1959) may still serve as a reference solution. The results of the pinched cylinder problem are shown in Table 3.7 and Fig. 3.15.

Although the Mindlin element with reduced integration provides a good approximation of the analytical solution, our formulation offers superior performance. The pattern of decreasing value of the displacement with increasing thickness of the shell is in excellent agreement with the analytical inextensional bending solution. It is worth mentioning that the analytical solution used here as a reference is not exact, as discussed above. Our formulation proves to be more accurate than the Mindlin

Table 3.7 Displacement under load [in] – Pinched cylinder

t [in]	Analytical	4-ABQ	Present
1	9.02E-05	1.08E-04	9.82E-05
1.2	5.22E-05	8.63E-05	6.08E-05
1.4	3.29E-05	5.38E-05	3.92E-05
1.6	2.2E-05	4.14E-05	2.84E-05
2	1.13E-05	2.39E-05	1.63E-05
2.5	5.77E-06	1.52E-05	1.13E-05

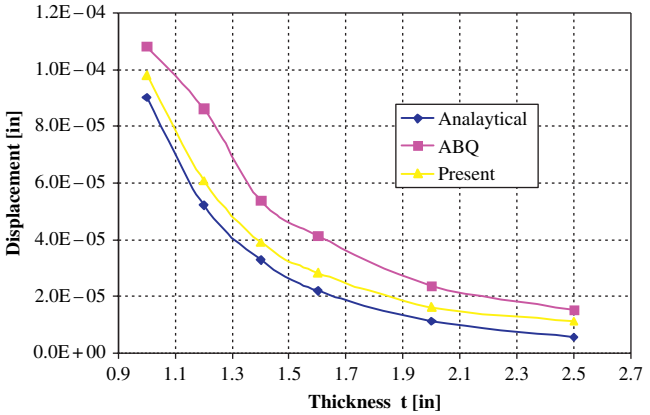

Fig. 3.15 Pinched cylinder – deflection under the load [in]

type of element in the analysis of thick shells. Moreover, the 4-ABQ element, as well as all the other elements using numerical integration, are dependent on the number of integration points. Although it is known that with appropriate choice of the number of integration points one can obtain an accurate result, the process is cumbersome, compared with the present algorithm with an explicit stiffness matrix and noneed for numerical integration during the finite element computations.

3.4 Summary

We evaluated the performance of the proposed finite element through a set of discriminating benchmark problems selected from the literature. The examples show that our formulation experiences neither shear locking nor spurious energy modes for thin shells. At the same time, in the analysis of thick shells it offers a superior performance than most of the formulations with which we compare it, providing very accurate results.

Despite careful considerations when interpolating the strains, the finite element suffers from mild membrane locking. An example of a pinched cylinder with a diaphragm, one of the most severe tests for both inextensional bending modes and complex membrane states, is given in Sect. 3.3.4. Although our formulation offered very accurate results and fast convergence in the case of the cylinder with radius $R = 300$ in, the mesh became too stiff when the radius was decreased to $R = 50$ in. Thus we conclude that the representation of the membrane strains can be inadequate and does not always ensure satisfaction of the inextensibility condition. This was also indicated by the results of the Scordelis-Lo roof problem in Sect. 3.3.5. The strain fields could be further refined to cure this problem. We found, however, that the quasi-conforming technique although very convenient, is also sensitive to changes in the interpolation of both strain and displacement fields. Approximation formulas that may seem reasonable from the physical point of view sometimes

produce results as much as 20% off the target solution. Refining the strain interpolation to get rid of membrane locking completely is therefore an iterative that can be tedious. The best solution is to construct the membrane displacement approximations dependent on the vertical displacement function w. The ratio of flexural and membrane rigidities should enter the membrane displacement interpolations, similarly to adopted Hu's functions for w and ϕ ((3.33), (3.34)), where a parameter λ (3.37) enforced a constraint of transverse shears reducing to zero in the case of thin shells. A similar parameter, dependent on the ratio of flexural and membrane rigidities, should be included in the displacement field such that the inextensibility condition is explicitly satisfied when the thickness of the shell decreases. Such a remedy could be successful, and the quasi-conforming technique, along with carefully devised inter-related displacement approximations, would be a powerful and efficient tool for constructing curved shell elements, despite its sensitivity.

Despite the above-discussed deficiencies, the finite element model we present here performs well in all of the tests undertaken. The model is also superior to many others in simulating the behavior of moderately thick and thick shells. Our formualation is therefore universal, applicable to thick and thin shells, plates, and beams; it shows good overall performance at the same time that it is computationally efficient.

References

Ashwell, D.G. and Sabir, A.B., (1972). A new cylindrical shell finite element based on simple independent strain functions. Int. J. Mech. Sci., 14, 171–183.

Belytschko, T., Liu, W.K., Ong, J.S.-J. (1984a). A consistent control of spurious singular modes in the 9-node Lagrange element for the Laplace and Mindlin plate equations. Comput. Meths. Appl. Mech. Eng., 44, 269–295.

Belytschko, T., Ong, J.S.-J., Liu, W.K., Kennedy, J.M. (1984b). Hourglass control in linear and non-linear problems, Comput. Meths. Appl. Mech. Eng., 43, 251–276.

Belytschko, T., Stolarski, H., Carpenter, N. (1984c). A C^0 triangular plate element with one-point quadrature. Int. J.Num. Meths. Eng., 20, 787–802.

Belytschko, T., Stolarski, H., Liu, W.K., Carpenter, N., Ong, J.S.-J. (1985). Stress projection for membrane and shear locking in shell finite elements. Comput. Methods Appl. Mech. Eng., 51, 221–258.

Cook, R.D. (1972). Two hybrid elements for analysis of thick and thin sandwich plates. Int. J.Num. Meths. Eng., 5, 277.

Cook, R.D., Malkus, D.S., Plesha, M.E. (1989). Concepts and Applications of Finite Element Analysis. 3rd edition, John Wiley & Sons, New York.

Cook, R.D., Malkus, D.S., Plesha, M.E., Witt, R.J. (2002). Concepts and Applications of Finite Element Analysis. 4th edition, John Wiley & Sons, New York.

Flugge, W. (1960). Stresses in Shells. Springer, New York.

Hibbit, Karlson & Sorensen, Inc. (2001). Abaqus, Theory Manual, Pawtucket, RI, USA

Hu, H-C. (1981). The Variational Principles in Elasticity and its Application. Scientific Publisher, Beijing.

Hughes, T.J.R. (1987). The Finite Element Method. Prentice-Hall, Englewood-Cliffs, NJ.

Hughes, T.J.R. and Hinton, E. (1986). Finite Element Methods for Plate and Shell Structures. Pineridge, Swansea, UK.

Koiter,W.T. (1960). A consistent first approximation in general theory of thin elastic shells. In Theory of Thin Elastic Shells, First IUTAM Symp. (Edited by W.T. Koiter), pp 12–33. North-Holland, Amsterdam.

Lindberg, G.M., Olson, M.D., Cowper, G.R. (1969). New developments in the finite element analysis of shells. Qart. Bull. Div. Mech. Eng. Natl. Aeronautical Establishment, 4, 1–99.

Liu, Y., Shi, G., Tang, L. (1984). Quasi-conforming elements for thick/thin beam and plate bending problems. J. DIT, 22, 3, 79–85.

Lu, H. and Liu, Y. (1981). Quasi-conforming element technique applied to double curvature shallow shells. J. DIT, 20, 1.

MacNeal, H.R. and Harder, R.L. (1985). A proposed standard set of problems to test finite element accuracy. Finite Elements Anal. Design, 1, 3–20. North-Holland.

Morley, L.S.D and Morris, A.J. (1978). Conflict between finite elements and shell theory, Royal Aircraft Establishment Report. London.

Sanders, J.L. (1959). An improved first approximation theory of thin shells. NASA Report24.

Scordelis, A.C. and Lo, K.S. (1969) Computer analysis of cylindrical shells. J. Am. Concrete Inst.; 61:539–561.

Shi, G. and Voyiadjis, G.Z. (1990). A simple C^0 quadrilateral thick/thin shell element based on the refined shell theory and the assumed strain fields. Int. J. Solids Struct., 27, 3, 283–298.

Shi, G. and Voyiadjis, G.Z. (1991a). Geometrically nonlinear analysis of plates by assumed strain element with explicit tangent stiffness. Comput. Struct., 41, 757–763.

Shi, G. and Voyiadjis, G.Z. (1991b). Simple and efficient shear flexible two node arch/beam and four node cylindrical shell/plate finite element. Int. J. Num. Meth. Eng., 31, 759–776.

Simo, J.C.; Fox, D.D. and Rifai, M.S. (1989a). On a stress resultant geometrically exact shell model. Comp. Meth. Appl. Mech. Eng., 73, 53–92, North-Holland.

Simo, J.C.; Fox, D.D. and Rifai, M.S. (1989b). On a stress resultant geometrically exact shell model. Part II: The linear theory. Comp Meth. Appl. Mech. Eng., 73, 53–92, North-Holland.

Stolarski, H. and Belytschko, T. (1981). Reduced integration for shallow-shell facet elements. New Concepts in Finite Element Analysis, Eds. T.J.R. Hughes, et. al., ASME, New York 179–194.

Stolarski, H. and Belytschko, T. (1982). Membrane locking and reduced integration for curved elements. J. Appl. Mech. 49, 172–177.

Tang, L., Chen, W. and Liu, Y. (1980). Quasi-conforming elements for finite element analysis. J. DIT, 19, 2.

Tang, L., Chen, W. and Liu, Y. (1983). String net function applications and quasi conforming technique. In Hybrid and Mixed Finite Element Methods, Wiley, New York

Timoshenko, S.P. and Woinowsky-Krieger, S. (1959). Theory of Plates. McGraw-Hill, Inc., New York.

Zienkiewicz, O.C. (1971). The Finite Element in Engineering Science. McGraw-Hill, London.

Zienkiewicz, O.C. (1978). The Finite Element Method, McGraw-Hill, New York.

Chapter 4
Geometrically Non-linear Finite Element Analysis of Thick Plates and Shells

4.1 Introduction

A problem of geometric non-linearity can be explained through the example of the simple beam. We consider a plane cantilever beam subjected to an end load, as shown in Fig. 4.1 (Cook et al., 1989).

Assuming that the beam is slender and the material linearly elastic, we seek the quasistatic deflections produced by the end load P. If the deflections are small, the linear theory is adequate to simulate the behavior of the beam. The reactant bending moment at the fixed end is $M = PL$, as the shortening of the moment arm e is negligible. For large displacements, e becomes significant and the reactant bending moment is $M = P(L - e)$. If the effect of large displacement is taken into account, the equilibrium equations must be written in the deformed configuration. This is because the deformation of the beam substantially alters the location of the external load P. The equations describing such an effect are non-linear and the nature of non-linearity is geometric.

Large displacement play an important role the investigation of the behavior of plates and shells. Certain parts of the structure under given loading conditions may undergo large rigid rotations and translations. Considering these effects is even more important in the elasto-plastic and damage analysis of shells. The regions of the structure deforming inelastically will most likely undergo large displacements. These can be approximated through geometrically non-linear analysis. Our objective is to present a reliable computational model for the elasto-plastic and damage

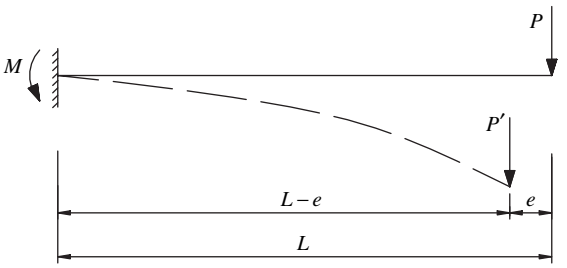

Fig. 4.1 Geometric non-linearity; cantilever beam under the end load

© Springer-Verlag Berlin Heidelberg 2008

analysis of shells; to achieve the desired accuracy, geometrical non-linearities must be considered.

One can usually distinguish two types of geometrical non-linearity when analyzing shells: large deformations and large rotations. Large deformations are attributed to the stretch of the middle surface of the shell undergoing large displacements. Large rotations are attributed to significant changes of the slope during the analysis. These changes also cause the transformation matrix of the coordinates to also change during the analysis. It is also possible to have rigid body motion without any strains. In that case, large rigid rotations and translations are considered, but the strains remain small.

For simplicity and conciseness, we examine only the most significant effects from the viewpoint of shell behavior. This leads us to include large rigid rotations and translations but not large strains. We use the Updated Lagrangian description, with the total rotations decomposed into large rigid and moderate relative rotations. The relative rotations and the derivatives of the in-plane displacements from two consecutive configurations can be considered small (Shi and Atluri, 1988; Shi and Voyiadjis, 1991a). Consequently, the quadratic terms of the derivatives of the in-plane displacement are negligible. We therefore have a non-linear analysis with large displacements and rotations but small strains. As shown below (Sect. 4.4, and Chaps. 5 and 6), such a treatment of the geometrical non-linearities is capable of simulating the shell behavior with sufficient accuracy. This is also convenient for the elasto-plastic modeling of shells in the stress resultant space. If the strains are small, then the assumption of additive decomposition of strains into elastic and plastic parts, commonly used in modeling of plasticity, can be extended to displacements. This allows use of the plastic node method in the elasto-plastic considerations.

Although the primary motivation for including large displacements in the analysis is to validate the plastic and damage investigations of shells, the procedure described in this chapter is universal and may be used as a stand-alone algorithm. The elastic shell model, which use developed with constitutive equations derived in Chap. 2, and elastic stiffness matrix in Chap. 3, is extended here to account for the geometrical non-linearities.

In the following sections, we briefly discuss the nature of the Updated Lagrangian description, used here in the treatment of geometric non-linearities. In Sect. 4.3, we present the kinematics of the shell followed by the derivation of the explicit tangent stiffness matrix in Sect. 4.4. Finally, we give a numerical example challenging the adopted concepts.

4.2 Updated Lagrangian Description

We adopt the Updated Lagrangian description, which has proven to be an effective method (Bathe, 1982; Flores and Onate, 2001; Horrigmoe and Bergan, 1978; Kebari and Cassell, 1992). In the Lagrangian description of a mechanical stressed problem, we study a coordinate frame in which the body under investigation is rigidly translated and rotated, and may also be deformed. This method is based on calculation of

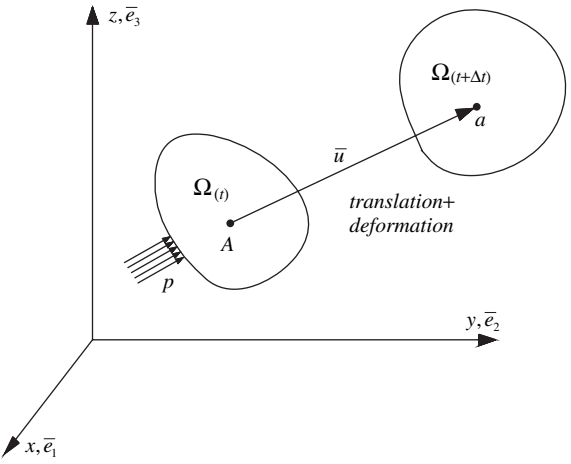

Fig. 4.2 Updated Lagrangian description

the increments of the displacements. In the Updated Lagrangian description, the reference configuration is in the state after the deformation, at time $t + \Delta t$, as opposed to the Total Lagrangian description, in which the reference configuration is at time t (Fig. 4.2). In the Updated Lagrangian description, the element local coordinates and local reference frame are continuously updated during the deformation. The transformation matrix given by Argyris (1982) is used to handle large rigid rotations.

4.3 Shell Kinematics

As discussed above we use the Updated Lagrangian description to study large displacements and rotations of the shell element. The coordinates of the nodal points are continuously updated during the deformation. The rotations are additively decomposed into large rigid rotations and moderate relative rotations (Shi and Voyiadjis, 1991a,b).

The structure under consideration is defined in the global, fixed-coordinate system **X**. We also have the local coordinate system **x**, surface coordinates at any nodal point $\mathbf{x}_s$, and base coordinates, which serve as a reference frame for the global degrees of freedom (Fig. 4.3).

4.3.1 Local Coordinates

To obtain the unit vector in the direction normal to the plane of the element, we first define two vectors, $\overrightarrow{41}$ and $\overrightarrow{42}$, connecting the origin of the coordinate system (point 4) to points 1 and 2, respectively. The cross product of these two vectors divided by its length, gives $\mathbf{e}_3$, as shown in Fig. 4.3 and given by (4.1):

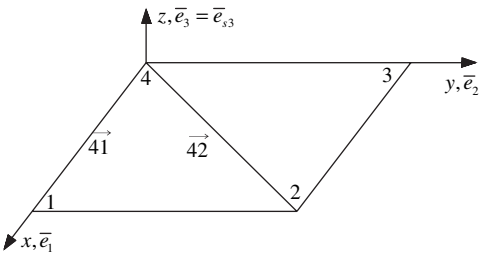

Fig. 4.3 Local coordinate system and normal vector $\mathbf{e}_{s3}$ (Voyiadjis and Woelke, 2006)

$$\mathbf{e}_3 = \frac{\overrightarrow{41} \times \overrightarrow{42}}{\left|\overrightarrow{41} \times \overrightarrow{42}\right|} \tag{4.1}$$

The unit vector $\mathbf{e}_2$ can be similarly obtained as a cross product of $\mathbf{e}_3$ and $\mathbf{e}_1$.

We may now determine the relation between the global coordinates $\mathbf{X}$ and element local coordinates in configuration k:

$$^k\mathbf{e} = {}^k\mathbf{R}\mathbf{E} \tag{4.2}$$

where $^k\mathbf{e}$ is the unit base vector of the local coordinates in configuration k, $\mathbf{E}$ is the unit base vector of the global coordinates, and $\mathbf{R}$ is a transformation matrix from local to global coordinates.

4.3.2 Surface Coordinates

The surface coordinate system $\mathbf{x}_S$ originates at each node of the element. As defined by Shi and Voyiadjis (1991a), the position and direction of this system are functions of rotations. Surface coordinates translate and rigidly rotate with the element. Consequently, $\mathbf{x}_{S3}$ is always normal to the surface of the element.

The finite rigid body rotation vector $\mathbf{V}$ is given by:

$$\mathbf{V} = \begin{bmatrix} \theta_1 \\ \theta_2 \\ \theta_3 \end{bmatrix} \tag{4.3}$$

where $\theta_1, \theta_2, \theta_3$ are rigid body rotations around x, y, z axes respectively.

The transformation matrix of large rotations $\mathbf{T}_\theta$, given by Argyris (1982) is used here:

$$\mathbf{T}_\theta = \exp\left(\tilde{\theta}\right) \tag{4.4}$$

with:

$$\tilde{\theta} = \tilde{\theta}_{ij} = e_{ijk}\theta_k, \quad k = 1, 2, 3 \tag{4.5}$$

where $\tilde{\theta}$ is a skew symmetric matrix and e_{ijk} is the permutation tensor. In the above equation, the indicial notation is used, with Einstein's summation convention. The transformation of the surface coordinates is therefore:

$$\mathbf{V}' = \mathbf{T}_\theta \mathbf{V} \tag{4.6}$$

where $\mathbf{V}'$ is a rigid body rotation vector transformed into a new position. Similarly, we can write a transformation of the surface coordinates for a given rotation vector θ_j resulting from configuration $k-1$ to k at node j:

$${}^k\mathbf{e}_s = \mathbf{T}_{\theta j}\, {}^{k-1}\mathbf{e}_s \tag{4.7}$$

where ${}^k\mathbf{e}_s$ are the unit base vectors of the surface coordinates at configuration k. Defining the transformation between $\mathbf{E}$ and ${}^k\mathbf{e}_s$ as:

$${}^k\mathbf{e}_s = {}^k\mathbf{R}_s \mathbf{E} \tag{4.8}$$

we rewrite (4.7) as:

$${}^k\mathbf{e}_s = \mathbf{T}_{\theta j}\, {}^{k-1}\mathbf{R}_s \mathbf{E} = {}^k\mathbf{R}_s\, {}^k\mathbf{R}^T {}^k\mathbf{e} = {}^k\mathbf{S}_j\, {}^k\mathbf{e} \tag{4.9}$$

where ${}^k\mathbf{R}^T$ is the transpose of ${}^k\mathbf{R}$ defined in (4.2), and ${}^k\mathbf{S}_j$ is a transformation matrix from local to the surface coordinate system. Note ${}^0\mathbf{R}_s$ is a 3×3 identity matrix for a flat plate.

4.3.3 Base Coordinates

The base coordinates defined by Horrigmoe and Bergan (1978) are adopted here as a common reference frame to which all element properties are transformed, prior to the assembly of the stiffness matrices. The base coordinates are defined by the combination of the fixed global and base coordinates.

The global degrees of freedom at node j are the incremental translations: ΔU_j, ΔV_j, ΔW_j in the directions of global coordinates X, Y, Z, respectively, and rotations Θ_{xj}, Θ_{yj} around x_S, y_S, respectively. The local degrees of freedom at node j are the incremental translations Δu_j, Δv_j, Δw_j in the directions of local coordinates x, y, z, respectively, and rotations ϕ_{xj}, ϕ_{yj} around x, y, respectively. The transformation of the increments of the displacements at node j from the local coordinate system $\Delta\mathbf{q}_{ej}$, to the corresponding base coordinates, $\Delta\mathbf{q}_{bj}$ can be written as:

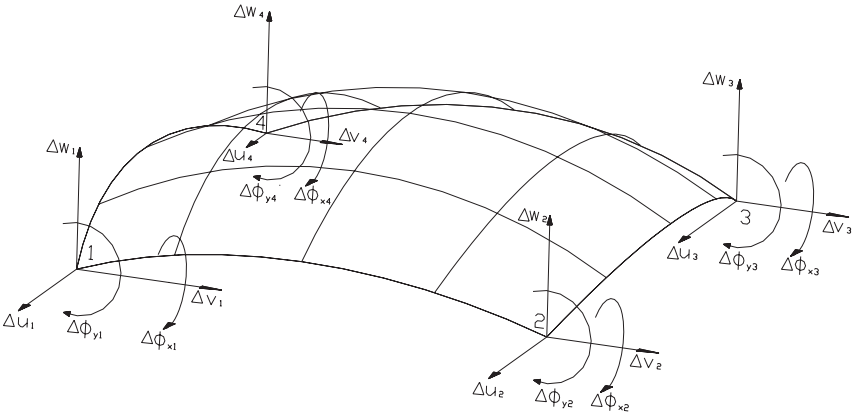

Fig. 4.4 Incremental degrees of freedom of shell element (Voyiadjis and Woelke, 2006)

$$\Delta \mathbf{q}_{bj} = \begin{Bmatrix} \Delta U_j \\ \Delta V_j \\ \Delta W_j \\ \Theta_{xj} \\ \Theta_{yj} \end{Bmatrix} = \begin{bmatrix} {}^k\mathbf{R}^T & 0 \\ 0 & {}^k\mathbf{s}_j \end{bmatrix} \begin{Bmatrix} \Delta u_j \\ \Delta v_j \\ \Delta w_j \\ \phi_{xj} \\ \phi_{yj} \end{Bmatrix} = {}^k\mathbf{T}_{bj} \Delta \mathbf{q}_{ej} \tag{4.10}$$

in which ${}^k\mathbf{s}_j$ is the upper left 2×2 submatrix of ${}^k\mathbf{S}_j$ defined in (4.9). The transformation matrix for the nodal displacement vector can be written as:

$$\Delta \mathbf{q}_b = {}^k\mathbf{T}_b \Delta \mathbf{q}_e \tag{4.11}$$

where ${}^k\mathbf{T}_b$ is composed of ${}^k\mathbf{T}_{bj}$ with $j = 1, 2, 3, 4$.

The vector of the local increments of nodal displacements is shown in Fig. 4.4 and given by (4.12):

$$\Delta \mathbf{q}_{ej} = \left\{ \Delta u_j, \Delta v_j, \Delta w_j, \Delta \phi_{xj}, \Delta \phi_{yj} \right\}^T \quad j = 1, 2, 3, 4 \tag{4.12}$$

4.4 Explicit Tangent Stiffness Matrix

In this geometrically non-linear analysis of plates and shells presented here, we use the shell constitutive equations derived in Chap. 2. These equations, transformed into a rectangular coordinate system are given by the (3.12), (3.13), (3.14), (3.15), (3.16), (3.17), (3.18), (3.19), (3.20), (3.21), (3.22), (3.23), (3.24), (3.25), (3.26). To determine the tangent stiffness matrix of the element, we define $\delta\boldsymbol{\varepsilon}_\mathbf{b}$, $\delta\boldsymbol{\varepsilon}_\mathbf{m}$, $\delta\boldsymbol{\varepsilon}_\mathbf{s}$ as virtual elastic bending, membrane, and transverse shear strains respectively (δ-virtual) and **M, N, Q** as stress couples and stress resultants of the element.

Rewriting the shell constitutive equations in the matrix form yields:

$$\mathbf{M} = \mathbf{D}\boldsymbol{\varepsilon}_\mathbf{b} \tag{4.13}$$

$$\mathbf{N} = \mathbf{S}\boldsymbol{\varepsilon}_\mathbf{m} \tag{4.14}$$

$$\mathbf{Q} = \mathbf{T}\boldsymbol{\varepsilon}_\mathbf{s} \tag{4.15}$$

where $\boldsymbol{\varepsilon}_\mathbf{b}$, $\boldsymbol{\varepsilon}_\mathbf{m}$, $\boldsymbol{\varepsilon}_\mathbf{s}$ are bending, membrane and shear strains respectively, defined by the (3.45), (3.46), (3.47) and rewritten here in the incremental form:

$$\boldsymbol{\varepsilon}_\mathbf{b} = \begin{Bmatrix} \dfrac{\partial \Delta\phi_x}{\partial x} \\ \dfrac{\partial \Delta\phi_y}{\partial y} \\ \dfrac{\partial \Delta\phi_x}{\partial y} + \dfrac{\partial \Delta\phi_y}{\partial x} \end{Bmatrix}, \quad \boldsymbol{\varepsilon}_\mathbf{m} = \begin{Bmatrix} \dfrac{\partial \Delta u}{\partial x} + \dfrac{\Delta w}{R} \\ \dfrac{\partial \Delta v}{\partial y} + \dfrac{\Delta w}{R} \\ \dfrac{\partial \Delta u}{\partial y} + \dfrac{\partial \Delta v}{\partial x} \end{Bmatrix}, \quad \boldsymbol{\varepsilon}_\mathbf{s} = \begin{Bmatrix} \dfrac{\partial \Delta w}{\partial x} - \phi_x - \dfrac{\Delta u}{R} \\ \dfrac{\partial \Delta w}{\partial y} - \phi_y - \dfrac{\Delta v}{R} \end{Bmatrix} \tag{4.16}$$

and **D, S, T** are bending, membrane and shear rigidities matrices, respectively, given by:

$$\mathbf{D} = D\begin{bmatrix} 1 & \nu & 0 \\ \nu & 1 & 0 \\ 0 & 0 & 1-\nu/2 \end{bmatrix}, \quad \mathbf{S} = S\begin{bmatrix} 1 & \nu & 0 \\ \nu & 1 & 0 \\ 0 & 0 & 1-\nu/2 \end{bmatrix}, \quad \mathbf{T} = T\begin{bmatrix} 1 & 0 \\ 0 & 1 \end{bmatrix} \tag{4.17}$$

D, T, S are defined by (3.26).

We also use the linearized equilibrium equations of the system at configuration $k+1$ in the Updated Lagrangian description, expressed by the principle of virtual work, which in finite element modeling takes the form:

$$\iint_\Omega \left(\delta\boldsymbol{\varepsilon}_\mathbf{b}{}^\mathbf{T}\mathbf{D}\boldsymbol{\varepsilon}_\mathbf{b} + \delta\boldsymbol{\varepsilon}_\mathbf{m}{}^\mathbf{T}\mathbf{S}\boldsymbol{\varepsilon}_\mathbf{m} + \delta\boldsymbol{\varepsilon}_\mathbf{s}{}^\mathbf{T}\mathbf{T}\boldsymbol{\varepsilon}_\mathbf{s}\right) dxdy + \iint_\Omega \delta\boldsymbol{\theta}^\mathbf{Tk}\mathbf{F}\boldsymbol{\theta} dxdy = {}^{k+1}R$$

$$- \iint_\Omega \left(\delta\boldsymbol{\varepsilon}_\mathbf{b}{}^\mathbf{Tk}\mathbf{M} + \delta\boldsymbol{\varepsilon}_\mathbf{m}{}^\mathbf{Tk}\mathbf{N} + \delta\boldsymbol{\varepsilon}_\mathbf{s}{}^\mathbf{Tk}\mathbf{Q}\right) dxdy \tag{4.18}$$

where ${}^{k+1}R$ is the total external virtual work at step $k+1$.

As discussed above, we use the quasi-conforming technique proposed by Tang et al. (1980, 1983) here to compute the element stiffness matrix. We therefore interpolate the strains directly. The compatibility equations are satisfied only in the weak sense, i.e., under the integral sign. Again, all the integrations are calculated analytically and the explicit form of the stiffness matrix is preserved.

The strain interpolation formulas are identical to those used in the linear elastic analysis in Chap. 3 ((3.45), (3.46), (3.47)). Following the same procedure as in Chap. 3, we obtain:

$$\boldsymbol{\varepsilon}_{\mathbf{b}} = \mathbf{P}_{\mathbf{b}}\mathbf{A}_{\mathbf{b}}{}^{-1}\mathbf{C}_{\mathbf{b}}\Delta\mathbf{q}^{\mathbf{e}} = \mathbf{B}_{\mathbf{b}}\Delta\mathbf{q}^{\mathbf{e}} \tag{4.19}$$

$$\boldsymbol{\varepsilon}_{\mathbf{m}} = \mathbf{P}_{\mathbf{m}}\mathbf{A}_{\mathbf{m}}{}^{-1}\mathbf{C}_{\mathbf{m}}\Delta\mathbf{q}^{\mathbf{e}} = \mathbf{B}_{\mathbf{m}}\Delta\mathbf{q}^{\mathbf{e}} \tag{4.20}$$

$$\boldsymbol{\varepsilon}_{\mathbf{s}} = \frac{1}{\Omega}\mathbf{C}_{\mathbf{b}}\Delta\mathbf{q}^{\mathbf{e}} = \mathbf{B}_{\mathbf{s}}\Delta\mathbf{q}^{\mathbf{e}} \tag{4.21}$$

In (4.18), $\boldsymbol{\theta}$ is the slope vector and ${}^{\mathbf{k}}\mathbf{F}$ is a membrane stress resultant matrix at step k given by:

$$\boldsymbol{\theta} = \begin{Bmatrix} \dfrac{\partial \Delta w}{\partial x} \\ \dfrac{\partial \Delta w}{\partial y} \end{Bmatrix}, \quad {}^{k}\mathbf{F} = \begin{bmatrix} {}^{k}N_x & {}^{k}N_{xy} \\ {}^{k}N_{xy} & {}^{k}N_y \end{bmatrix} \tag{4.22}$$

The slope field $\boldsymbol{\theta}$ is evaluated in the same way as the strain fields, using the quasi-conforming technique (Tang et al., 1980, 1983). A bilinear interpolation as given by Shi and Voyiadjis (1991a) is used to approximate the slope field:

$$\boldsymbol{\theta} = \begin{bmatrix} 1 & x & y & xy & 0 & 0 & 0 & 0 \\ 0 & 0 & 0 & 0 & 1 & x & y & xy \end{bmatrix} \begin{Bmatrix} \beta_1 \\ \beta_2 \\ \beta_3 \\ \cdots \\ \beta_7 \\ \beta_8 \end{Bmatrix} = \mathbf{P}\boldsymbol{\beta} \tag{4.23}$$

where $\mathbf{P}$ denotes the trial function matrix and $\boldsymbol{\beta}$ is a vector of undetermined parameters, calculated the same way as the vector of strain parameters $\boldsymbol{\alpha}$ used to approximate the strain fields (equations (3.50), (3.51), (3.52)):

$$\boldsymbol{\beta} = \mathbf{A}^{-1}\mathbf{C}\Delta\mathbf{q}^{e}, \quad \mathbf{A} = \iint_{\Omega} \mathbf{P}^{\mathbf{T}}\mathbf{P}\, dxdy, \quad \mathbf{C}\Delta\mathbf{q}^{e} = \iint_{\Omega} \mathbf{P}^{\mathbf{T}}\boldsymbol{\theta}\, dxdy \tag{4.24}$$

The slope field $\boldsymbol{\theta}$ is therefore expressed in terms of the slope-displacement matrix $\mathbf{G}$:

$$\boldsymbol{\theta} = \mathbf{P}\mathbf{A}^{-1}\mathbf{C}\Delta\mathbf{q}^{\mathbf{e}} = \mathbf{G}\Delta\mathbf{q}^{\mathbf{e}} \tag{4.25}$$

The matrix $\mathbf{A}$ appearing in (4.24) can easily be evaluated, as was shown in Chap. 3. The matrix $\mathbf{C}$ in (4.24) can be evaluated through the quasi-conforming technique as follows (Shi and Voyiadjis, 1990):

$$
\begin{aligned}
C_{1i}\Delta q_{ei} &= \int_{\Omega} \frac{\partial \Delta w}{\partial x} dxdy = \oint \Delta w n_x ds, \quad (i = 1, 2, 3, \ldots, N_{ed}) \\
C_{2i}\Delta q_{ei} &= \int_{\Omega} \frac{\partial \Delta w}{\partial x} x dxdy = \oint \Delta w x n_x ds - \int_{\Omega} \Delta w dxdy \\
&= \oint \Delta w x n_x ds - \int_{-1}^{1}\int_{-1}^{1} \Delta w(\xi, \eta) |J| d\xi d\eta \\
C_{3i}\Delta q_{ei} &= \int_{\Omega} \frac{\partial \Delta w}{\partial x} y dxdy = \oint \Delta w y n_x ds \\
C_{4i}\Delta q_{ei} &= \int_{\Omega} \frac{\partial \Delta w}{\partial x} xy dxdy = \oint \Delta w x y n_x ds - \int_{\Omega} \Delta w y dxdy \\
&= \oint \Delta w x y n_x ds - \int_{-1}^{1}\int_{-1}^{1} \Delta w(\xi, \eta)\, y(\xi, \eta) |J| d\xi d\eta
\end{aligned}
\tag{4.26}
$$

where N_{ed} denotes the number of the nodal displacement variables in an element; $n_x = \cos(\mathbf{n}, x)$ is the cosine of the angle between the normal vector to the boundary and a direction of the x axis; s is the tangential coordinate along an element boundary; $|J|$ is the Jacobian; and $\Delta w(\xi, \eta)$ is an interpolation of the transverse displacement of the element in the isoparametric coordinates. We use the cubic interpolation of Δw along the boundary of the elements given by Hu (1981) to evaluate the **C** matrix:

$$
\begin{aligned}
\Delta w(s) = &\left[1 - \xi + \lambda\left(\xi - 3\xi^2 + 2\xi^3\right)\right]\Delta w_i \\
&+ \left[\xi - \xi^2 + \lambda\left(\xi - 3\xi^2 + 2\xi^2\right)\right]\frac{l}{2}\Delta\phi_{si} \\
&+ \left[\xi - \lambda\left(\xi - 3\xi^2 + 2\xi^3\right)\right]\Delta w_j \\
&+ \left[-\xi + \xi^2 + \lambda\left(\xi - 3\xi^2 + 2\xi^2\right)\right]\frac{l}{2}\Delta\phi_{sj} \\
\xi = \frac{2s}{l_{ij}}; \quad -\frac{l}{2} \le s \le \frac{l}{2}; \quad -1 \le \xi \le 1; \quad &\lambda = \frac{1}{\left(1 - 12\dfrac{D}{TL^2}\right)}
\end{aligned}
\tag{4.27}
$$

where l is the length of the side of the element; $\Delta\phi_{si}, \Delta\phi_{sj}$ are tangential rotations at nodes i and j, respectively, and D, T are flexural and transverse shear rigidities, respectively. The influence of parameter λ was discussed in the previous chapter.

Using (4.25), the virtual work principle given by (4.18) can now be rewritten as:

$$\iint_{\Omega} \left(\delta\boldsymbol{\varepsilon}_{\mathbf{b}}{}^{\mathbf{T}}\mathbf{D}\boldsymbol{\varepsilon}_{\mathbf{b}} + \delta\boldsymbol{\varepsilon}_{\mathbf{m}}{}^{\mathbf{T}}\mathbf{S}\boldsymbol{\varepsilon}_{\mathbf{m}} + \delta\boldsymbol{\varepsilon}_{\mathbf{s}}{}^{\mathbf{T}}\mathbf{T}\boldsymbol{\varepsilon}_{\mathbf{s}}\right) dxdy + \delta\Delta\mathbf{q}^{e^{\mathbf{T}}}\mathbf{K}_{\mathbf{g}}\Delta\mathbf{q}^{e}$$
$$= {}^{k+1}R - \iint_{\Omega} \left(\delta\boldsymbol{\varepsilon}_{\mathbf{b}}{}^{\mathbf{Tk}}\mathbf{M} + \delta\boldsymbol{\varepsilon}_{\mathbf{m}}{}^{\mathbf{Tk}}\mathbf{N} + \delta\boldsymbol{\varepsilon}_{\mathbf{s}}{}^{\mathbf{Tk}}\mathbf{Q}\right) dxdy \tag{4.28}$$

where $\mathbf{K_g}$ is the initial stress matrix defined as:

$$\mathbf{K_g} = \iint_{\Omega} \mathbf{G}^{\mathbf{Tk}}\mathbf{F}\mathbf{G}dxdy \tag{4.29}$$

Substituting (4.19), (4.20), (4.21) into the right side of (4.28), we write:

$$\iint_{\Omega} \left(\delta\boldsymbol{\varepsilon}_{\mathbf{b}}{}^{\mathbf{Tk}}\mathbf{M} + \delta\boldsymbol{\varepsilon}_{\mathbf{m}}{}^{\mathbf{Tk}}\mathbf{N} + \delta\boldsymbol{\varepsilon}_{\mathbf{s}}{}^{\mathbf{Tk}}\mathbf{Q}\right) dxdy = \delta\Delta\mathbf{q}^{\mathbf{T}}\Delta\mathbf{f} \tag{4.30}$$

where $\mathbf{f}$ is the internal force vector resulting from the unbalanced forces in configuration k and is expressed as:

$$\mathbf{f} = \iint_{\Omega} \left(\mathbf{B}_{\mathbf{b}}{}^{\mathbf{Tk}}\mathbf{M} + \mathbf{B}_{\mathbf{m}}{}^{\mathbf{Tk}}\mathbf{N} + \mathbf{B}_{\mathbf{s}}{}^{\mathbf{Tk}}\mathbf{Q}\right) dxdy \tag{4.31}$$

Similarly, substitution of (4.19), (4.20), (4.21) and (4.30) into (4.28) yields:

$$\sum_{elem} \delta\Delta\mathbf{q}^{e^{\mathbf{T}}} \left(\mathbf{K_e} + \mathbf{K_g}\right) \Delta\mathbf{q}^{e} = {}^{k+1}R - \sum_{elem} \delta\Delta\mathbf{q}^{e^{\mathbf{T}}}\Delta\mathbf{f} \tag{4.32}$$

where $\mathbf{K_e}$ is a linear elastic stiffness matrix of the element given by:

$$\mathbf{K_e} = \iint_{\Omega} \left(\mathbf{B_b}{}^{\mathbf{T}}\mathbf{D}\mathbf{B_b} + \mathbf{B_m}{}^{\mathbf{T}}\mathbf{S}\mathbf{B_m} + \mathbf{B_s}{}^{\mathbf{T}}\mathbf{T}\mathbf{B}_s\right) dxdy \tag{4.33}$$

Redefining the total external virtual work as:

$${}^{k+1}R = {}^{k+1}R^{*}\delta\Delta\mathbf{q} \tag{4.34}$$

we finally obtain:

$$\left(\mathbf{K_e} + \mathbf{K_g}\right) \Delta\mathbf{q}^{e} - {}^{k+1}R^{*} + \Delta\mathbf{f} = 0 \tag{4.35}$$

or:

$$\mathbf{K_{eg}}\Delta\mathbf{q} = {}^{k+1}R^{*} - \Delta\mathbf{f} \tag{4.36}$$

where:

$$\mathbf{K_{eg}} = \mathbf{K_e} + \mathbf{K_g} \tag{4.37}$$

The tangent stiffness matrix given by equation (4.37) is similar to that presented by Shi and Voyiadjis (1990). Our formulation however, is much more general, as it is universal and suitable for analysis of plates, shells, and beams.

One of the most important features of the derived tangent stiffness is its explicit form. This is because application of the quasi-conforming technique in the formulation of both the linear elastic stiffness matrix and the initial stress stiffness matrix allows all of the integrations to be performed analytically. This makes our model extremely efficient in terms of computer time and power, at the same time that it is mathematically consistent. All the matrices of the stiffness matrix of the element can be integrated analytically and exactly, without use of the numerical selective reduced integration.

4.5 Numerical Example

For the purpose of analysis, we developed a finite element code in programming language Fortran 95. A modified Newton-Raphson technique was used to solve a system of non-linear, incremental equations. The external forces in the system of the (4.36) are balanced by the iteration scheme. The local increments at the iterations are calculated using the arc-length method (Crisfield, 1991). The results obtained by our model were computed using a personal computer. Further explanation of the numerical techniques used here is provided in Chap. 7.

The example used to verify the validity and accuracy of our model is that of a pinched hemispherical shell. This benchmark problem is commonly used to test the performance of shell elements with the influence of the large displacements taken into account. The results obtained by means of our formulation here will be compared with other formulations available in the literature. Table 4.1 gives the references used here, as well as their abbreviations.

We consider a pinched hemispherical shell (Morley Sphere) with an 18^0 hole at the top, subjected to four point loads alternating in sign at 90^0 intervals on the equator. Because of symmetry, we model only a quadrant. The geometry, deformed shape, and material properties are shown in Fig. 4.5. The linear elastic solution of the problem often serves as a benchmark problem for linear analysis of shells

Table 4.1 Models used and abbreviations

Name	Description
F&O	Numerical solution of pinched hemispherical shell by Flores and Onate (2001)
SIMO	Numerical solution of pinched hemispherical shell by Simo et al. (1990)
W&V	The present formulation without shear forces included in the yield function

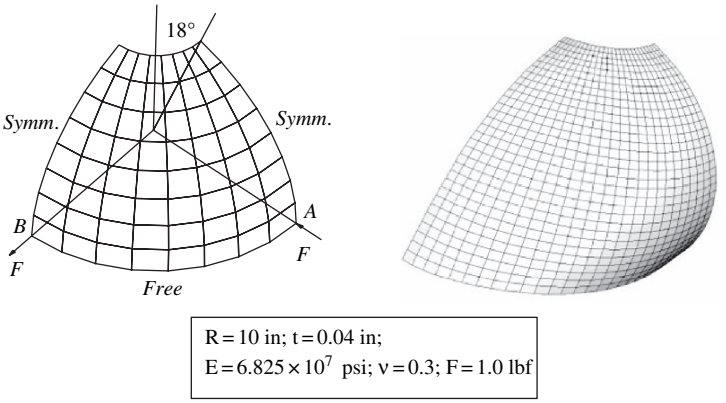

Fig. 4.5 Pinched hemispherical shell (Morley Sphere): geometry, deformed shape, and material properties (Voyiadjis and Woelke, 2006)

(Morley and Morris, 1978; Belytschko et al., 1985; MacNeal and Harder, 1985; Simo et al., 1989a,b; Shi and Voyiadjis, 1991a; Voyiadjis and Woelke, 2006). Ample sections of the shell rigidly rotate under these loading conditions; hence, precise modeling of the rigid body motion is essential for good performance in this test (Belytschko et al., 1985). Simo et al., (1990) as well as Parish (1995), Hauptmann and Schweizerhof (1998), and Flores and Onate (2001) used the same problem with an increased load factor to examine the capabilities of their models in the description of large deformations. We compare the results provided by our formulation with those by Simo et al. and Flores and Onate. In the case of geometrically non-linear analysis, the deflections under alternating forces are not equal; we therefore plot the equilibrium path for both points of application of the load – A and B. The load displacement path is plotted in Fig. 4.6.

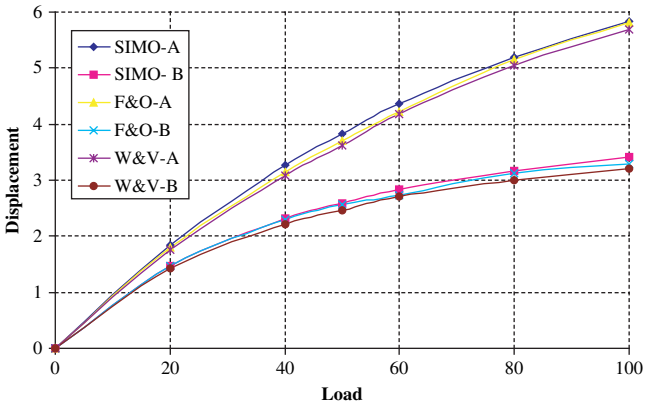

Fig. 4.6 Pinched hemispherical shell (Morley Sphere) – Equilibrium paths (**A**-point under an inward load, **B**-point under an outward load) (Voyiadjis and Woelke, 2006)

The displacements calculated with our model are very accurate and compare very well with the reference solutions, confirming that it gives adequate representation of large displacements.

The reliability of our formulation will be further verified through a series of discriminating examples in Chap. 5, where the elasto-plastic behavior of shells is investigated. The large displacement representation is crucial for accurate predictions of the load-displacement curve for both plates and shells undergoing inelastic deformations. Hence, close approximations of the elasto-plastic equilibrium path and collapse load confirm the robustness of the large displacement formulation.

4.6 Summary

We evaluated the ability of our model to simulate large rigid rotations and translations in shells with a numerical example in Sect. 4.5. The displacements calculated with the model are very accurate and compare excellently with the reference solutions.

Because certain sections of the structure deforming inelastically usually undergo large displacements, representation of geometrical non-linearities is crucial for the accuracy of elasto-plastic and damage analysis of shells. If the computational model for the elasto-plastic analysis of shells with large rotations performs well in the elasto-plastic analysis, it also confirms, although indirectly, the adequate representation of large displacements. We discuss the results of the elasto-plastic investigations in Chap. 5.

To thoroughly examine the functioning of our algorithm in the description of large displacements in shells, further testing would be necessary. We discuss the ability of, model to simulate the plasticity and damage in plates and shells in the following chapters.

References

Argyris, J. (1982). An excursion into large rotations. Comp. Meth. Appl. Mech. Eng., 32, 85–155

Bathe, K.J. (1982). Finite Element Procedures in Engineering Analysis. Prentice-Hall, Englewood Cliffs, NJ.

Belytschko, T., Stolarski, H., Liu, W.K., Carpenter, N., Ong, J.S.-J. (1985). Stress projection for membrane and shear locking in shell finite elements. Comp. Meth. Appl. Mech. Eng., 51, 221–258.

Cook, R.D., Malkus, D.S., Plesha, M.E. (1989). Concepts and applications of finite element analysis. 3rd edition, John Wiley & Sons, New York.

Crisfield, M.A. (1991). Non-linear Finite element Analysis of Solids and Structures. Vol. 1. John Wiley & Sons Ltd, New York.

Flores, F.G. and Onate, E. (2001). A basic thin shell triangle with only translational DOFs for large strain plasticity. Int. J. Num. Meth. Eng., 51, 57–83.

Hauptmann, R., Schweizerhof, K. (1998). A systematic development of ‘solid-shell’ element formulations for linear and non-linear analyses employing only displacement degrees of freedom. Int. J. Num. Meth. Engng., 42, 49–69.

Horrigmoe, G. and Bergan, P.G. (1978). Nonlinear analysis of free form shells by flat elements. Comp. Meth. Appl. Mech. Eng., 16, 11–35.

Hu, H-C. (1981). The Variational Principles in Elasticity and its Application. Scientific Publisher, Beijing.

Kebari, H. and Cassell, A.C. (1992). A stabilized 9-node non-linear shell element. Int. J. Num. Meth. Eng., 35, 37–61.

MacNeal, H.R. and Harder, R.L. (1985). A proposed stadard set of problems to test finite element accuracy. Finite Elem. Anal. Design, 1, 3–20. North-Holland.

Morley, L.S.D and Morris, A.J. (1978). Conflict between finite elements and shell theory. Royal Aircraft Establishment Report. London.

Parish, H. (1995). A continuum-based shell theory for non-linear applications. Int. J. Num. Meth. Eng., 38, 1855–1883.

Shi, G. and Atluri, S.N. (1988). Elasto-plastic large deformation analysis of space frames: A plastic-hinge and stress-based explicit derivation of tangent stiffnesses. Int. J. Num. Meth. Eng., 26, 589–615.

Shi, G. and Voyiadjis, G.Z. (1990). A simple C^0 quadrilateral thick/thin shell element based on the refined shell theory and the assumed strain fields. Int. J. Solids Struct., 27, 3, 283–298.

Shi, G. and Voyiadjis, G.Z. (1991a). Geometrically nonlinear analysis of plates by assumed strain element with explicit tangent stiffness. Comp. Struct., 41, 757–763.

Shi, G. and Voyiadjis, G.Z. (1991b). Simple and efficient shear flexible two node arch/beam and four node cylindrical shell/plate finite element. Int. J. Num. Meth. Eng., 31, 759–776.

Simo, J.C.; Fox, D.D. and Rifai, M.S. (1989a). On a stress resultant geometrically exact shell model. Comp. Meth. Appl. Mech. Eng., 73, 53–92. North-Holland

Simo, J.C.; Fox, D.D. and Rifai, M.S. (1989b). On a stress resultant geometrically exact shell model. Part II: The linear Theory. Comp Meth. Appl. Mech. Eng., 73, 53–92. North-Holland

Simo, J.C.; Fox, D.D. and Rifai, M.S. (1990). On a stress resultant geometrically exact shell model. Part III: Computational Aspects of the Nonlinear Theory. Comp. Meth. Appl. Mech. Eng., 79, 21–70. North-Holland

Tang, L., Chen, W. and Liu, Y. (1980). Quasi-conforming elements for finite element analysis. J. DIT, 19, 2.

Tang, L., Chen, W. and Liu, Y. (1983). String net function applications and quasi conforming technique. In Hybrid and Mixed Finite Element Methods, Wiley, New York.

Voyiadjis, G.Z. and Woelke, P. (2006). General non-linear finite element analysis of thick plates and shells. Int. J. Solids Struct., 43, 2209–2242.

Chapter 5
Elasto-Plastic Geometrically Non-linear Finite Element Analysis of Thick Plates and Shells

5.1 Introduction

In this chapter, the computational model for the analysis of shells presented in the previous chapters is further developed to simulate the elasto-plastic behavior of plates and shells with the effect of large rotations considered. The shell constitutive equations given in Chap. 2 are again adopted as a base for the formulation. A simple C^0 quadrilateral, geometrically non-linear shell element presented in Chapter 4 is extended to account for material non-linearities.

We adopt the non-layered approach and the plastic node method (Ueda and Yao, 1982) in the treatment of material non-linearities. We use the Iliushin's yield function expressed in terms of stress resultants and stress couples (Iliushin, 1956), modified to investigate the development of plastic deformations across the thickness (Crisfield, 1981a), as well as the influence of the transverse shear forces on the plastic behavior of plates and shells (Shi and Voyiadjis, 1992). Both isotropic and kinematic hardening rules are included in the yield function, with the latter derived on the basis of the Armstrong and Frederick evolution equation of backstress (Armstrong and Frederick, 1966), thus reproducing the Bauschinger effect.

The strongest motivation for the advances in shell elements is not only accuracy but computational efficiency. Shells can be analyzed by means of solid, three-dimensional elements, defined in the stress space. This, however, can require prohibitively large storage in the computer. The shell elements based on the shell constitutive equations, relating stress resultants and stress couples to strains have proven to be as accurate as the stress-based elements, while while less expensive; they are capable of approximating the exact solutions of problems with complicated geometry and boundary conditions. Moreover, the purpose of most analysis and design procedures used by structural engineers is to determine the internal forces and bending moments in the structure to enable a design able to resist those forces. Ideally, the analysis directed to the engineering community is performed in the stress resultant space. Nevertheless, using the stress resultant models in the elasto-plastic investigations has been cumbersome, mainly because of a lack of suitable yield functions expressed in terms of the forces and moments, capable of representing the progressive plastification of the cross section, the influence of all the components of the stress tensor on plastic behavior, and isotropic and kinematic hardening effects.

G.Z. Voyiadjis, P. Woelke, *Elasto-Plastic and Damage Analysis of Plates and Shells*,

© Springer-Verlag Berlin Heidelberg 2008

The most important feature of the our framework is an ablity to obtain an accurate, stress resultant-based yield surface that accounts for the gradual growth of the plastic curvatures, influence of the shear forces on yielding, and isotropic and kinematic hardening rules, that represent the Bauschinger effect. Application of such a yield surface is convenient from an engineering point of view, as it allows taking the full advantage of the shell elements not only in the elastic, but also in the plastic zone, making the algorithm highly efficient. The approach is effective because, unlike in the layered approach where the yield function is expressed in terms of the stresses, discretization through the thickness is unnecessary. Furthermore, it leaves room for further enhancements allowing for example approximation of the effects of damage and/or rate dependence. Damage of shells is discussed in Chap. 6. These advances lead to the objective of performing a full and comprehensive analysis of shells through the use of internal forces and moments.

All of the assumptions made in previous chapters are still valid. We again use the shell equations presented in Chap. 2. We adopt the linear elastic stiffness matrix, derived in Chap. 3 and the large displacements examined in Chap. 4. The advantage of the explicit form of the elastic stiffness matrix, obtained by means of the quasi-conforming technique (Tang et al., 1980, 1983), is even more evident in non-linear computations where the stiffness matrix must be evaluated many times during the analysis. As we follow the non-layered approach, numerical integration is not performed at any stage of the analysis. All the integrals are calculated analytically, with the results later introduced into a computer code.

The order of this chapter is as follows: in Sect. 5.2 the yield surface with the flow and hardening rules are derived. The elasto-plastic, large displacement stiffness matrix is formulated in Sect. 5.3. The numerical examples verifying the performance of the constitutive equation, as well as the numerical procedure, are given in Sect. 5.4.

5.2 Yield Criterion and Hardening Rule

5.2.1 Iliushin's Yield Function (Iliushin, 1956)

As discussed in the Introduction, we use a yield criterion expressed in terms of stress resultants and couples, similar to the Iliushin's yield function modified to account for the progressive development of the plastic curvatures and shear forces, as given by Shi and Voyiadjis (1992). The Iliushin's yield function F can be written as:

$$F = \frac{M^2}{{M_0}^2} + \frac{N^2}{{N_0}^2} + \frac{1}{\sqrt{3}} \frac{|MN|}{M_0 N_0} - \frac{Y(k)}{{\sigma_0}^2} = 0 \tag{5.1}$$

or:

$$F = \frac{|M|}{M_0} + \frac{N^2}{{N_0}^2} - \frac{Y(k)}{{\sigma_0}^2} = 0 \tag{5.2}$$

where N and M are the stress intensities given by:

$$N^2 = {N_x}^2 + {N_y}^2 - N_x N_y + 3{N_{xy}}^2 \tag{5.3}$$

$$M^2 = {M_x}^2 + {M_y}^2 - M_x M_y + 3{M_{xy}}^2 \tag{5.4}$$

$$MN = M_x N_x + M_y N_y - \frac{1}{2} M_x N_y - \frac{1}{2} M_y N_x + 3{M_{xy}}^2 \tag{5.5}$$

and M_0 and N_0 are, respectively, the moment capacity of the cross section when the plastic hinge has formed, i.e., the cross section is fully plastic, and the normal force capacity of the cross section given by:

$$M_0 = \frac{\sigma_0 h^2}{4},\ N_0 = \sigma_0 h \tag{5.6}$$

The symbol σ_0 is the uniaxial yield stress; $Y(k)$ is a material parameter, which depends on the isotropic hardening parameter k; h is the thickness of the shell, and $|.|$ denotes the absolute value; and N_x, N_y, N_{xy} and M_x, M_y, M_{xy} are the stress resultants and stress couples, respectively, defined in terms of the strains of the shell by (3.18), (3.19), (3.20), (3.21), (3.22), (3.23), (3.24), (3.25) and shown in Fig. 5.1.

5.2.2 *Influence of the Shear Forces*

The form of the yield condition given by (5.1) can be easily derived from the von Mises function and the definition of normal stresses at top and bottom surfaces of the shell, as shown by Bieniek and Funaro (1976). To examine the influence of the transverse shear forces on the plastic behavior of shells, the yield surface given by (5.1) must be modified. We include the transverse shear forces Q_x, Q_y (Fig. 5.1) by altering the stress intensity given by (5.3) following (Shi and Voyiadjis, 1992):

$$N^2 = {N_x}^2 + {N_y}^2 - N_x N_y + 3\left({N_{xy}}^2 + {Q_x}^2 + {Q_y}^2\right) \tag{5.7}$$

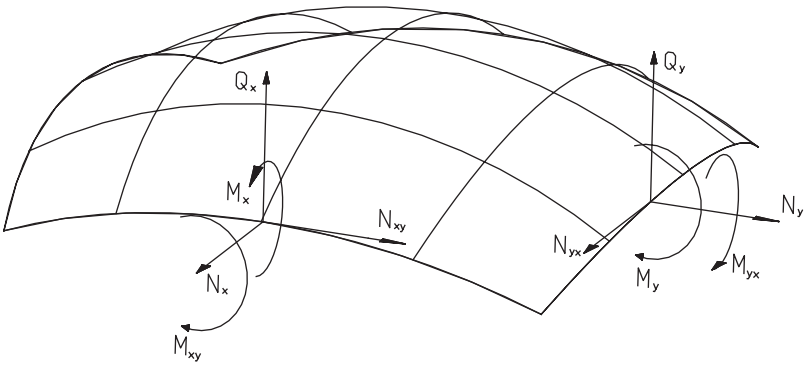

Fig. 5.1 Stress resultants on a shell element (Voyiadjis and Woelke, 2006)

We show below, that the representation of the shear forces in thick plastic plates and shells can be very important under certain conditions.

5.2.3 Development of the Plastic Hinge

For a bending dominant situation, according to (5.1) or (5.2), the structure will behaves linearly until the entire cross section is plastic, i.e., the plastic hinge has formed. In reality, however, plastic curvature develops progressively from the outer fibers of the shell or plate, and the material behaves non-linearly as soon as the outer fibers start to yield. To account for the development of plastic curvature across the thickness, Crisfield (1981a) introduced a plastic curvature parameter $\alpha\,(\bar{\kappa}^p)$ into the (5.1), (5.2):

$$F = \frac{M^2}{\alpha^2 {M_0}^2} + \frac{N^2}{{N_0}^2} + \frac{1}{\sqrt{3}\alpha}\frac{|MN|}{M_0 N_0} - \frac{Y(k)}{{\sigma_0}^2} = 0 \tag{5.8}$$

or:

$$F = \frac{|M|}{\alpha M_0} + \frac{N^2}{{N_0}^2} - \frac{Y(k)}{{\sigma_0}^2} = 0 \tag{5.9}$$

where α was chosen such that αM_0 follows the uniaxial moment-plastic curvature relation:

$$\alpha = 1 - \frac{1}{3}\exp\left(-\frac{8}{3}\bar{\kappa}^p\right) \tag{5.10}$$

$$\bar{\kappa}^p = \sum \Delta\bar{\kappa}^p = \frac{Eh}{\sqrt{3}\sigma_0}\sum\left(\left(\Delta{\kappa_x}^p\right)^2 + \left(\Delta{\kappa_y}^p\right)^2 + \Delta{\kappa_x}^p\Delta{\kappa_y}^p + \left(\Delta{\kappa_{xy}}^p\right)^2/4\right)^{1/2} \tag{5.11}$$

$\bar{\kappa}^p$ is the equivalent plastic curvature $\Delta{\kappa_x}^p$, $\Delta{\kappa_y}^p$ and $\Delta{\kappa_{xy}}^p$ are the increments of the plastic curvatures. For $\bar{\kappa}^p = 0, \alpha = 2/3$ and we obtain $\alpha M_0 = \dfrac{\sigma_0 t^2}{6}$ which represents the moment capacity at first yield. If, however, $\bar{\kappa}^p = \infty \rightarrow \alpha = 1$ we obtain the moment capacity of the fully plastic cross section. Therefore, through the introduction of the plastic curvature parameter α we account for the progressive development of the plastic curvatures and predict the first yield.

5.2.4 Bauschinger Effect and Kinematic Hardening Rule

The Bauschinger effect is a phenomenon observed in the experimental tests of metals. For most metals the stress–strain curve in a simple compression test is almost identical to that in a simple tension test. If, however, the specimen is plastically prestrained in tension and the load is then reversed, the stress–strain curve in compression differs considerably from the curve that, would be obtained on reloading

Fig. 5.2 Bauschinger effect

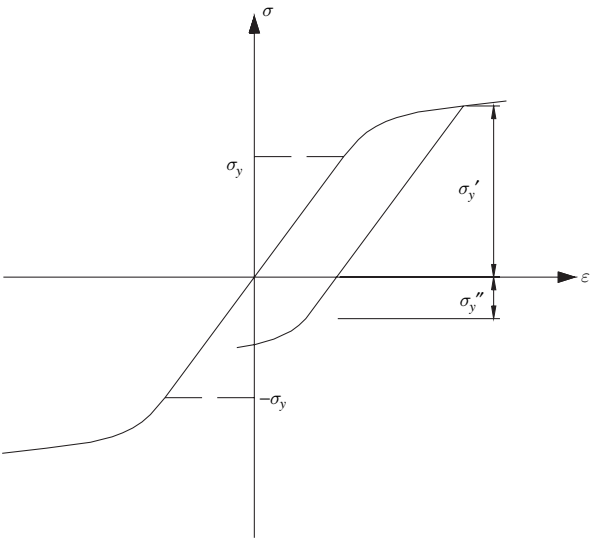

the specimen in tension, or on loading the undisturbed specimen in compression. As shown in Fig. 5.2 for the specimen with the preloading $\sigma_y{}'$ in tension, its corresponding compression yielding occurs at the stress level $\sigma_y{}''$, which is less than the initial yield stress σ_y and much less than the subsequent yield point $\sigma_y{}'$. The Bauschinger effect and is usually present when there is a load reversal. This indicates that the strain is not a function of the stress alone, but depends on the previous loading history. Thus, the material is load path dependent (Chen and Han, 1988). To model the Bauschinger effect requires an accurate kinematic hardening rule, which represents the rigid body motion of the yield surface in the stress or stress resultant space. The shape and orientation of the initial surface is maintained. Our work focuses on development of a stress resultant-based model; hence, the need for such a kinematic hardening rule.

Bieniek and Funaro (1976) introduced residual bending moments ("hardening parameters"), allowing for description of the Bauschinger effect. These were later successfully applied for dynamic (Bieniek et al., 1976) and viscoplastic dynamic (Atkatsh et al., 1982, 1983) analysis of shells. To correctly determine the rigid translation of the yield surface in the stress resultant space, we need not only residual bending moments, but also residual normal and shear forces. These hardening parameters are related directly to backstress, representing the center of the yield surface in the stress space. We introduce a new kinematic hardening rule for plates and shells, with residual stress resultants, derived directly from the evolution of the backstress given by Armstrong and Frederick (1966). The yield surface is expressed as:

$$F^* = \frac{|M^*|}{\alpha M_0} + \frac{(N^*)^2}{{N_0}^2} - \frac{Y(k)}{{\sigma_0}^2} = 0 \tag{5.12}$$

where:

$$\begin{aligned}\left(N^*\right)^2 &= \left(N_x - {N_x}^*\right)^2 + \left(N_y - {N_y}^*\right)^2 - \left(N_x - {N_x}^*\right)\left(N_y - {N_y}^*\right) \\ &\quad + 3\left[\left(N_{xy} - {N_{xy}}^*\right)^2 + \left(Q_x - {Q_x}^*\right)^2 + \left(Q_y - {Q_y}^*\right)^2\right]\end{aligned} \tag{5.13}$$

$$\begin{aligned}\left(M^*\right)^2 &= \left(M_x - {M_x}^*\right)^2 + \left(M_y - {M_y}^*\right)^2 - \left(M_x - {M_x}^*\right)\left(M_y - {M_y}^*\right) \\ &\quad + 3\left(M_{xy} - {M_{xy}}^*\right)^2\end{aligned} \tag{5.14}$$

and ${M_x}^*$, ${M_y}^*$, ${M_{xy}}^*$, ${N_x}^*$, ${N_y}^*$, ${N_{xy}}^*$, ${Q_x}^*$, ${Q_y}^*$ are previously described residual bending moments, normal forces, and shear forces, respectively. We now proceed to the definition of the kinematic hardening parameters. For conciseness, we use indicial notation in the derivation, and engineering notation only for the final result. The Armstrong and Frederick's evolution of backstress ρ_{ij} is given by:

$$\Delta\rho_{ij} = c\Delta{\varepsilon_{ij}}^p - a\rho_{ij}\Delta{\varepsilon_{eq}}^p \tag{5.15}$$

where a and c are material constants and the equivalent plastic strain increment is:

$$\Delta{\varepsilon_{eq}}^p = \sqrt{\frac{2}{3}\Delta{\varepsilon_{ij}}^p\Delta{\varepsilon_{ij}}^p} \tag{5.16}$$

The backstress represents the center of the translated yield surface in the stress space. It has the same dimension as the stress tensor. To compute the stress resultants we need to integrate the stresses over the thickness of the shell. We use the same definition to derive the hardening parameters, which represent the center of the yield surface in the stress resultant space. We therefore need to integrate the backstress over the thickness of the shell or plate to obtain residual normal and shear forces and bending moments. The definitions of the increments of hardening parameters are:

$$\Delta{N_{ij}}^* = \int_{-h/2}^{h/2} \Delta\rho_{ij}\,dz \tag{5.17}$$

$$\Delta{M_{ij}}^* = \int_{-h/2}^{h/2} \Delta\rho_{ij}z\,dz \tag{5.18}$$

Substituting (5.15) into (5.17) we obtain:

$$\Delta{N_{ij}}^* = \int_{-h/2}^{h/2} \left(c\Delta{\varepsilon_{ij}}^p - a\rho_{ij}\Delta{\varepsilon_{eq}}^p\right) dz \tag{5.19}$$

The increments of plastic strains $\Delta\varepsilon_{ij}{}^{p}$ in (5.19) are membrane strains, due to normal forces only. These are constant across the thickness of the shell; therefore, we can write:

$$\Delta N_{ij}{}^{*} = ch\Delta\varepsilon_{ij}{}^{p} - ah\rho_{ij}\Delta\varepsilon_{eq}{}^{p} \tag{5.20}$$

Defining the hardening parameters similarly as stress resultants:

$$h\rho_{ij} = N_{ij}{}^{*} \tag{5.21}$$

we rewrite (5.21) as:

$$\Delta N_{ij}{}^{*} = ch\Delta\varepsilon_{ij}{}^{p} - aN_{ij}{}^{*}\Delta\varepsilon_{eq}{}^{p} \tag{5.22}$$

Constants a and c are similar to Bieniek and Funaro (1976):

$$a = c = \beta_1 (1 - F)\frac{1}{h}\frac{N_0}{\varepsilon_0} \tag{5.23}$$

where N_0 and ε_0 are given by:

$$N_0 = \sigma_0 h,\ \varepsilon_0 = \sigma_0 / E \tag{5.24}$$

where F is a yield surface given in (5.9) and h is the thickness of the plate and β_1 is a constant. We therefore obtain:

$$\Delta N_{ij}{}^{*} = \beta_1 (1 - F)\frac{N_0}{\varepsilon_0}\left[\Delta\varepsilon_{ij}{}^{p} - \frac{1}{h}N_{ij}{}^{*}\Delta\varepsilon_{eq}{}^{p}\right] \tag{5.25}$$

Similarly, substituting (5.15) into (5.18) we determine the increments of the residual bending moments:

$$\Delta M_{ij}{}^{*} = \int_{-h/2}^{h/2} \left(c\Delta\varepsilon_{ij}{}^{p} - a\rho_{ij}\Delta\varepsilon_{eq}{}^{p}\right) z dz \tag{5.26}$$

where $\Delta\varepsilon_{ij}{}^{p}$ and $\Delta\varepsilon_{eq}{}^{p}$ are:

$$\Delta\varepsilon_{ij}{}^{p} = z\Delta\kappa_{ij}{}^{p} \tag{5.27}$$

$$\Delta\varepsilon_{eq}{}^{p} = \sqrt{\frac{2}{3}z^2\Delta\kappa_{ij}{}^{p}\Delta\kappa_{ij}{}^{p}} \tag{5.28}$$

Substituting (5.27) into (5.26) and integrating it we have:

$$\Delta {M_{ij}}^* = c\frac{h^3}{12}\Delta {\kappa_{ij}}^p - a\frac{h^3}{12}\rho_{ij}\Delta {\kappa_{eq}}^p \tag{5.29}$$

$$\Delta {M_{ij}}^* = c\frac{h^3}{12}\Delta {\kappa_{ij}}^p - a\frac{h}{2}{M_{ij}}^*\Delta {\kappa_{eq}}^p \text{ where } \rho_{ij}\frac{h^2}{6} = {M_{ij}}^* \tag{5.30}$$

The constants a and c are expressed similarly to those in (5.23):

$$a = c = \beta_2(1-F)\frac{12}{h^3}\frac{M_0}{\kappa_0} \tag{5.31}$$

which leads to:

$$\Delta {M_{ij}}^* = \beta_2(1-F)\frac{M_0}{\kappa_0}\left[\Delta {\kappa_{ij}}^p - \frac{6}{h^2}{M_{ij}}^*\Delta {\kappa_{eq}}^p\right] \tag{5.32}$$

The hardening parameters can now be rewritten in engineering notation as:

$$\begin{aligned}
&If\ F^* = 1\ and\ \nabla F^* > 0\ (plastic\ loading)\\
&\Delta {N_x}^* = \beta_1(1-F)\frac{N_0}{\varepsilon_0}\left[\Delta {\varepsilon_x}^p - \frac{1}{h}{N_x}^*\Delta {\varepsilon_{eq}}^p\right]\\
&\Delta {N_y}^* = \beta_1(1-F)\frac{N_0}{\varepsilon_0}\left[\Delta {\varepsilon_y}^p - \frac{1}{h}{N_y}^*\Delta {\varepsilon_{eq}}^p\right]\\
&\Delta {N_{xy}}^* = \beta_1(1-F)\frac{N_0}{\varepsilon_0}\left[\Delta {\varepsilon_{xy}}^p - \frac{1}{h}{N_{xy}}^*\Delta {\varepsilon_{eq}}^p\right]\\
&\Delta {Q_x}^* = \beta_1(1-F)\frac{N_0}{\varepsilon_0}\left[\Delta {\varepsilon_{xz}}^p - \frac{1}{h}{Q_x}^*\Delta {\varepsilon_{eq}}^p\right]\\
&\Delta {Q_y}^* = \beta_1(1-F)\frac{N_0}{\varepsilon_0}\left[\Delta {\varepsilon_{yz}}^p - \frac{1}{h}{Q_y}^*\Delta {\varepsilon_{eq}}^p\right]
\end{aligned} \tag{5.33}$$

$$\begin{aligned}
&\Delta {M_x}^* = \beta_2(1-F)\frac{M_0}{\kappa_0}\left[\Delta {\kappa_x}^p - \frac{6}{h^2}{M_x}^*\Delta {\kappa_{eq}}^p\right]\\
&\Delta {M_y}^* = \beta_2(1-F)\frac{M_0}{\kappa_0}\left[\Delta {\kappa_y}^p - \frac{6}{h^2}{M_y}^*\Delta {\kappa_{eq}}^p\right]\\
&\Delta {M_{xy}}^* = \beta_2(1-F)\frac{M_0}{\kappa_0}\left[\Delta {\kappa_{xy}}^p - \frac{6}{h^2}{M_{xy}}^*\Delta {\kappa_{eq}}^p\right]
\end{aligned} \tag{5.34}$$

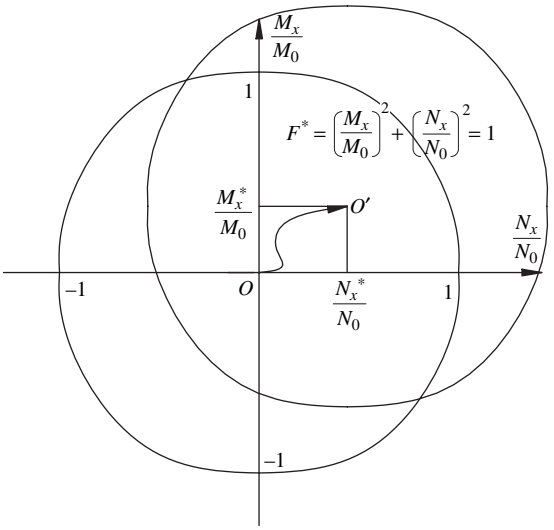

Fig. 5.3 Yield surface on $N_x M_x$ plane – interpretation of kinematic hardening parameter, O' is the center of transferred yield surface

$$If\ F^* < 1\ and\ \nabla F^* \leq 0\ (unloading\ or\ neutral\ loading)$$

$$\Delta N_x{}^* = \Delta N_y{}^* = \Delta N_{xy}{}^* = \Delta Q_x{}^* = \Delta Q_y{}^* = \Delta M_x{}^* = \Delta M_y{}^* = \Delta M_{xy}{}^* = 0 \tag{5.35}$$

Parameters β_1 and β_2 in the above formulation control the membrane force-membrane strain and moment-curvature relations. A value of $\beta_1 = \beta_2 = 2.0$ is found to be of sufficient accuracy in the representation of the behavior of shells.

We arrive at a final form of the yield function expressed in terms of stress resultants and couples, with isotropic and kinematic hardening rules. A graphic representation of the yield surface given by (5.12) on the $N_x M_x$ plane with $\alpha = 1$ and $Y = {\sigma_0}^2$ is shown in Fig. 5.3 (Woelke and Voyiadjis, 2005). Point O' denotes the transferred center of the yield surface.

5.3 Explicit Elasto-Plastic Tangent Stiffness Matrix with Large Displacements

We adopt the plastic node method (Ueda and Yao, 1982), i.e., the plastic deformations are considered to be concentrated in the plastic hinges. The yield function is checked only at each node of the finite element. If the combination of stress resultants satisfies the yield condition, that node is considered plastic. In this method the inelastic deformations are considered only at the nodes, while the interior of the element remains elastic.

When node i of the element becomes plastic, the yield function takes the form:

$$F^*{}_i\left(\mathbf{N_i}, \mathbf{Q_i}, \mathbf{M_i}, \mathbf{N^*_i}, \mathbf{Q^*_i}, \mathbf{M^*_i}, k\right) = 0 \tag{5.36}$$

where:

$$\mathbf{N_i} = \begin{Bmatrix} N_x \\ N_y \\ N_{xy} \end{Bmatrix}; \quad \mathbf{Q_i} = \begin{Bmatrix} Q_x \\ Q_y \end{Bmatrix}; \quad \mathbf{M_i} = \begin{Bmatrix} M_x \\ M_y \\ M_{xy} \end{Bmatrix} \tag{5.37}$$

$$\mathbf{N^*_i} = \begin{Bmatrix} N^*{}_x \\ N^*{}_y \\ N^*{}_{xy} \end{Bmatrix}; \quad \mathbf{Q^*_i} = \begin{Bmatrix} Q^*{}_x \\ Q^*{}_y \end{Bmatrix}; \quad \mathbf{M^*_i} = \begin{Bmatrix} M^*{}_x \\ M^*{}_y \\ M^*{}_{xy} \end{Bmatrix} \tag{5.38}$$

At the same time, the stress resultants must remain on the yield surface, i.e., the consistency condition must be satisfied:

$$\begin{aligned} &\frac{\partial F^*{}_i}{\partial \mathbf{M_i}} d\mathbf{M_i} + \frac{\partial F^*{}_i}{\partial \mathbf{N_i}} d\mathbf{N_i} + \frac{\partial F^*{}_i}{\partial \mathbf{Q_i}} d\mathbf{Q_i} + \frac{\partial F^*{}_i}{\partial \mathbf{M^*_i}} d\mathbf{M^*_i} \\ &+ \frac{\partial F^*{}_i}{\partial \mathbf{N^*_i}} d\mathbf{N^*}_i + \frac{\partial F^*{}_i}{\partial \mathbf{Q^*_i}} d\mathbf{Q^*_i} + \frac{\partial F^*{}_i}{\partial k} d\mathbf{k_i} = 0 \end{aligned} \tag{5.39}$$

We assume additive decomposition of strains into elastic and plastic parts:

$$\varepsilon = \varepsilon^e + \varepsilon^p \tag{5.40}$$

The associated flow rule is used here to determine the increments of plastic strains:

$$\Delta\kappa_x{}^p = \sum_{i=1}^{NPN} \Delta\lambda_i \frac{\partial F^*{}_i}{\partial M_{xi}} \tag{5.41}$$

where NPN is the number of plastic nodes in the element and $d\lambda_i$ is a plastic multiplier. The remaining increments of the plastic strains are obtained the same way. The plastic strain fields are interpolated as in the linear elastic analysis ((3.45), (3.46), (3.47)) rewritten here in the incremental form:

$$\Delta\boldsymbol{\varepsilon}_\mathbf{b}^\mathbf{p} = \begin{Bmatrix} \Delta\kappa_x{}^p \\ \Delta\kappa_y{}^p \\ 2\Delta\kappa_{xy}{}^p \end{Bmatrix}, \; \Delta\boldsymbol{\varepsilon}_\mathbf{m}^\mathbf{p} = \begin{Bmatrix} \Delta\varepsilon_x{}^p \\ \Delta\varepsilon_y{}^p \\ 2\Delta\varepsilon_{xy}{}^p \end{Bmatrix}, \; \Delta\boldsymbol{\varepsilon}_\mathbf{s}^\mathbf{p} = \begin{Bmatrix} \Delta\gamma_{xz}{}^p \\ \Delta\gamma_{yz}{}^p \end{Bmatrix} \tag{5.42}$$

or:

$$\Delta\boldsymbol{\varepsilon}_{\mathbf{b}} = \begin{Bmatrix} \dfrac{\partial \Delta\phi_x}{\partial x} \\ \dfrac{\partial \Delta\phi_y}{\partial y} \\ \dfrac{\partial \Delta\phi_x}{\partial y} + \dfrac{\partial \Delta\phi_y}{\partial x} \end{Bmatrix},\ \Delta\boldsymbol{\varepsilon}_{\mathbf{m}} = \begin{Bmatrix} \dfrac{\partial \Delta u}{\partial x} + \dfrac{\Delta w}{R} \\ \dfrac{\partial \Delta v}{\partial y} + \dfrac{\Delta w}{R} \\ \dfrac{\partial \Delta u}{\partial y} + \dfrac{\partial \Delta v}{\partial x} \end{Bmatrix},\ \Delta\boldsymbol{\varepsilon}_{\mathbf{s}} = \begin{Bmatrix} \dfrac{\partial \Delta w}{\partial x} - \phi_x - \dfrac{\Delta u}{R} \\ \dfrac{\partial \Delta w}{\partial y} - \phi_y - \dfrac{\Delta v}{R} \end{Bmatrix} \tag{5.43}$$

The assumption of an additive decomposition of strains can be extended to displacements, provided that the strains are small (Ueda and Yao, 1982; Shi and Voyiadjis, 1992). Although we take into account geometric non-linearities, we consider only large rigid rotations and translations, but small strains. We write:

$$q = q^e + q^p \tag{5.44}$$

Following the work of Shi and Voyiadjis (1992) we approximate the increments of plastic displacements by the increments of plastic strains. The plastic rotation $\Delta{\phi_x}^p$ is a function of both $\Delta{\kappa_x}^p$ and $\Delta{\kappa_{xy}}^p$, as can be deduced from (5.43). Assuming that increment of plastic nodal rotation $\Delta{\phi_{xi}}^p$ is proportional to the increment of elastic nodal rotation, $\Delta\phi_{xi}$ we express the former as:

$$\begin{aligned} \Delta{\phi_{xi}}^p &= \lim_{\delta\Omega\to 0} \iint_{\delta\Omega_i} \left[\Delta{\kappa_x}^p + \frac{\Delta{\phi_{xi}}^2}{\Delta{\phi_{xi}}^2 + \Delta{\phi_{yi}}^2} 2\Delta{\kappa_{xy}}^p \right] dxdy \\ &= \Delta\lambda_i \left[\frac{\partial {F^*}_i}{\partial M_{xi}} + \frac{2\Delta{\phi_{xi}}^2}{\Delta{\phi_{xi}}^2 + \Delta{\phi_{yi}}^2} \frac{\partial {F^*}_i}{\partial M_{xyi}} \right] \end{aligned} \tag{5.45}$$

where $\delta\Omega_i$ represents the infinitesimal neighborhood of node i. The vector of incremental nodal plastic displacements of the element at node i can then be expressed as:

$$\Delta\mathbf{q_i^p} = \mathbf{a_i}\Delta\lambda_i \tag{5.46}$$

with $\mathbf{a_i}$ given by:

$$\begin{aligned} {\mathbf{a_i}}^{\mathbf{T}} = &\left\{ \frac{\partial {F^*}_i}{\partial N_{xi}} + p_u \frac{\partial {F^*}_i}{\partial N_{xyi}};\ \frac{\partial {F^*}_i}{\partial N_{yi}} + p_v \frac{\partial {F^*}_i}{\partial N_{xyi}};\ \frac{\partial {F^*}_i}{\partial Q_{xi}} + \frac{\partial {F^*}_i}{\partial Q_{yi}};\right. \\ &\left. \frac{\partial {F^*}_i}{\partial M_{xi}} + p_{\phi x} \frac{\partial {F^*}_i}{\partial M_{xyi}};\ \frac{\partial {F^*}_i}{\partial M_{yi}} + p_{\phi y} \frac{\partial {F^*}_i}{\partial M_{xyi}} \right\} \\ p_u = &\frac{2\Delta{u_i}^2}{\Delta{u_i}^2 + \Delta{v_i}^2};\ p_v = \frac{2\Delta{v_i}^2}{\Delta{u_i}^2 + \Delta{v_i}^2};\ p_{\phi x} = \frac{2\Delta{\phi_{xi}}^2}{\Delta{\phi_{xi}}^2 + \Delta{\phi_{yi}}^2}; \\ p_{\phi y} = &\frac{2\Delta{\phi_{yi}}^2}{\Delta{\phi_{xi}}^2 + \Delta{\phi_{yi}}^2} \end{aligned} \tag{5.47}$$

Equations (5.46) and (5.47) indicate that the plastic displacements at the nodes are functions of the stress resultants only at this node (Shi and Voyiadjis, 1992). Therefore, we can write the vector of increments of nodal plastic displacements as:

$$\Delta \mathbf{q^p} = \begin{bmatrix} \mathbf{a_1} & \mathbf{0} & \mathbf{0} \\ \mathbf{0} & \mathbf{a_i} & \mathbf{0} \\ \mathbf{0} & \mathbf{0} & \mathbf{a_{NPN}} \end{bmatrix} \begin{Bmatrix} \Delta\lambda_1 \\ \Delta\lambda_i \\ \Delta\lambda_{\mathbf{NPN}} \end{Bmatrix} = \mathbf{a}\Delta\boldsymbol{\lambda} \tag{5.48}$$

As with the geometrically non-linear analysis presented in Chap. 4, to determine the tangent stiffness matrix of the element we define $\delta\boldsymbol{\varepsilon}_\mathbf{b}$, $\delta\boldsymbol{\varepsilon}_\mathbf{m}$, $\delta\boldsymbol{\varepsilon}_\mathbf{s}$ as virtual elastic bending, membrane and transverse shear strains, respectively (δ-virtual), and **M,N,Q** as stress couples and stress resultants of the element. We also use the same linearized equilibrium equations of the system at configuration $k+1$ in the Updated Lagrangian description, expressed by the principle of the virtual work, which in finite element modeling takes the form:

$$\begin{aligned} \iint_\Omega \left(\delta\boldsymbol{\varepsilon}_\mathbf{b}^{\mathbf{T}}\mathbf{D}\boldsymbol{\varepsilon}_\mathbf{b} + \delta\boldsymbol{\varepsilon}_\mathbf{m}^{\mathbf{T}}\mathbf{S}\boldsymbol{\varepsilon}_\mathbf{m} + \delta\boldsymbol{\varepsilon}_\mathbf{s}^{\mathbf{T}}\mathbf{T}\boldsymbol{\varepsilon}_\mathbf{s}\right) dxdy + \iint_\Omega \delta\boldsymbol{\theta}^{\mathbf{Tk}}\mathbf{F}\boldsymbol{\theta} dxdy = {}^{k+1}R \\ - \iint_\Omega \left(\delta\boldsymbol{\varepsilon}_\mathbf{b}^{\mathbf{Tk}}\mathbf{M} + \delta\boldsymbol{\varepsilon}_\mathbf{m}^{\mathbf{Tk}}\mathbf{N} + \delta\boldsymbol{\varepsilon}_\mathbf{s}^{\mathbf{Tk}}\mathbf{Q}\right) dxdy \end{aligned} \tag{5.49}$$

where ${}^{k+1}R$ is the total external virtual work at step $k+1$, $\boldsymbol{\theta}$ is the slope vector, and $^{\mathbf{k}}\mathbf{F}$ is a membrane stress resultant matrix at step k given by (4.22). Following the procedure described in Chap. 4, we derive the initial stress stiffness matrix. Equation (4.18) can be expressed as:

$$\iint_\Omega \left(\delta\boldsymbol{\varepsilon}_\mathbf{b}^{\mathbf{T}}\mathbf{D}\boldsymbol{\varepsilon}_\mathbf{b} + \delta\boldsymbol{\varepsilon}_\mathbf{m}^{\mathbf{T}}\mathbf{S}\boldsymbol{\varepsilon}_\mathbf{m} + \delta\boldsymbol{\varepsilon}_\mathbf{s}^{\mathbf{T}}\mathbf{T}\boldsymbol{\varepsilon}_\mathbf{s}\right) dxdy + \delta\Delta\mathbf{q}^{e\mathbf{T}}\mathbf{K_g}\Delta\mathbf{q}^e = {}^{k+1}\ R - \delta\Delta\mathbf{q}^{\mathbf{T}}\Delta\mathbf{f} \tag{5.50}$$

where $\mathbf{K_g}$ is the initial stress matrix defined as in Chap. 4:

$$\mathbf{K_g} = \iint_\Omega \mathbf{G}^{\mathbf{Tk}}\mathbf{F}\mathbf{G} dxdy \tag{5.51}$$

and $\mathbf{f}$ is the internal force vector resulting from the unbalanced forces in configuration k expressed as:

$$\mathbf{f} = \iint_\Omega \left(\mathbf{B_b}^{\mathbf{Tk}}\mathbf{M} + \mathbf{B_m}^{\mathbf{Tk}}\mathbf{N} + \mathbf{B_s}^{\mathbf{Tk}}\mathbf{Q}\right) dxdy \tag{5.52}$$

We now rewrite (5.50), using (5.40), written in a matrix form as:

$$\begin{aligned} \iint_\Omega \left[\left(\delta\boldsymbol{\varepsilon}_\mathbf{b}^{e\mathbf{T}} + \delta\boldsymbol{\varepsilon}_\mathbf{b}^{p\mathbf{T}}\right)\mathbf{M} + \left(\delta\boldsymbol{\varepsilon}_\mathbf{m}^{e\mathbf{T}} + \delta\boldsymbol{\varepsilon}_\mathbf{m}^{p\mathbf{T}}\right)\mathbf{N} + \left(\delta\boldsymbol{\varepsilon}_\mathbf{s}^{e\mathbf{T}} + \delta\boldsymbol{\varepsilon}_\mathbf{s}^{p\mathbf{T}}\right)\mathbf{Q}\right] dxdy \\ + \delta\Delta\mathbf{q}^{e\mathbf{T}}\mathbf{K_g}\Delta\mathbf{q}^e = {}^{k+1}R - \delta\Delta\mathbf{q}^{\mathbf{T}}\Delta\mathbf{f} \end{aligned} \tag{5.53}$$

Rearranging terms and writing the above equation in incremental form, we have:

$$\iint_{\Omega} \left(\delta\Delta{\boldsymbol{\varepsilon}_{\mathbf{b}}}^{e\mathbf{T}}\Delta\mathbf{M} + \delta\Delta{\boldsymbol{\varepsilon}_{\mathbf{m}}}^{e\mathbf{T}}\Delta\mathbf{N} + \delta\Delta{\boldsymbol{\varepsilon}_{\mathbf{s}}}^{e\mathbf{T}}\Delta\mathbf{Q}\right) dxdy + \iint_{\Omega} \left(\delta\Delta{\boldsymbol{\varepsilon}_{\mathbf{b}}}^{p\mathbf{T}}\Delta\mathbf{M} + \delta\Delta{\boldsymbol{\varepsilon}_{\mathbf{m}}}^{p\mathbf{T}}\Delta\mathbf{N} + \delta\Delta{\boldsymbol{\varepsilon}_{\mathbf{s}}}^{p\mathbf{T}}\Delta\mathbf{Q}\right) dxdy + \delta\Delta\mathbf{q}^{e\mathbf{T}}\mathbf{K_g}\Delta\mathbf{q}^{e} = {}^{k+1}R - \delta\Delta\mathbf{q}^{\mathbf{T}}\Delta\mathbf{f} \quad (5.54)$$

Substituting (5.41) into (5.54) we obtain:

$$\begin{aligned}&\iint_{\Omega} \left(\delta\Delta{\boldsymbol{\varepsilon}_{\mathbf{b}}}^{e^{\mathbf{T}}}\Delta\mathbf{M} + \delta\Delta{\boldsymbol{\varepsilon}_{\mathbf{m}}}^{e^{\mathbf{T}}}\Delta\mathbf{N} + \delta\Delta{\boldsymbol{\varepsilon}_{\mathbf{s}}}^{e^{\mathbf{T}}}\Delta\mathbf{Q}\right) dxdy \\ &\quad + \sum_{i=1}^{NPN} \delta\Delta\lambda_i \left[\frac{\partial {F^*}_i}{\partial\mathbf{M_i}} d\mathbf{M_i} + \frac{\partial {F^*}_i}{\partial\mathbf{N_i}} d\mathbf{N_i} + \frac{\partial {F^*}_i}{\partial\mathbf{Q_i}} d\mathbf{Q_i}\right] + \delta\Delta\mathbf{q}^{e^{\mathbf{T}}}\mathbf{K_g}\Delta\mathbf{q}^{e} \\ &= {}^{k+1}R - \delta\Delta\mathbf{q}^{\mathbf{T}}\Delta\mathbf{f}\end{aligned} \quad (5.55)$$

Using (3.66), (3.67), (3.68), (3.69), (3.70), (3.71), (3.72), (3.73), (3.74), (3.75), (3.76), (3.77), (3.78), (3.79), (3.80), (3.81), as well as the consistency condition given by (5.39), we may write:

$$\begin{aligned}&\delta\Delta\mathbf{q}^{e\mathbf{T}}\left(\mathbf{K_e}+\mathbf{K_g}\right)\Delta\mathbf{q}^{e} \\ &\quad - \sum_{i=1}^{NPN} \delta\Delta\lambda_i \left[\frac{\partial {F^*}_i}{\partial\mathbf{M^*_i}} d\mathbf{M^*_i} + \frac{\partial {F^*}_i}{\partial\mathbf{N^*_i}} d\mathbf{N^*_i} + \frac{\partial {F^*}_i}{\partial\mathbf{Q^*_i}} d\mathbf{Q^*_i} + \frac{\partial {F^*}_i}{\partial\mathbf{k}} d\mathbf{k_i}\right] \\ &= {}^{k+1}R - \delta\Delta\mathbf{q}^{\mathbf{T}}\Delta\mathbf{f}\end{aligned} \quad (5.56)$$

where $\mathbf{K_e}$ is the linear elastic stiffness matrix given by (3.83).

Similarly to (5.47) we define the following relations:

$$\begin{aligned}\mathbf{a_{bi}}^{\mathbf{T}} &= \frac{\partial {F^*}_i}{\partial\mathbf{M^*}_i} = \left\{\frac{\partial {F^*}_i}{\partial {M^*}_{xi}};\ \frac{\partial {F^*}_i}{\partial {M^*}_{yi}};\ \frac{\partial {F^*}_i}{\partial {M^*}_{xyi}}\right\}; \\ \mathbf{a_{mi}}^{\mathbf{T}} &= \frac{\partial {F^*}_i}{\partial\mathbf{N^*}_i} = \left\{\frac{\partial {F^*}_i}{\partial {N^*}_{xi}};\ \frac{\partial {F^*}_i}{\partial {N^*}_{yi}};\ \frac{\partial {F^*}_i}{\partial {N^*}_{xyi}}\right\}; \\ \mathbf{a_{si}}^{\mathbf{T}} &= \frac{\partial {F^*}_i}{\partial\mathbf{Q^*}_i} = \left\{\frac{\partial {F^*}_i}{\partial {Q^*}_{xi}};\ \frac{\partial {F^*}_i}{\partial {Q^*}_{yi}}\right\};\end{aligned} \quad (5.57)$$

Substituting (5.41) into (5.33) and (5.34) we obtain:

$$\begin{aligned}&d{M_x}^* = \Delta{M_x}^* \\ &= \beta_2 (1 - F) \frac{M_0}{\kappa_0} \Delta\lambda \left[\frac{\partial F^*}{\partial M_x} - \frac{6}{h^2} {M_x}^* \sqrt{\frac{2}{3}\left[\left(\frac{\partial F^*}{\partial M_x}\right)^2 + \left(\frac{\partial F^*}{\partial M_y}\right)^2 + \left(\frac{\partial F^*}{\partial M_{xy}}\right)^2\right]}\right]\end{aligned} \quad (5.58)$$

and similarly for the remaining hardening parameters. Vectors of hardening parameters therefore yield:

$$d\mathbf{N}^*_{\mathbf{i}} = \begin{Bmatrix} \Delta N^*_x \\ \Delta N^*_y \\ \Delta N^*_{xy} \end{Bmatrix} = \Delta\boldsymbol{\lambda}\mathbf{A}_{\mathbf{mi}};\ d\mathbf{Q}^*_{\mathbf{i}} = \begin{Bmatrix} \Delta Q^*_x \\ \Delta Q^*_y \end{Bmatrix} = \Delta\boldsymbol{\lambda}\mathbf{A}_{\mathbf{si}} \tag{5.59}$$

and:

$$d\mathbf{M}^*_{\mathbf{i}} = \begin{Bmatrix} \Delta M^*_x \\ \Delta M^*_y \\ \Delta M^*_{xy} \end{Bmatrix} = \Delta\boldsymbol{\lambda}\mathbf{A}_{\mathbf{bi}} \tag{5.60}$$

where $\mathbf{A_{mi}}$, $\mathbf{A_{si}}$, $\mathbf{A_{bi}}$ are given by:

$$\mathbf{A_{mi}} = \begin{Bmatrix} \beta_1(1-F)\dfrac{N_0}{\varepsilon_0}\left[\dfrac{\partial F^*}{\partial N_x} - \dfrac{1}{h}N_x{}^*\sqrt{\dfrac{2}{3}\left[\left(\dfrac{\partial F^*}{\partial N_x}\right)^2 + \left(\dfrac{\partial F^*}{\partial N_y}\right)^2 + \left(\dfrac{\partial F^*}{\partial N_{xy}}\right)^2\right]}\right] \\ \beta_1(1-F)\dfrac{N_0}{\varepsilon_0}\left[\dfrac{\partial F^*}{\partial N_y} - \dfrac{1}{h}N_y{}^*\sqrt{\dfrac{2}{3}\left[\left(\dfrac{\partial F^*}{\partial N_x}\right)^2 + \left(\dfrac{\partial F^*}{\partial N_y}\right)^2 + \left(\dfrac{\partial F^*}{\partial N_{xy}}\right)^2\right]}\right] \\ \beta_1(1-F)\dfrac{N_0}{\varepsilon_0}\left[\dfrac{\partial F^*}{\partial N_{xy}} - \dfrac{1}{h}N_{xy}{}^*\sqrt{\dfrac{2}{3}\left[\left(\dfrac{\partial F^*}{\partial N_x}\right)^2 + \left(\dfrac{\partial F^*}{\partial N_y}\right)^2 + \left(\dfrac{\partial F^*}{\partial N_{xy}}\right)^2\right]}\right] \end{Bmatrix} \tag{5.61}$$

$$\mathbf{A_{si}} = \begin{Bmatrix} \beta_1(1-F)\dfrac{N_0}{\varepsilon_0}\left[\dfrac{\partial F^*}{\partial Q_x} - \dfrac{1}{h}Q_x{}^*\sqrt{\dfrac{2}{3}\left[\left(\dfrac{\partial F^*}{\partial Q_x}\right)^2 + \left(\dfrac{\partial F^*}{\partial Q_y}\right)^2\right]}\right] \\ \beta_1(1-F)\dfrac{N_0}{\varepsilon_0}\left[\dfrac{\partial F^*}{\partial Q_y} - \dfrac{1}{h}Q_y{}^*\sqrt{\dfrac{2}{3}\left[\left(\dfrac{\partial F^*}{\partial Q_x}\right)^2 + \left(\dfrac{\partial F^*}{\partial Q_y}\right)^2\right]}\right] \end{Bmatrix}$$

$$\mathbf{A_{bi}} = \begin{Bmatrix} \beta_2(1-F)\dfrac{M_0}{\kappa_0}\left[\dfrac{\partial F^*}{\partial M_x} - \dfrac{6}{h^2}M_x{}^*\sqrt{\dfrac{2}{3}\left[\left(\dfrac{\partial F^*}{\partial M_x}\right)^2 + \left(\dfrac{\partial F^*}{\partial M_y}\right)^2 + \left(\dfrac{\partial F^*}{\partial M_{xy}}\right)^2\right]}\right] \\ \beta_2(1-F)\dfrac{M_0}{\kappa_0}\left[\dfrac{\partial F^*}{\partial M_y} - \dfrac{6}{h^2}M_x{}^*\sqrt{\dfrac{2}{3}\left[\left(\dfrac{\partial F^*}{\partial M_x}\right)^2 + \left(\dfrac{\partial F^*}{\partial M_y}\right)^2 + \left(\dfrac{\partial F^*}{\partial M_{xy}}\right)^2\right]}\right] \\ \beta_2(1-F)\dfrac{M_0}{\kappa_0}\left[\dfrac{\partial F^*}{\partial M_{xy}} - \dfrac{6}{h^2}M_x{}^*\sqrt{\dfrac{2}{3}\left[\left(\dfrac{\partial F^*}{\partial M_x}\right)^2 + \left(\dfrac{\partial F^*}{\partial M_y}\right)^2 + \left(\dfrac{\partial F^*}{\partial M_{xy}}\right)^2\right]}\right] \end{Bmatrix}$$

Following the work of Shi and Voyiadjis (1992) we also define the isotropic hardening parameter as:

$$\mathbf{H}\Delta\boldsymbol{\lambda} = \begin{bmatrix} H_1 & 0 & 0 \\ 0 & H_i & 0 \\ 0 & 0 & H_{NPN} \end{bmatrix} \begin{Bmatrix} \Delta\lambda_1 \\ \Delta\lambda_i \\ \Delta\lambda_{NPN} \end{Bmatrix} = -\begin{Bmatrix} \dfrac{\partial F^*{}_1}{\partial k_1}dk_1 \\ \dfrac{\partial F^*{}_i}{\partial k_i}dk_i \\ \dfrac{\partial F^*{}_{NPN}}{\partial k_{NPN}}dk_{NPN} \end{Bmatrix} \tag{5.62}$$

where k is represented by the amount of plastic work, i.e. $d\mathbf{k_i} = \mathbf{N_i} d\boldsymbol{\varepsilon}_\mathbf{m}^\mathbf{p} + \mathbf{M_i} d\boldsymbol{\varepsilon}_\mathbf{b}^\mathbf{p}$. We substitute (5.57), (5.59) and (5.62) into (5.56) to obtain:

$$\begin{aligned}\delta\Delta\mathbf{q}^{e\mathbf{T}} \left(\mathbf{K}+\mathbf{K_g}\right)\Delta\mathbf{q}^e + \delta\Delta\boldsymbol{\lambda}^\mathbf{T}\left[\mathbf{H}-\mathbf{a_b}^\mathbf{T}\mathbf{A_b}-\mathbf{a_m}^\mathbf{T}\mathbf{A_m}-\mathbf{a_s}^\mathbf{T}\mathbf{A_s}\right]\Delta\boldsymbol{\lambda} \\ = {}^{k+1}R - \delta\Delta\mathbf{q}^\mathbf{T}\Delta\mathbf{f}\end{aligned} \tag{5.63}$$

or using (5.44) and (5.46):

$$\begin{aligned}&\left(\delta\Delta\mathbf{q}^\mathbf{T} - \delta\Delta\mathbf{q}^{p\mathbf{T}}\right)\left(\mathbf{K}+\mathbf{K_g}\right)\Delta\mathbf{q}^e + \delta\Delta\boldsymbol{\lambda}^\mathbf{T}\left[\mathbf{H}-\mathbf{a_b}^\mathbf{T}\mathbf{A_b}-\mathbf{a_m}^\mathbf{T}\mathbf{A_m}-\mathbf{a_s}^\mathbf{T}\mathbf{A_s}\right]\Delta\boldsymbol{\lambda} \\ &\quad - {}^{k+}R + \delta\Delta\mathbf{q}^\mathbf{T}\Delta\mathbf{f} = \delta\Delta\mathbf{q}^\mathbf{T}\left[\left(\mathbf{K}+\mathbf{K_g}\right)\Delta\mathbf{q}^e - {}^{k+1}R^* + \Delta\mathbf{f}\right] \\ &\quad + \delta\Delta\boldsymbol{\lambda}^\mathbf{T}\left[-\mathbf{a}^\mathbf{T}\left(\mathbf{K}+\mathbf{K_g}\right)\Delta\mathbf{q}^e + \left(\mathbf{H}-\mathbf{a_b}^\mathbf{T}\mathbf{A_b}-\mathbf{a_m}^\mathbf{T}\mathbf{A_m}-\mathbf{a_s}^\mathbf{T}\mathbf{A_s}\right)\Delta\boldsymbol{\lambda}\right] = 0\end{aligned} \tag{5.64}$$

with:

$${}^{k+1}R = {}^{k+1}R^*\delta\Delta\mathbf{q} \tag{5.65}$$

By the virtue of the variational method, (5.64) gives:

$$\begin{aligned}&\left(\mathbf{K}+\mathbf{K_g}\right)\Delta\mathbf{q}^e - {}^{k+1}R^* + \Delta\mathbf{f} = 0 \\ &-\mathbf{a}^\mathbf{T}\left(\mathbf{K}+\mathbf{K_g}\right)\Delta\mathbf{q}^e + \left(\mathbf{H}-\mathbf{a_b}^\mathbf{T}\mathbf{A_b}-\mathbf{a_m}^\mathbf{T}\mathbf{A_m}-\mathbf{a_s}^\mathbf{T}\mathbf{A_s}\right)\Delta\boldsymbol{\lambda} = 0\end{aligned} \tag{5.66}$$

Substituting (5.44) and (5.46) into the above equations we get:

$$\left(\mathbf{K}+\mathbf{K_g}\right)\Delta\mathbf{q}^e - {}^{k+1}R^* + \Delta\mathbf{f} = \left(\mathbf{K}+\mathbf{K_g}\right)\left(\Delta\mathbf{q} - \mathbf{a}\Delta\boldsymbol{\lambda}\right) = {}^{k+1}R^* - \Delta\mathbf{f} \tag{5.67}$$

$$-\mathbf{a}^\mathbf{T}\left(\mathbf{K}+\mathbf{K_g}\right)\left(\Delta\mathbf{q} - \mathbf{a}\Delta\boldsymbol{\lambda}\right) + \left(\mathbf{H}-\mathbf{a_b}^\mathbf{T}\mathbf{A_b}-\mathbf{a_m}^\mathbf{T}\mathbf{A_m}-\mathbf{a_s}^\mathbf{T}\mathbf{A_s}\right)\Delta\boldsymbol{\lambda} = 0 \tag{5.68}$$

Equation (5.68) leads to:

$$\Delta\boldsymbol{\lambda} = \left[\mathbf{a}^\mathbf{T}\left(\mathbf{K}+\mathbf{K_g}\right)\mathbf{a} + \left(\mathbf{H}-\mathbf{a_b}^\mathbf{T}\mathbf{A_b}-\mathbf{a_m}^\mathbf{T}\mathbf{A_m}-\mathbf{a_s}^\mathbf{T}\mathbf{A_s}\right)\right]^{-1}\mathbf{a}^\mathbf{T}\left(\mathbf{K}+\mathbf{K_g}\right)\Delta\mathbf{q} \tag{5.69}$$

Equation (5.67) becomes:

$$\mathbf{K_{epg}}\Delta\mathbf{q} = {}^{k+1}R^* - \Delta\mathbf{f} \tag{5.70}$$

where $\mathbf{K_{epg}}$ is the elasto-plastic, large displacement stiffness matrix of the element, given by:

$$\begin{aligned}&\mathbf{K_{epg}} = \left(\mathbf{K}+\mathbf{K_g}\right) \\ &\left\{\mathbf{I} - \mathbf{a}\left[\mathbf{a}^\mathbf{T}\left(\mathbf{K}+\mathbf{K_g}\right)\mathbf{a} + \left(\mathbf{H}-\mathbf{a_b}^\mathbf{T}\mathbf{A_b}-\mathbf{a_m}^\mathbf{T}\mathbf{A_m}-\mathbf{a_s}^\mathbf{T}\mathbf{A_s}\right)\right]^{-1}\mathbf{a}^\mathbf{T}\left(\mathbf{K}+\mathbf{K_g}\right)\right\}\end{aligned} \tag{5.71}$$

The tangent stiffness matrix given by (5.71) is similar to that presented by Shi and Voyiadjis (1992). As our formulation accounts for large displacements the stiffness

matrix of the element contains the initial stress matrix $\mathbf{K_g}$. More important however, the above-derived stiffness matrix describes not only isotropic hardening, by means of the parameter $\mathbf{H}$, but kinematic hardening, through matrices $\mathbf{A_b}$, $\mathbf{A_m}$, $\mathbf{A_s}$, which are not determined by curve fitting but derived explicitly from the evolution equation of the backstress given by Armstrong and Frederick (1966). We therefore have a non-layered finite element formulation with shell constitutive equations, yield condition, flow, and hardening rules expressed in terms of membrane and shear forces and bending moments. All the variables used here, namely the stress resultants and couples, as well as the residual stress resultants and couples, representing the center of the yield surface, are rigorously derived from stresses and backstresses.

A significant feature of the derived tangent stiffness is its explicit form. The linear elastic stiffness matrix and initial stress matrix are determined by the quasi-conforming technique. We do not use through-the-thickness integration, as our procedure is for the non-layered model with the yield condition expressed in terms of stress couples and resultants.

5.4 Numerical Examples

A finite element code written in the programming language Fortran 95 for the purpose of the geometrically non-linear analysis was further enhanced to model the elasto-plastic behavior. As before, we used the modified Newton-Raphson technique to solve a system of non-linear, incremental equations. To overcome the singularity problem appearing at the limit point, we adopted the arc-length method (Crisfield, 1991) to determine the local load increment for each iteration. A return to the yield surface algorithm was also implemented (Crisfield, 1991). The results delivered by our model were computed on a personal computer. Some of the reference solutions obtained with the layered approach (ABAQUS) were determined using a Silicon Graphics Onyx 3200 system. Computational and programming issues are discussed in detail in Chap. 7.

The accuracy of our formulation is verified through a series of discriminating examples. We solve only non-linear examples to test the reliability of the elasto-plastic framework presented in this chapter. The problems were chosen to challenge and demonstrate the most important features of our model:

- Representation of progressive development of plastic deformation until the plastic hinge is formed;
- Influence of the transverse shear forces on plastic behavior of thick plates, beams, and shells of general shape;
- Elasto-plastic behavior of structures of interest upon reversal of loading (representation of Bauschinger effect through kinematic hardening); and
- Description of large displacements and rotations.

We compare the performance of the our procedure with other formulations available in the literature. Table 5.1 gives the references used, and their abbreviations.

Table 5.1 References used with abbreviations

Name	Description
ABQ-L	ABAQUS layered model with von Mises type yield criterion and Ziegler kinematic hardening rule (Hibbit, Karlson & Sorensen, Inc., 2001)
C&H	Bounds for collapse load – analytical solution of cylindrical shell Chen and Han (1988)
HOD	Analytical solution given by Hodge (1959)
O&HNL	Owen and Hinton Non-Layered Model based on Mindlin plate theory and Iliushin's Yield Criterion (1980)
O&HL	Owen and Hinton Layered Model based on Mindlin plate theory and von Mises Yield Criterion (1980)
V&W-Q	The present formulation with shear forces included in the yield function (Voyiadjis and Woelke, 2006)
V&W	The present formulation without shear forces included in the yield function (Voyiadjis and Woelke, 2006)

5.4.1 Simply Supported Elasto-Plastic Beam

The importance of the transverse shear forces in the approximation of the collapse load of thick beams, plates, and shells is known to be significant. Neglecting transverse shears in the assessment of the maximum load carrying capacity of the structure may lead to predictions that are not conservative. Accurate and safe approximations should result in a decreasing value of the maximum load factor with increasing thickness. To test the accuracy of our formulation in accounting for shear deformation, we consider a simply supported beam of length $2L = 20\,in.$ subjected to a concentrated load $2P = 20\,lb$ at its mid-point. The Young's modulus is $E = 10.5 \times 10^6\ psi$, yield stress $\sigma = 500\ psi$, and width of the beam is $b = 0.15\,in.$ We compute the load factor of the beam as a function of thickness. The analytical solution of this problem given by Hodge (1959) serves as a reference solution. The geometry of the problem, as well as the material and section properties, are given in Fig. 5.4. The comparison of the results provided by our formulation, compared with the reference solutions are given in Fig. 5.5.

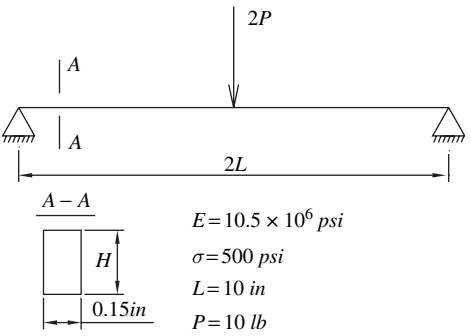

Fig. 5.4 Simply supported beam – geometry and material properties (Voyiadjis and Woelke, 2006)

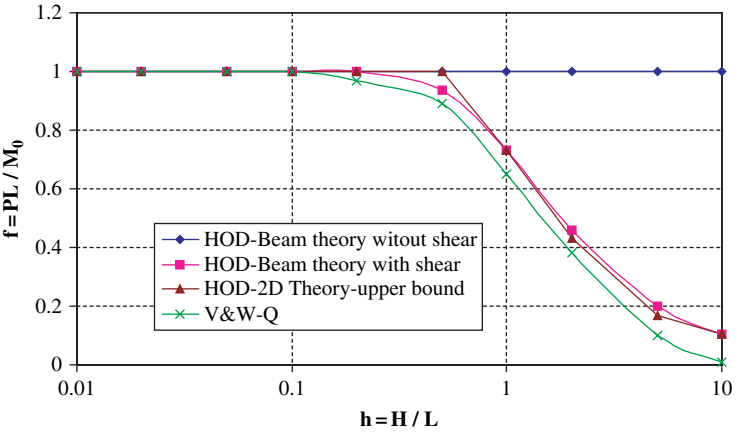

Fig. 5.5 Simply supported beam – results of the analysis: collapse load as a function of thickness (Voyiadjis and Woelke, 2006)

As seen in Fig. 5.5, our formulation agrees very well with analytical results of this problem by Hodge (1959). We observe a substantial drop in the load factor for thick beams. Note that, for practical purposes only a certain range of H is significant. When the thickness of the beam, plate, or shell reaches 50% of its total length, we clearly enter into a purely academic problem, although it is still valuable for illustrative purposes.

The reduction of the load factor is very significant even for moderately thick beams, i.e., $H = 0.5L$ (total length of the beam is $2L$), which is closely approximated here.

5.4.2 Simply Supported Plate

The following example corroborates the accuracy of our formulation in the prediction of the first yield in plates, as well as the description of the load-displacement response under cyclic loads. We examine only material non-linearities, to allow for comparison with the reference solution by Owen and Hinton (1980).

We consider a square ($L = 1.0$ m) simply supported plate subjected to a uniformly distributed load $q = 1.0\,kPa$. Young's modulus is $E = 10.92\,kPa$, Poisson's ratio $\nu = 0.3$, yield stress $\sigma = 1600\,kPa$, and thickness of the plate $t = 0.01\,m$. The geometry and material properties are shown in Fig. 5.6.

We compare the results obtained with our finite element model, with those published by Owen and Hinton (1980), using layered and non-layered model (O&HL, O&HNL – Table 5.1). The load-deflection responses are shown in Fig. 5.7.

One of our objectives is to account for the progressive plasticization of the cross section by means of a non-layered model. In a layered model, used here as a reference, we track the development of the plastic deformation directly, as stresses are

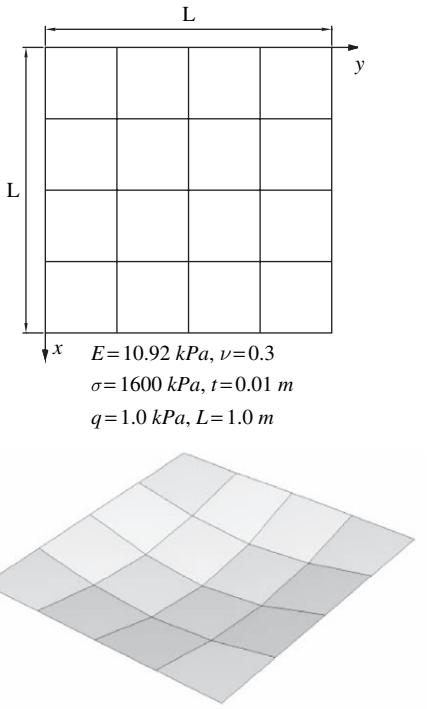

Fig. 5.6 Simply supported plate – geometry, material properties and deformed shape (Voyiadjis and Woelke, 2006)

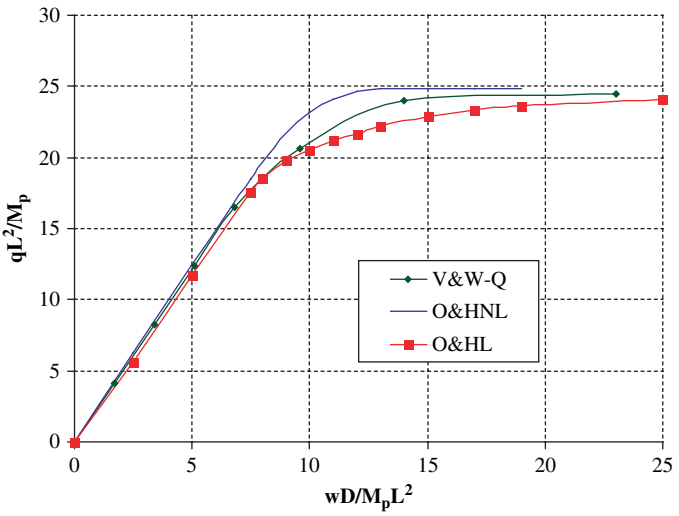

Fig. 5.7 Simply supported plate – Load-displacement curves (Voyiadjis and Woelke, 2006)

calculated at several different levels (layers) in the model. In a layered model, we operate in a stress resultant and stress couples space. The plastic bending moment is calculated under the assumption of a fully plastic cross section. Hence, unless steps are taken to alleviate this problem, the cross section can only be either fully elastic or fully plastic, with no intermediate states.

As seen in Fig. 5.7, our approach provides a very good approximation of plastic strains growing gradually from the outer fibers to the mid-plane.

A main thrusts of our work is development of a physically sound kinematic hardening rule for non-layered plates and shells, correctly representing not only moment-curvature relationship, but normal force-normal strain and shear force-shear strain relationships upon complete reversal of loading. We therefore need to show the importance of all the hardening parameters $\mathbf{N}^*$, $\mathbf{Q}^*$, $\mathbf{M}^*$. The simply supported plate under a uniformly distributed load is a problem in which the normal forces are negligible. The residual forces $\mathbf{N}^*$ are also negligible. The influence of these is investigated in the following examples.

The plate example is a bending dominant problem and the moment curvature relation is of primary importance. The load-displacement curve takes the shape of a moment-curvature relation. Figure 5.8 shows the load-deflection curves for the plate shown in Fig. 5.6, in the case of reverse loading condition. The ABAQUS layered model with kinematic hardening rule is used as a reference. Our approximation is very close to the one by the layered approach, as seen in Fig. 5.8. This confirms that the definition of residual bending moments $\mathbf{M}^*$ in the hardening rule is sound and produces accurate results.

For the thickness of the plate $t = 0.01\,m$, the influence of the transverse shear forces on the plastic behavior is very small. In this case, the residual transverse shear forces $\mathbf{Q}^*$ do not matter either. With increasing thickness of the plate, we observe

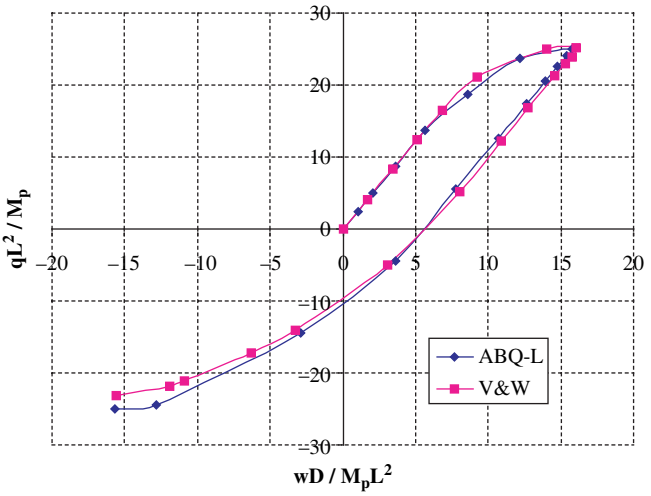

Fig. 5.8 Simply supported plate – Load-displacementresponse (Voyiadjis and Woelke, 2006)

the increasing importance of the transverse shear forces, as was shown by Shi and Voyiadjis (1992). We show here that for thick plates, both transverse shear forces and residual transverse shear forces play a very important role.

We now consider the same rectangular simply supported plate as in Fig. 5.6. The thickness of the plate, however, is increased to $t = 0.35\,m$, and a uniform load to $q = 850\,kPa$, and the yield stress reduced to $\sigma = 1200\,kPa$. The thickness of the plate is now 35% of its length; hence, we expect a significant reduction of the load factor of the plate, due to the influence of the shear forces. Again, we compare the results with the layered model, with the influence of transverse shear taken into account. The results are presented in Fig. 5.9. A diamond line denoted by ABQ-L indicates a layered approach with shear forces considered. This approach serves as a reference solution.

As expected, the influence of the shear forces on the approximations of the collapse load is significant. The analysis in which the transverse shear forces are not considered leads to a nearly 20% higher prediction of maximum load carried by the plate. Neglecting the shear forces when analyzing thick plates, shells and beams potentially leads to overprediction of the ultimate load carried by the structure.

When loading is reversed and applied in the opposite direction, until yielding occurs at the top surface of the plate, the residual shear forces $\mathbf{Q}^*$ become dominant in the analysis.

Our model reproduces very well the lowered yield point upon reversal of loading, and offers a solution close to that of the layered approach. We therefore conclude

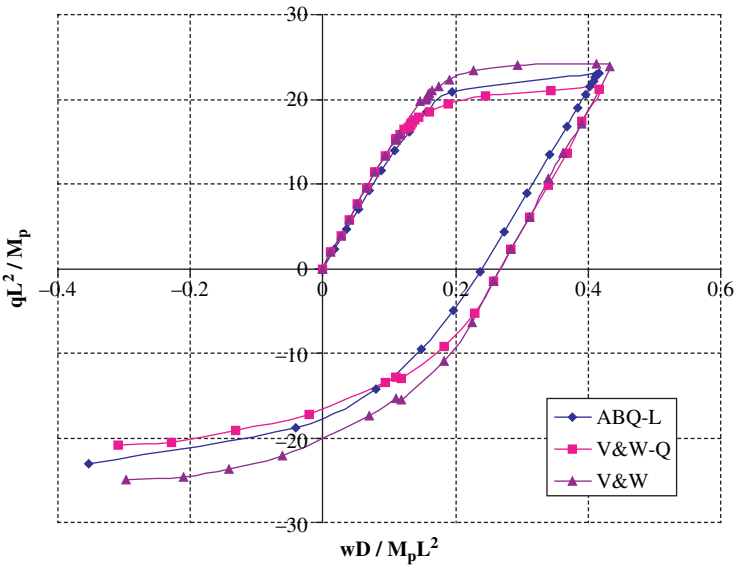

Fig. 5.9 Simply supported thick plate – Load –displacement response (Voyiadjis and Woelke, 2006)

that the representation of the residual shear forces as kinematic hardening parameters is physically sound and capable of delivering highly accurate results.

The effect of the shear forces on the plastic behavior and maximum load carrying capacity is correctly recognized. As expected, because of the increasing significance of transverse shears, the results show a reduction of the limit load for thick plates, shells, and beams.

5.4.3 Cylindrical Shell Subjected to Ring of Pressure

The previous example showed the validity of the definition of the residual bending moments and residual shear forces as kinematic hardening parameters. The derivation of the residual membrane forces is based on the same assumptions, thus we expect them to be as reliable as the shear forces and bending moments. As the membrane forces in bending of plates are negligible, the results of the previous example do not confirm the soundness of the formulation of the residual normal forces. To do so, we investigate a cylindrical shell under a ring of pressure. The geometry, deformed shape of a cylinder, octant, and material parameters are shown in Fig. 5.10.

Membrane forces play an important role here. If the structure is loaded into a plastic zone, then unloaded and loaded in the opposite direction, the residual membrane forces are also significant. The results of the analysis are compared with those of the "through the thickness integration" (layered) method in Fig. 5.11.

Again, our non-layered model with a new kinematic hardening rule is robust and agrees excellently with the layered approach. The latter, however, requires many more operations for non-linear calculations, as the yield function and consistency condition must be checked separately at each layer.

The problem presented here was originally investigated by Drucker (1954) and later by Chen and Han, (1988), who analytically determined the bounds for the collapse load of the cylinder. These bounds are given by:

$$1.5 \leq \frac{P}{\sigma_0 h \left(\frac{h}{R}\right)^{1/2}} \leq 2.0 \tag{5.72}$$

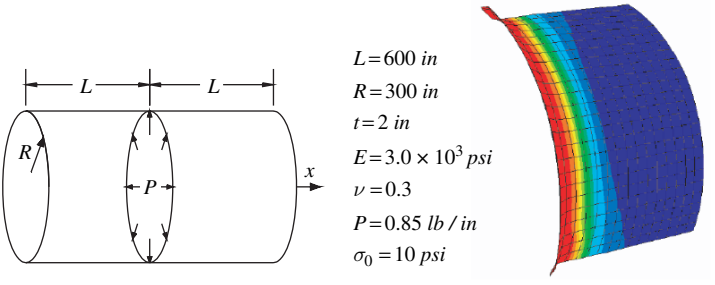

Fig. 5.10 Cylindrical shell subjected to a ring of pressure and a deformed shape (Woelke et al. 2006)

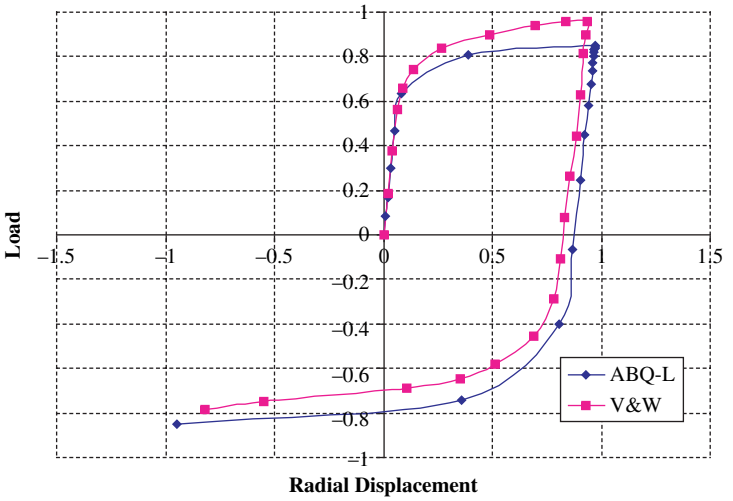

Fig. 5.11 Equilibrium path for a cylinder subjected to a ring of pressure (Voyiadjis and Woelke, 2006)

Assessment of the collapse load of structures is of paramount importance from an engineering point of view. We therefore examine the functionality of our model in the determining the maximum load carried by the cylinder. Equation (5.12) serves as a target solution. The collapse load as a function of thickness of the shell is shown in Fig. 5.12.

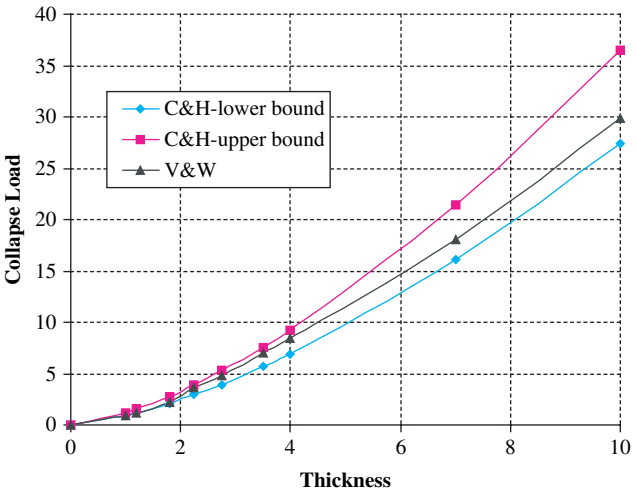

Fig. 5.12 Collapse load for a cylinder subjected to a ring of pressure Predictions of the maximum load carried by the cylinder are accurate and fall within the analytical bounds (Voyiadjis and Woelke, 2006)

Note that for the case of a very thick shell, the results approach the lower bound solution. This is because the shear forces become more and more important for thick shells, causing a reduction in the load carrying capacity.

5.4.4 Spherical Dome Subjected to Ring of Pressure

The problem of a spherical dome with an 18^0 hole at the top, subjected to a ring of pressure, is solve to establish the wide range of applicability of our method. This is an important engineering problem, as well as a discriminating test of accuracy

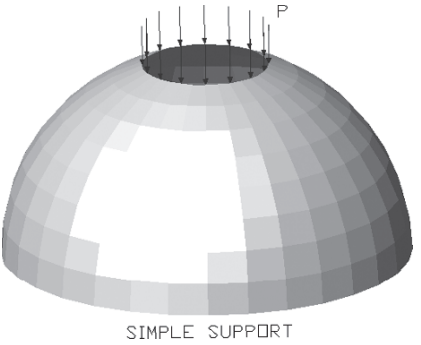

$R = 10\ in$
$t = 0.04\ in$
$E = 6.82 \times 10^7\ psi$
$\nu = 0.3$
$\sigma_0 = 125\ psi$

Fig. 5.13 Spherical dome with an 18^0 cut-out; geometry and material properties (Voyiadjis and Woelke, 2006)

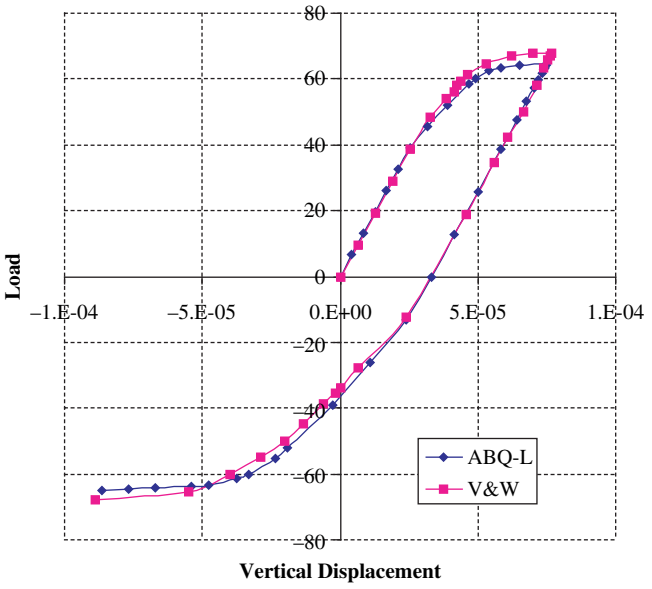

Fig. 5.14 Spherical dome with an 18^0 cut-out; Load –displacement curves (Voyiadjis and Woelke, 2006)

of the finite element representation in the behavior of shells. We again study the performance of the yield function and the kinematic hardening rule. Geometrical and material data are shown in Fig. 5.13.

The structure is loaded into a plastic zone and the pressure is reversed. The kinematic hardening rule is applied to determine the equilibrium path. The layered approach again serves as a reference. The load-displacement curves are plotted in Fig. 5.14.

The approximation of the equilibrium path obtained by our approach agrees very well with the adopted target solution, showing again the validity of our assumptions. The lowered yield point is correctly reproduced by the yield surface defined here.

Although this framework is robust for plates and shells of general shape, it performs best with spherical shells. This is to be expected, as the shell constitutive equations we use were derived by means of spherical strains, and then generalized with the finite element method.

5.5 Summary

We evaluated the reliability of our concepts through a series of benchmark problems that were selected to challenge and demonstrate the most important features of our model. In all the cases, the results were very close to the reference solutions, demonstrating that the model is well grounded.

The effect of the shear forces on the plastic behavior and maximum load carrying capacity is correctly recognized. As expected, because of the increasing significance of transverse shears, the results show a reduction of the load factor for thick plates, shells, and beams.

The progressive plastification of the cross section is also closely approximated. Typically, in the non-layered approach the load displacement relation is linear until the plastic hinge is developed. Any yielding occurring before the section is fully plastic is neglected. Through a modification introduced by Crisfield (1981a), the first yield of the outer fibers can be predicted, as was also confirmed here.

A spherical dome problem (Sect. 5.4.4) confirms that, although our framework is robust for plates and shells of general shape, it performs best in the case of spherical shells. This is to be expected, as the shell constitutive equations we used were derived by means of spherical strains and to be generalized with the finite element method.

The Bauschinger effect can only be numerically observed only if the method used features a reliable kinematic hardening rule. The one use propose was defined in a stress resultant space, which is effective in terms of structural analysis. The lowered yield point upon load reversal was correctly determined here for both plates and shells confirming that the definition of the “hardening parameters” is sound and capable of delivering very accurate results. It is worth noting the importance of the material constants in the definition of the hardening parameters. Correct determination of these constants is critical for the dependability of the kinematic hardening

rule. Our calibration of the constants was based on the reference solutions; ideally, they should be determined from extensive experimental data. Furthermore, the analysis results provided by our model, which are of course approximate, should be compared with experimental results, rather than with other approximations, based on a different theoretical formulation (Bieniek and Funaro, 1976).

It is important that the elasto-plastic analysis is a continuation of the formulation developed in the preceding chapters. Consequently, any limitations and deficiencies experienced in the elastic and geometrically non-linear investigations will persist.

The approximation introduced on the elasto-plastic level of the model that can be subject to critique uses a plastic node method, which presumes the concentration of the plastic deformation in the nodes of the elements, while the interior remains elastic. Clearly, the spread of inelastic deformations will occur in many cases. The results of our analysis show, however, that any errors that arise from a plastic node method are in significant, even for coarse meshes.

The elasto-plastic formulation we present offers a reliable yield surface and a new kinematic hardening rule in the stress resultant space. It delivers precise results of the non-linear analysis of shells under cyclic loading, yet it is relatively simple and very efficient.

References

Armstrong, P.J. and Frederick, C.O. (1966). A Mathematical Representation of the Multiaxial Bauschinger Effect. (CEGB Report RD/B/N/731). Berkeley Laboratories, R&D Department, California.

Atkatsh, R.S., Bieniek, M.P., Sandler, I.S. (1982). Theory of Viscoplastic Shells for Dynamic Response. Technical report DNA-TR-81-50, Weidlinger Associates, New York.

Atkatsh, R.S., Bieniek, M.P., Sandler, I.S. (1983). Theory of Viscoplastic Shells for Dynamic Response. J. Appl. Mech., 50, 131–136.

Bieniek, M.P. and Funaro, J.R. (1976). Elasto-plastic behaviour of plates and shells. Technical Report DNA 3584A, Weidlinger Associates, New York.

Bieniek, M.P. and Funaro, J. R., Baron, M.L. (1976). Numerical Analysis of the Dynamic Response of Elasto-Plastic Shells. Technical Report No. 20, November 1976, Weidlinger Associates, New York.

Chen, W. and Han, D. (1988). Plasticity for Structural Engineers. Springer-Verlag, New York.

Crisfield, M.A. (1981a). Finite element analysis for combined material and geometric nonlinearities. In W. Wunderlich et al. (eds.) Nonlinear Finite Element Analysis in Structural Mechanics, Springer-Verlag, New York, pp. 325–338.

Crisfield, M.A. (1981b). A fast incremental/iterative solution procedure that handles 'snap-through'. Comp. Stuct., 13, 55–62.

Crisfield, M.A. (1991). Non-linear Finite element Analysis of Solids and Structures. Vol. 1. John Wiley & Sons Ltd, New York.

Drucker, D.C. (1954). Limit Analysis of Cylindrical Shells Under Axially Symmetric Loading. Proc. 1st Midwestern Conf. Solid Mech., Urbana, Illinoi, pp. 158–163.

Hibbit, Karlson & Sorensen, Inc. (2001). Abaqus, Theory Manual, Pawtucket, RI, USA.

Hodge, P.G. (1959). Plastic Analysis of Structures. McGraw-Hill, New York.

Iliushin, A.A. (1956). Plastichnost', Gostekhizdat, Moscow (in Russian).

Owen, D.R.J. and Hinton, E. (1980). Finite Elements in Plasticity: Theory and Practice, Pineridge Press, Swansea, UK.

Shi, G. and Voyiadjis, G.Z. (1992). A simple non-layered finite element for the elasto-plastic analysis of shear flexible plates. Int. J. Num. Meth. Eng., 33, 85–99.

Tang, L., Chen, W. and Liu, Y. (1980). Quasi-conforming elements for finite element analysis. J. DIT, 19(2).

Tang, L., Chen, W. and Liu, Y. (1983). String net function applications and quasi conforming technique. In Hybrid and Mixed Finite Element Methods, Wiley, NY.

Ueda, Y. and Yao, T. (1982). The plastic node method of plastic analysis. Comp. Meth. Appl. Mech. Eng. 34, 1089–1104.

Voyiadjis, G.Z. and Woelke, P. (2006). General non-linear finite element analysis of thick plates and shells. Int. J. Solids Struct., 43, 2209–2242.

Woelke, P. and Voyiadjis, G.Z. (2005). A stress resultant based yield surface with kinematic hardening and isotropic damage due to microvoids for isotropic plates and shells. Proceedings of McMat2005, 2005 Joint ASME/ASCE/SES Conference on Mechanics and Materials, June 1–3, Baton Rouge, Louisiana, USA.

Woelke, P., Chan, K.K., Daddazio, R., Abboud, N. (2006) “Stress Resultant Based Elasto-Viscoplastic Thick Shell Model.” 77th Shock and Vibration Symposium Proceedings, Monterrey, CA.

Chapter 6
Elasto-Plastic Geometrically Non-linear Finite Element Analysis of Thick Plates and Shells With Damage Due to Microvoids

6.1 Introduction

In this chapter we introduce the effects of damage into the computational model for the analysis of plates and shells. All previously made assumptions pertaining to the shell theory, shell element, geometrically non-linear, and elasto-plastic investigations presented in the preceding chapters are employed here. The characteristics of the present damage formulation, as well as the published literature, were already discussed in Chap. 1. Thus, we only briefly review the features of the damage model developed.

The experimental results (Bluhm and Morrissey, 1965; Fisher, 1980; Roy et al., 1981) show that the degradation of material properties of ductile metals in the elastic range due to damage effects is negligible. Hence, the damage considered here is a phenomenon induced by the plastic strain and any damage occurring in the elastic zone is disregarded.

Following the discussion given in Chap. 1, we adopt an isotropic scalar damage parameter. In the isotropic representation of damage, the stiffness of the material is reduced according to the same relation in all directions. For a better description of the anisotropic effects, the second order damage tensor, which is capable of representing different levels of material degradation in different directions, is often used (Abu Al-Rub and Voyiadjis, 2003; Doghri, 2000; Lubarda and Krajcinovic, 1993; Murakami, 1988; Seweryn and Mroz, 1998; Voyiadjis and Abu-Lebdeh, 1993; Voyiadjis and Deliktas, 2000a, b; Voyiadjis and Kattan, 1991, 1992a, b, 1999; Voyiadjis and Park, 1997, 1999; Voyiadjis and Venson, 1995).

One complexity in using anisotropic damage variables is the need to determine of numerous material parameters, which describe the directional dependency of the evolution of damage. Extensive experimental data are required to calibrate these constants with sufficient accuracy and consistency. The isotropic damage formulation requires determination of fewer constants (two in the case of our analysis), yet it is capable of delivering very accurate results. For our investigation of the behavior of isotropic plates and shells, we consider the isotropic scalar parameter in the representation of damage to be satisfactory. The effects of anisotropy are not accounted for.

G.Z. Voyiadjis, P. Woelke, *Elasto-Plastic and Damage Analysis of Plates and Shells*,

© Springer-Verlag Berlin Heidelberg 2008

The isotropic porosity parameter defined by Duszek-Perzyna and Perzyna (1994) is used to describe damage effects in plates and shells. The evolution of porosity given by Duszek-Perzyna and Perzyna (1994), reduced to a rate-independent case, consists of three terms responsible for the cracking of the second-phase particles, debonding of the second-phase particles from the matrix material, and void growth controlled only by plastic flow phenomena. The first term (cracking of the second-phase particles) is dependent only on the stress, which allows for variation of damage, even without plastic flow.

This makes the formulation universal and capable of correctly describing the material behavior under all loading conditions, including the hydrostatic stress for the case of isotropic damage conditions. Here, we consider only the most important effects from the point of view of structural analysis of isotropic homogenous plates and shells. Loading conditions are assumed to be static, and the evolution of porosity is reduced to represent only the void growth. Although the effects of the microcracks can be important for investigations of the material behavior, observations of ductile fracture in metals (Beachem, 1963; Gurland and Plateau, 1963) led to the conclusion that this process may involve the generation of considerable porosity through nucleation and growth of voids (Gurson, 1977). The influence of the growth of microvoids is considered decisive in the modeling of ductile isotropic material. Thus we consider only damage due to microvoids.

Like Gurson (1975, 1977), as well as Duszek-Perzyna and Perzyna (1994), we incorporate the porosity parameter into the yield function, obtaining a yield criterion and flow rule for porous ductile materials with a strong coupling between plasticity and damage. The yield function given by Duszek-Perzyna and Perzyna (1994), which could be directly related to Gurson's model (1975, 1977), is expressed in terms of the stress resultants and stress couples, similarly to Iliushin's yield function (1956), following the procedure presented by Bieniek and Funaro (1976). The yield surface derived here is very similar to that presented by Woelke and Voyiadjis (2005) with kinematic hardening parameters in the form as well as of residual normal and shear forces, residual bending moments. It is, however, enhanced to account for the reduction of the stiffness caused by the damage effects, represented by the porosity parameter.

The stiffness matrix presented in Chap. 5 was derived by means of the principle of virtual work and the plastic node method (Ueda and Yao, 1982), which assumes the inelastic deformations to be concentrated in the plastic hinges. Following the work of Shi and Voyiadjis (1992, 1993), we adopt the plastic node method to derive the elasto-plastic, damage stiffness matrix of the element. The explicit form of the stiffness matrix is therefore preserved, i.e., numerical integration is not performed, which makes our formulation very effective and accurate (see below).

Our formulation offers a simple and convenient way to achieve a detailed analysis of shells that is accurate and mathematically consistent. Its simplicity and computational efficiency make it particularly useful for structural analysis. Below we verify the assumptions, as well as the derivation, through the discriminating numerical examples.

In the following sections, we first formulate a loading surface with the previously used isotropic and kinematic hardening rules, featuring a strong coupling between plasticity and damage. An associated flow rule and evolution of porosity representing damage is defined. In Sect. 6.3, we derive the explicit tangent stiffness matrix, and in Sect. 6.4, we present the numerical examples that challenge our procedure.

6.2 Yield and Damage Criterion

As discussed above, we derive here a yield criterion for porous metals expressed in terms of the stress resultants and couples, similar to the yield function derived in Chap. 5, and modified to account for the damage effects. The Iliushin's yield function F is given by (5.1), (5.2), (5.3), (5.4), (5.5), (5.6), repeated here for convenience:

$$F = \frac{M^2}{{M_0}^2} + \frac{N^2}{{N_0}^2} + \frac{1}{\sqrt{3}} \frac{|MN|}{M_0 N_0} - \frac{Y(k)}{{\sigma_0}^2} = 0 \tag{6.1}$$

or:

$$F = \frac{|M|}{M_0} + \frac{N^2}{{N_0}^2} - \frac{Y(k)}{{\sigma_0}^2} = 0 \tag{6.2}$$

where:

$$N^2 = {N_x}^2 + {N_y}^2 - N_x N_y + 3{N_{xy}}^2 \tag{6.3}$$

$$M^2 = {M_x}^2 + {M_y}^2 - M_x M_y + 3{M_{xy}}^2 \tag{6.4}$$

$$MN = M_x N_x + M_y N_y - \frac{1}{2} M_x N_y - \frac{1}{2} M_y N_x + 3{M_{xy}}^2 \tag{6.5}$$

$$M_0 = \frac{\sigma_0 h^2}{4}, \quad N_0 = \sigma_0 h \tag{6.6}$$

In the above relations σ_0 is the uniaxial yield stress; $Y(k)$ is a material parameter, which depends on the isotropic hardening parameter k; h is the thickness of the shell; and $|.|$ is the absolute value.

The form of the yield condition given by (6.2) can be derived from the von Mises function and the definition of normal stresses at the top and bottom surfaces of the shell, as shown by Bieniek and Funaro, (1976). Here, however, we use the yield criterion for porous ductile metals as originally proposed by Gurson (1975, 1977) and modified by Perzyna (1984b) and Dornowski and Perzyna (2000). Although it is similar in form to the von Mises equation (also referred to as Huber-Mises-Hencky equation), it accounts for the isotropic damage effects through the dependence of the first invariant of stress and the evolution of porosity. The plastic potential function defined by Dornowski and Perzyna (2000) can be written as:

$$f = \sqrt{\frac{3}{2} S_{ij} S_{ij} + n\xi {\sigma_{ii}}^2}, \quad i, j = 1, 2, 3 \tag{6.7}$$

where S_{ij} is the deviatoric stress tensor given by:

$$S_{ij} = \sigma_{ij} - \frac{1}{3}\sigma_{kk}\delta_{ij} \tag{6.8}$$

In the above relation σ_{ij} is a stress tensor given by:

$$\sigma_{ij} = \frac{N_{ij}}{h} \pm \frac{6M_{ij}}{h^2} \tag{6.9}$$

where N_{ij} are normal forces, M_{ij} are bending moments, h is a thickness of the shell, and δ_{ij} is a Kronecker delta. The parameter n in (6.7) is a material constant, determined by Perzyna (1984b): $n = 1.2587$ (for ductile metals).

The parameter ξ in (6.7) is a porosity parameter given by Gurson (1975, 1977) and modified by Duszek-Perzyna and Perzyna (1994):

$$\Delta\xi = k_1 \Delta\sigma_{ii} + k_2 \Delta\sigma_{ij} \Delta {\varepsilon_{ij}}^p + k_3 \Delta {\varepsilon_{ii}}^p \tag{6.10}$$

where k_1, k_2, k_3 denote the material constants, and $\Delta\sigma$ and $\Delta\varepsilon^p$ are the increments of stress and plastic strain, respectively.

The first two terms in the above equation are responsible for nucleation due to cracking of the second-phase particles and debonding of the second-phase particles from the matrix material. The third term depicts the growth of voids and is controlled only by the plastic flow. The main term is the growth term. We assume that from the metallurgical investigations of the isotropic material forming a plate or a shell, we can determine the initial porosity $\xi\,(t = 0) = \xi_0$; we shall consider only the growth term in the evolution of porosity, i.e.:

$$\Delta\xi = k_3 \Delta {\varepsilon_{ii}}^p \tag{6.11}$$

Equations (6.7), (6.8), (6.9), (6.10), (6.11) are written using indicial notation and a summation convention. Rewriting (6.11) in engineering notation yields:

$$\Delta\xi = k_3 \left(\Delta {\varepsilon_x}^p + \Delta {\varepsilon_y}^p + \Delta {\varepsilon_z}^p\right) \tag{6.12}$$

where $\Delta {\varepsilon_x}^p; \Delta {\varepsilon_y}^p; \Delta {\varepsilon_z}^p$ are increments of normal plastic strains due to both membrane and bending actions in *x, y, z* directions respectively. $\Delta {\varepsilon_x}^p$ and $\Delta {\varepsilon_y}^p$ can be written as:

$$\begin{aligned} \Delta {\varepsilon_x}^p &= \Delta {\varepsilon_{mx}}^p + \Delta {\varepsilon_{bx}}^p = \Delta {\varepsilon_{mx}}^p + z\Delta {\kappa_x}^p \\ \Delta {\varepsilon_y}^p &= \Delta {\varepsilon_{my}}^p + \Delta {\varepsilon_{by}}^p = \Delta {\varepsilon_{my}}^p + z\Delta {\kappa_y}^p \end{aligned} \tag{6.13}$$

where $\Delta\varepsilon_{mx}{}^{p}$ and $\Delta\varepsilon_{my}{}^{p}$ are the increments of plastic strains due to membrane action only, in *x, y* directions, respectively; $\Delta\varepsilon_{bx}{}^{p}$ and $\Delta\varepsilon_{by}{}^{p}$ are the increments of plastic strains due to bending action only, in *x, y* directions, respectively; z is the distance from the mid-plane to the plane under consideration; and $\Delta\kappa_x{}^{p}$, $\Delta\kappa_y{}^{p}$ are the increments of plastic curvatures at the mid-surface in planes parallel to the *xz, yz* planes, respectively. The maximum normal plastic strain caused by bending occurs at $z = h/2$, which leads to:

$$\begin{aligned}\Delta\varepsilon_x{}^{p} &= \Delta\varepsilon_{mx}{}^{p} + \frac{h}{2}\Delta\kappa_x{}^{p}\\ \Delta\varepsilon_y{}^{p} &= \Delta\varepsilon_{my}{}^{p} + \frac{h}{2}\Delta\kappa_y{}^{p}\end{aligned} \tag{6.14}$$

Substituting (6.14) into (6.12) and neglecting $\Delta\varepsilon_z{}^{p}$, we obtain:

$$\Delta\xi = k_3\left[\Delta\varepsilon_{mx}{}^{p} + \Delta\varepsilon_{my}{}^{p} + \frac{h}{2}\left(\Delta\kappa_x{}^{p} + \Delta\kappa_y{}^{p}\right)\right] \tag{6.15}$$

We now proceed to the determination of the plastic potential function expressed in terms of the stress resultants and couples. For conciseness, we neglect radial and transverse shear stresses in this current derivation. Later transverse shear forces will be introduced into the yield condition. Equation (6.7) can be written using the engineering notation:

$$f = \frac{1}{\sqrt{2}}\sqrt{\left[\left(\sigma_x - \sigma_y\right)^2 + \sigma_x{}^2 + \sigma_y{}^2 + 6\tau_{xy}{}^2 + n\xi\left(\sigma_x + \sigma_y\right)^2\right]} \tag{6.16}$$

where σ_x, σ_y are the normal stresses in the *x,y* directions, respectively, and τ_{xy} is a shear stress on the *xy* plane.

We define the yield condition as:

$$\frac{1}{\sqrt{2}}\sqrt{\left[\left(\sigma_x - \sigma_y\right)^2 + \sigma_x{}^2 + \sigma_y{}^2 + 6\tau_{xy}{}^2 + n\xi\left(\sigma_x + \sigma_y\right)^2\right]} = \sigma_0 \tag{6.17}$$

where σ_0 denotes the uniaxial yield stress.

Substituting of (6.9) into (6.17) and using some manipulations results in the following relation:

$$\frac{N^2}{N_0{}^2} + \frac{M^2}{M_{0E}{}^2} \pm 2\frac{NM}{N_0 M_{0E}} = 1 \tag{6.18}$$

where:

$$N^2 = \left(1 + \frac{1}{2}n\xi\right)\left({N_x}^2 + {N_y}^2\right) - (1 - n\xi)\, N_x N_y + 3{N_{xy}}^2$$
$$M^2 = \left(1 + \frac{1}{2}n\xi\right)\left({M_x}^2 + {M_y}^2\right) - (1 - n\xi)\, M_x M_y + 3{M_{xy}}^2 \tag{6.19}$$
$$NM = \left(1 + \frac{1}{2}n\xi\right)\left(N_x M_x + N_y M_y\right) - \frac{1}{2}(1 - n\xi)\left(M_y N_x + M_x N_y\right) + 3N_{xy}M_{xy}$$

and:

$$N_0 = \sigma_0 h, \quad M_{0E} = \frac{\sigma_0 h^2}{6} \tag{6.20}$$

Both the top and bottom surfaces of the shell should be considered, in order to obtain the larger value of the term $\pm 2\dfrac{NM}{N_0 M_{0E}}$. We ensure representation of the most negative effect by writing the (6.18) in the form (Bieniek and Funaro, 1976; Bieniek et al., 1976):

$$\frac{N^2}{{N_0}^2} + \frac{M^2}{{M_{0E}}^2} + 2\frac{|NM|}{N_0 M_{0E}} = 1 \tag{6.21}$$

The yield surface given above is similar to Iliushin's yield function (1956) given by (6.1). To derive (6.1), we follow the procedure presented by Bieniek and Funaro (1976), which is essentially the surface fitting approach. We write (6.21) as:

$$a\frac{N^2}{{N_0}^2} + b\frac{M^2}{{M_{0E}}^2} + c\frac{|NM|}{N_0 M_{0E}} = 1 \tag{6.22}$$

We determine the parameters *a,b,c* by considering the special loading cases separately. If we account for membrane forces only, we see that for $a = 1$ we obtain the exact limit condition. Similarly, if we take a pure bending case, (6.22) produces exact results for $b = \dfrac{M_{0E}^2}{M_0^2}$. To find c, we investigate the loading case corresponding to the maximum value of the ratio $\dfrac{NM}{N_0 M_{0E}}$, which occurs if $N_x = N_y$, $M_x = M_y$ and $N_{xy} = M_{xy} = 0$. The stress distribution in the cross section in this case is shown in Fig. 6.1.

Based on the stress distribution in Fig. 6.1, we may calculate the normal force:

$$N_x = \int_{-h/2}^{h/2} \sigma_x dz = \int_{-h/2}^{-h/2\sqrt{3}} -\sigma_0 dz + \int_{-h/2\sqrt{3}}^{h/2} \sigma_0 dz = \frac{\sigma_0 h}{\sqrt{3}} \tag{6.23}$$

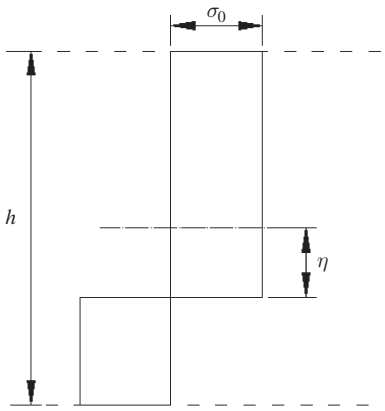

Fig. 6.1 Stress distribution corresponding to maximum $\frac{NM}{N_0 M_{0E}}$ ($\eta = h/2\sqrt{3}$) (Woelke et al., 2006)

Using (6.20), we write:

$$\frac{{N_x}^2}{{N_0}^2} = \frac{1}{3} \tag{6.24}$$

Similarly, we obtain:

$$\frac{M^2}{{M_{0E}}^2} = \frac{4{M_0}^2}{9{M_{0E}}^2} \quad \text{and} \quad \frac{NM}{N_0 M_{0E}} = 2\sqrt{3}\frac{M_0}{9M_{0E}} \tag{6.25}$$

Substitution of (6.24), (6.25) and the above-determined parameters $a = 1$ and $b = \frac{{M_{0E}}^2}{{M_0}^2}$ into the (6.22) yields:

$$\frac{1}{3} + \frac{{M_{0E}}^2}{{M_0}^2}\frac{4{M_0}^2}{9{M_{0E}}^2} + 2\sqrt{3}c\frac{M_0}{9M_{0E}} = 1 \tag{6.26}$$

which leads to:

$$c = \frac{M_{0E}}{\sqrt{3}M_0} \tag{6.27}$$

Substituting the parameters *a,b,c* into (6.22) we arrive at the limit yield surface as defined by Iliushin:

$$F = \frac{M^2}{{M_0}^2} + \frac{N^2}{{N_0}^2} + \frac{1}{\sqrt{3}}\frac{|MN|}{M_0 N_0} = 1 \tag{6.28}$$

The stress intensities are given by (6.19); unlike in the original Iliushin's yield function, they account for the damage effects.

In Chap. 5, were introduced several other modifications to the Iliushin's yield surface for a better description of the plastic behavior of shells. We adopt the same modifications of the yield function in this chapter. We include the transverse shear forces Q_x, Q_y by expanding one of the stress intensities in (6.19), as in the previous chapter, cf. (Shi and Voyiadjis, 1992):

$$N^2 = \left(1 + \frac{1}{2}n\xi\right)\left({N_x}^2 + {N_y}^2\right) - (1 - n\xi)\, N_x N_y + 3\left({N_{xy}}^2 + {Q_x}^2 + {Q_y}^2\right) \quad (6.29)$$

Shi and Voyiadjis (1992) showed that the influence of the shear forces on plastic behavior of thick plates and shells could be very important.

In Sect. 5.2.3 a plastic curvature parameter $\alpha\,(\bar{\kappa}^p)$ was incorporated into (6.28), to account for the development of the plastic curvature across the thickness (Crisfield, 1981a):

$$F = \frac{M^2}{\alpha^2 {M_0}^2} + \frac{N^2}{{N_0}^2} + \frac{1}{\sqrt{3}\alpha}\frac{|MN|}{M_0 N_0} - \frac{Y(k)}{{\sigma_0}^2} = 0 \quad (6.30)$$

or:

$$F = \frac{|M|}{\alpha M_0} + \frac{N^2}{{N_0}^2} - \frac{Y(k)}{{\sigma_0}^2} = 0 \quad (6.31)$$

where α and $\bar{\kappa}^p$ were given by (5.10), (5.11).

We used a material parameter $Y\,(k)$, in (6.30), (6.31), which depends on the isotropic hardening parameter k, similarly to (6.1), (6.2).

In Sect. 5.2.4, we derived a stress resultant-based kinematic hardening rule, allowing for the correct predictions of the Bauschinger effect. Adopting the same hardening rule here, we express the yield surface as:

$$F^* = \frac{|M^*|}{\alpha M_0} + \frac{(N^*)^2}{{N_0}^2} - \frac{Y(k)}{{\sigma_0}^2} = 0 \quad (6.32)$$

where:

$$\begin{aligned}\left(N^*\right)^2 = {} & \left(1 + \frac{1}{2}n\xi\right)\left[\left(N_x - {N_x}^*\right)^2 + \left(N_y - {N_y}^*\right)^2\right] \\ & - (1 - n\xi)\left(N_x - {N_x}^*\right)\left(N_y - {N_y}^*\right) \\ & + 3\left[\left(N_{xy} - {N_{xy}}^*\right)^2 + \left(Q_x - {Q_x}^*\right)^2 + \left(Q_y - {Q_y}^*\right)^2\right] \end{aligned} \quad (6.33)$$

$$\begin{aligned}\left(M^*\right)^2 = {} & \left(1 + \frac{1}{2}n\xi\right)\left[\left(M_x - {M_x}^*\right)^2 + \left(M_y - {M_y}^*\right)^2\right] \\ & - (1 - n\xi)\left(M_x - {M_x}^*\right)\left(M_y - {M_y}^*\right) + 3\left(M_{xy} - {M_{xy}}^*\right)^2 \end{aligned} \quad (6.34)$$

In the above relations $M_x{}^*$, $M_y{}^*$, $M_{xy}{}^*$, $N_x{}^*$, $N_y{}^*$, $N_{xy}{}^*$, $Q_x{}^*$, $Q_y{}^*$ are the residual bending moments, and normal and shear forces, respectively, that were derived in the previous chapter and given by (5.33), (5.34), (5.35). We repeat them for completeness:

$$
\begin{aligned}
&If\, F^* = 1 \; and \; \nabla F^* > 0 \; (plastic\; loading)\\
&\Delta N_x{}^* = \beta_1 (1-F)\frac{N_0}{\varepsilon_0}\left[\Delta \varepsilon_x{}^p - \frac{1}{h} N_x{}^* \Delta \varepsilon_{eq}{}^p\right]\\
&\Delta N_y{}^* = \beta_1 (1-F)\frac{N_0}{\varepsilon_0}\left[\Delta \varepsilon_y{}^p - \frac{1}{h} N_y{}^* \Delta \varepsilon_{eq}{}^p\right]\\
&\Delta N_{xy}{}^* = \beta_1 (1-F)\frac{N_0}{\varepsilon_0}\left[\Delta \varepsilon_{xy}{}^p - \frac{1}{h} N_{xy}{}^* \Delta \varepsilon_{eq}{}^p\right]\\
&\Delta Q_x{}^* = \beta_1 (1-F)\frac{N_0}{\varepsilon_0}\left[\Delta \varepsilon_{xz}{}^p - \frac{1}{h} Q_x{}^* \Delta \varepsilon_{eq}{}^p\right]\\
&\Delta Q_y{}^* = \beta_1 (1-F)\frac{N_0}{\varepsilon_0}\left[\Delta \varepsilon_{yz}{}^p - \frac{1}{h} Q_y{}^* \Delta \varepsilon_{eq}{}^p\right]
\end{aligned}
\tag{6.35}
$$

$$
\begin{aligned}
&\Delta M_x{}^* = \beta_2 (1-F)\frac{M_0}{\kappa_0}\left[\Delta \kappa_x{}^p - \frac{6}{h^2} M_x{}^* \Delta \kappa_{eq}{}^p\right]\\
&\Delta M_y{}^* = \beta_2 (1-F)\frac{M_0}{\kappa_0}\left[\Delta \kappa_y{}^p - \frac{6}{h^2} M_y{}^* \Delta \kappa_{eq}{}^p\right]\\
&\Delta M_{xy}{}^* = \beta_2 (1-F)\frac{M_0}{\kappa_0}\left[\Delta \kappa_{xy}{}^p - \frac{6}{h^2} M_{xy}{}^* \Delta \kappa_{eq}{}^p\right]
\end{aligned}
\tag{6.36}
$$

$$
\begin{aligned}
&If\; F^* < 1 \; and \; \nabla F^* \le 0 \; (unloading\; or\; neutral\; loading)\\
&\Delta N_x{}^* = \Delta N_y{}^* = \Delta N_{xy}{}^* = \Delta Q_x{}^* = \Delta Q_y{}^* = \Delta M_x{}^* = \Delta M_y{}^* = \Delta M_{xy}{}^* = 0
\end{aligned}
\tag{6.37}
$$

Note that by setting the porosity parameter to zero, i.e., $\xi = 0$, the yield surface given by (6.32), (6.33), (6.34) reduces to that given by (5.12), (5.13), (5.14), where the damage effects were not considered.

The meaning of the material parameters β_1 and β_2 in the above formulation was explained in Chap. 5.

We arrive at a final form of the yield function for ductile porous metals, given by (6.32), (6.33), (6.34) and (6.35), (6.36), (6.37), expressed in terms of the stress resultants and couples, with isotropic and kinematic hardening. This is a convenient form of the yield surface for the analysis of shells, accounting for the damage effects through the evolution of porosity. A graphic representation of the yield surface on the $N_x M_x$ plane with $\alpha = 1$ and $Y = \sigma_0^2$ is shown in Fig. 5.3.

6.3 Explicit Tangent Stiffness Matrix

We follow the same procedure as in the preceding chapter to derive the tangent stiffness matrix. The plastic node method is used in the derivation, i.e., the plastic deformations and damage are considered to be concentrated in the plastic hinges. The yield function is checked only at each node of the finite elements. If the combination of stress resultants satisfies the yield condition, that node is considered to be plastic, which triggers the void growth, as we consider the porosity to be a function of the plastic flow. Thus, the inelastic deformations are considered only at the nodes, and the interior of the element remains elastic.

When node i of the element becomes plastic, the yield function takes the form:

$$F^*{}_i\left(\mathbf{N_i}, \mathbf{Q_i}, \mathbf{M_i}, \mathbf{N^*{}_i}, \mathbf{Q^*{}_i}, \mathbf{M^*{}_i}, \mathbf{k_i}, \boldsymbol{\xi}_\mathbf{i}\right) = 0 \tag{6.38}$$

where:

$$\mathbf{N_i} = \begin{Bmatrix} N_x \\ N_y \\ N_{xy} \end{Bmatrix}; \quad \mathbf{Q_i} = \begin{Bmatrix} Q_x \\ Q_y \end{Bmatrix}; \quad \mathbf{M_i} = \begin{Bmatrix} M_x \\ M_y \\ M_{xy} \end{Bmatrix} \tag{6.39}$$

$$\mathbf{N^*{}_i} = \begin{Bmatrix} N^*{}_x \\ N^*{}_y \\ N^*{}_{xy} \end{Bmatrix}; \quad \mathbf{Q^*{}_i} = \begin{Bmatrix} Q^*{}_x \\ Q^*{}_y \end{Bmatrix}; \quad \mathbf{M^*{}_i} = \begin{Bmatrix} M^*{}_x \\ M^*{}_y \\ M^*{}_{xy} \end{Bmatrix} \tag{6.40}$$

At the same time, the stress resultants must remain on the loading surface, i.e., the consistency condition must be satisfied:

$$\begin{aligned} &\frac{\partial F^*{}_i}{\partial \mathbf{M_i}} d\mathbf{M_i} + \frac{\partial F^*{}_i}{\partial \mathbf{N_i}} d\mathbf{N_i} + \frac{\partial F^*{}_i}{\partial \mathbf{Q_i}} d\mathbf{Q_i} + \frac{\partial F^*{}_i}{\partial \mathbf{M^*{}_i}} d\mathbf{M^*{}_i} + \frac{\partial F^*{}_i}{\partial \mathbf{N^*{}_i}} d\mathbf{N^*{}_i} + \frac{\partial F^*{}_i}{\partial \mathbf{Q^*{}_i}} d\mathbf{Q^*{}_i} \\ &\quad + \frac{\partial F^*{}_i}{\partial \mathbf{k_i}} d\mathbf{k_i} + \frac{\partial F^*{}_i}{\partial \boldsymbol{\xi}_\mathbf{i}} d\boldsymbol{\xi}_\mathbf{i} = 0 \end{aligned} \tag{6.41}$$

We assume an additive decomposition of strains into elastic and plastic parts:

$$\varepsilon = \varepsilon^e + \varepsilon^p \tag{6.42}$$

The associated flow rule is used to determine the increments of plastic strains:

$$\Delta {\kappa_x}^p = \sum_{i=1}^{NPN} \Delta\lambda_i \frac{\partial F^*{}_i}{\partial M_{xi}} \quad \text{and} \quad \Delta {\varepsilon_x}^p = \sum_{i=1}^{NPN} \Delta\lambda_i \frac{\partial F^*{}_i}{\partial N_{xi}} \tag{6.43}$$

where *NPN* is the number of plastic nodes in the element and $\Delta\lambda_i$ is a plastic multiplier. The remaining increments of the plastic strains are obtained the same way. The

plastic strain fields are interpolated as in the linear elastic analysis, ((3.45), (3.46), (3.47)) given here in the incremental form:

$$\Delta\boldsymbol{\varepsilon}_{\mathbf{b}}^{\mathbf{p}} = \begin{Bmatrix} \Delta\kappa_x{}^p \\ \Delta\kappa_y{}^p \\ 2\Delta\kappa_{xy}{}^p \end{Bmatrix}, \quad \Delta\boldsymbol{\varepsilon}_{\mathbf{m}}^{\mathbf{p}} = \begin{Bmatrix} \Delta\varepsilon_x{}^p \\ \Delta\varepsilon_y{}^p \\ 2\Delta\varepsilon_{xy}{}^p \end{Bmatrix}, \quad \Delta\boldsymbol{\varepsilon}_{\mathbf{s}}^{\mathbf{p}} = \begin{Bmatrix} \Delta\gamma_{xz}{}^p \\ \Delta\gamma_{yz}{}^p \end{Bmatrix} \tag{6.44}$$

The evolution of the porosity parameter representing damage is given by (6.15), repeated here for convenience:

$$\Delta\xi = k_3 \left[\Delta\varepsilon_x{}^p + \Delta\varepsilon_y{}^p + \frac{h}{2}\left(\Delta\kappa_x{}^p + \Delta\kappa_y{}^p\right) \right] \tag{6.45}$$

The assumption of an additive decomposition of strains can be extended to displacements, provided that the strains are small (Shi and Voyiadjis, 1992; Ueda and Yao, 1982). Although we take into account geometric non-linearities, we consider only large rigid rotations and translations, but small strains. Thus, we write:

$$q = q^e + q^p \tag{6.46}$$

Following the work of Shi and Voyiadjis (1992), we approximate the increments of plastic displacements by the increments of plastic strains. The plastic rotation $\Delta\phi_x{}^p$ is a function of both $\Delta\kappa_x{}^p$ and $\Delta\kappa_{xy}{}^p$, as can be deduced from (6.44). Assuming that the increment of the plastic nodal rotation $\Delta\phi_{xi}{}^p$ is proportional to the increment of the elastic nodal rotation $\Delta\phi_{xi}$, we express the former as:

$$\begin{aligned} \Delta\phi_{xi}{}^p &= \lim_{\delta\Omega\to 0} \iint_{\delta\Omega_i} \left[\Delta\kappa_x{}^p + \frac{\Delta\phi_{xi}{}^2}{\Delta\phi_{xi}{}^2 + \Delta\phi_{yi}{}^2} 2\Delta\kappa_{xy}{}^p \right] dxdy \\ &= \Delta\lambda_i \left[\frac{\partial F^*{}_i}{\partial M_{xi}} + \frac{2\Delta\phi_{xi}{}^2}{\Delta\phi_{xi}{}^2 + \Delta\phi_{yi}{}^2} \frac{\partial F^*{}_i}{\partial M_{xyi}} \right] \end{aligned} \tag{6.47}$$

where $\delta\Omega_i$ represents the infinitesimal neighborhood of node i. The vector of incremental nodal plastic displacements of the element at node i can then be expressed as:

$$\Delta\mathbf{q}_{\mathbf{i}}^{\mathbf{p}} = \mathbf{a}_{\mathbf{i}}\Delta\lambda_i \tag{6.48}$$

with $\mathbf{a_i}$ given by:

$$\mathbf{a_i}^{\mathbf{T}} = \left\{ \frac{\partial F^*_i}{\partial N_{xi}} + p_u \frac{\partial F^*_i}{\partial N_{xyi}}; \frac{\partial F^*_i}{\partial N_{yi}} + p_v \frac{\partial F^*_i}{\partial N_{xyi}}; \frac{\partial F^*_i}{\partial Q_{xi}} + \frac{\partial F^*_i}{\partial Q_{yi}}; \right.$$
$$\left. \frac{\partial F^*_i}{\partial M_{xi}} + p_{\phi x} \frac{\partial F^*_i}{\partial M_{xyi}}; \frac{\partial F^*_i}{\partial M_{yi}} + p_{\phi y} \frac{\partial F^*_i}{\partial M_{xyi}} \right\}$$
$$p_u = \frac{2\Delta u_i{}^2}{\Delta u_i{}^2 + \Delta v_i{}^2}; \quad p_v = \frac{2\Delta v_i{}^2}{\Delta u_i{}^2 + \Delta v_i{}^2}; \tag{6.49}$$
$$p_{\phi x} = \frac{2\Delta \phi_{xi}{}^2}{\Delta \phi_{xi}{}^2 + \Delta \phi_{yi}{}^2}; \quad p_{\phi y} = \frac{2\Delta \phi_{yi}{}^2}{\Delta \phi_{xi}{}^2 + \Delta \phi_{yi}{}^2}$$

Equations (6.48) and (6.49) indicate that the plastic displacements at the nodes are functions only of stress resultants at this node. We therefore, we write the vector of increments of the nodal plastic displacements, as:

$$\Delta \mathbf{q^p} = \begin{bmatrix} \mathbf{a_1} & \mathbf{0} & \mathbf{0} \\ \mathbf{0} & \mathbf{a_i} & \mathbf{0} \\ \mathbf{0} & \mathbf{0} & \mathbf{a_{NPN}} \end{bmatrix} \begin{Bmatrix} \Delta\lambda_1 \\ \Delta\lambda_i \\ \Delta\lambda_{NPN} \end{Bmatrix} = \mathbf{a}\Delta\boldsymbol{\lambda} \tag{6.50}$$

To determine the tangent stiffness matrix of the element, we use the definition of the virtual elastic bending, membrane, and transverse shear strains, respectively: $\delta\boldsymbol{\varepsilon}_\mathbf{b}$, $\delta\boldsymbol{\varepsilon}_\mathbf{m}$, $\delta\boldsymbol{\varepsilon}_\mathbf{s}$ (δ-virtual) and the stress couples and stress resultants of the element **M, N, Q** from the preceding chapters. We again use the linearized equilibrium equations of the system at configuration $k+1$ in the Updated Lagrangian description, expressed by the principle of the virtual work, which in finite element modeling takes the form:

$$\iint_\Omega \left(\delta\boldsymbol{\varepsilon}_\mathbf{b}{}^{\mathbf{T}}\mathbf{D}\boldsymbol{\varepsilon}_\mathbf{b} + \delta\boldsymbol{\varepsilon}_\mathbf{m}{}^{\mathbf{T}}\mathbf{S}\boldsymbol{\varepsilon}_\mathbf{m} + \delta\boldsymbol{\varepsilon}_\mathbf{s}{}^{\mathbf{T}}\mathbf{T}\boldsymbol{\varepsilon}_\mathbf{s}\right) dxdy + \iint_\Omega \delta\boldsymbol{\theta}^{\mathbf{Tk}}\mathbf{F}\boldsymbol{\theta} dxdy$$
$$= {}^{k+1}R - \iint_\Omega \left(\delta\boldsymbol{\varepsilon}_\mathbf{b}{}^{\mathbf{Tk}}\mathbf{M} + \delta\boldsymbol{\varepsilon}_\mathbf{m}{}^{\mathbf{Tk}}\mathbf{N} + \delta\boldsymbol{\varepsilon}_\mathbf{s}{}^{\mathbf{Tk}}\mathbf{Q}\right) dxdy \tag{6.51}$$

where ${}^{k+1}R$ is the total external virtual work at step $k+1$, $\boldsymbol{\theta}$ is the slope vector, and ${}^{\mathbf{k}}\mathbf{F}$ is a membrane stress resultant matrix at step k given by:

$$\boldsymbol{\theta} = \begin{Bmatrix} \dfrac{\partial \Delta w}{\partial x} \\ \dfrac{\partial \Delta w}{\partial y} \end{Bmatrix}, \quad {}^{\mathbf{k}}\mathbf{F} = \begin{bmatrix} {}^kN_x & {}^kN_{xy} \\ {}^kN_{xy} & {}^kN_y \end{bmatrix} \tag{6.52}$$

The slope field $\boldsymbol{\theta}$ is evaluated the same way as in Chap. 4. Using the equations derived in Chap. 5, we rewrite (6.51) as:

$$\iint_{\Omega} \left(\delta\boldsymbol{\varepsilon_b}^{\mathbf{T}}\mathbf{D}\boldsymbol{\varepsilon_b} + \delta\boldsymbol{\varepsilon_m}^{\mathbf{T}}\mathbf{S}\boldsymbol{\varepsilon_m} + \delta\boldsymbol{\varepsilon_s}^{\mathbf{T}}\mathbf{T}\boldsymbol{\varepsilon_s}\right) dxdy + \delta\Delta\mathbf{q}^{e\mathbf{T}}\mathbf{K_g}\Delta\mathbf{q}^{e} = {}^{k+1}R - \delta\Delta\mathbf{q}^{\mathbf{T}}\Delta\mathbf{f} \tag{6.53}$$

where $\mathbf{K_g}$ is the initial stress matrix defined as in Chap. 4:

$$\mathbf{K_g} = \iint_{\Omega} \mathbf{G}^{\mathbf{Tk}}\mathbf{F}\mathbf{G}dxdy \tag{6.54}$$

and $\mathbf{f}$ is the internal force vector resulting from the unbalanced forces in configuration k and expressed as:

$$\mathbf{f} = \iint_{\Omega} \left(\mathbf{B_b}^{\mathbf{Tk}}\mathbf{M} + \mathbf{B_m}^{\mathbf{Tk}}\mathbf{N} + \mathbf{B_s}^{\mathbf{Tk}}\mathbf{Q}\right) dxdy \tag{6.55}$$

We now rewrite (6.53) using (6.42) as:

$$\begin{aligned}\iint_{\Omega} \left[\left(\delta\boldsymbol{\varepsilon_b}^{e\mathbf{T}} + \delta\boldsymbol{\varepsilon_b}^{p\mathbf{T}}\right)\mathbf{M} + \left(\delta\boldsymbol{\varepsilon_m}^{e\mathbf{T}} + \delta\boldsymbol{\varepsilon_m}^{p\mathbf{T}}\right)\mathbf{N} + \left(\delta\boldsymbol{\varepsilon_s}^{e\mathbf{T}} + \delta\boldsymbol{\varepsilon_s}^{p\mathbf{T}}\right)\mathbf{Q}\right] dxdy \\ + \delta\Delta\mathbf{q}^{e\mathbf{T}}\mathbf{K_g}\Delta\mathbf{q}^{e} = {}^{k+1}R - \delta\Delta\mathbf{q}^{\mathbf{T}}\Delta\mathbf{f}\end{aligned} \tag{6.56}$$

Rearranging terms and writing the above equation in incremental form, we obtain:

$$\begin{aligned}&\iint_{\Omega} \left(\delta\Delta\boldsymbol{\varepsilon}_{\mathbf{b}}^{e\mathbf{T}}\Delta\mathbf{M} + \delta\Delta\boldsymbol{\varepsilon}_{\mathbf{m}}^{e\,\mathbf{T}}\Delta\mathbf{N} + \delta\Delta\boldsymbol{\varepsilon}_{\mathbf{s}}^{e\mathbf{T}}\Delta\mathbf{Q}\right) dxdy \\ &\quad + \iint_{\Omega} \left(\delta\Delta\boldsymbol{\varepsilon}_{\mathbf{b}}^{p\mathbf{T}}\Delta\mathbf{M} + \delta\Delta\boldsymbol{\varepsilon}_{\mathbf{m}}^{p\,\mathbf{T}}\Delta\mathbf{N} + \delta\Delta\boldsymbol{\varepsilon}_{\mathbf{s}}^{p\mathbf{T}}\Delta\mathbf{Q}\right) dxdy \\ &\quad + \delta\Delta\mathbf{q}^{e\mathbf{T}}\mathbf{K_g}\Delta\mathbf{q}^{e} = {}^{k+1}R - \delta\Delta\mathbf{q}^{\mathbf{T}}\Delta\mathbf{f}\end{aligned} \tag{6.57}$$

Substituting (6.43) into (6.57), we obtain:

$$\begin{aligned}&\iint_{\Omega} \left(\delta\Delta\boldsymbol{\varepsilon_b}^{e\mathbf{T}}\Delta\mathbf{M} + \delta\Delta\boldsymbol{\varepsilon_m}^{e\mathbf{T}}\Delta\mathbf{N} + \delta\Delta\boldsymbol{\varepsilon_s}^{e\mathbf{T}}\Delta\mathbf{Q}\right) dxdy \\ &\quad + \sum_{i=1}^{NPN} \delta\Delta\lambda_i \left[\frac{\partial F^*{}_i}{\partial\mathbf{M_i}}d\mathbf{M_i} + \frac{\partial F^*{}_i}{\partial\mathbf{N_i}}d\mathbf{N_i} + \frac{\partial F^*{}_i}{\partial\mathbf{Q_i}}d\mathbf{Q_i}\right] \\ &\quad + \delta\Delta\mathbf{q}^{e\mathbf{T}}\mathbf{K_g}\Delta\mathbf{q}^{e} = {}^{k+1}R - \delta\Delta\mathbf{q}^{\mathbf{T}}\Delta\mathbf{f}\end{aligned} \tag{6.58}$$

Using (3.68), (3.69), (3.70), (3.71), (3.72), (3.73), as well as the consistency condition given by (6.41), we write:

$$\begin{aligned}&\delta\Delta\mathbf{q}^{e\mathbf{T}}\left(\mathbf{K_e}+\mathbf{K_g}\right)\Delta\mathbf{q}^{e}\\&-\sum_{i=1}^{NPN}\delta\Delta\lambda_i\left[\frac{\partial F^*{}_i}{\partial\mathbf{M^*_i}}d\mathbf{M^*_i}+\frac{\partial F^*{}_i}{\partial\mathbf{N^*_i}}d\mathbf{N^*_i}+\frac{\partial F^*{}_i}{\partial\mathbf{Q^*_i}}d\mathbf{Q^*_i}+\frac{\partial F^*{}_i}{\partial\mathbf{k_i}}d\mathbf{k_i}+\frac{\partial F^*{}_i}{\partial\boldsymbol{\xi}_\mathbf{i}}d\boldsymbol{\xi}_i\right]\\&=^{k+1}R-\delta\Delta\mathbf{q}^{\mathbf{T}}\Delta\mathbf{f}\end{aligned}\tag{6.59}$$

where $\mathbf{K_e}$ is the linear elastic stiffness matrix given by (3.80). Similarly to (5.57), we define:

$$\begin{aligned}&\mathbf{a_b}^{\mathbf{T}}=\frac{\partial F^*{}_i}{\partial\mathbf{M^*_i}}=\begin{bmatrix}\mathbf{a_{b1}}^{\mathbf{T}}&\mathbf{0}&\mathbf{0}\\\mathbf{0}&\mathbf{a_{bi}}^{\mathbf{T}}&\mathbf{0}\\\mathbf{0}&\mathbf{0}&\mathbf{a_{bNPN}}^{\mathbf{T}}\end{bmatrix},\ \mathbf{a_m}^{\mathbf{T}}=\frac{\partial F^*{}_i}{\partial\mathbf{N^*_i}}=\begin{bmatrix}\mathbf{a_{m1}}^{\mathbf{T}}&\mathbf{0}&\mathbf{0}\\\mathbf{0}&\mathbf{a_{mi}}^{\mathbf{T}}&\mathbf{0}\\\mathbf{0}&\mathbf{0}&\mathbf{a_{mNPN}}^{\mathbf{T}}\end{bmatrix},\\&\mathbf{a_s}^{\mathbf{T}}=\frac{\partial F^*{}_i}{\partial\mathbf{Q^*_i}}=\begin{bmatrix}\mathbf{a_{s1}}^{\mathbf{T}}&\mathbf{0}&\mathbf{0}\\\mathbf{0}&\mathbf{a_{si}}^{\mathbf{T}}&\mathbf{0}\\\mathbf{0}&\mathbf{0}&\mathbf{a_{sNPN}}^{\mathbf{T}}\end{bmatrix},\mathbf{a_\xi}^{\mathbf{T}}=\frac{\partial F^*{}_i}{\partial\boldsymbol{\xi}_\mathbf{i}}=\begin{bmatrix}a_{\xi1}&\mathbf{0}&\mathbf{0}\\\mathbf{0}&a_{\xi i}&\mathbf{0}\\\mathbf{0}&\mathbf{0}&a_{\xi NPN}\end{bmatrix}\end{aligned}\tag{6.60}$$

and:

$$\begin{aligned}\mathbf{a_{bi}}^{\mathbf{T}}&=\left\{\frac{\partial F^*{}_i}{\partial M^*{}_{xi}};\frac{\partial F^*{}_i}{\partial M^*{}_{yi}};\frac{\partial F^*{}_i}{\partial M^*{}_{xyi}}\right\};\\\mathbf{a_{mi}}^{\mathbf{T}}&=\left\{\frac{\partial F^*{}_i}{\partial N^*{}_{xi}};\frac{\partial F^*{}_i}{\partial N^*{}_{yi}};\frac{\partial F^*{}_i}{\partial N^*{}_{xyi}}\right\};\\\mathbf{a_{si}}^{\mathbf{T}}&=\left\{\frac{\partial F^*{}_i}{\partial Q^*{}_{xi}};\frac{\partial F^*{}_i}{\partial Q^*{}_{yi}}\right\};\\a_{\xi i}&=\frac{\partial F^*{}_i}{\partial\xi_i};\end{aligned}\tag{6.61}$$

Substituting (6.43) into (6.35) and (6.36), we obtain:

$$\begin{aligned}&dM_x{}^*=\Delta M_x{}^*\\&=\beta_2(1-F)\frac{M_0}{\kappa_0}\Delta\lambda\left[\frac{\partial F^*}{\partial M_x}-\frac{6}{h^2}M_x{}^*\sqrt{\frac{2}{3}\left[\left(\frac{\partial F^*}{\partial M_x}\right)^2+\left(\frac{\partial F^*}{\partial M_y}\right)^2+\left(\frac{\partial F^*}{\partial M_{xy}}\right)^2\right]}\right]\end{aligned}\tag{6.62}$$

and similarly for the remaining hardening parameters. Vectors of the hardening parameters therefore yield:

$$d\mathbf{N}^*_{\mathbf{i}} = \begin{Bmatrix} \Delta N^*_{xi} \\ \Delta N^*_{yi} \\ \Delta N^*_{xyi} \end{Bmatrix} = \mathbf{A_m}\Delta\boldsymbol{\lambda}; d\mathbf{Q}^*_{\mathbf{i}} = \begin{Bmatrix} \Delta Q^*_{xi} \\ \Delta Q^*_{yi} \end{Bmatrix} = \mathbf{A_s}\Delta\boldsymbol{\lambda}; \tag{6.63}$$

and

$$d\mathbf{M}^*_{\mathbf{i}} = \begin{Bmatrix} \Delta M^*_{xi} \\ \Delta M^*_{yi} \\ \Delta M^*_{xyi} \end{Bmatrix} = \mathbf{A_b}\Delta\boldsymbol{\lambda} \tag{6.64}$$

where $\mathbf{A_m}$, $\mathbf{A_s}$, $\mathbf{A_b}$ are given by:

$$\begin{gathered} \mathbf{A_m} = \begin{bmatrix} \mathbf{A_{m1}} & \mathbf{0} & \mathbf{0} \\ \mathbf{0} & \mathbf{A_{mi}} & \mathbf{0} \\ \mathbf{0} & \mathbf{0} & \mathbf{A_{mNPN}} \end{bmatrix}, \mathbf{A_b} = \begin{bmatrix} \mathbf{A_{b1}} & \mathbf{0} & \mathbf{0} \\ \mathbf{0} & \mathbf{A_{bi}} & \mathbf{0} \\ \mathbf{0} & \mathbf{0} & \mathbf{A_{bNPN}} \end{bmatrix}, \\ \mathbf{A_s} = \begin{bmatrix} \mathbf{A_{s1}} & \mathbf{0} & \mathbf{0} \\ \mathbf{0} & \mathbf{A_{si}} & \mathbf{0} \\ \mathbf{0} & \mathbf{0} & \mathbf{A_{sNPN}} \end{bmatrix} \end{gathered} \tag{6.65}$$

$\mathbf{A_{mi}}$, $\mathbf{A_{si}}$, $\mathbf{A_{bi}}$ are given by (5.61).

The evolution equation for the porosity parameter can be obtained by substitution of (6.43) into (6.45):

$$d\xi_i = \Delta\xi_i = k_3\Delta\lambda_i \left[\frac{\partial F^*_i}{\partial N_{xi}} + \frac{\partial F^*_i}{\partial N_{yi}} + \frac{h}{2}\left(\frac{\partial F^*_i}{\partial M_{xi}} + \frac{\partial F^*_i}{\partial M_{yi}} \right) \right] = A_{\xi i}\Delta\lambda_i \tag{6.66}$$

Again, we apply the plastic node method to derive the matrix form of the above equation:

$$d\boldsymbol{\xi}_{\mathbf{i}} = \Delta\boldsymbol{\xi}_{\mathbf{i}} = \mathbf{A}_{\boldsymbol{\xi}}\Delta\boldsymbol{\lambda} \tag{6.67}$$

where:

$$\mathbf{A}_{\xi} = \begin{bmatrix} A_{\xi 1} & 0 & 0 \\ 0 & A_{\xi i} & 0 \\ 0 & 0 & A_{\xi NPN} \end{bmatrix} \tag{6.68}$$

and:

$$A_{\xi i} = k_3 \left[\frac{\partial F^*_i}{\partial N_{xi}} + \frac{\partial F^*_i}{\partial N_{yi}} + \frac{h}{2}\left(\frac{\partial F^*_i}{\partial M_{xi}} + \frac{\partial F^*_i}{\partial M_{yi}} \right) \right] \tag{6.69}$$

Following the work of Shi and Voyiadjis (1992) we also define the isotropic hardening parameter as:

$$\mathbf{H}\Delta\boldsymbol{\lambda} = \begin{bmatrix} H_1 & 0 & 0 \\ 0 & H_i & 0 \\ 0 & 0 & H_{NPN} \end{bmatrix} \begin{Bmatrix} \Delta\lambda_1 \\ \Delta\lambda_i \\ \Delta\lambda_{NPN} \end{Bmatrix} = - \begin{Bmatrix} \dfrac{\partial F^*{}_1}{\partial k_1} dk_1 \\ \dfrac{\partial F^*{}_i}{\partial k_i} dk_i \\ \dfrac{\partial F^*{}_{NPN}}{\partial k_{NPN}} dk_{NPN} \end{Bmatrix} \tag{6.70}$$

We now substitute (6.60), (6.63), (6.67) and (6.70) into (6.59) to obtain:

$$\begin{aligned} &\delta\Delta\mathbf{q}^{e\mathbf{T}} \left(\mathbf{K_e} + \mathbf{K_g}\right) \Delta\mathbf{q}^e + \delta\Delta\boldsymbol{\lambda}^{\mathbf{T}} \left[\mathbf{H} - \mathbf{a_b}^{\mathbf{T}}\mathbf{A_b} - \mathbf{a_m}^{\mathbf{T}}\mathbf{A_m} - \mathbf{a_s}^{\mathbf{T}}\mathbf{A_s} - \mathbf{a_\xi}^{\mathbf{T}}\mathbf{A_\xi}\right] \Delta\boldsymbol{\lambda} \\ &\quad = {}^{k+1}R - \delta\Delta\mathbf{q}^{\mathbf{T}}\Delta\mathbf{f} \end{aligned} \tag{6.71}$$

Using equations (6.46) and (6.48) in equation (6.71), we write:

$$\begin{aligned} &\left(\delta\Delta\mathbf{q}^{\mathbf{T}} - \delta\Delta\mathbf{q}^{p\mathbf{T}}\right) \left(\mathbf{K_e} + \mathbf{K_g}\right) \Delta\mathbf{q}^e + \delta\Delta\boldsymbol{\lambda}^{\mathbf{T}} \left[\mathbf{H} - \mathbf{a_b}^{\mathbf{T}}\mathbf{A_b} - \mathbf{a_m}^{\mathbf{T}}\mathbf{A_m} - \mathbf{a_s}^{\mathbf{T}}\mathbf{A_s} - \mathbf{a_\xi}^{\mathbf{T}}\mathbf{A_\xi}\right] \Delta\boldsymbol{\lambda} \\ &\quad - {}^{k+1}R + \delta\Delta\mathbf{q}^{\mathbf{T}}\Delta\mathbf{f} = \delta\Delta\mathbf{q}^{\mathbf{T}} \left[\left(\mathbf{K_e} + \mathbf{K_g}\right) \Delta\mathbf{q}^e - {}^{k+1}R^* + \Delta\mathbf{f}\right] \\ &\quad + \delta\Delta\boldsymbol{\lambda}^{\mathbf{T}} \left[-\mathbf{a}^{\mathbf{T}} \left(\mathbf{K_e} + \mathbf{K_g}\right) \Delta\mathbf{q}^e + \left(\mathbf{H} - \mathbf{a_b}^{\mathbf{T}}\mathbf{A_b} - \mathbf{a_m}^{\mathbf{T}}\mathbf{A_m} - \mathbf{a_s}^{\mathbf{T}}\mathbf{A_s} - \mathbf{a_\xi}^{\mathbf{T}}\mathbf{A_\xi}\right) \Delta\boldsymbol{\lambda}\right] = 0 \end{aligned} \tag{6.72}$$

with

$${}^{k+1}R = {}^{k+1}R^* \delta\Delta\mathbf{q} \tag{6.73}$$

By virtue of the variational method, equation (6.72) gives:

$$\begin{aligned} &\left(\mathbf{K_e} + \mathbf{K_g}\right) \Delta\mathbf{q}^e - {}^{k+1}R^* + \Delta\mathbf{f} = 0 \\ &\quad - \mathbf{a}^{\mathbf{T}} \left(\mathbf{K_e} + \mathbf{K_g}\right) \Delta\mathbf{q}^e + \left(\mathbf{H} - \mathbf{a_b}^{\mathbf{T}}\mathbf{A_b} - \mathbf{a_m}^{\mathbf{T}}\mathbf{A_m} - \mathbf{a_s}^{\mathbf{T}}\mathbf{A_s} - \mathbf{a_\xi}^{\mathbf{T}}\mathbf{A_\xi}\right) \Delta\boldsymbol{\lambda} = 0 \end{aligned} \tag{6.74}$$

Substituting equations (6.46) and (6.48) into the above equations we obtain:

$$\left(\mathbf{K_e} + \mathbf{K_g}\right) \Delta\mathbf{q}^e - {}^{k+1}R^* + \Delta\mathbf{f} = \left(\mathbf{K_e} + \mathbf{K_g}\right) (\Delta\mathbf{q} - \mathbf{a}\Delta\boldsymbol{\lambda}) = {}^{k+1}R^* - \Delta\mathbf{f} \tag{6.75}$$

$$- \mathbf{a}^{\mathbf{T}} \left(\mathbf{K_e} + \mathbf{K_g}\right) (\Delta\mathbf{q} - \mathbf{a}\Delta\boldsymbol{\lambda}) + \left(\mathbf{H} - \mathbf{a_b}^{\mathbf{T}}\mathbf{A_b} - \mathbf{a_m}^{\mathbf{T}}\mathbf{A_m} - \mathbf{a_s}^{\mathbf{T}}\mathbf{A_s} - \mathbf{a_\xi}^{\mathbf{T}}\mathbf{A_\xi}\right) \Delta\boldsymbol{\lambda} = 0 \tag{6.76}$$

Equation (6.76) leads to:

$$\Delta\boldsymbol{\lambda} = \left[\mathbf{a}^{\mathbf{T}} \left(\mathbf{K_e} + \mathbf{K_g}\right) \mathbf{a} + \left(\mathbf{H} - \mathbf{a_b}^{\mathbf{T}}\mathbf{A_b} - \mathbf{a_m}^{\mathbf{T}}\mathbf{A_m} - \mathbf{a_s}^{\mathbf{T}}\mathbf{A_s} - \mathbf{a_\xi}^{\mathbf{T}}\mathbf{A_\xi}\right)\right]^{-1} \mathbf{a}^{\mathbf{T}} \left(\mathbf{K_e} + \mathbf{K_g}\right) \Delta\mathbf{q} \tag{6.77}$$

Equation (6.75) becomes:

$$\mathbf{K_{epdg}}\Delta\mathbf{q} = {}^{k+1}R^* - \Delta\mathbf{f} \tag{6.78}$$

where $\mathbf{K_{epg}}$ is the elasto-plastic, damage, large displacement stiffness matrix of the element, given by:

$$\mathbf{K_{epdg}} = \left(\mathbf{K_e} + \mathbf{K_g}\right)$$
$$\left\{\mathbf{I} - \mathbf{a}\left[\mathbf{a}^{\mathbf{T}}\left(\mathbf{K_e} + \mathbf{K_g}\right)\mathbf{a} + \left(\mathbf{H} - \mathbf{a_b}^{\mathbf{T}}\mathbf{A_b} - \mathbf{a_m}^{\mathbf{T}}\mathbf{A_m} - \mathbf{a_s}^{\mathbf{T}}\mathbf{A_s} - \mathbf{a_\xi}^{\mathbf{T}}\mathbf{A_\xi}\right)\right]^{-1}\mathbf{a}^{\mathbf{T}}\left(\mathbf{K_e} + \mathbf{K_g}\right)\right\} \tag{6.79}$$

The tangent stiffness matrix given by (6.79) is similar to that presented by Shi and Voyiadjis (1992). As our formulation accounts for large displacements, the stiffness matrix of the element contains the initial stress matrix $\mathbf{K_g}$. The stiffness matrix derived above describes not only isotropic hardening, by means of the parameter $\mathbf{H}$, but kinematic hardening, through parameters $\mathbf{A_b}$, $\mathbf{A_m}$, $\mathbf{A_s}$, which are not determined by curve fitting but derived explicitly from the evolution equation of the backstress given by Armstrong and Frederick (1966).

The most important characteristic described in this chapter is consistent and convenient incorporation of the damage effects into the yield condition and stiffness matrix, by means of $\mathbf{A_\xi}$ matrix. We therefore have a non-layered finite element formulation with shell constitutive equations, yield condition for porous ductile metals, and flow and hardening rules expressed in terms of the membrane and shear forces and bending moments. All the variables used here, namely the porosity function, stress resultants, and couples as well as the residual stress resultants and couples representing the center of the yield surface, are rigorously derived.

6.4 Numerical Examples

We enhanced a finite element computer program previously developed for the elasto-plastic considerations in programming language Fortran 95 to account for the damage effects due to microvoids. A modified Newton-Raphson technique was used to solve a system of non-linear, incremental equations. To overcome the singularity problem appearing at the limit point, the arc-length method (Crisfield, 1983, 1991) was adopted to determine the local load increment for each iteration. We also used an algorithm to return to the yield surface (Crisfield, 1991). We computed our results delivered by the current model were on a personal computer. Some of the reference solutions obtained with the layered approach (ABAQUS) were determined using a Silicon Graphics Onyx 3200 system.

The accuracy of the description of the elasto plastic and damage behavior of shells is verified through discriminating numerical examples. This chapter is a continuation of the previous ones, where linear elastic and elasto-plastic formulations were given. The most important novel feature of the present algorithm is the description of isotropic damage in plates and shells. The examples we present were selected to challenge mainly the representation of the evolution of damage in shells and the associated reduction of stiffness.

Table 6.1 gives the references used here and their abbreviations.

Table 6.1 Models used with abbreviations

Name	Description
V&W-E	Present formulation – elastic analysis
V&W-EP	Present formulation – elasto-plastic analysis
V&W-EPD	Present formulation – elasto-plastic, damage analysis

6.4.1 Clamped Square Plate Subjected to a Central Point Load

In this example, we consider a square plate with all the edges fixed, with an aspect ratio $L/h = 20$, where L is the length of the plate and h is the thickness. The plate is subjected to a central point load. Because of symmetry only a quarter of the plate needs to be examined due to symmetry. This problem was analyzed by Shi and Voyiadjis (1993), by means of the 4×4 mesh of finite elements. The same mesh of 4×4 elements per quarter of the plate will be used here. The geometry of the problem and the material properties are given in Fig. 6.2.

The equilibrium path is a universal curve providing most of the information about functioning of the model independently of whether the deformation of the structure is governed by the bending, membrane, or shear strains. We study the equilibrium path for this problem. The material parameters n and k_3 appearing in (6.7) and (6.11) are: $n = 1.2587$, $k_3 = 0.09$, as determined by Perzyna (1984b) See also Woelke et al., 2006b. The central deflection of the plate as a function of the applied load is given in Fig. 6.3. Shi and Voyiadjis (1993) obtained the critical load for this problem without the influence of damage, of $P_c = 10M_0$. They also showed the substantial reduction of stiffness of the structure when damage was considered. The critical load of the damaged plate was about $P_c = 8M_0$. The result of (Woelke et al., 2006) analysis with the influence of damage considered yields approximately the same

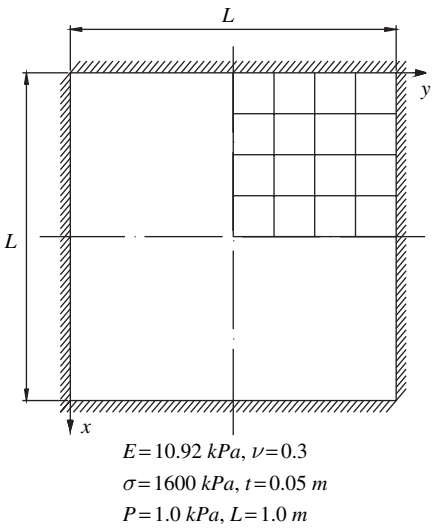

Fig. 6.2 Clamped square plate subjected to a central point load – geometry and material properties (Woelke et al., 2006)

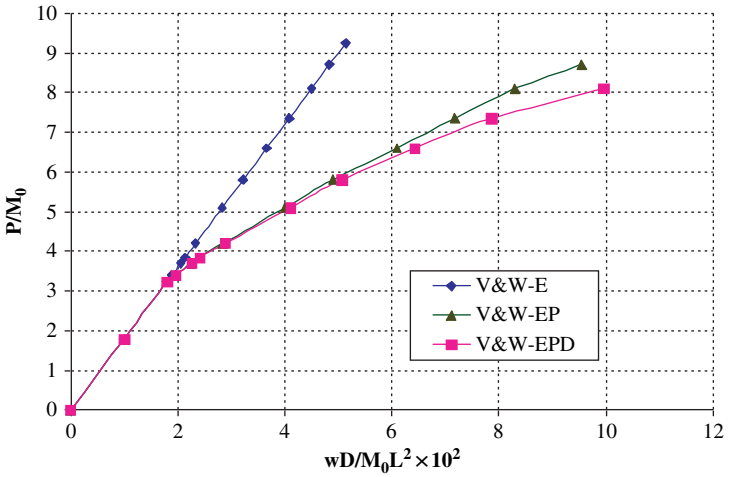

Fig. 6.3 Clamped square plate subjected to a central point load – load displacement curve (Woelke et al., 2006)

critical load $P_c = 8M_0$. As expected, the damage variable only becomes significant when the structure deforms plastically. This is because the evolution of damage is neglected in the elastic zone. Our formulation performs robustly in this test.

6.4.2 Spherical Dome Subjected to Ring of Pressure

The problem of a spherical dome with an 18^0 hole at the top, subjected to a ring of pressure, was investigated in the previous chapter. It was shown by Voyiadjis and Woelke (2004) that the stress resultant-based shell model with the kinematic hardening rule given by (6.35), (6.36) is capable of correctly predicting the elasto-plastic behavior of shells, including the Bauschinger effect. In this chapter, we revisit the problem of the spherical dome subjected to a ring of pressure, to establish the ability of our formulation to approximate damage due to microvoids. As discussed above, the structure is loaded into a plastic zone and the pressure then reversed. We examine the elasto-plastic load-displacement curve and compare the results with the curve obtained with the influence of damage taken into account, to test the functioning and accuracy of the presented yield surface for ductile porous metals, defined in the stress resultant space. The material parameters n and k_3 are the same as in example 7.1: $n = 1.2587,\ k_3 = 0.09$. Geometrical and material data are presented in Fig. 6.4 and the resulting load-displacement curves are plotted in Fig. 6.5.

Through the introduction of the porosity function, which characterizes damage into the yield function, we obtain a strong coupling between plasticity and damage. The damage variable is dependent on the plastic deformation; therefore, through application of a robust kinematic hardening rule, we can model the evolution of damage in the structure loaded into the plastic zone in tension and, after

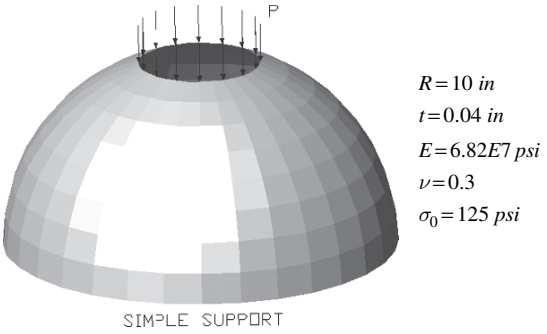

Fig. 6.4 Spherical dome with an 18^0 cut-out; geometry and material properties (Woelke et al., 2006)

the load has been reversed, in compression (Fig. 6.5). The lowered yield point due to the Bauschinger effect is again correctly approximated. The reduction of stiffness caused by damage initiated by the inelastic strains is significant. It leads to a decrease of the ultimate load carried by the structure by about 10%. It is a very significant factor in terms of the engineering analysis of critically important structures.

Figure 6.6 presents a plot of porosity ξ as a function of load. As the evolution of porosity representing growth of voids is a function of the plastic strains, we see growth of voids only when plasticity occurs. In reality, the porosity in the material will not be zero, even with only elastic strains. The level of porosity in the elastic range is, however, negligible and thus is not accounted for in this work. At the load level of approximately $P = 63\,lb/in$ we observe a clear plateau in Fig. 6.6. This means that this load level is the ultimate load carried by the structure. The porosity will most likely grow without application of any additional loading leading to a

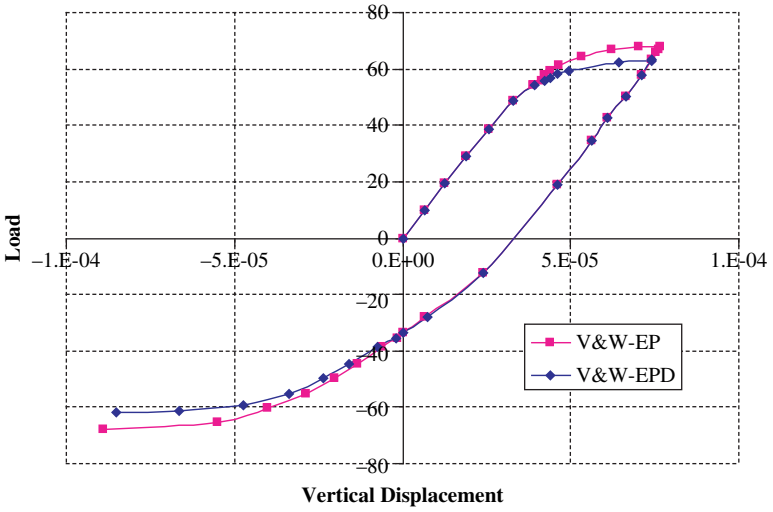

Fig. 6.5 Spherical dome with an 18^0 cut-out – load displacement curve (Woelke et al., 2006)

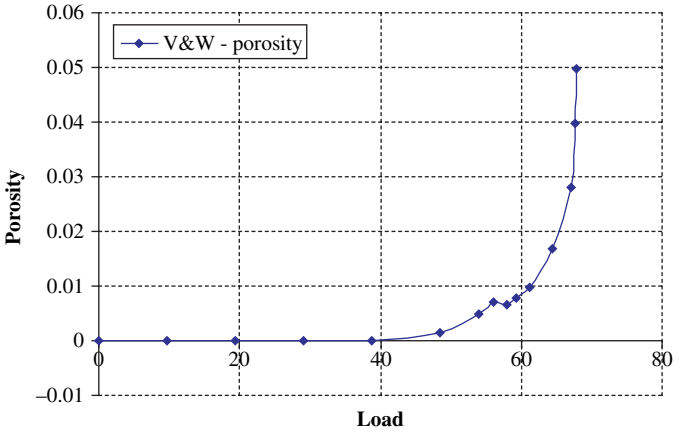

Fig. 6.6 Spherical dome with an 18^0 cut-out – load-porosity curve (Woelke et al., 2006)

local fracture and ultimately collapse of the structure. The collapse will therefore occur at the load level approximately 8% lower than that predicted by the elasto-plastic analysis. Based on the level of porosity, at the first sign of unloading the fracture criterion could be postulated, which would provide additional tools for the modeling of shells. Such a criterion should, however, be verified by the experimental results for various materials and structures, along with all the material parameters necessary for the damage description. As shown in Figs. 6.5 and 6.6, our approach provides a good approximation of the evolution of damage of modeled structures, confirming the validity of the original assumptions. Once again, the computational cost of the calculations is much lower than in the case of shell elements with a layered approach. This is because of the explicit form of the stiffness matrix and the application of the single loading surface with damage variable incorporated. A three-dimensional analysis with the solid elements would be even more expensive. For some problems with a complicated geometry, the computational cost of the finite element procedure may be decisive.

6.5 Summary

The reliability of our concept was evaluated through example problems. In the example in Sect. 6.4.2, the plot of porosity versus load was given, based on which the fracture criterion could be formulated. The example in Sect. 6.4.2 also showed that not considering damage in the analysis of plates and shells could lead to overprediction of the ultimate load carried by the structure. Unfortunately, there is a limited amount of data regarding the evolution of damage in plates and shells that could be used as references. Moreover, it is unrealistic to verify the damage formulation based on comparisons with results obtained by approximate methods. As discussed in previous chapters, the functioning of this algorithm should be tested against

experimental results, particularly in the case of damage. References providing information about the damage in structures based on experiments are even more difficult to find than numerical estimates. Our formulation incorporating damage is conceptually correct, based on the limited references; in addition, our results show the expected pattern of the reduction of stiffness caused by the evolution of damage.

Similarly to the kinematic hardening rule presented in Chap. 5, there are material constants n, k_3 defining the constitutive relations. Determination of these constants is critical to the accuracy of the model. We found the model to be highly sensitive to changes in the values of n, k_3, as well as the parameters defining the kinematic hardening rule. In fact, the results of the analysis obtained using damage formulation could be closely approximated by manipulation of the material parameters in the kinematic hardening rule and the corresponding damage effects that were not considered here. Although this is an interesting observation, such an approach cannot be considered constitutive modeling of the damage phenomenon.

The strongest advantage of our method is its simplicity and efficiency. By means of the quasi-conforming technique the elastic stiffness matrix is calculated explicitly. A non-layered approach allows for the elasto-plastic calculation without discretization of the shell through the thickness. Thus, the tangent stiffness matrix computed here is also given explicitly and numerical integration is not used. This makes the procedure extremely efficient computationally. The isotropic damage variable inserted into the yield criterion expressed in terms of the stress resultant and stress couples provides an additional tool for simulating the behavior of plates and shells, without substantially complicating the analysis. The porosity parameter representing damage due to void growth only is used here. This can be regarded as a limitation of our model, as the influence of nucleation caused by microcracks is very important for certain applications. Our model, however, is based on the evolution of porosity as defined by Duszek-Perzyna and Perzyna (1994), who reported very good results in modeling ductile metals. According to this reference, the influence of microcracks is very important when analyzing metal matrix composites because of cracking of the reinforcing fibers. In the case of homogenous and isotropic shells, the void growth is decisive in the analysis and thus, is the only damage-causing phenomenon we describe.

Only two additional material parameters need be determined to account for damage, as opposed to the higher order approximations advocated by many authors, where sometimes tremendous amounts of experimental data are necessary to calibrate all the required material constants. This would be the case if higher-order damage tensors were used. Moreover, while a more advanced procedure would be needed to model the elasto-plastic and damage behavior of materials, the accuracy of our analysis in terms of structural analysis is satisfactory. Many variables simulating the material behavior lose their significance when the structure made of the material is investigated. This is confirmed by the sensitivity of the model to material parameters defining the kinematic hardening rule, as discussed in the previous paragraph (See also Woelke et al. 2008. In view of the above arguments, as well as the accuracy of the numerical results presented in this chapter, our representation of damage in plates and shells is robust and useful.

There is no "best" comprehensive shell model. Any given formulation will always perform better than others for certain applications. Our formulation is no exception. It has its limitations and is likely to yield more accurate results for certain problems and slightly less accurate for others. Our model realizes the concept of shell elements built on reliable constitutive equations, in the elasto-plastic and damage modeling of plates and shells. It offers flexibility, accuracy, and efficiency. The soundness of all the assumptions was verified and confirmed by a series of challenging numerical examples that confirmed the model's reliability. Thus, the shell formulation developed and presented here is a significant advancement in the area of plates and shells.

References

Abu Al-Rub, R.K. and Voyiadjis, G. (2003). On the coupling of anisotropic damage and plasticity models for ductile materials. Int. J. Solids Struct., 40, 11, 2611–2643.

Armstrong, P.J. and Frederick, C.O. (1966). A Mathematical Representation of the Multiaxial Bauschinger Effect. (CEGB Report RD/B/N/731). Berkeley Laboratories, R&D Department, California.

Beachem, C.D. (1963). An electron fractographic study of the influence of plastic strain conditions upon ductile rapture processes in metals. Trans. A.S.M., 56, 318–326.

Bieniek, M.P. and Funaro, J.R. (1976). Elasto-plastic behaviour of plates and shells. Technical Report DNA 3584A, Weidlinger Associates, New York.

Bieniek, M.P., Funaro, J.R., Baron, M.L. (1976). Numerical Analysis of the Dynamic Response of Elasto-Plastic Shells. Technical Report No. 20, November 1976, Weidlinger Associates, New York.

Bluhm, J.I., and Morrissey, R.J. (1965). Fracture in a Tensile Specimen. Proc. First Int. Conf. On Fracture, Sendai, Japan, September. In T. Yakobori, T. Kawasaki and J.L. Swedlow (eds.), Vol. 3, pp. 1739–1780.

Crisfield, M.A. (1981a). Finite element analysis for combined material and geometric nonlinearities. In W. Wunderlich et al. (eds.) Nonlinear Finite Element Analysis in Structural Mechanics, Springer-Verlag, New York, pp. 325–338.

Crisfield, M.A. (1981b). A fast incremental/iterative solution procedure that handles 'snap-through'. Comp. Stuct., 13, 55–62.

Crisfield, M.A. (1983). An arc-length method including line searches and accelerations. Int. J. Num. Meth. Eng., 19, 1269–1289.

Crisfield, M.A. (1991). Non-linear Finite Element Analysis of Solids and Structures. Vol. 1. John Wiley & Sons Ltd, New York.

Doghri, I. (2000). Mechanics of Deformable Solids: Linear and Nonlinear, Analytical and Computational Aspects. Springer, Germany.

Dornowski, W. and Perzyna P. (2000). Localization phenomena in thermo-viscoplastic flow processes under cyclic dynamic loadings. Comp. Assis. Mech. Eng. Sci., 7, 117–160.

Duszek-Perzyna, M.K. and Perzyna, P. (1993). Adiabatic shear band localization in elastic-plastic single crystals. Int. J. Solids Struct., 30, 1, 61–89.

Duszek-Perzyna, M.K. and Perzyna, P. (1994). Analysis of the influence of different effects on criteria for adiabatic shear band localization in inelastic solids. In R.C. Batra and H.M. Zbib (eds.). Material Instabilities: Theory and Applications, ASME Congress, Chicago, 9–11 November. AMD-Vol. 183/MD-Vol. 50, pp. 59–85.

Duszek-Perzyna, M.K. and Perzyna, P. (1998). Analysis of anisotropy and plastic spin effects on localization phenomena. Arch. Appl. Mech., 68, 352–374, Springer-Verlag, New York.

Fisher, J.R. (1980). Void Nucleation in Spheroidized Steels During Tensile Deformation. Ph.D. Thesis, Brown University.

Gurland, J. and Plateau, J. (1963). The Mechanism of Ductile Rupture of Metals Containing Inclusions. Trans. A.S.M., 56, 443–454.

Gurson, A.L. (1975). Plastic flow and fracture behaviour of ductile materials incorporating void nucleation, growth and interaction, PhD Thesis, Brown University.

Gurson, A.L. (1977). Continuum theory of ductile rapture by void nucleation and growth – Part I – Yield criteria and flow rules for porous ductile media. J. Eng. Mater. Technol., 99, 2–15.

Iliushin, A.A. (1956). Plastichnost', Gostekhizdat, Moscow (in Russian).

Lubarda, V.A. and Krajcinovic, D. (1993). Damage tensors and the crack density distribution. Int. J. Solids Struct., 30, 2859–2877.

Murakami, S. (1988). Mechanical modeling of material damage. J. Appl. Mech., Transact. ASME, 55, 2, 280–286.

Perzyna, P. (1984b). Constitutive modeling of dissipative solids for postcritical behaviour and fracture. ASME, J. Eng. Mater. Technol., 106, 410–419.

Perzyna, P. and Drabik, A. (1989). Description of micro-damage process by porosity parameter for nonlinear viscoplasticity. Arch. Mech., 41, 895–908.

Roy, G.L., Embury, J.D., Edward, G., and Ashby, M.F. (1981). A model of ductile fracture based on the nucleation an growth of voids. Acta Metall., 29, 1509–1522.

Seweryn, A. and Mroz, Z. (1998). On the criterion of damage evolution for variable multiaxial stress states. Int. J. Solids Struct. 35, 1589–1616.

Shi, G and Voyiadjis, G.Z. (1992). A simple non-layered finite element for the elasto-plastic analysis of shear flexible plates. Int. J. Num. Meth. Eng., 33, 85–99.

Shi, G and Voyiadjis, G.Z. (1993). A computational model for FE ductile plastic damage analysis of plate bending. J.Appl. Mech., 60, 749–758.

Ueda, Y., Yao, T. (1982). The plastic node method of plastic analysis. Comp. Meth. Appl. Mech. Eng., 34, 1089–1104.

Voyiadjis, G.Z. and Abu-Lebdeh, (1993). Damage model for concrete using bounding surface concept. J. Eng. Mech., 119, 9, 1865–1885.

Voyiadjis, G.Z. and Deliktas, B. (2000a). A coupled anisotropic damage model for the inelastic response of composite materials. Comp. Meth. Appl. Mech. Eng., 183, 159–199.

Voyiadjis, G.Z., Deliktas, B. (2000b). Multi-scale analysis of multiple damage mechanics coupled with inelastic behavior of composite materials. Mech. Res. Commun., 27, 3, 295–300.

Voyiadjis, G.Z. and Kattan, P.I. (1991). Effect of transverse normal strain on the bending of thick circular plates on the elastic foundation subjected to surface loads. Int. J. Mech. Sci., 33, 6, 413–433.

Voyiadjis, G.Z. and Kattan, P.I. (1992a). A plasticity-damage theory for large deformations of solids. Part I: Theoretical formulation. Int. J. Eng. Sci., 30, 1089–1108.

Voyiadjis, G.Z. and Kattan, P.I. (1992b). Finite strain plasticity and damage in constitutive modeling of metals with spin tensors. Appl. Mech. Rev., 45, S95–S109.

Voyiadjis, G.Z. and Kattan, P.I. (1999). Advances in Damage Mechanics: Metals and Metal Matrix Composites. Elsevier, Oxford.

Voyiadjis, G.Z. and Park, T. (1997). Local and interfacial damage analysis of metal matrix composites using finite element method. Eng. Fract. Mech., 56, 4, 483–511.

Voyiadjis, G.Z. and Park, T. (1999). Kinematics of damage for finite strain plasticity. Int. J. Eng. Sci., 37, 7, 803–830.

Voyiadjis, G.Z. and Venson, A.R. (1995). Experimental damage investigaion of a SiC-Ti aluminade metal matrix composite. Int. J. Damage Mech., 4, 338–361.

Woelke, P. and Voyiadjis, G.Z. (2005). A stress resultant based yield surface with kinematic hardening and isotropic damage due to microvoids for isotropic plates and shells. Proceedings of McMat2005, 2005 Joint ASME/ASCE/SES Conference on Mechanics and Materials, June 1–3, Baton Rouge, Louisiana, USA.

Woelke, P., Voyiadjis, G.Z. and Perzyna, P. (2006). Elasto-plastic finite element analysis of shells with damage due to microvoids. Int. J. Numer. Moth. Eng., 68, 3, 338–380. 2008.

Woelke, P., Chan, K.K., Abboud, N., Daddazio, R., Hapij, A. and Voyiadjis, G.Z. (2006b). Damage model for analysis of isotripic shells using EPSA. 77th Shock and Vibration Symposium Proceedings, Monterrey, CA, USA.

Woelke, P., Abboud, N., Daddazio, R. and Voyiadjis, G. (2008). Localization, damage and fracture modeling in shell structures. Proceedings of World Congress of Computational Mechanics, Venice, Italy.

Chapter 7
Non-linear Post Buckling Finite Element Analysis of Plates and Shells

7.1 Introduction

In this chapter we present the nonlinear post-buckling analysis of plates and shells by the finite element method, using the four-node C^0 strain element. As previously, the element tangent stiffness matrix is given explicitly, i.e., without any numerical integration, which results in a computationally efficient algorithm.

The buckling behavior of plates and shells differents from that of columns. A slender straight column subjected to gradually increasing compressive loads at its ends, becomes unstable and buckles when the applied loads reach a certain value called the critical load. The column, in general, collapses completely when a slight incremental load is applied beyond the critical load. The load-carrying capacity of plates and shells, however, differs significantly from the critical loads predicted by the stability analysis. This can be demonstrated by large discrepancies between results given by the classical stability theory of plates and shells and by experimental observations. Von Karman and Tsien (1939) first showed that such buckling behavior of plates and shells is caused by the highly unstable and nonlinear post-buckling phenomenon exhibited by thin structures. The nonlinear post-buckling analysis of plates and shells is necessary for correct prediction of the load-carrying capacity of these structures. As it is difficult to obtain rigorous analytical solutions of nonlinear post-buckling problems in most cases, numerical methods must be adopted.

Because of the increased use of shells and plates in the aerospace and nuclear industries, instability analysis of these structures has become more important in recent years. With the advent of computers and the finite element technique, the engineer's ability to solve complex structural problems has greatly improved. Numerous finite element models for the large displacement and post-buckling analysis of plates and shells have been suggested (Murray and Willson, 1969; Gallagher and Thomas, 1973; Sabir and Lock, 1973; Wood and Zienkiewicz, 1977; Horrigmoe and Bergan, 1978; Bathe and Dvorkin, 1986; Noor et al., 1989; Kim and Voyiadjis, 1999). In most nonlinear finite elements, however, the element matrices are evaluated through numerical integration, which is computationally expensive, especially in nonlinear analysis where the element matrices must be evaluated numerous times.

G.Z. Voyiadjis, P. Woelke, *Elasto-Plastic and Damage Analysis of Plates and Shells*,

© Springer-Verlag Berlin Heidelberg 2008

An assumed strain shell element, with five degrees of freedom at each node, was developed for nonlinear post buckling analysis by Voyiadjis and Shi (1992). The element formulation is based on the Updated Lagrangian description, the von Karman assumption, and the quasi-conforming element method (an assumed strain method – Tang et al., 1980, 1983). The four-node quadrilateral element can reduce to the corresponding three-node triangular element.

The formulation of the explicit element tangent stiffness matrix is similar to that presented in Chap. 4. The emphasis here is on evaluation of the initial surface coordinates for large deformation analysis of shells. The post-buckling analysis using our algorithm is performed on a number of structures and compared with the existing analytical/numerical solutions where they are available. These numerical examples demonstrate that our nonlinear plate element is efficient and accurate.

7.2 Element Tangent Stiffness Matrix

The element considered here is the four-node quadrilateral strain element; each node has five degrees of freedom, three translations, and two rotations. The element formulation for the nonlinear analysis of plates and shells was presented in the previous chapters. Here we use this element for the post-buckling analysis of plates and shells. For convenience, we repeat some of the equations derived in previous chapters.

7.2.1 Element Stiffness in Local Coordinates

The von Karman assumptions and Updated Lagrangian description are used here to derive the element tangent stiffness matrix. In the finite element modeling of transverse shear deformable plates using a generalized displacement method, the incremental bending strains $\boldsymbol{\varepsilon}_{\mathbf{b}}$, membrane strains $\boldsymbol{\varepsilon}_{\mathbf{m}}$, transverse shear strains $\boldsymbol{\varepsilon}_{\mathbf{s}}$, and slopes $\boldsymbol{\theta}$ of an element defined in the element local coordinates take the form (Shi and Voyiadjis, 1990, 1991a,c):

$$\boldsymbol{\varepsilon}_{\mathbf{b}} = \begin{Bmatrix} \dfrac{\partial \Delta\phi_x}{\partial x} \\ \dfrac{\partial \Delta\phi_y}{\partial y} \\ \dfrac{\partial \Delta\phi_x}{\partial y} + \dfrac{\partial \Delta\phi_y}{\partial x} \end{Bmatrix} = \mathbf{B}_{\mathbf{b}} \Delta \mathbf{q}_{\mathbf{e}} \tag{7.1}$$

$$\boldsymbol{\varepsilon}_{\mathbf{m}} = \begin{Bmatrix} \dfrac{\partial \Delta u}{\partial x} \\ \dfrac{\partial \Delta v}{\partial y} \\ \dfrac{\partial \Delta u}{\partial y} + \frac{\partial \Delta v}{\partial x} \end{Bmatrix} = \mathbf{B}_{\mathbf{m}} \Delta \mathbf{q}_{\mathbf{e}} \tag{7.2}$$

$$\boldsymbol{\varepsilon}_{\mathbf{s}} = \begin{Bmatrix} \dfrac{\partial \Delta w}{\partial x} - \Delta \phi_x \\ \dfrac{\partial \Delta w}{\partial y} - \Delta \phi_y \end{Bmatrix} = \mathbf{B}_{\mathbf{s}} \Delta \mathbf{q}_{\mathbf{e}} \tag{7.3}$$

and

$$\boldsymbol{\theta} = \begin{Bmatrix} \dfrac{\partial \Delta w}{\partial x} \\ \dfrac{\partial \Delta w}{\partial y} \end{Bmatrix} = \mathbf{G} \Delta \mathbf{q}_{\mathbf{e}} \tag{7.4}$$

where Δw is the increment of the generalized transverse displacement across the plate thickness; $\Delta \phi_x$ and $\Delta \phi_y$ are the increments of generalized rotations of cross-sections of the plate; $\Delta \mathbf{q}_{\mathbf{e}}$ is the vector of increments of the nodal displacements of the element under consideration; and $\mathbf{B}_{\mathbf{b}}, \mathbf{B}_{\mathbf{m}}, \mathbf{B}_{\mathbf{s}}$, and $\mathbf{G}$ are, respectively, the bending strain, membrane strain, transverse shear strain and slope-displacement matrices. Using the principle of virtual work, the element tangent stiffness matrix in the element local coordinates (x, y) at configuration k takes the form (Horrigmoe and Bergan, 1978):

$$\mathbf{K} = \mathbf{K}_{\mathbf{e}} + \mathbf{K}_{\mathbf{g}} \tag{7.5}$$

where

$$\mathbf{K}_{\mathbf{e}} = \iint_{\Omega} \left(\mathbf{B}_{\mathbf{b}}{}^{\mathbf{T}} \mathbf{D} \mathbf{B}_{\mathbf{b}} + \mathbf{B}_{\mathbf{m}}{}^{\mathbf{T}} \mathbf{S} \mathbf{B}_{\mathbf{m}} + \mathbf{B}_{\mathbf{s}}{}^{\mathbf{T}} \mathbf{T} \mathbf{B}_{s} \right) dxdy \tag{7.6}$$

$$\mathbf{K}_{\mathbf{g}} = \iint_{\Omega} \mathbf{G}^{\mathbf{Tk}} \mathbf{F} \mathbf{G} dxdy \tag{7.7}$$

$${}^{\mathbf{k}}\mathbf{F} = \begin{bmatrix} {}^{k}N_x & {}^{k}N_{xy} \\ {}^{k}N_{xy} & {}^{k}N_y \end{bmatrix} \tag{7.8}$$

in which $\boldsymbol{\Omega}$ is the element domain; **D, S**, and **T** are, respectively, the plate bending, stretching, and shearing rigidity matrixes; and ${}^{\mathbf{k}}\mathbf{F}$ is the in-plane stress resultant matrix at configuration k. In (7.5), $\mathbf{K}_{\mathbf{e}}$ is the linear part of the tangent stiffness matrix

$\mathbf{K}$ and $\mathbf{K_g}$ is the nonlinear part of $\mathbf{K}$. As shown in (7.7), $\mathbf{K_g}$ is associated with the in-plane stress resultants and takes into account the geometric nonlinearity including the post-buckling behavior. As shown by Voyiadjis and Shi (1992), the element strain-displacement matrices $\mathbf{B_b}$, $\mathbf{B_m}$, $\mathbf{B_s}$, as well as the slope-displacement matrix $\mathbf{G}$, can be evaluated by the quasi-conforming element method (Tang et al., 1980, 1983). The starting point in the formulation of a quasi-conforming element is to interpolate element strain fields in terms of the undetermined strain parameters that are the element local quantities. For example, the bending strains $\boldsymbol{\varepsilon_b}$ defined in (7.1) can be approximated as:

$$\boldsymbol{\varepsilon_b} \approx \mathbf{P_b}\boldsymbol{\alpha_b} \tag{7.9}$$

where $\mathbf{P_b}$ is the interpolation function matrix (usually a polynomial function) and $\boldsymbol{\alpha_b}$ is the element strain parameter vector. If $\mathbf{W_b}$ is the test functions matrix, the weak form of (7.1) and (7.9) can be written as:

$$\int_{\Omega} \mathbf{W_b}\left(\boldsymbol{\varepsilon_b} - \mathbf{P_b}\boldsymbol{\alpha_b}\right) \mathbf{d\Omega} = \mathbf{0} \tag{7.10}$$

To obtain a symmetric stiffness matrix, the test functions can be taken as $\mathbf{W_b} = \mathbf{P_b^T}$. Carrying out the integration, the above equation leads to:

$$\mathbf{A_b}\boldsymbol{\alpha_b} = \mathbf{C_b}\boldsymbol{\Delta q_e} \text{ or } \boldsymbol{\alpha_b} = \mathbf{A_b}^{-1}\mathbf{C_b}\boldsymbol{\Delta q_e} \tag{7.11}$$

where:

$$\mathbf{A_b} = \int_{\Omega} \mathbf{P_b}^{\mathbf{T}}\mathbf{P_b} d\boldsymbol{\Omega}; \quad \mathbf{C_b}\boldsymbol{\Delta q_e} = \int_{\Omega} \mathbf{P_b}^{\mathbf{T}}\boldsymbol{\varepsilon_b} d\boldsymbol{\Omega} \tag{7.12}$$

where $\mathbf{A_b}$ is a symmetric and nonsingular square matrix and $\mathbf{C_b}$ is the element strain discretization matrix. Substituting for $\boldsymbol{\alpha_b}$ in (7.9) from (7.11) and using (7.1) and (7.9) yields:

$$\mathbf{B_b} = \mathbf{P_b}\mathbf{A_b}^{-1}\mathbf{C_b} \tag{7.13}$$

Similarly, we obtain:

$$\mathbf{B_m} = \mathbf{P_m}\mathbf{A_m}^{-1}\mathbf{C_m} \tag{7.14}$$

$$\mathbf{B_s} = \mathbf{P_s}\mathbf{A_s}^{-1}\mathbf{C_s} \tag{7.15}$$

$$\mathbf{G} = \mathbf{P_\theta}\mathbf{A_\theta}^{-1}\mathbf{C_\theta} \tag{7.16}$$

where $\mathbf{P_b}$, $\mathbf{P_m}$, $\mathbf{P_s}$, and $\mathbf{P_\theta}$ are the interpolation function matrices for element bending, membrane, transverse shear strains and slope field, respectively. Equations (7.9), (7.10), (7.11), (7.12), (7.13), (7.14), (7.15), (7.16) indicate that the

element strain fields in quasi-conforming elements are obtained from integration instead of the differentiation used in the conventional assumed displacement elements. For the four-node quadrilateral element considered here, the following strain interpolation matrices are used:

$$\mathbf{P_b} = \begin{bmatrix} 1\ x\ y\ xy & 0 & 0 \\ 0 & 1\ x\ y\ xy & 0 \\ 0 & 0 & 1\ x\ y \end{bmatrix} \tag{7.17}$$

$$\mathbf{P_m} = \begin{bmatrix} 1 & y & 0 & 0 & 0 \\ 0 & 0 & 1 & x & 0 \\ 0 & 0 & 0 & 0 & 1 \end{bmatrix} \tag{7.18}$$

$$\mathbf{P_s} = \begin{bmatrix} 1 & 0 \\ 0 & 1 \end{bmatrix} \tag{7.19}$$

$$\mathbf{P_\theta} = \begin{bmatrix} 1 & x & y & xy & 0 & 0 & 0 & 0 \\ 0 & 0 & 0 & 0 & 1 & x & y & xy \end{bmatrix} \tag{7.20}$$

$\mathbf{A_b}$, $\mathbf{C_b}$, $\mathbf{A_m}$, $\mathbf{C_m}$, $\mathbf{A_s}$, $\mathbf{C_s}$, $\mathbf{A_\theta}$ and $\mathbf{C_\theta}$ are given explicitly. Substituting (7.13), (7.14), (7.15), (7.16) into (7.6) and (7.7) gives:

$$\begin{aligned} \mathbf{K_e} = {} & \mathbf{C_b}^{\mathrm{T}}\mathbf{A_b}^{-1} \int_\Omega \mathbf{P_b}^{\mathrm{T}}\mathbf{D}\mathbf{P_b} dx dy \mathbf{A_b}^{-1}\mathbf{C_b} \\ & + \mathbf{C_m}^{\mathrm{T}}\mathbf{A_m}^{-1} \int_\Omega \mathbf{P_m}^{\mathrm{T}}\mathbf{S}\mathbf{P_m} dx dy \mathbf{A_m}^{-1}\mathbf{C_m} \\ & + \mathbf{C_s}^{\mathrm{T}}\mathbf{A_s}^{-1} \int_\Omega \mathbf{P_s}^{\mathrm{T}}\mathbf{T}\mathbf{P_s} dx dy \mathbf{A_s}^{-1}\mathbf{C_s} \end{aligned} \tag{7.21}$$

$$\mathbf{K_g} = \mathbf{C_\theta}^{\mathrm{T}}\mathbf{A_\theta}^{-1} \int_\Omega \mathbf{P_\theta}^{\mathrm{T}}\mathbf{F}\mathbf{P_\theta} dx dy \mathbf{A_\theta}^{-1}\mathbf{C_\theta} \tag{7.22}$$

The integrals in (7.21) and (7.22) can be carried out explicitly, as the integrands are simple polynomials. Consequently, the element tangent stiffness matrix can be obtained explicitly, i.e., without numerical integration. Compared with the nonlinear elements obtained through numerical integration, the explicit form of the element tangent stiffness matrix presented here makes the resulting element computationally very efficient.

The element nodal force vector evaluated in the element local coordinates at configuration k is given by:

$$\mathbf{f} = \iint_{\Omega} \left(\mathbf{B_b}^{\mathbf{Tk}}\mathbf{M} + \mathbf{B_m}^{\mathbf{Tk}}\mathbf{N} + \mathbf{B_s}^{\mathbf{Tk}}\mathbf{Q} \right) dxdy \tag{7.23}$$

in which $\mathbf{B_b}$, $\mathbf{B_m}$ and $\mathbf{B_s}$ are defined in (7.13), (7.14), (7.15); ${}^{\mathbf{k}}\mathbf{M}$, ${}^{\mathbf{k}}\mathbf{N}$, and ${}^{\mathbf{k}}\mathbf{Q}$ are the stress couple, in-plane stress, and transverse shear stress resultant vectors, respectively, which take the form:

$${}^{\mathbf{k}}\mathbf{M} = \begin{Bmatrix} {}^{k}M_x \\ {}^{k}M_y \\ {}^{k}M_{xy} \end{Bmatrix}, \quad {}^{\mathbf{k}}\mathbf{N} = \begin{Bmatrix} {}^{k}N_x \\ {}^{k}N_y \\ {}^{k}N_{xy} \end{Bmatrix}, \quad {}^{\mathbf{k}}\mathbf{Q} = \begin{Bmatrix} {}^{k}Q_x \\ {}^{k}Q_x \end{Bmatrix} \tag{7.24}$$

Corresponding to the strain interpolation functions given in (7.17), (7.18), (7.19), a bilinear field for ${}^{\mathbf{k}}\mathbf{M}$ and ${}^{\mathbf{k}}\mathbf{N}$ and a constant function for ${}^{\mathbf{k}}\mathbf{Q}$ are used here. Similar to (7.21) and (7.22), the integrals in (7.23) can also be carried out explicitly.

7.2.2 Initial Surface Coordinates for Large Deformation Analysis

A surface coordinate system associated with each nodal point is adopted (see also Chap. 4). This allows efficient definition of the global rotational degrees of freedom. After deformation from configuration $k-1$ to k, there are three rotational components ($\theta_1,\ \theta_2,\ \theta_3$) at a nodal point, and the nodal surface coordinates at node i will undergo a finite rigid body rotation with components ($\theta_1,\ \theta_2,\ \theta_3$). The initial surface coordinates for a flat plate take the form of a 3×3 identity matrix. The initial surface coordinates for shells are presented here.

If $\mathbf{E}$ is the unit base vectors of the fixed global coordinates, and ${}^{\mathbf{k}}\mathbf{e}$ and ${}^{\mathbf{k}}\mathbf{e_s}$ are, respectively, the unit base vectors of the element local coordinates and the nodal surface coordinates at configuration k, then the relations between ${}^{\mathbf{k}}\mathbf{e}$ and $\mathbf{E}$ as well as between ${}^{\mathbf{k}}\mathbf{e_s}$ and $\mathbf{E}$ are:

$${}^{\mathbf{k}}\mathbf{e} = {}^{\mathbf{k}}\mathbf{R}\mathbf{E} \tag{7.25}$$

$${}^{\mathbf{k}}\mathbf{e_s} = {}^{\mathbf{k}}\mathbf{R_s}\mathbf{E} \tag{7.26}$$

${}^{\mathbf{k}}\mathbf{R}$ can be easily determined by the nodal coordinates of the element under consideration. The determination of ${}^{\mathbf{k}}\mathbf{R_s}$ is presented below. Note that ${}^{\mathbf{k}}\mathbf{e}$ is associated with a finite element and is updated with the changes of the element nodal coordinates, while ${}^{\mathbf{k}}\mathbf{e_s}$ is related to a nodal point and rotates rigidly with the deformations of this nodal point.

The transformation from ${}^{\mathbf{k-1}}\mathbf{e_s}$ to ${}^{\mathbf{k}}\mathbf{e_s}$ at node i can be written as:

$${}^{k}e_{si} = T_{\theta i}{}^{k-1}e_{si} = T_{\theta i}{}^{k-1}R_{si}E = {}^{k}R_{si}E \tag{7.27}$$

where $T_{\theta i}$ s the transformation matrix for large rotations at node i and is given by:

$$T_{\theta i} = \exp\left(\widehat{\Theta}_i\right) \tag{7.28}$$

$$\widehat{\Theta}_i = \widehat{\Theta}_{mn} = \varepsilon_{mnk}\theta_k \quad (m, n, k = 1, 2, 3) \tag{7.29}$$

where ε_{mnk} is the permutation tensor. For the initial surface coordinates ${}^{o}e_s = \{{}^{o}e_{s1}, {}^{o}e_{s2}, {}^{o}e_{s3}\}$ at a nodal point of a shell, ${}^{o}e_{s3}$ is chosen to coincide with the outward normal of the undeformed shell surface at the point, and ${}^{o}e_{s1}$ and ${}^{o}e_{s2}$ are given by:

$${}^{0}e_{s1} = \frac{E_2 \times {}^{0}e_{s3}}{\left|E_2 \times {}^{0}e_{s3}\right|} \tag{7.30}$$

$${}^{0}e_{s2} = {}^{0}e_{s3} \times {}^{0}e_{s1} \tag{7.31}$$

where E_2 is the second component of the unit base vectors E of the fixed global coordinates, and the symbol $\times$ denotes the cross-product. Equations (7.25) and (7.27) yield the transformation between $\mathbf{{}^{k}e_s}$ and $\mathbf{{}^{k}e}$ at node i of an element as:

$${}^{k}e_{si} = {}^{k}R_{si}\ {}^{k}R_i{}^{T}\ {}^{k}e_i = {}^{k}S_i\ {}^{k}e_i \tag{7.32}$$

where

$${}^{k}S_i = {}^{k}R_{si}\ {}^{k}R_i{}^{T} \tag{7.33}$$

Note that ${}^{k}S_i$ is not only associated with a nodal point but also dependent on the element.

7.2.3 Transformation of Element Stiffness Matrix

In this study, each node has five degrees of freedom, i.e., three translations and two rotations. At node i of an element, the degrees of freedom defined in the element local coordinates are the incremental translations Δu_i, and Δv_i, as well as Δw_i in the directions of ${}^{k}e_1$, ${}^{k}e_2$, and ${}^{k}e_3$, respectively, under consideration and two incremental rotations $\Delta\varphi_{xi}$ and $\Delta\varphi_{yi}$ about ${}^{k}e_2$ and ${}^{k}e_1$. The global degrees of freedom at the same node are the incremental translations ΔU_{1i}, ΔU_{2i}, and ΔU_{3i} measured in the directions of the fixed global coordinates E_j $(j = 1, 2, 3)$, respectively, as well as rotations $\Delta\varphi_{s1i}$ and $\Delta\varphi_{s2i}$ about ${}^{k}e_{s2}$ and ${}^{k}e_{s1}$, respectively, of the surface coordinate system ${}^{k}e_s$ at the nodal point. The coordinates that combine the element local coordinates with the nodal surface coordinates are called the "base coordinates". The transformation of the incremental displacement parameters at node i from an

element local coordinates, Δq_{ei}, to the corresponding base coordinates, Δq_{bi}, takes the form:

$$\Delta q_{bi} = \begin{Bmatrix} \Delta U_{1i} \\ \Delta U_{2i} \\ \Delta U_{3i} \\ \Delta \varphi_{s1i} \\ \Delta \varphi_{s2i} \end{Bmatrix} = \begin{bmatrix} {}^{k}R^{T} & 0 \\ 0 & {}^{k}s_i{}^{*} \end{bmatrix} \begin{Bmatrix} \Delta u_i \\ \Delta v_i \\ \Delta w_i \\ \Delta \varphi_{xi} \\ \Delta \varphi_{yi} \end{Bmatrix} = {}^{k}T_{bi} \Delta q_{ei} \tag{7.34}$$

in which ${}^{k}s_i{}^{*}$ is the upper left 2×2 submatrix of matrix ${}^{k}S$ at node i as defined in (7.33) but with a different sequence. Consequently, the global displacement vector Δq_b and the local displacement vector Δq_e for the element have the following relationship:

$$\Delta q_b = {}^{k}T_b \Delta q_e \tag{7.35}$$

For the four-node element considered here, ${}^{k}T_b$ is given by:

$${}^{k}T_b = \begin{bmatrix} {}^{k}T_{b1} & 0 & 0 & 0 \\ 0 & {}^{k}T_{b2} & 0 & 0 \\ 0 & 0 & {}^{k}T_{b3} & 0 \\ 0 & 0 & 0 & {}^{k}T_{b4} \end{bmatrix} \tag{7.36}$$

Using (7.35), the element tangent stiffness matrix evaluated in the element coordinates, $\mathbf{K}$, given by (7.5), (7.6), (7.7) can be transformed into that corresponding to the base coordinates, $\mathbf{K_b}$:

$$\mathbf{K_b} = {}^{\mathbf{k}}\mathbf{T_b}\mathbf{K}{}^{\mathbf{k}}\mathbf{T_b}{}^{\mathbf{T}} \tag{7.37}$$

Similarly, the element internal nodal force vector $\mathbf{f_b}$ in the base coordinates is given by:

$$\mathbf{f_b} = {}^{\mathbf{k}}\mathbf{T_b}\mathbf{f} \tag{7.38}$$

7.3 Solution Algorithm

Following the common assembling procedure, one obtains the nodal equilibrium equations of a system for configuration $k + 1$ given by:

$$\mathbf{K}_g \Delta \mathbf{q_g} = \Delta \mathbf{P} + \mathbf{F_{unb}} \tag{7.39}$$

where

$$\mathbf{K}_g \Delta \mathbf{q_g} = \sum_{elem} \mathbf{K_b} \Delta \mathbf{q_b} \tag{7.40}$$

$$\mathbf{F_{unb}} = {}^{k}\mathbf{P} - \sum_{elem} \mathbf{f_b} \tag{7.41}$$

where $\mathbf{K_g}$, $\mathbf{\Delta q_g}$, and $\mathbf{F_{unb}}$ are, respectively, the assembled global stiffness matrix, the nodal displacement increment vector, and the unbalanced force vector of the system; $\mathbf{\Delta P}$ is the load increment vector from configurations k to $k + 1$; and ${}^{k}\mathbf{P}$ is the total load vector up to configuration k. The unbalanced forces $\mathbf{F_{unb}}$ in (7.41) are due to geometric nonlinearities of the system.

We adopt the Newton-Raphson method to solve the incremental system equations in (7.39) in which the unbalanced forces are resolved through iterations. The load increments $\mathbf{\Delta P}$ are determined by the arc length method (Crisfield, 1981; Riks, 1972; Wempner, 1971), which is a very effective and efficient approach to dealing with snap-through and other post-buckling problems. Detailed descriptions of both Newton-Raphson arc-length methods are given in Chap. 9. The convergence criterion used here is:

$$\frac{|\Delta q_{g'}|}{|\Delta q_g|} \leq e_{tol} \tag{7.42}$$

in which $|\Delta q_{g'}|$ is the norm of the displacement increments obtained in the latest iteration, $|\Delta q_g|$ is the norm of the total displacement increments obtained during the current increment, and e_{tol} is a prescribed value of error tolerance. The value of $e_{tol} = 0.0001$ is used here.

7.4 Numerical Examples

The post-buckling analysis of a number of structures is presented in this section. All the shapes of the elements used in this section rectangular, quadrilateral, and triangular are the variations of the four-noded quadrilateral strain element presented in previous chapters. The numerical solutions obtained by our element are compared with the existing analytical/numerical solutions where available.

7.4.1 The Williams' Toggle Frame

The Williams' toggle is shown schematically in Fig. 7.1, together with the material properties and load condition (the units used are in/lb to compare our results with others directly). The toggle under the central load exhibits snap-through behavior. Four rectangular elements are used for the discretization of a half-span of the toggle. The curves of the central deflection and horizontal reaction at the fixed end versus the applied load are shown in Fig. 7.1. The numerical solutions given by Wood and Zienkiewicz (1977), as well as by Kondoh and Atluri (1986) are also plotted for comparison. Our results agree well with the reference solutions.

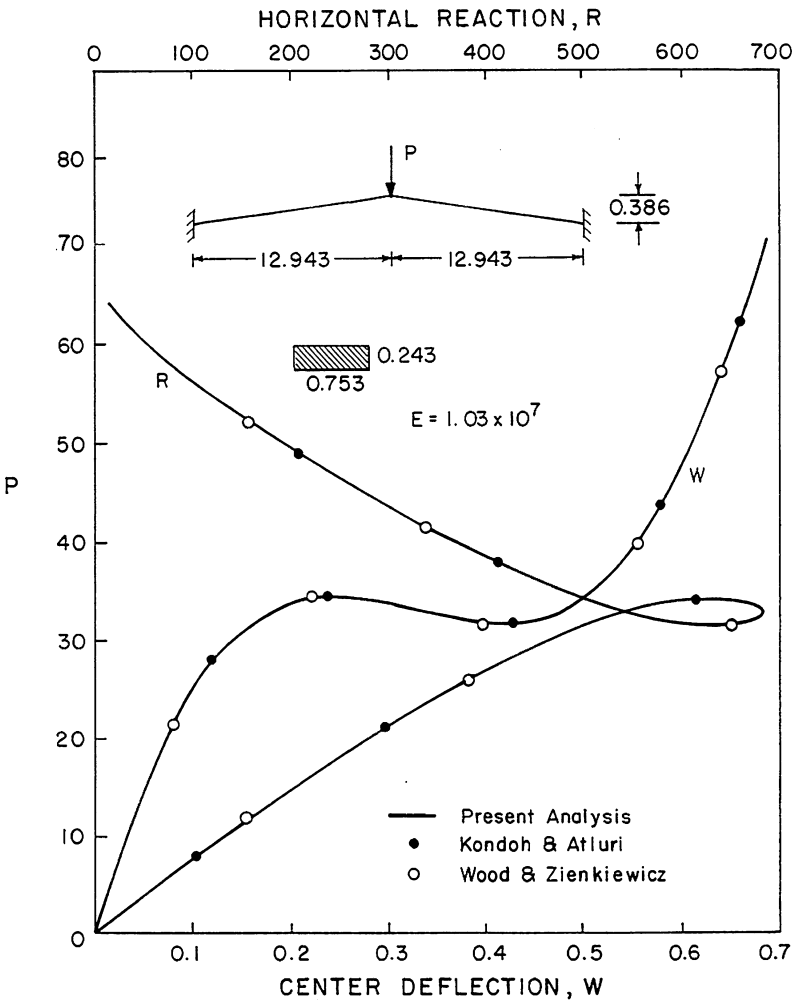

Fig. 7.1 Load-deflection and load-reaction curves of William's Toggle frame (Voyiadjis and Shi, 1992)

7.4.2 Simply Supported Circular Plate Subjected to Edge Pressure

In this example we investigate a thin simply supported circular plate subjected to a uniform comprehensive normal stress along the edge. The geometry and material properties of the circular plate are given in Fig. 7.2. The critical edge pressure is $q_{crit} = \dfrac{4.24D}{R^2h}$ (Friedrichs and Stoker, 1942), where D, R and h are the bending rigidity, radius, and thickness of the circular plate, respectively. The load-carrying capability of this plate, however, is far beyond the critical load. The buckling pattern of the circular plate is symmetric about the plate center (Friedrichs and Stoker,

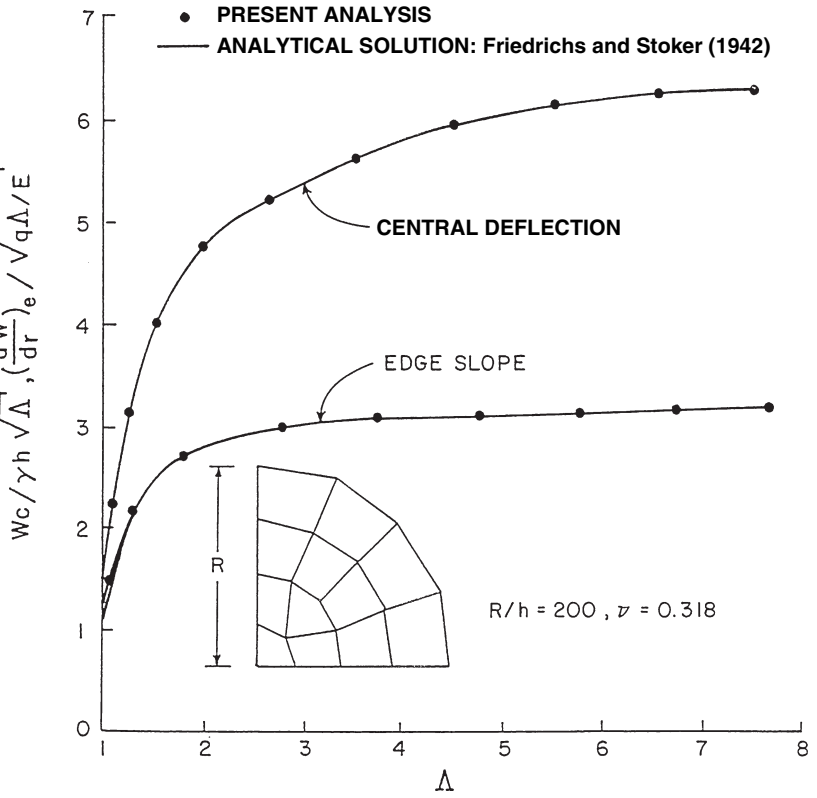

Fig. 7.2 Central deflection and edge-slope curves beyond the critical load for a simply supported circular plate subjected to edge compression (Voyiadjis and Shi, 1992)

1942). Therefore, we consider only one quarter of the plate. Twelve quadrilateral elements are used, as shown in Fig. 7.2. A lateral disturbance force $P = \dfrac{2\pi\ Rhq}{1000}$ is introduced. The deflection at the center and the slope at the edge against the load parameter $\Lambda = \dfrac{q}{q_{crit}}$ beyond the critical load are plotted in Fig. 7.2. The parameter γ used in the load-deflection curve is defined as $\gamma = 1/\sqrt{12(1-\nu^2)}$. The numerical results are in good agreement with the analytical solutions given by Friedrichs and Stoker (1942).

7.4.3 Rectangular Plate Subjected to In-Plane Load

This example concerns the post-buckling analysis of a simply supported rectangular plate subjected to a uniaxial compression along the shorter edges. The in-plane displacements of the simply supported plate are constrained such that the longitudinal

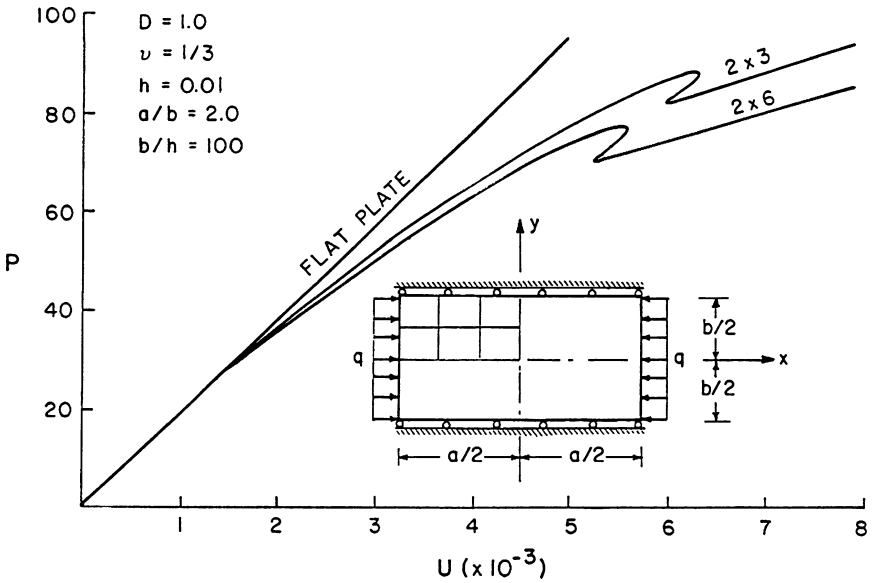

Fig. 7.3 Rectangular plate subjected to in-plane load (Voyiadjis and Shi, 1992)

edges can move freely in the tangential direction but are completely restrained in the normal direction. The geometric and material data of the plate are shown in Fig. 7.3. These data are the same as those used by Allman (1982). In Allman's paper, however, each transverse end of the plate is assumed to be compressed by a force applied through a rigid end-block. Under the given boundary and loading conditions, this rectangular plate has a symmetric buckling mode. Consequently, only one-quarter of the plate needs be analyzed.

The rectangular plate undergoes single wave buckling in the transverse direction. It can have a higher buckling mode in the longitudinal direction when the load is large enough. To account more accurately for the higher buckling mode, 2×3 and 2×6 meshes are considered. The 2×3 mesh and boundary conditions are shown in Fig. 7.3. A small lateral disturbance force is applied at the plate center. The plot of displacement in the longitudinal direction U versus the in-plane load P is shown in Fig. 7.3, where U and P are defined, respectively, as:

$$U = \frac{1}{b} \int_0^b u\left(\frac{-a}{2}, y\right) dy \tag{7.43}$$

$$P = bq \tag{7.44}$$

The deflections along the central longitudinal line of the plate corresponding to various load values obtained by 2×6 mesh are shown in Fig. 7.4. Note that the plate undergoes buckling from one wave to three waves when the load reaches a certain

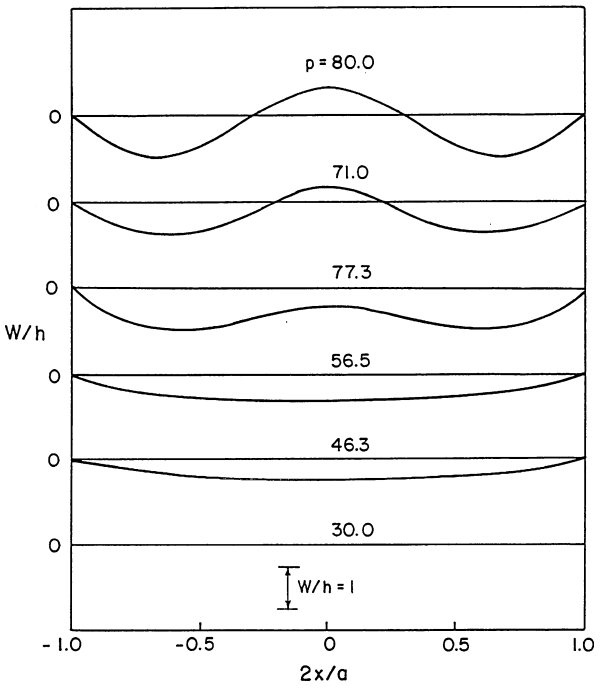

Fig. 7.4 Rectangular plate subjected to in-plane load – deflection along the central, longitudinal line (Voyiadjis and Shi, 1992)

value. Figure 7.3 shows that the plate can be in equilibrium in more than one buckle pattern in certain load regions. Figures 7.3 and 7.4 also show that the stiffness of the plate becomes negative when the central deflection crosses its initial equilibrium configuration after the large deflection. Allman (1982) also showed that the plate can be in equilibrium in more than one buckling mode. The local drop in force is observed, however, at the limit point of the $U - P$ curve. Such behavior makes the slope of the curve become infinite at the corresponding point.

7.4.4 Cylindrical Shell Under a Central Load

The geometry and material properties of the circular cylindrical shell under consideration are shown in Fig. 7.5. The shell is subjected to a concentrated central load as shown in Fig. 7.5. The longitudinal edges of the shell have all the translational degrees of freedom restrained while rotations are free. All the curved edges are free. Only one-quarter of the shell is analyzed here because of the symmetry, and a 4×4 mesh is used. Both triangular and quadrilateral elements are used. The central deflection as a function of applied load is plotted in Fig. 7.6. The numerical solution obtained by Horrigmore and Bergan (1978) is also shown for comparison.

The results we obtained from the flat three-noded triangular elements agree very well with the solution given by Horrigmore and Bergan (1978), while the results given by the flat rectangular elements are stiffer. The difference in the behavior of

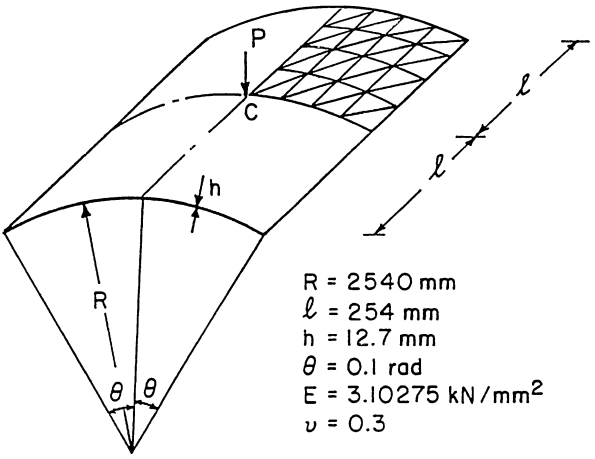

Fig. 7.5 Cylindrical shell – geometry, material properties and finite element mesh (Voyiadjis and Shi, 1992)

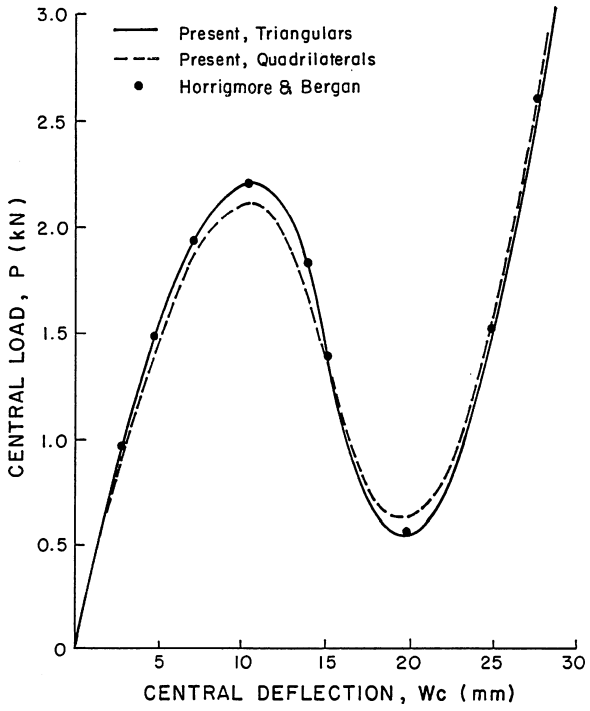

Fig. 7.6 Cylindrical shell – Load-displacement curve (Voyiadjis and Shi, 1992)

the triangular and rectangular elements can be attributed to the fact that the triangular elements represent the deformed geometry of the shell more accurately than the quadrilateral elements. Yang and Saigal (1985) solved the same problem using a higher-order curved shell element (48 degrees of freedom) and a 2×2 mesh for a quarter of the shell. Even though fewer elements are used in Yang and Saigal's solution, more nodal degrees of freedom are used compared with the finite elements

used here. The simple flat plate elements presented by Horrigmore and Bergan (1978) and in our study give results with the same accuracy as Yang and Saigal's higher-order curved element. This indicates that the lower-order plate elements can lead to increased computational efficiency in nonlinear shell analysis.

7.4.5 Spherical Shell Subjected to Central Load

Figure 7.7 shows a spherical shell subjected to a concentrated load at its apex. All the translational degrees of freedom on the edges are restrained, while rotations are free. A 5×5 mesh of triangular elements is used for one-quarter of the spherical shell. The resulting load-deflection curve at the apex, obtained by sixteen increments, is shown in Fig. 7.7. Results obtained by Horrigmore and Bergan (1978), where twenty-nine increments were used, are shown for comparison. Our analysis agrees very well with Horrigmore and Bergan's numerical solution. This example is also studied by Bathe and Ho (1981) by means of the flat three-node triangular elements and mesh identical to that used here. Bathe and Ho (1981) obtained similar results, but the maximum central displacement $W_c = 298.35\,mm$ was obtained using nineteen load increments.

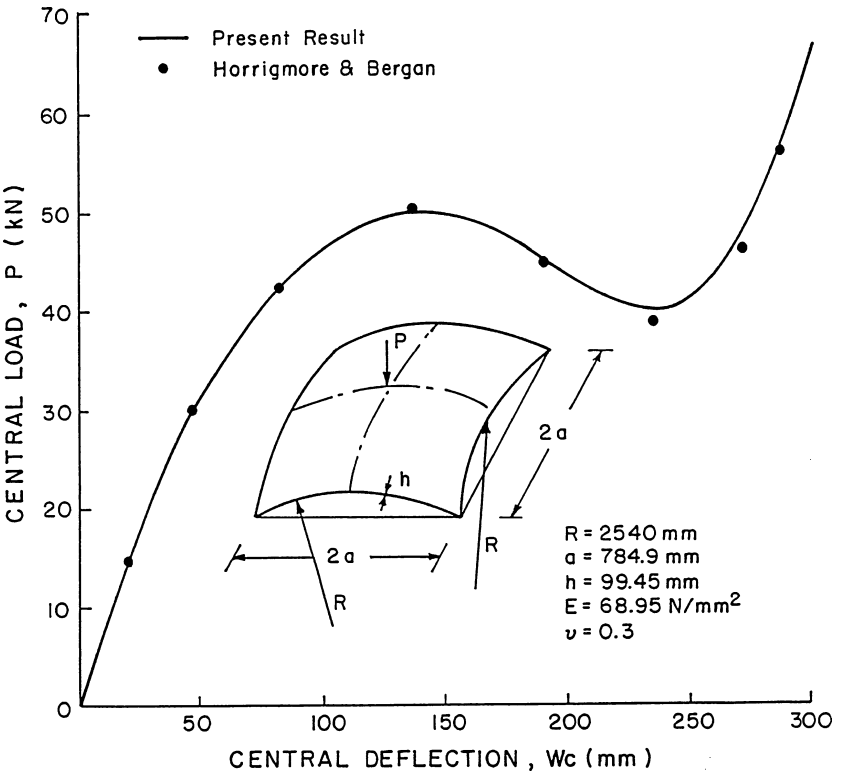

Fig. 7.7 Spherical shell under a central load (Voyiadjis and Shi, 1992)

7.5 Summary

The four-node quadrilateral strain element is used here for nonlinear post-buckling shell analysis. The von Karman assumptions and the Updated Lagrangian description are used to derive the element tangent stiffness matrix. The transformation matrix of large rotations proposed by Argyris (1982) is adopted to account for the large rigid rotations. By means of the quasi-conforming method, the element tangent stiffness matrix is calculated explicitly. As the element tangent stiffness matrices must be evaluated numerous times in a nonlinear analysis, this feature makes our formulation very efficient computationally.

The nonlinear post-buckling analysis of a number of structures is presented and compared with the analytical/numerical solutions of other works. The examples show that the four-node strain element presented here is not only simple and computationally efficient but accurate.

References

Allman, D.J., (1982). Improved finite element method for the large displacement bending and post buckling analysis of thin plates. Int. J. Solids Struct., 18, 737–762.

Argyris, J., (1982). An excursion into large rotations. Comput. Meth. Appl. Mech. Eng., 32, 85–155.

Bathe, K.J. and Dvorkin, Z.N., (1986). A formulation of general shell elements – The use of mixed interpolation of tensional components. IJNME, 22, 697–722.

Bathe, K.J. and Ho, L.W., (1981). A simple and effective element for analysis of general shell structures. J. Comp. Struct., 13, 673–681.

Crisfield, M.A., (1981). A fast incremental interactive solution procedure that handles snap-through. Comp. Struct., 13, 52–62.

Friedrichs, K.O. and Stoker, J.J., (1942). Buckling of the circular plate beyond the critical thrust. J. Appl. Mech., ASME, 9, A7–A14.

Gallagher, R.H. and Thomas, G.R., (1973). The finite element in plate and shell instability analysis. Proc. Fourth Australian Conf. Mech. Struct. Materials, Brisbane, Australia, pp. 77–86.

Horrigmore, G. and Bergan, P.G. (1978). Nonlinear analysis of free form shells by flat elements. Comp. Meth. Appl. Mech. Eng. 16, 11–35.

Kim, K., and Voyiadjis, G.Z., (1999). Buckling strength prediction of CFRP cylindrical panels using finite element method. J. Compos. A: Appl. Sci. Manuf., 30, 1093–1104.

Kondoh, K. and Atluri, S. N., (1986). A simplified finite element method for large deformation, post-buckling analysis of large frames, using explicitly derived tangent stiffness matrices. IJNME, 23, 69–90.

Murray, D. W. and Willson, E. L., (1969). Finite-element post-buckling analysis of thin elastic plates. AIAA J., 7, 1915–1920.

Noor, A. K., Belytschko, T. and Simo, J. C., (1989). Analytical and Computational Models of Shells, ASME, New York, 640.

Riks, E., (1972). The application of Newton's method to the problem of elastic stability. J. Appl. Mech., ASME, 39, 1060–1066.

Sabir, A. B. and Lock, A. C., (1973). The application of finite elements to the large deflection geometrically non-linear behavior of cylindrical shells, In C. A. Brebbia and H. Tottenham (eds.), Variational Methods in Engineering, Southampton University Press, Southampton, Vol. 7, 66–75

Shi, G. and Voyiadjis, G.Z. (1990). A simple C^0 quadrilateral thick/thin shell element based on the refined shell theory and the assumed strain fields. Int. J. Solids Struct., 27, 3, 283–298.

Shi, G. and Voyiadjis, G.Z. (1991a). Geometrically nonlinear analysis of plates by assumed strain element with explicit tangent stiffness. Comp. Struct., 41, 757–763.

Shi, G. and Voyiadjis, G.Z. (1991b). Simple and efficient shear flexible two node arch/beam and four node cylindrical shell/plate finite element. Int. J. Num. Meth. Eng., 31, 759–776.

Shi, G. and Voyiadjis, G.Z., (1991c). Efficient and accurate four-node quadrilateral C^0 plate bending elements based on assumed strain fields. IJNME, 32, 1041–1055.

Tang, L., Chen, W. and Liu, Y. (1980). Quasi-conforming elements for finite element analysis. J. DIT, 19, 2.

Tang, L., Chen, W. and Liu, Y. (1983). String net function applications and quasi conforming technique. In Hybrid and Mixed Finite Element Methods, Wiley, NY.

von Karman, T. and Tsien, H.-S., (1939). The buckling of spherical shells by external pressure. J. Aero. Scoi., 7, 43–50.

Voyiadjis, G.Z. and Shi, G. (1992). Nonlinear postbuckling analysis of plates and shells by four-noded strain element. AIAA J., 30, 4, 1110–1116.

Wempner, G.A., (1971). Discrete approximation related to nonlinear theories of solids. Int. J. Solids Struct., 7, 1581–1599.

Wood, R.D. and Zienkiewicz, O.C., (1977), Geometrically nonlinear finite element analysis of beams, frames, arches, and axisymmetric shells. Comp. Struct., 7, 725–735.

Yang, T. Y. and Saigal, S., (1985). A curved quadrilateral element for static analysis of shells with geometric and material nonlinearities. IJNME, 21, 617–635.

Chapter 8
Determination of Transverse Shear Stresses and Delamination in Composite Laminates Using Finite Elements

8.1 Introduction

In this chapter, we present a simple and efficient method of analysis for the shear flexible shells and composite laminates using the finite element framework discussed in the previous chapters (See also Woelke et al. 2008).

Transverse shear strains and stresses are especially important in the analysis of composite laminates. This is because advanced filamentary composite materials are susceptible to thickness effects, as their effective transverse shear modulus is substantially smaller than the effective elastic modulus in the fiber direction. Moreover, increasing use of composite laminates in various branches of industry requires analysis of these structures beyond the elastic behavior and up to failure. Composite laminates have various modes of failure: delamination, debonding, fiber cracking, and matrix yielding and cracking. Thus, determination of the accurate distribution of transverse shear stresses across the thickness of the laminate demands special attention.

One of the most common failure modes is delamination caused by the transverse shear stresses. To accurately model composite plates and shells and address the issues related to failure, it is necessary to include transverse shear stresses in analyses. We use a description of shear effects based on the Mindlin-Reissner theory of plates, modified to improve the model's accuracy. The Mindlin-Reissner theory leads to a constant distribution of the transverse shear stresses across the laminate thickness. This representation is inexact, as the transverse shear stress function is actually parabolic through the thickness of the lamina and not continuous through the laminate. To improve the accuracy of shear stress prediction, a shear correction function is applied, obtaining a parabolic distribution of shear stresses across the thickness of the laminate without changing the definitions of the shell kinematics. The correction function satisfies the boundary conditions, enforcing zero shear stresses on the outer surfaces of the laminas. Although using a second-order strain function through the thickness of the composite laminate is a significant improvement over a constant one, it still results in an undesired strain continuity through the thickness. Substantial stiffness variations of the individual laminas lead to "jumps" of the shear stress gradients at lamina interfaces. As failure analysis focuses on stresses, we adopt a transformed section method that assumes a continuous shear strain distribution. The transverse shear stresses are calculated using the effective

G.Z. Voyiadjis, P. Woelke, *Elasto-Plastic and Damage Analysis of Plates and Shells*,

© Springer-Verlag Berlin Heidelberg 2008

section properties, i.e., first and second moments of area, allowing for accurate determination of the stress distribution through the thickness. The formulation is a generalization of the effective section method commonly applied in composite beams. This allows prediction of the aforementioned "jumps" in the shear stress gradients through the thickness of the composite laminate.

A Tsai-Hill interactive, anisotropic failure criterion is used to account for the influence of transverse shear stresses. To enable prediction of the failure mode, the maximum stress criterion is modified to include shear stresses.

Our formulation is simple and computationally inexpensive, and it yields accurate results without employing higher-order displacement interpolations. It is implemented into the explicit dynamic finite element codes EPSA and FLEX (WAI, 1998; Vaughan, 2005).

This chapter contains six sections. Following the Introduction, Sect. 8.2 discusses shell kinematics. Section 8.3 presents the constitutive equations. Section 8.4 discusses failure criteria in composite laminates, and Section 8.5 presents numerical examples demonstrating the accuracy of our computational model's results. Finally, Sect. 8.6 gives the summary.

8.2 Kinematics of the Shell

The thick shell formulation, which uses Mindlin kinematics, is, according to Reddy's classification (Putcha and Reddy, 1986; Reddy, 1984, 1989; Reddy et al., 1989), a single-layer shear deformation formulation. It accounts for a constant state of transverse shear strains across the thickness of a composite laminate. It is not a layerwise formulation, which would require higher-order interpolation functions to approximate variation of axial displacement through the thickness of the composite laminate. Use of a layerwise formulation to model composite laminates would require major changes in the kinematics of the shell element, which would make the element more complex and could negatively affect code reliability.

The displacement-based shear deformation formulations are developed using a displacement field of the form Putcha and Reddy (1986):

$$\begin{aligned} u(x, y, z, t) &= u_0 - z\left[-\alpha\frac{\partial w}{\partial x} - \beta\phi_x - \gamma\frac{4}{3}\left(\frac{z}{h}\right)^2\left(\phi_x + \frac{\partial w}{\partial x}\right)\right] \\ v(x, y, z, t) &= v_0 - z\left[-\alpha\frac{\partial w}{\partial y} + \beta\phi_y - \gamma\frac{4}{3}\left(\frac{z}{h}\right)^2\left(-\phi_y + \frac{\partial w}{\partial y}\right)\right] \\ w(x, y, z, t) &= w\,(x, y, t) \end{aligned} \tag{8.1}$$

where u, v, w are the displacement components in the (x, y, z) directions respectively, at time t; u_0, v_0 are displacement of the middle surface; ϕ_x and ϕ_y are the angles of rotation of the transverse normal around x and y axes, respectively; and h is the thickness of the composite laminate. The above relations can easily be reduced to a

classical thin shell formulation by setting $\alpha = 1, \beta = 0, \gamma = 0$. Here, a single-layer shear deformation formulation is obtained by setting $\alpha = 0, \beta = 1, \gamma = 0$:

$$u = u_0 + z\phi_x \text{ and } v = v_0 - z\phi_y \tag{8.2}$$

with ϕ_x, ϕ_y given as:

$$\phi_x = -\frac{\partial w}{\partial x} + \gamma_{xz} \text{ and } \phi_y = \frac{\partial w}{\partial y} - \gamma_{yz} \tag{8.3}$$

where γ_{xz}, γ_{yz} are the transverse shear strains in the xz and yz planes, respectively.

Equations (8.2) and (8.3) express the following hypothesis: plane sections originally perpendicular to the middle surface remain plane after the deformation but not perpendicular to the middle surface (Fig. 8.1). The formulation is therefore related to the Mindlin-Reissner theory of plates.

The plate or shell considered here is assumed to be a laminated surface with a thickness h. At any point of the shell, the membrane strains and curvatures in a rectangular coordinate system (x, y, z) are given by the following equations:

$$e_x = \frac{\partial u}{\partial x} \tag{8.4}$$

$$e_y = \frac{\partial v}{\partial y} \tag{8.5}$$

$$e_{xy} = \frac{1}{2}\left(\frac{\partial u}{\partial y} + \frac{\partial v}{\partial x}\right) \tag{8.6}$$

$$\kappa_x = \frac{\partial \phi_x}{\partial x} = \frac{\partial}{\partial x}\left(-\frac{\partial w}{\partial x} + \gamma_{xz}\right) \tag{8.7}$$

$$\kappa_y = \frac{\partial \phi_y}{\partial y} = \frac{\partial}{\partial y}\left(\frac{\partial w}{\partial y} - \gamma_{yz}\right) \tag{8.8}$$

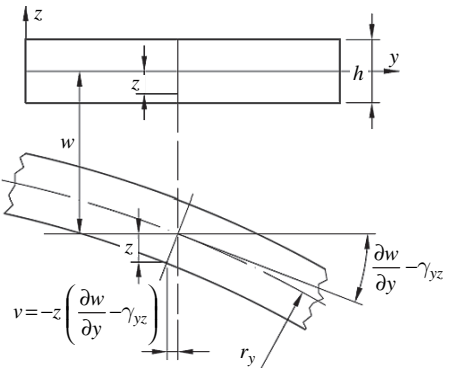

Fig. 8.1 Transverse shear deformations (Woelke et al., 2006b)

$$\kappa_{xy} = \frac{1}{2}\left(\frac{\partial \phi_x}{\partial y} + \frac{\partial \phi_y}{\partial x}\right) \tag{8.9}$$

The transverse shear strains are calculated using the following equations:

$$\gamma_{xz} = \frac{\partial w}{\partial x} + \phi_x \tag{8.10}$$

$$\gamma_{yz} = \frac{\partial w}{\partial y} - \phi_y \tag{8.11}$$

where $2\varepsilon_{xz} = \gamma_{xz};\ 2\varepsilon_{yz} = \gamma_{yz}$.

In (8.4), (8.5), (8.6), (8.7), (8.8), (8.9), (8.10), (8.11) z is a measure of the distance between the middle surface of the shell and the surface under consideration; e_x, e_y are membrane strains; e_{xy} is in-plane shear strain; and $\kappa_x, \kappa_y, \kappa_{xy}$ are curvatures at the mid-surface in planes parallel to the *xz, yz*, and *xy* planes, respectively; *u, v, w* are the displacements along the *x, y, z* axes, respectively; γ_{xz}, γ_{yz} are transverse shear strains in *xz* and *yz* planes respectively; and ϕ_x, ϕ_y are angles of rotation of the cross-sections that were normal to the mid-surface of the undeformed shell (see Fig. 8.1). The total normal strains due to both membrane and bending deformation in *x, y* directions, respectively, can be written as follows:

$$\varepsilon_x = e_x + z\kappa_x \quad and \quad \varepsilon_y = e_y - z\kappa_y \tag{8.12}$$

8.3 Lamina Constitutive Equations

For a lamina of constant thickness h and made of an orthotropic material (the plate having a plane of elastic symmetry parallel to the *xy* plane), the constitutive equations relating stresses $\boldsymbol{\sigma}$ to strains $\boldsymbol{\varepsilon}$ for a layer can be written in the principal material directions (1, 2, 3) as:

$$\begin{Bmatrix} \sigma_1 \\ \sigma_2 \\ \sigma_4 \\ \sigma_5 \\ \sigma_6 \end{Bmatrix} = \begin{bmatrix} Q_{11} & Q_{12} & 0 & 0 & 0 \\ Q_{12} & Q_{22} & 0 & 0 & 0 \\ 0 & 0 & 2Q_{44} & 0 & 0 \\ 0 & 0 & 0 & 2Q_{55} & 0 \\ 0 & 0 & 0 & 0 & 2Q_{66} \end{bmatrix} \begin{Bmatrix} \varepsilon_1 \\ \varepsilon_2 \\ \varepsilon_{23} \\ \varepsilon_{13} \\ \varepsilon_{12} \end{Bmatrix} \tag{8.13}$$

where the transverse normal stresses σ_3 are neglected. The principal material directions (1, 2, 3) are shown in Fig. 8.2, defined for a single lamina:

The quantities Q_{ij} in (8.13) form the stiffness matrix and are expressed as follows (Sloan, 1979; Vinson and Sierakowski, 1987):

$$\begin{aligned} &Q_{11} = E_{11}/\Delta, \quad Q_{22} = E_{22}/\Delta, \quad Q_{12} = \nu_{21}E_{11}/\Delta \\ &Q_{44} = G_{23}, \quad Q_{55} = G_{13}, \quad Q_{66} = G_{12}, \quad \Delta = 1 - \nu_{12}\nu_{21} \end{aligned} \tag{8.14}$$

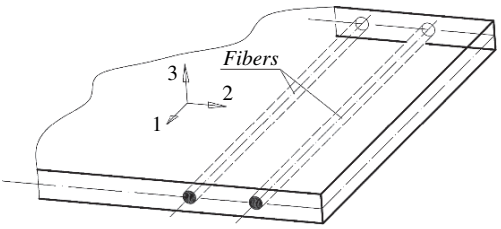

Fig. 8.2 Principal material directions for an individual layer (local coordinate system); 1 is the direction of the fibers (Woelke et al., 2006b)

where E_{11}, E_{22} are Young's moduli of the composite in 11 and 22 directions, respectively; G_{23}, G_{13}, G_{12} are shear moduli of the composite in 23, 13, and 12 directions, respectively; and ν_{12} is a Poisson's ratio in 12 direction. Directions are defined as in the theory of elasticity, where the first subscript defines the normal to the plane under consideration and the second subscript defines the direction.

Note that $\varepsilon_{23} = (1/2G_{23})\sigma_4$, $\varepsilon_{13} = (1/2G_{13})\sigma_5$, and $\varepsilon_{12} = (1/2G_{12})\sigma_6$; thus, coefficients "2" appear in the Q_{ij} matrix.

The transformation matrix from the local (lamina) to global (laminate) coordinate system is given by matrix **T** (see Figs. 8.2 and 8.3):

$$\begin{Bmatrix}\sigma_1\\ \sigma_2\\ \sigma_3\\ \sigma_4\\ \sigma_5\\ \sigma_6\end{Bmatrix} = \mathbf{T}\begin{Bmatrix}\sigma_x\\ \sigma_y\\ \sigma_z\\ \sigma_{yz}\\ \sigma_{xz}\\ \sigma_{xy}\end{Bmatrix}; \quad \begin{Bmatrix}\varepsilon_1\\ \varepsilon_2\\ \varepsilon_3\\ \varepsilon_{23}\\ \varepsilon_{13}\\ \varepsilon_{12}\end{Bmatrix} = \mathbf{T}\begin{Bmatrix}\varepsilon_x\\ \varepsilon_y\\ \varepsilon_z\\ \varepsilon_{yz}\\ \varepsilon_{xz}\\ \varepsilon_{xy}\end{Bmatrix} \quad where \quad \mathbf{T} = \begin{bmatrix} m^2 & n^2 & 0 & 0 & 0 & 2mn \\ n^2 & m^2 & 0 & 0 & 0 & -2mn \\ 0 & 0 & 1 & 0 & 0 & 0 \\ 0 & 0 & 0 & m & -n & 0 \\ 0 & 0 & 0 & n & m & 0 \\ -mn & mn & 0 & 0 & 0 & (m^2 - n^2) \end{bmatrix}$$

$$m = \cos\theta; \quad n = \sin\theta \tag{8.15}$$

where θ is the angle between the positive x direction of the global coordinate system and the direction of the fibers 1 (Fig. 8.3). An inverse of the transformation matrix $\mathbf{T}^{-1}$ can easily be found by replacing θ with $-\theta$ in **T**.

Using (8.13), (8.14), (8.15) we calculate the stresses in each lamina of the composite laminate. To calculate the stress resultants and stress couples M_x, M_y,

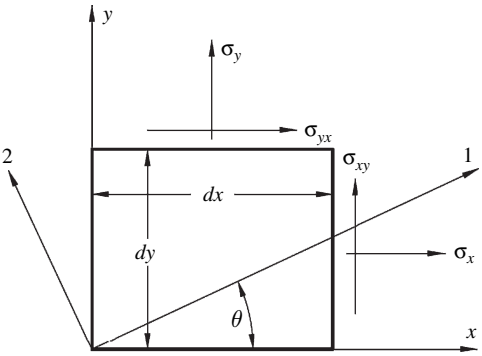

Fig. 8.3 Lamina (local) coordinate system – 123 and laminate (global) coordinate system – xyz (Woelke et al., 2006b)

$M_{xy}, N_x, N_y, N_{xy}, Q_x, Q_y$ in the laminate, we use definitions of normal and shear forces, as well as bending moments commonly used in beam, plate, and shell theory:

$$\begin{Bmatrix} N_x \\ N_y \\ N_{xy} \\ N_{xz} \\ N_{yz} \end{Bmatrix} = \int_{-h/2}^{h/2} \begin{Bmatrix} \sigma_x \\ \sigma_y \\ \sigma_{xy} \\ \sigma_{xz} \\ \sigma_{yz} \end{Bmatrix} dz; \quad \begin{Bmatrix} M_x \\ M_y \\ M_{xy} \end{Bmatrix} = \int_{-h/2}^{h/2} \begin{Bmatrix} \sigma_x \\ \sigma_y \\ \sigma_{xy} \end{Bmatrix} z\, dz \tag{8.16}$$

The positive directions of the stress resultants, consistent with their definitions given by (8.16), are shown in Fig. 8.4.

The shear correction factor of 5/6 is often applied in the definition of the transverse shear forces in (8.16). This is because transverse shear strains are defined according to the Mindlin plate theory, where the strain is constant over the thickness. The stresses are obtained by multiplying strains by a shear modulus (8.13), which leads to a constant distribution of the shear stresses across the thickness of the composite laminate. In reality, however, shear stresses σ_{xz} and σ_{yz} are quadratic functions of thickness coordinate z, and in absence of the traction boundary conditions on the outer surfaces of the shell, they should vanish on the top and bottom surfaces, i.e., $z = \pm h/2 \rightarrow \sigma_{xz} = \sigma_{yz} = 0$. If these boundary conditions are not satisfied, the integration of constant stresses over the thickness will not yield accurate values of the transverse shear forces without application of the shear correction factor. The value of the shear correction factor is derived by equating the strain energy for the exact parabolic function of shear stress to the strain energy of the approximate constant shear stress, acting over a modified area. The shear strain energy of a beam is given by:

$$U_s = \frac{1}{2}\int_V \frac{\tau_{zx}^2}{G} dV = \frac{1}{2}\int_V G\gamma_{zx}^2 dV = \frac{5}{2}\frac{Gbh}{6}\int_0^L \left(\frac{dw}{dx} - \phi_x\right)^2 dx \tag{8.17}$$

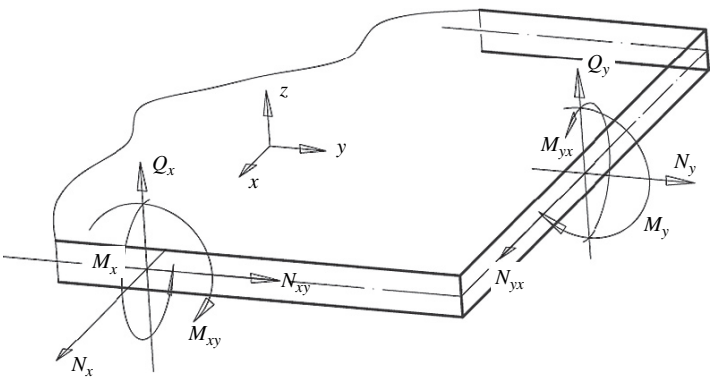

Fig. 8.4 Stress resultants on shell element (Woelke et al., 2006a)

To obtain the same energy for a uniform stress σ_{xz}, the stresses need to act on a modified area $A = (5/6)bh$, where b and h are the width and thickness of the beam.

Application of the shear correction factor results in accurate computations of transverse shear forces. Transverse shear stresses are still uniform, however, which may lead to incorrect failure prediction of individual laminas and of the composite laminate. To correct this deficiency without redefining the kinematics of the shell, it is necessary to modify the strains by applying not only a shear correction factor, but the shape function $f(z)$. The function describing the variation of shear stresses across the thickness is obtained from the equilibrium equations of stresses and is given by:

$$f(z) = \frac{5}{6}\frac{3}{2}\left[1 - \left(\frac{2z}{h}\right)^2\right] \tag{8.18}$$

The shape function obtained by (8.18) is introduced into the formulation, resulting in a parabolic distribution of the stresses across the thickness. This representation is not exact, as the real strain function is not continuous through the thickness of the composite laminate, owing to the stiffness variation of the individual laminas (see Sect. 8.5.1). It is, however, convenient, as it does not require redefinition of the kinematics of the shell.

One of the most common failure modes in composite laminates is delamination, which is driven by the transverse shear stresses. On one hand, accurate determination of transverse shear stresses is important and the aforementioned parabolic distribution might be insufficient. On the other hand, a mathematically consistent formulation ensuring convergence to the analytical solution requires adoption of a higher-order kinematics of the shell, which is cumbersome, especially when used in explicit finite element codes such as EPSA and FLEX. To avoid these difficulties while obtaining accurate representation of the shear stresses through the thickness, we use a transformed section method. This approach, which has been used in the analytical calculation of composite beams, can easily be extended to plates and shells. In the case of the beam, the cross section built of several materials is transformed into an equivalent cross section of a single material on which the resisting forces and the neutral axis are the same as on the original section. The usual flexure formula is then applied to the new section (Ugural and Fenster, 1995). The equivalent cross section is found by multiplying the width of each lamina by a so-called modular ratio, given by:

$$n = \frac{E_x}{E_2} \tag{8.19}$$

where E_x is Young's modulus of a considered lamina in the global x direction and E_2 is Young's modulus of a lamina in the direction perpendicular to the fiber. We therefore have for the lamina oriented at 0°, $n = E_1/E_2 \geq 1$ and for the lamina oriented at 90°, $n = 1$. The width of each lamina is then multiplied by its respective modular ratio to form the equivalent cross section, shown in Fig. 8.5.

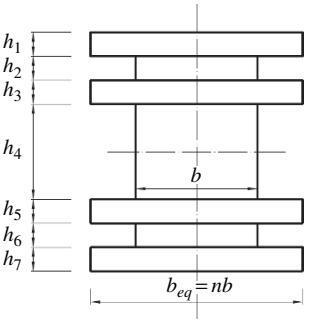

Fig. 8.5 Equivalent cross section of the composite beam (Woelke et al., 2006b)

Having established the equivalent cross section, we can determine the equivalent area and first and second moment of area, which can be used to calculate the displacements, strains, and stresses. In the case of plates and shells, the geometric cross-section characteristics of individual laminas are multiplied by the modular factor given by:

$$\begin{aligned} E_{equ\_x} &= E_1 \cos^2\theta + E_2 \sin^2\theta \\ E_{equ\_y} &= E_2 \cos^2\theta + E_1 \sin^2\theta \end{aligned} \tag{8.20}$$

where E_{equ_x} and E_{equ_y} are the modular factors of the lamina in global x and y directions, respectively; E_1 and E_2 are Young's moduli of the lamina in directions 1 (fiber direction) and 2 (direction perpendicular to the fibers), respectively; and θ is the angle between a positive x direction of a global coordinate system and a direction of the fibers 1, (Fig. 8.3). The equivalent cross-section area of the lamina is therefore:

$$A_{xi} = h_i E_{equ\_xi} \quad where \quad i = 1, k \tag{8.21}$$

where k is the number of laminas and h_i is the thickness of the $i - th$ lamina. The equivalent area of the laminate can be obtained by adding the equivalent areas:

$$A_x = \sum_{i=1}^{k} A_{xi} \tag{8.22}$$

Similarly, the equivalent first and second moment of area are given by:

$$\begin{aligned} Q_x &= \sum_{i=1}^{k} h_i z_i E_{equ\_xi} \\ I_x &= \sum_{i=1}^{k} \left(\frac{h_i^3}{12} + h_i z_i^2 \right) E_{equ\_xi} \quad where \quad i = 1, k \end{aligned} \tag{8.23}$$

where z_i is the distance between the center axes of the lamina and composite laminate.

The transverse shear stresses can now be calculated:

$$\sigma_{xz} = \frac{Q_x N'_{xz}}{I_x} \; ; \quad \sigma_{yz} = \frac{Q_{yx} N'_{yz}}{I_y} \tag{8.24}$$

where N'_{xz} and N'_{yz} are transverse shear forces calculated not by means of (8.16), but through direct integration of transverse shear strains multiplied by the shear correction factor given by (8.18):

$$N'_{xz} = \int_{-h/2}^{h/2} G_{xz} f(z) \varepsilon_{xz} \; ; \quad N'_{yz} = \int_{-h/2}^{h/2} G_{yz} f(z) \varepsilon_{yz} \tag{8.25}$$

where $G_{xz} = G_{13}$ and $G_{yz} = G_{23}$. As mentioned above, application of the shear correction factor results in the accurate computation of transverse shear forces. Substituting these forces into (8.24), along with previously obtained equivalent cross-section characteristics, allows for accurate determination of the non-continuous distribution of the transverse shear stresses across the thickness of the shell.

The above constitutive equations are universal for both plates and shells. They are implemented into the explicit finite element codes EPSA and FLEX. The composite shell element used is flat, with constant strains and 4 nodes and 5 degrees of freedom per node, i.e., linear velocities $\dot{u}, \dot{v}, \dot{w}$ in x, y, z directions, respectively, and angular velocities $\dot{\phi}_x, \dot{\phi}_y$ around y and x axes, respectively. The curvature of the shell is modeled through finite element discretization. The positive directions of the degrees of freedom are the same as the positive directions of the stress resultants (see Fig. 8.4).

Details of the kinematics of the element, integration scheme, and anti-hourglassing procedure are given by Flanagan and Belytschko (1981).

8.4 Failure Criteria for Composite Laminates

Some of the most common failure criteria for composite laminates are discussed in WAI (2005). Here, transverse shear stresses were introduced into the composite model. Transverse shear stresses are important in failure investigation of composite laminates, primarily because they cause delamination. To consider the influence of shear stresses on failure prediction, we modify a maximum stress criterion as follows: the composite begins to fail if $F \geq 1$, where F is given by:

$$F = \max\left(\left| \frac{\sigma_{11}}{X} \right|, \left| \frac{\sigma_{22}}{Y} \right|, \left| \frac{\sigma_{12}}{S_{12}} \right|, \left| \frac{\sigma_{13}}{S_{13}} \right|, \left| \frac{\sigma_{23}}{S_{23}} \right| \right) \tag{8.26}$$

where $\sigma_{11}, \sigma_{22}, \sigma_{12}, \sigma_{13}, \sigma_{23}$ are the stresses in the principal material directions, and X, Y, S_{12}, S_{13}, S_{23} are, respectively, tensile or compressive strength in 11 and 22 directions and shear strengths in 12, 13, 23 directions. The maximum stress criterion is especially useful, as it allows for predictions of the failure modes. With the appropriate experimental data, the transverse shear strength of the composite laminate could be determined. This would allow anticipation of failure by delamination, substantially improving the modeling of failure in composite laminates.

We also modify an interactive anisotropic Tsai-Hill criterion to account for transverse shear stresses. Although this criterion is commonly used, it usually considers only a plane state of stress. To include transverse shear stresses in the failure analysis of composite laminates, we use an interactive Tsai-Hill criterion in the following form:

$$F = \frac{{\sigma_{11}}^2}{X^2} - \frac{\sigma_{11}\sigma_{22}}{X^2} + \frac{{\sigma_{22}}^2}{Y^2} + \left(\frac{\sigma_{12}}{S_{12}}\right)^2 + \left(\frac{\sigma_{23}}{S_{23}}\right)^2 + \left(\frac{\sigma_{13}}{S_{13}}\right)^2 \tag{8.27}$$

According to this criterion the individual lamina fails if $F \geq 1$. The Tsai-Hill criterion in the form given by (8.27) is introduced separately into EPSA. We therefore have both a plane stress version of the Tsai-Hill criterion and the form given by (8.27), which accounts for transverse shear stresses.

The above criteria are commonly used in the analysis of composite laminates. They are based, however, on the assumption that the structure is linear until failure occurs. When the failure criterion is satisfied, the lamina is typically eroded. In reality however, satisfying the failure criterion (such as Tsai-Hill) could indicate, for example, local fiber cracking, in which case the laminate continues to carry the reduced load. To represent failure in composite laminates, plasticity and elastic and inelastic damage must be invoked. Use of the experimental data necessary to calibrate the model would allow prediction of yielding and cracking of the matrix, cracking of the fibers, debonding of the fibers from the matrix material, and delamination. We will describe such failure in composites in future work.

8.5 Implementation and Numerical Examples

We implemented our formulation into dynamic finite element codes EPSA and FLEX using the programming language Fortran 95. The novel feature of the model, i.e., the calculation of the transverse shear stresses does not require any changes to the laminated shell element that would negatively affect its convergence rate. The convergence of the laminated shell elements in EPSA and FLEX are discussed by Vaughan (2005) and WAI (1998).

Both EPSA and FLEX use an explicit time integration scheme, which does not require any nonlinear equation solver (e.g., Newton-Raphson technique). Consequently, explicit time integration is convenient for implementation of advanced material constitutive models. The disadvantage of the explicit methods as opposed to

implicit time integration lies in conditional stability. The solution is stable only if the timestep size is equal to or lower than a critical value (Courant stability criterion). The critical timestep is a function of the maximum frequency of the analyzed structure. In this analysis, the choice of timestep size is such that the Courant stability criterion is satisfied and stability of the solution ensured.

We investigate the reliability of our approach through a series of discriminating examples. The problems are selected to demonstrate and challenge new features of the formulation, i.e., representation of transverse shear deformation and transverse shear stresses in the analysis of layered composites.

The importance of shear deformation in the analysis of composite structures is widely known and has been discussed by many authors. Our objective here is to confirm that our description of the shear effects is reliable and leads to improvement in the accuracy of analyses of composite structures.

8.5.1 Laminated Composite Strip under Three-Point Bending

We consider a simply supported 7-layer symmetric beam with a central line load. This problem is a commonly used composite benchmark (Hardy, 2001). The stacking sequence and orientation of the fibers is as follows: 0/90/0/90/0/90/0, where the center ply is four times as thick as the others. The geometry of the beam including the stacking sequence is shown in Fig. 8.6.

The length of the beam is $L = 50\,mm$, the line load $P = 10\,N/mm$ is applied at point E, and material properties are: $E_1 = 1.0E5\,MPa,\ E_2 = 5.0E3\,MPa,\ G_{12} = 3.0E3\,MPa,\ G_{13} = G_{23} = 2.0E3\,MPa$, and $\nu_{12} = 0.4$, $\nu_{12} = 0.3$.

To confirm that our formulation reliably represents of the shear effects and is therefore applicable to the analysis of thick composite shells, we investigate the vertical displacement under the load (point E), bending stresses at the same location, and transverse shear stresses at point D (see Fig. 8.6). All of these values can be

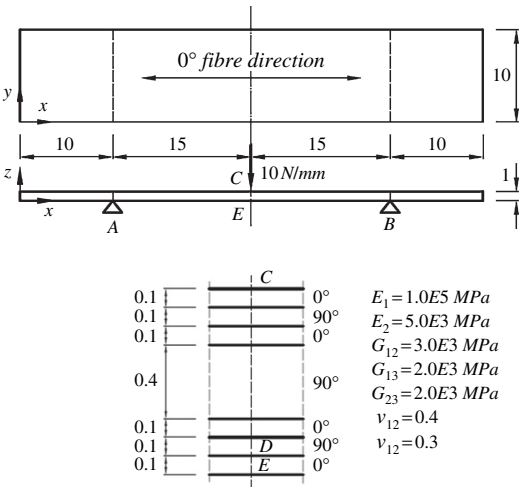

Fig. 8.6 Simply supported laminated beam subjected to central line load with material properties (Hardy, 2001)

calculated analytically using a transformed section method. In this method, a cross section composed of several materials is transformed into an equivalent cross section of a single material on which the resisting forces and neutral axis are the same as on the original section. The usual flexure formula is then applied to the new section (Ugural and Fenster, 1995).

The equivalent cross section is obtained by multiplying the width of each lamina by a so-called modular ratio, given by:

$$n = \frac{E_x}{E_2} \tag{8.28}$$

where E_x is Young's modulus of a considered lamina in the global x direction and E_2 is Young's modulus of the lamina in the direction perpendicular to the fiber. We therefore have for the lamina oriented at 0^o, $n = E_1/E_2 = 20$, and for the lamina oriented at 90^o, $n = 1$. The width of each lamina is then multiplied by the appropriate modular ratio to form the equivalent cross section, shown in Fig. 8.7.

Having established the equivalent cross section, we can determine its moment of inertia using Steiner's theorem (Parallel Axis Theorem):

$$I_{eq} = \sum_{j=1}^{m} \left(\frac{b_j h^3}{12} + b_j h {d_j}^2 \right)_j = 10.9667\ mm^4 \tag{8.29}$$

where m is a number of sub-areas (Fig. 8.7); b_j is a width of considered sub-area; h is the total thickness of the composite laminate; and d_j is the distance between the neutral axes of the laminate and lamina. Using the equivalent moment of inertia, we calculate the displacement under the load due to bending and shear actions. We apply the virtual unit force at point C to determine the displacement by means of the virtual work principle:

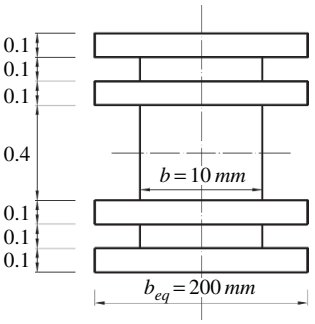

Fig. 8.7 Equivalent cross section of the composite beam (Woelke et al., 2006b)

$$w = w_M + w_Q = \int_L \frac{M\bar{M}}{E_2 I_{eq}} dx + \int_L \frac{6\,Q\bar{Q}}{5\,G_{13}A_{eq}} dx = \frac{PL^3}{48E_2 I_{eq}} + \frac{3PL}{10G_{13}A} = -1.07\,mm \tag{8.30}$$

where M,Q are bending moment and shear force functions, respectively; $\bar{M}$, $\bar{Q}$ are virtual bending moment and shear force, respectively; $L = 30\,mm$, (see Fig. 8.6); 5/6 is a shear correction factor (see (8.16), (8.17)); and A is the area of the cross section.

The problem described above is modeled using 20 composite shell elements based on the thin shell and thick shell formulations. We compare the time histories obtained using the two formulations, as well as a final numerical solution to the analytical result given by (8.30). Figure 8.8 shows the time history for the vertical displacement at point E (Fig. 8.6), calculated without accounting for shear stresses and after transverse shears have been introduced:

In Fig. 8.8, as expected, the displacement calculated with shear stresses taken into account ($w = -1.069\,mm$) is slightly larger than that calculated with shear effects not taken into account ($w = -1.054\,mm$). Both values, however, compare well with the reference solution ($w = -1.07\,mm$). We therefore conclude that shear stresses do not significantly affect the response of the structure under consideration. The situation changes, however, if the transverse shear moduli G_{13} and G_{23} are significantly smaller than the in-plane shear modulus G_{12}. If $G_{13} = G_{23} = 250\,MPa$ the displacement calculated using (8.30) is:

$$for \quad G_{13} = G_{23} = 250\ MPa: \quad w = w_M + w_Q = -1.026 - 0.36 = -1.386\,mm \tag{8.31}$$

The significant increase (nearly 26%) in the displacement is caused mainly by transverse shear action only, while the deformation caused by bending does not

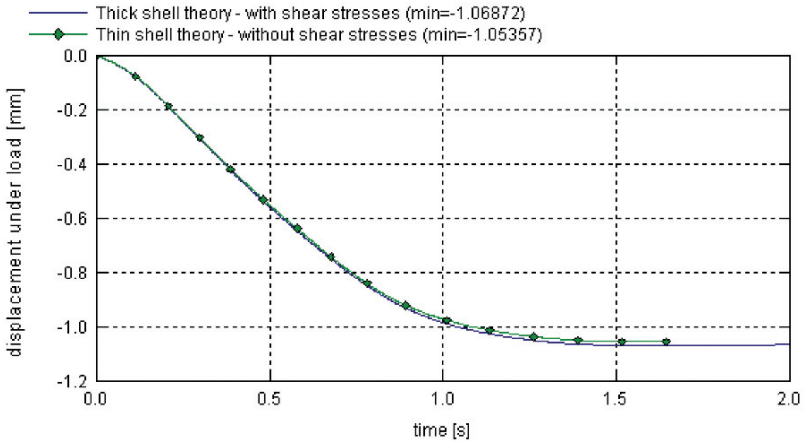

Fig. 8.8 Displacement time histories (displacement under load) (Woelke et al., 2006b)

change. In this case, only a formulation that features a reliable representation of the shear effects is capable of delivering an accurate solution.

Figure 8.9 shows the time histories of displacement under load calculated, as above, with EPSA composite shell elements based on the thin shell formulation, without taking shear stresses into account, and on the thick shell formulation, accounting for shear stresses. The significant difference between the results obtained by means of the thin and thick shell formulations is attributed to the influence of shear stresses. Our thick shell formulation delivers a value of displacement under load ($w = -1.3838\,mm$) that practically matches the reference solution obtained by (8.31) ($w = -1.386\,mm$). The thin shell formulation correctly predicts only the bending part of the deformation, while the shear part is entirely neglected (see Fig. 8.9).

For further verification, we compare the values of maximum bending stresses and transverse shear stresses computed using EPSA-III, with the reference solution calculated analytically. The maximum bending stress is given by:

$$\sigma_x = \frac{nM}{I_{eq}}\frac{h}{2} = \pm\frac{nPLh}{8I_{eq}} = \pm 683.89\ MPa \tag{8.32}$$

where n is given by (8.28), M is the bending moment at midspan of the beam (under the load), and h is the thickness of the composite laminate. The transverse shear stress (interlaminar shear) between the jth and the $(j+1)th$ can be calculated from equilibrium of stresses. At the top layer ($z = \pm 0.4\,mm$), we have:

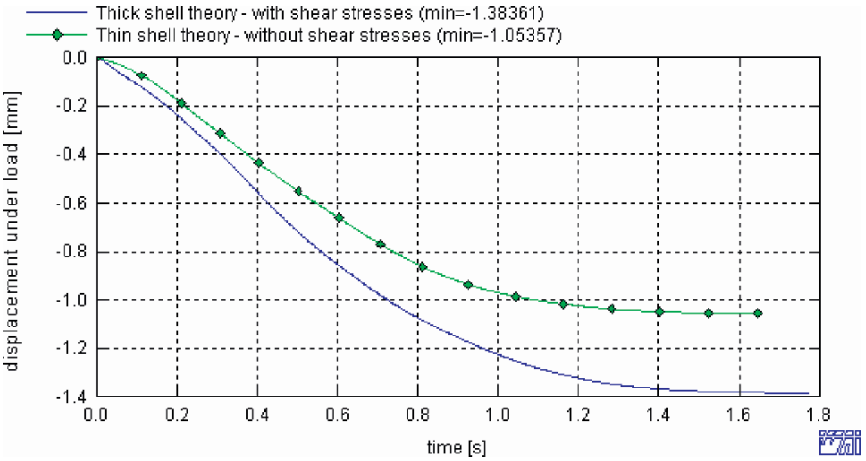

Fig. 8.9 Displacement time histories (displacement under load) with reduced shear modulus G_{13} (Woelke et al., 2006b)

Table 8.1 Comparison of analytical and numerical results (A and E are shown in Fig. 8.6)

	Analytical solution	EPSA thin shell	EPSA thick quadratic	EPSA thick TSM*
Displacement at E [mm]	1.07	1.054	1.069	1.069
Displacement at E [mm], (reduced G_{13})	1.386	1.054	1.384	1.384
Shear force between A and E [kN]	0.05	0.05	0.05	0.05
Shear stress at $D(z = \pm 0.4\,mm)$ [MPa]	−4.103	–	−2.620	−4.131
Bending moment at E [kNm]	7.5E-4	7.51E-4	7.51E-4	7.51E-4
Bending stress at E [MPa]	683.89	684.96	684.96	684.96

* Note: TSM – Transformed Section Method.

$$\sigma_{xz} = -\int_{0.4}^{0.5} \frac{\partial \sigma_x}{\partial x} dz = -\int_{0.4}^{0.5} \frac{\partial}{\partial x}\left(\frac{n\ 0.05xz}{I_{eq}}\right) dz = -4.103\ MPa \tag{8.33}$$

Table 8.1 compares the analytical and numerical values of displacements and bending stresses, as well as shear forces and bending moments, and Fig. 8.10 presents the transverse shear stress distribution.

The interlaminar shear stress at $z = \pm 0.4\,mm$, determined using our model, is $\sigma_{xz} = -4.134\,MPa$ (Fig. 8.10), which compares very well with the analytical solution obtained by (8.33) ($\sigma_{xz} = -4.103\,MPa$). The distribution of the transverse shear stresses, as calculated by the transformed section method, also agrees closely with the reference solution. Table 8.1 and Fig. 8.10 compare the formulations. Note that, although application of the second-order shape function significantly improves model accuracy over the constant distribution, it leads to inaccuracies in shear

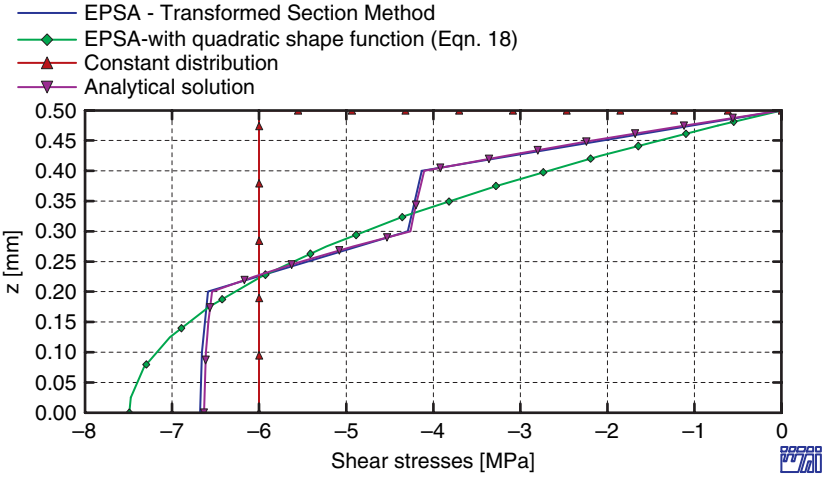

Fig. 8.10 Distribution of transverse shear stress σ_{xz} [MPa] across the thickness of the composite laminate (Axis of symmetry $z = 0.0$) (Woelke et al., 2006b)

stresses. This negatively affects the failure prediction capability of the model. The transformed section method allows for reliable shear stress distribution calculations, and it is simple and efficient. In all of the approaches considered, the integration of stresses through the thickness yields accurate results for the shear forces.

The displacements calculated by means of the thin shell formulation are accurate only when shear effects are negligible. When the transverse shear modulus is significantly smaller than the in-plane shear modulus, the thin shell formulation does not produce accurate results. The displacements calculated by means of the thick shell formulation almost exactly match the reference solutions, verifying that our thick shell formulation reliably represents of the shear effects and can be used successfully to model the behavior of thick composite plates, shells, and beams.

8.5.2 Composite Cylinder under Internal Pressure

In the previous example, we confirmed that our thick shell formulation correctly represents the increased shear flexibility caused by the differences between in-plane and out-of-plane shear moduli. Taking into account shear stresses in the analysis of thin shells can lead, however, to numerical deficiency commonly referred to as shear locking. A reliable shell model correctly predicts shear modes of deformation in the case of both thin and thick shells, without suffering from shear locking. To verify that we have avoided this numerical deficiency, we consider a long cylinder composed of two layers. The internal layer is an isotropic material and the external layer an orthotropic material. The cylinder is subjected to internal pressure (see Fig. 8.11). Properties of the cylinder are given in Table 8.2.

Because of symmetry, only an octant of the cylinder need be considered. The mesh of 160 EPSA shell elements, used to model cylinderoctant, is shown in Fig. 8.12.

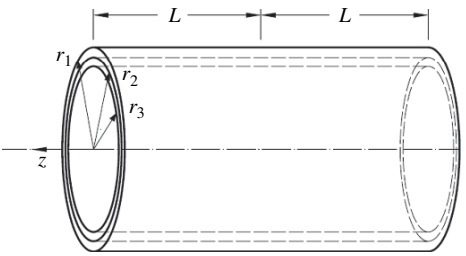

Fig. 8.11 Composite cylinder under internal pressure (Woelke et al., 2006b)

Table 8.2 Material properties and dimensions of the pinched cylinder

	Dimensions [mm]	$L = 100.0,\ r_1 = 27.0,\ r_2 = 25.0,\ r_3 = 23.0$
	Loading	Internal pressure: $p = 200\,MPa$
	Layer 1 (Inner)	Isotropic: $E = 2.1E5\ MPa,\ \nu = 0.3$
Material	Layer 2 (Outer)	Orthotropic: $E_1 = 1.3E5\,MPa,\ E_2 = 5.0E3\ MPa,$
Properties		$\nu_{12} = 0.3,\ G_{12} = 1.0E4\ MPa,\ G_{13} = 500\ MPa$

Note: Direction 1 is a hoop direction; 2 is a z direction.

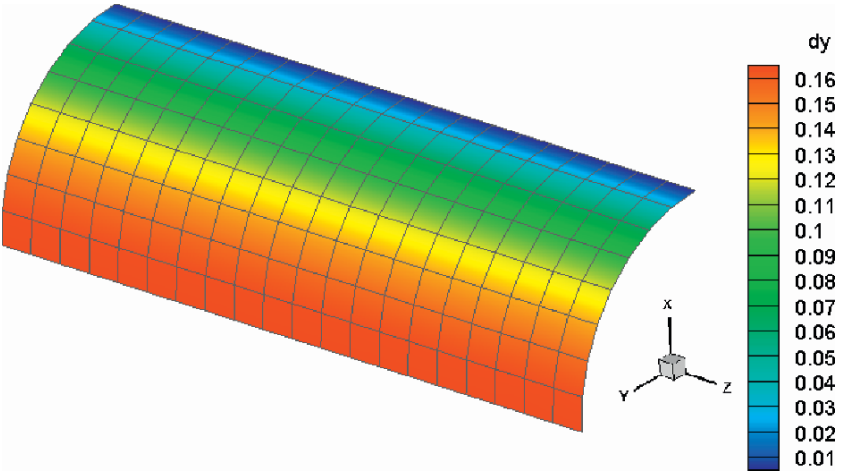

Fig. 8.12 Finite element mesh and displacements of an octant of the cylinder (Woelke et al., 2006b)

We investigate the radial displacement of the cylinder (see Fig. 8.11), calculated by means of the thin and thick shell formulations. The outer shell layer is orthotropic, the inner layer is isotropic, and the cylinder is relatively thin. The loads are resisted mainly by the membrane action of the shell, and shear effects are negligible. Despite the fact that the in-plane shear modulus (G_{12}) of layer 2 is much larger than the out-of-plane shear modulus (G_{13}), the difference between displacements obtained from the two formulations should not be significant. The time histories of displacement under load determined using the thin and thick shell formulations are shown in Fig. 8.13.

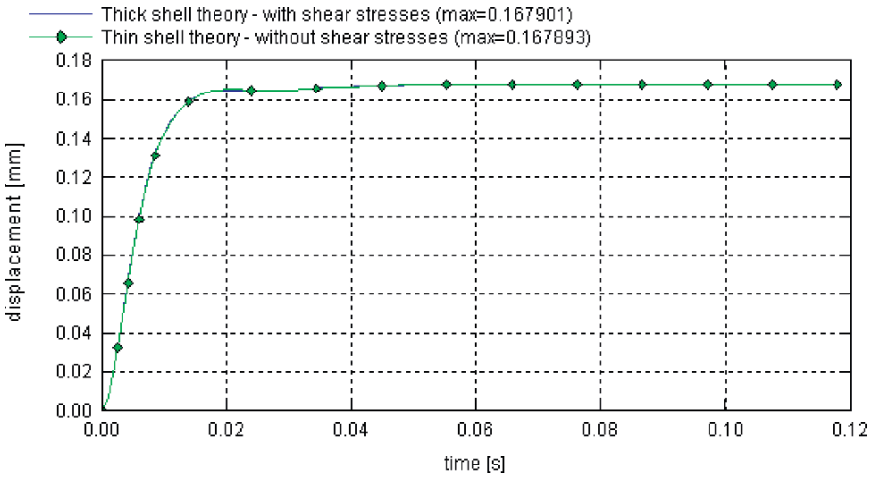

Fig. 8.13 Time history plots for radial displacements (Woelke et al., 2006b)

In Fig. 8.13 the radial displacements calculated using the thin and thick shell formulations practically coincide. Because, as discussed above, shear effects are negligible, this result confirms the reliability of the thick shell formulation.

8.5.3 Cylindrical Shell Subjected to Ring of Pressure

As discussed in the Introduction, our main objective is to account for the influence of transverse shear strains and stresses on the behavior of composite laminates. In Sects. 8.5.1 and 8.5.2, the composite problems were investigated, confirming the reliability of the current thick shell formulation for composite structures. A reliable layered shell formulation should produce accurate results of the analysis of laminated isotropic plates and shells. In this section, we analyze a layered isotropic shell to further confirm the effectiveness of the model.

We consider a cylindrical shell subjected to the ring of pressure. The geometry and material parameters are shown in Fig. 8.14. Because of symmetry, we need consider only an octant of a shell, which is modeled using finite element mesh, as shown in Fig. 8.12.

We analyze the problem using EPSA layered shell elements, based on the thin shell formulation, and compare the results with those obtained using the thick composite shell elements accounting for transverse shear deformation. First, we consider a cylinder with thickness $t = 0.5\,mm$. Shells in which the ratio of the radius of the curvature and thickness is higher than 50 are usually considered thin. In this case, the results delivered by EPSA thin-layered shell element, previously shown to be reliable, will be sufficiently accurate. Solving the problem using the thick layered shell formulation presented here should therefore produce similar results. We compare the radial displacements at midspan of the cylinder, determined by thin and thick shell formulations. The time history plots are shown in Fig. 8.15.

Figure 8.15 shows that, as expected, the results produced by the thin and thick shell formulations are practically identical. Shear effects are negligible in this problem, as correctly recognized by the thick layered shell model.

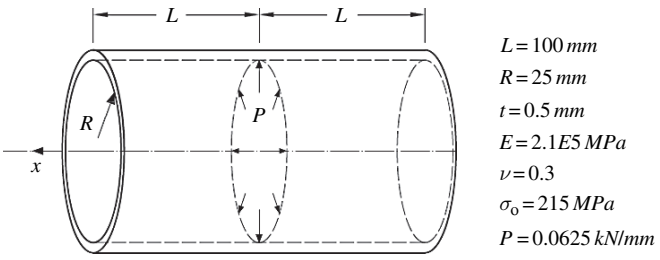

Fig. 8.14 Cylindrical shell subjected to a ring of pressure (Woelke et al., 2006b)

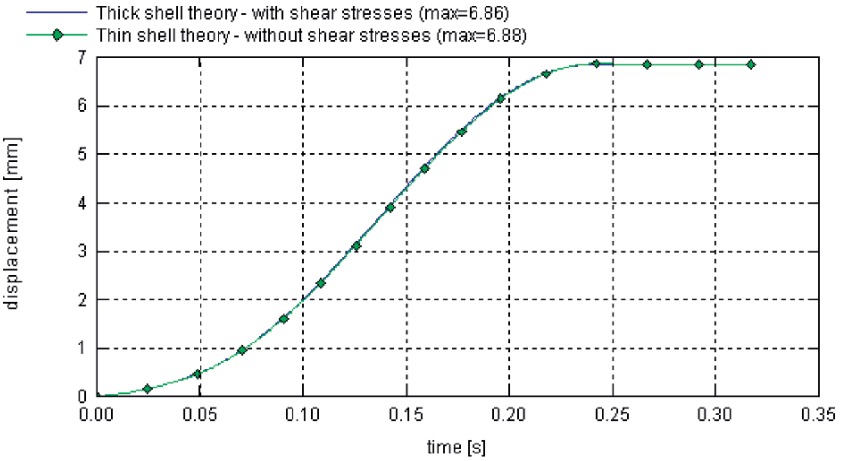

Fig. 8.15 Radial displacements for a cylinder subjected to a ring of pressure ($t = 0.5\,mm$) (Woelke et al., 2006b)

We increase the thickness of the cylinder to $t = 5\,mm$ and the pressure to $P = 1.0\,kN/mm$ and again compare the radial displacements obtained from the two formulations. The displacement time history plots are shown in Fig. 8.16.

Displacement calculated using our thick shell formulation is 17% larger than that obtained without accounting for shear stresses. At the same time, the bending moments and axial forces determined by the thick and thin shell formulations are approximately the same (see Fig. 8.17). This significant discrepancy between

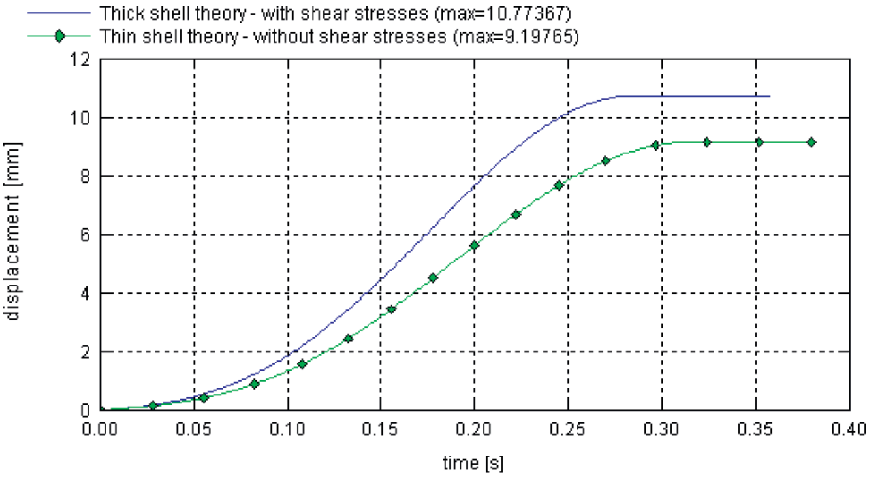

Fig. 8.16 Radial displacement for a cylinder subjected to a ring of pressure ($t = 5\,mm$) (Woelke et al., 2006b)

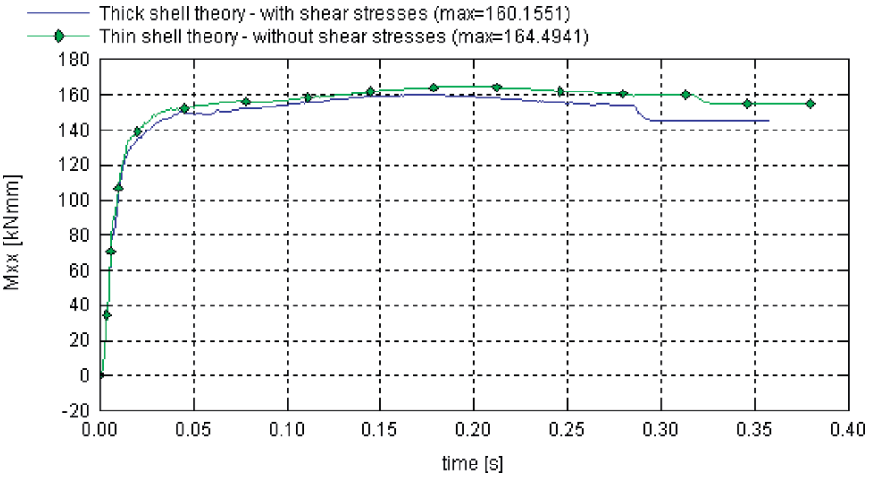

Fig. 8.17 Bending moment at midspan of the cylinder subjected to a ring of pressure ($t = 5\,mm$) (Woelke et al., 2006b)

displacement values is attributed to the increased influence of the transverse shear effects, which are correctly represented in our model.

8.6 Summary

Accounting for out-of-plane shear strains and stresses is necessary for the accurate modeling of the elasto-plastic behavior of thick plates and shells. In the case of composite laminates, the influence of transverse shear stresses is even more important. This is because of the orthotropic nature of these structures and the often significant difference between in-plane and out-of-plane shear moduli. As this leads to increased shear flexibility of the composites, neglecting shear effects can result in an unsafe design. Moreover, transverse shear stresses cause delamination in composites, one of the most important failure modes. Our formulation makes it possible to account for transverse shear stresses in failure criteria. With the use of appropriate experimental data, this can result in greatly improved failure predictions for composite laminates.

EPSA is an explicit code that features a constant strain, flat shell element. The equation of motion is solved locally, without assembling the stiffness matrix of the structure. Neither shear nor membrane locking is experienced, as shown in Sect. 8.5. The anti-hourglass procedure is given by Flanagan and Belytschko (1981).

The numerical examples in Sect. 8.7 were selected to challenge the most important features of this work, i.e., representation of transverse shear effects in composite laminates and elasto-plastic investigations of isotropic shells. Because of a lack of appropriate experimental data, we do not discuss the failure prediction capability of the model. We will address this capability in their future work. In all of the analyzed

cases, the results are accurate, confirming that the model is well grounded. EPSA layered composite finite elements are therefore capable of delivering accurate approximations of the structural behavior of thin and thick beams, plates, shells, and composite laminates.

References

Flanagan, D.P. and Belytschko, T. (1981), A uniform strain hexahedron and quadrilateral with orthogonal hourglass control. Int. J. Num. Meth. Eng., 17, 679–706.

Hardy, S. (2001) Composite Benchmarks. NAFEMS, Ref: R0031, Issue 2.

Putcha, N.S. and Reddy, J.N. (1986). A refined mixed shear flexible finite element for the nonlinear analysis of laminated plates. Comput. Struct., 22, 4, 529–538.

Reddy, J.N. (1984). A simple high-order theory for laminated composite plates. J. Appl. Mech., 51, 745–752.

Reddy, J.N. (1989). On refined computational models composite laminates. Int. J. Num. Meths. Eng. 27, 361–382.

Reddy, J.N., Barbero, E.J., Teply, J.L. (1989). A plate bending element based on a generalized laminate plate theory. Int. J. Num. Meths. Eng., 28, 2275–2292.

Sloan, J.G. (1979). The Behavior of Rectangular Composite Material Plates Under Lateral and Hydrothermal Loads. MMAE Thesis. University of Delaware.

Ugural, A.C. and Fenster, S.K. (1995) Advanced Strength and Applied Elasticity. Third Edition, Prentice Hall.

Vaughan, D.K., "FLEX Users's Guide," Report UG8298, Weidlinger Associates, Los Altos, CA, May 1983 plus updates through 2005.

Vinson, J.R. and Sierakowski, R.L. (1987). The Behavior of Structures Composed of Composite Materials. Kluwer Academic Publishers, Dordrecht.

WAI, (1998), EPSA-III, Theoretical Guidebook. Weidlinger Associates.

Woelke, P., Chan, K.K., Daddazio, R., Abboud, N. (2006a). Stress Resultant Based Elasto-Viscoplastic Thick Shell Model. 77th Shock and Vibration Symposium Proceedings, Monterrey, CA.

Woelke, P., Chan, K.K., Daddazio, R. and Abboud, N. and Voyiadjis, G.Z (2006b) Analysis of Shear Flexible Layered Isotropic and Composite Shells By EPSA. 77th Shock and Vibration Symposium Proceedings, Monterrey, CA.

Woelke, P., Chan, K.K., Daddazio, R., Abboud, N. and Voyaidjis, G.Z. (2008). A Simple Method of Determination of Transverse Shear Stresses and Delamination in Composite Laminates Using Finite Elements. Submitted to IJMS, December 2007.

Chapter 9
Numerical Methods and Computational Algorithms

9.1 Introduction

In this chapter use discuss the numerical techniques and computational algorithms used in our work. Together the equations derived, form a procedure for a comprehensive analysis of thick plates and shells. Given the complexity of the constitutive equations, analytical solutions would be possible only for specific problems. Recent developments in computer technology, as well as numerical methods, provide a powerful tool that allows approximations of the sometimes very complicated systems of equations, used to describe engineering problems. To take advantage of this tool, a set of instructions must be given to the computer, which defines in suitable form the sequence of operations required to solve a given problem (Ketter and Prawel, 1969).

We gradually built a computer program, Voyiadjis-Woelke-SHELLS, based on the shell constitutive equations presented in the preceding chapters, as well as on the computer program published by Voyiadjis and Shi (1990). The programming language was Fortran 95, along with the Compaq Visual Fortran compiler, version 6.6.C. We conducted our analyses on a personal computer. Some of the reference solutions were computed using the commercial finite element program ABAQUS installed on a Silicon Graphics Onyx 3200 workstation.

Below, we discuss computational issues and numerical techniques of the computer program. First, we present a method for solving a system of linear algebraic equations. We then discuss the solution scheme of the non-linear equations followed by the overall structure of the program.

9.2 Linear Elastic Analysis – System of Linear Algebraic Equations

In Chapter 3 we formulated a shell finite element, based on the shell constitutive equations derived in Chap. 2. The stiffness matrix of the element **K** was determined using a quasi-conforming technique. This method allows for the explicit determination of **K** without a need for numerical integration. Once the stiffness

G.Z. Voyiadjis, P. Woelke, *Elasto-Plastic and Damage Analysis of Plates and Shells*,

© Springer-Verlag Berlin Heidelberg 2008

matrix is calculated, the analysis involves a solution of the system of linear algebraic equations given by:

$$\mathbf{Kq} = \mathbf{R} \tag{9.1}$$

where **K** is the stiffness matrix of the structure given by equation (3.83), **q** is a vector of unknown nodal displacements of the structure, and **R** is an external load vector. In a linear problem, the coefficients of the stiffness matrix do not depend on the unknowns. There are many different methods of successive elimination of the unknowns, which is a direct way of solving simultaneous linear equations. One of the most popular elimination method the Gauss method, is used here. It is demonstrated through consideration of a system of equations of the form:

$$\begin{aligned} a_{11}x_1 + a_{12}x_2 + a_{13}x_3 + \ldots + a_{1n}x_n &= c_1 \\ a_{21}x_1 + a_{22}x_2 + a_{23}x_3 + \ldots + a_{2n}x_n &= c_2 \\ \ldots\ldots\ldots\ldots\ldots\ldots\ldots\ldots\ldots\ldots\ldots\ldots & \\ a_{n1}x_1 + a_{n2}x_2 + a_{n3}x_3 + \ldots + a_{nn}x_n &= c_n \end{aligned} \tag{9.2}$$

To solve the above equations requires two stages, i.e., forward elimination and backward substitution. The former involves eliminating the unknowns from the system of equations. For $a_{11} \neq 0$, the first of the (9.2) can be written as:

$$x_1 + b_{12}x_2 + b_{13}x_3 + \ldots + b_{1n}x_n = b_{1m} \tag{9.3}$$

where

$$b_{1j} = \frac{a_{1j}}{a_{11}},\ j > 1 \text{ and } m = n + 1 \tag{9.4}$$

An $(n-1)$ set of equations in the unknowns $x_2, x_3, \ldots, x_n$ is obtained by successive elimination between (9.3) and the latter $(n-1)$ equations of (9.2). Dividing the coefficients of the first equation in this new set by the leading element a_{22-1} gives the following equation (Ketter and Prawel, 1969):

$$x_2 + b_{23-1}x_3 + \ldots + b_{2n-1}x_n = b_{2m-1} \tag{9.5}$$

where

$$b_{2j-1} = \frac{a_{2j-1}}{a_{22-1}}, \quad j > 2 \tag{9.6}$$

By continuing the process, the leading equation of the $(n-2)$ system can be written as:

$$x_3 + b_{34-2}x_4 + \ldots + b_{3n-2}x_n = b_{3m-2} \tag{9.7}$$

and

$$b_{3j-2} = \frac{a_{3j-2}}{a_{33-2}}, \quad j > 3 \tag{9.8}$$

When $(n-1)$ eliminations have been carried out, we have:

$$x_n = b_{nm-(n-1)} \tag{9.9}$$

where:

$$b_{nm-(n-1)} = \frac{a_{nm-(n-1)}}{a_{nn-(n-1)}} \tag{9.10}$$

We follow backward substitution to determine the remaining $(n-1)$ values of the unknown x.

The total number of multiplications and divisions necessary to solve a set of n linear simultaneous algebraic equations by the single division Gauss elimination procedure described above is given by (Ketter and Prawel, 1969):

$$\frac{n}{3}\left(n^2 + 3n - 1\right) \tag{9.11}$$

Following the above sequence, the vector of unknown nodal displacements $\mathbf{q}$ is determined.

9.3 Non-linear Analysis – System of Non-linear Algebraic Equations

Several classes of non-linear problems of interest in many branches of science and engineering can be reduced to the solution of a system of simultaneous equations in which the coefficients are dependent on some functions of the prime variables (Zienkiewicz, 1978). Here, we are concerned only with the investigation of the geometrically non-linear and elasto-plastic-damage problems. The use of finite element discretization in a large class of non-linear problems results in a system of simultaneous equations of the same form as (9.1):

$$\mathbf{Kq} = \mathbf{R} \tag{9.12}$$

The coefficients of the stiffness matrix $\mathbf{K}$ are, however, dependent on the unknowns $\mathbf{q}$. This is a main distinction between the non-linear problem and a linear one, in which the equation coefficients are independent. In the case of stress path-dependent models, such as those in plasticity, the result is a system of functional equations even harder to solve than the typical non-linear algebraic equations. The numerical solution of the system of non-linear equations is much more complicated

than the system of linear equations. Direct solution of (9.12) is generally impossible necessitating an iterative scheme (Owen and Hinton, 1980). This leads to a computational cost for the analysis of the non-linear problems 10–100 times greater than the that for linear approximation for the same number of degrees of freedom. Nevertheless, advances in computer technology have decreased computing costs and non-linear calculations are undertaken much more frequently than in the past. In addition, there is greater demand for structural redundancy, which requires more sophisticated analysis (Cook et al., 1989).

The method of solution of the system of non-linear equation we adopt here, a modified Newton-Raphson technique, is discussed below.

9.3.1 *Modified Newton-Raphson Method – Combined Incremental/Iterative Solutions*

Analysis of a non-linear problem requires an iterative scheme, such as a Newton Raphson method. During any step of the iterative process expression (9.12) is not satisfied unless convergence has occurred. A system of residual forces may be assumed to exist so that (Owen and Hinton, 1980):

$$\boldsymbol{\Psi} = \mathbf{K}\mathbf{q} - \mathbf{R} \neq 0 \tag{9.13}$$

The residual forces $\boldsymbol{\Psi}$ can be interpreted as a measure of the departure of (9.12) from the equilibrium. As $\mathbf{K}$ is a function of $\mathbf{q}$ and possibly its derivatives, at any stage of the process the residual forces are functions of the displacement vector, i.e., $\boldsymbol{\Psi} = \boldsymbol{\Psi}(\mathbf{q})$. If the true solution to the problem exists at $\mathbf{q}^r + \Delta\mathbf{q}^r$, then the Newton-Raphson approximation for the general term of the residual force vector $\boldsymbol{\Psi}^r$ is:

$$\Psi_i^r = -\sum_{j=1}^{N} \Delta q_j^r \left(\frac{\partial \Psi_i}{\partial q_j}\right)^r \tag{9.14}$$

in which N is the total number of variables in the system and the superscript r denotes the r^{th} approximation of the true solution. Substituting for Ψ_i from (9.13), the complete expression for all the residual components can be written in matrix form:

$$\boldsymbol{\Psi}\left(\mathbf{q}^r\right) = -\mathbf{J}\left(\mathbf{q}^r\right)\Delta\mathbf{q}^r \tag{9.15}$$

where $\mathbf{J}$ is a Jacobian matrix with a typical term given by:

$$J_{ij} = \left(\frac{\partial \Psi_i}{\partial q_j}\right)^r = k_{ij}^r + \sum_{k=1}^{m} \left(\frac{\partial k_{ik}}{\partial q_j}\right)^r q_k^r \tag{9.16}$$

and k_{ij} is the general term of the stiffness matrix. The last term in (9.16) gives rise to non-symmetric terms in the Jacobian matrix. We retain these terms for the sake of a better convergence (Owen and Hinton, 1980).

The explicit form of the non-linear terms in (9.16) depends on the way in which the stiffness coefficients k_{ij} depend on the unknowns $\mathbf{q}$. The terms in the Jacobian matrix can be assembled to give the general expression:

$$\mathbf{J}(\mathbf{q}) = \mathbf{K}(\mathbf{q}) + \mathbf{K}'(\mathbf{q}) \tag{9.17}$$

where $\mathbf{K}'(\mathbf{q})$ contains only the unsymmetric terms. Finally, the Newton-Raphson process can be written using (9.15) and (9.17) in the following form:

$$\Delta\mathbf{q}^r = -\left[\mathbf{J}\left(\mathbf{q}^r\right)\right]^{-1}\boldsymbol{\Psi}\left(\mathbf{q}^r\right) = \left[\mathbf{K}\left(\mathbf{q}^r\right) + \mathbf{K}'\left(\mathbf{q}^r\right)\right]^{-1}\boldsymbol{\Psi}\left(\mathbf{q}^r\right) \tag{9.18}$$

The above relation allows the correction to the vector of unknowns $\mathbf{q}$ to be obtained from the residual force vector $\boldsymbol{\Psi}$ for any iteration. The iterative approach must be followed, with the vector $\mathbf{q}$ corrected at each stage according to equation (9.18) until convergence. The technique is shown schematically for a single variable case in Fig. 9.1.

Solution of the non-linear problem is achieved when the residual force $\boldsymbol{\Psi}$ vanishes, as this is a direct measure of the lack of equilibrium of the governing equation. First, a trial value $\mathbf{q}^0$ of the unknown is assumed, and the material stiffness associated with this value is calculated according to the prescribed $\mathbf{K}-\mathbf{q}$ relationship. The residual force is then calculated from (9.13) and the Jacobian matrix from (9.16). The correction of the first assumed value $\Delta\mathbf{q}^0$ can be found from (9.18), giving an improved approximation to the solution $\mathbf{q}^1 = \mathbf{q}^0 + \Delta\mathbf{q}^0$. The process is then repeated until the residual force $\boldsymbol{\Psi}$ vanishes or is sufficiently small. The Newton-Raphson process generally gives relatively rapid and stable convergence.

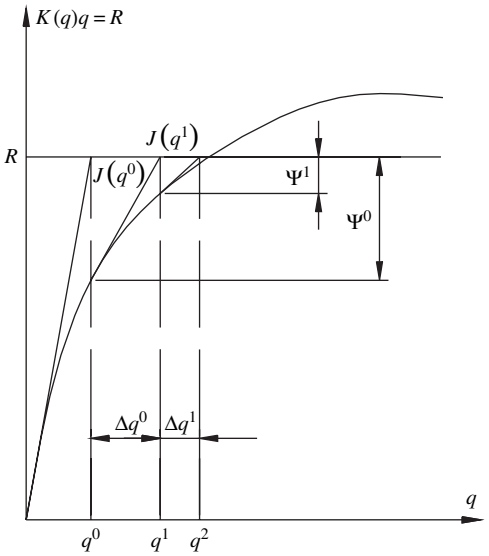

Fig. 9.1 The Newton-Raphson method for a single variable problem-convex $K - q$ relation

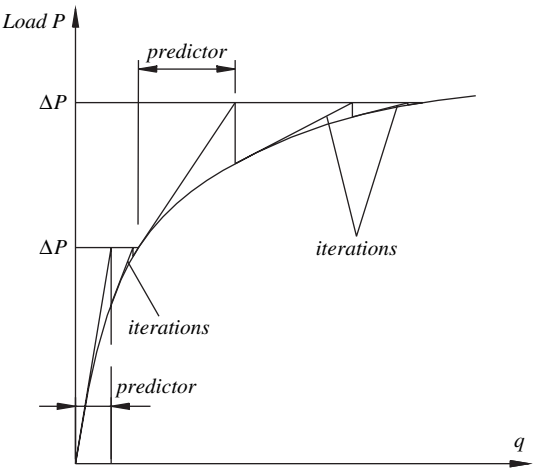

Fig. 9.2 A combination of incremental predictors with Newton-Raphson iterations

This iterative technique provides only a single point solution, as we apply only a single increment of load and then iterate until convergence. In practice, however, one generally needs a complete load-displacement response (equilibrium path). To determine the equilibrium path, we combine the incremental and iterative solution procedures. First, we apply an increment of load and then with a tangential stiffness matrix, we obtain a starting solution q^0, as shown in Fig. 9.1. This first step of the solution is called a "predictor". After computing the first predictor, we apply the iterations until the solution converges. Another increment of loading is then applied and the process repeated until the desired load level is reached. This method is commonly referred to as a "modified Newton-Raphson" technique or "combined incremental/iterative solution". Figure 9.2 shows this process.

9.3.2 The Arc-Length Technique

Our computational model is intended for the non-linear elasto-plastic and damage analysis of shells. Comprehensive modeling of structures requires determination of the entire equilibrium path until collapse occurs. Solution of the system of non-linear equations by means of the combined incremental/iterative algorithms discussed in Sect. 7.3.1, can lead to problems near the limit point, where the stiffness of the structure approaches zero. This can result in a singularity problem and potentially large errors in the results. To overcome this shortcoming, we use the arc-length method. Use of this technique in structural analysis was originally proposed by Riks (1979) and Wempner (1971), later modified by Crisfield (1983, 1991 and 1997).

To begin our demonstration of the arc-length method, we write the equilibrium equations in the following form (Crisfield, 1991):

$$\mathbf{g}(\mathbf{q}, \lambda) = \mathbf{F}_i(\mathbf{q}) - \lambda \mathbf{F}_{ef} = \mathbf{0} \tag{9.19}$$

where $\mathbf{F}_i$ is a vector of the internal forces, which are functions of the displacements $\mathbf{q}$; the vector $\mathbf{F}_{ef}$ is a fixed internal loading vector; and the scalar parameter λ is a load level parameter that multiplies $\mathbf{F}_{ef}$. The arc-length method is used to find the intersection of the curve described by (9.19) with the curve $s = \text{constant}$, where s is the arc length, defined by:

$$s = \int ds \tag{9.20}$$

and

$$ds = \sqrt{\left(d\mathbf{q}^T d\mathbf{q} + d\lambda^2 \vartheta^2 \mathbf{F}_{ef}{}^T \mathbf{F}_{ef}\right)} \tag{9.21}$$

The scaling parameter ϑ in (9.21) accounts for the fact that the load contribution depends on the adopted scaling between the load and displacement terms. For the arc-length method, we replace the differential form of (9.21) with the incremental form:

$$a = \left(\Delta\mathbf{q}^T \Delta\mathbf{q} + \Delta\lambda^2 \vartheta^2 \mathbf{F}_{ef}{}^T \mathbf{F}_{ef}\right) - \Delta l^2 = 0 \tag{9.22}$$

where Δl is a fixed radius of the desired intersection (Fig. 9.3). The vector $\Delta\mathbf{q}$ and the scalar parameter $\Delta\lambda$ are incremental (not iterative) and relate to the last

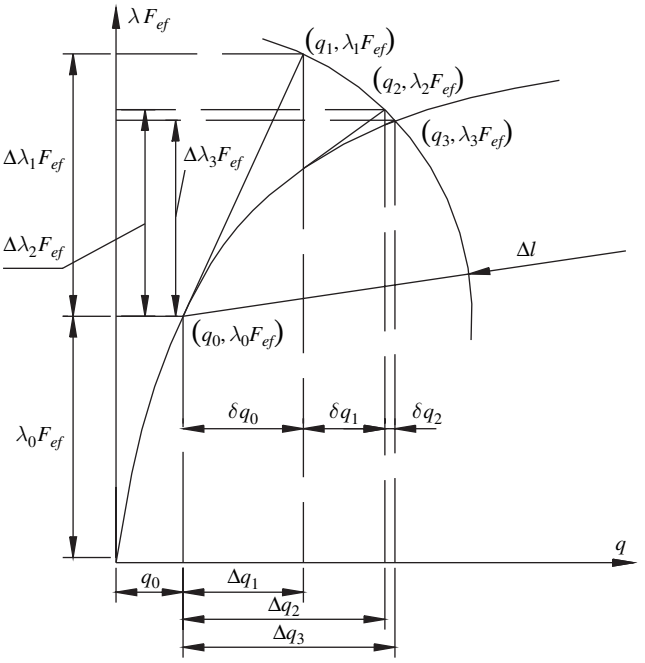

Fig. 9.3 Spherical arc-length method (Crisfield, 1991)

converged equilibrium state. The essence of the arc-length method is that the load parameter λ is a variable. An additional constraint expression that allows us to determine that variable is (9.22).

The Newton-Raphson technique with the load parameter accounted for can be introduced via a truncated Taylor series. Using (9.19) and (9.22) we write:

$$\mathbf{g}_n = \mathbf{g}_o + \frac{\partial \mathbf{g}}{\partial \mathbf{q}}\delta\mathbf{q} + \frac{\partial \mathbf{g}}{\partial \lambda}\delta\lambda = \mathbf{g}_o + \mathbf{K}_t\delta\mathbf{q} - \mathbf{F}_{ef}\delta\lambda = 0 \tag{9.23}$$

$$a_n = a_o + 2\Delta\mathbf{q}^T\delta\mathbf{q} + 2\Delta\lambda\delta\lambda\vartheta^2{\mathbf{F}_{ef}}^T\mathbf{F}_{ef} = 0 \tag{9.24}$$

where the subscript n means "new" and the subscript o means "old". We then directly introduce the constraint of (9.24) for the displacement control for a single point. To this end, an iterative displacement $\delta\mathbf{q}$ is split into two parts. The change of the displacement at the unknown load level $\lambda_n = \lambda_o + \delta\lambda$ becomes:

$$\delta\mathbf{q} = -\mathbf{K}_t^{-1}\mathbf{g}\left(\mathbf{q}_o, \lambda\right) = -\mathbf{K}_t^{-1}\left(\mathbf{F}_i\left(\mathbf{q}_o\right) - \lambda_n\mathbf{F}_{ef}\right) = -\mathbf{K}_t^{-1}\left(\mathbf{g}\left(\mathbf{q}_o, \lambda_o\right) - \delta\lambda\mathbf{F}_{ef}\right) \tag{9.25}$$

The above equation can also be written as (Crisfield, 1991):

$$\delta\mathbf{q} = -\mathbf{K}_t^{-1}\mathbf{g}_o + \delta\lambda\mathbf{K}_t^{-1}\mathbf{F}_{ef} = \delta\bar{\mathbf{q}} + \delta\lambda\delta\mathbf{q}_t \tag{9.26}$$

where:

$$\delta\mathbf{q}_t = \mathbf{K}_t^{-1}\mathbf{F}_{ef} \text{ and } \delta\bar{\mathbf{q}} = -\mathbf{K}_t^{-1}\mathbf{g}_o \tag{9.27}$$

The symbol $\delta\bar{\mathbf{q}}$ is the iterative change that would arise from the standard load-controlled Newton-Raphson method (at a fixed load level λ_o), and $\delta\mathbf{q}_t$ is the displacement vector corresponding to a fixed load vector $\mathbf{F}_{ef}$. After calculating $\delta\mathbf{q}$ from (9.26), we update the incremental displacements as:

$$\Delta\mathbf{q}_n = \Delta\mathbf{q}_o + \delta\mathbf{q} = \Delta\mathbf{q}_o + \delta\bar{\mathbf{q}} + \delta\lambda\delta\mathbf{q}_t \tag{9.28}$$

where $\delta\lambda$ is the only unknown. The increment $\delta\lambda$ can be found from equation (9.22), which can be expressed as:

$$\left(\Delta\mathbf{q}_o{}^T\Delta\mathbf{q}_o + \Delta{\lambda_o}^2\vartheta^2{\mathbf{F}_{ef}}^T\mathbf{F}_{ef}\right) = \left(\Delta\mathbf{q}_n{}^T\Delta\mathbf{q}_n + \Delta{\lambda_n}^2\vartheta^2{\mathbf{F}_{ef}}^T\mathbf{F}_{ef}\right) = \Delta l^2 \tag{9.29}$$

Substituting (9.28) into the above we obtain a scalar quadratic equation:

$$a_1\delta\lambda^2 + a_2\delta\lambda + a_3 = 0 \tag{9.30}$$

where:

$$\begin{aligned} a_1 &= \delta\mathbf{q}_t{}^T \delta\mathbf{q}_t + \vartheta^2 \mathbf{F}_{ef}{}^T \mathbf{F}_{ef} \\ a_2 &= 2\delta\mathbf{q}_t \left(\Delta\mathbf{q}_o + \delta\overline{\mathbf{q}}\right) + 2\Delta\lambda_o \vartheta^2 \mathbf{F}_{ef}{}^T \mathbf{F}_{ef} \\ a_3 &= \left(\Delta\mathbf{q}_o + \delta\overline{\mathbf{q}}\right)^T \left(\Delta\mathbf{q}_o + \delta\overline{\mathbf{q}}\right) - \Delta l^2 + \Delta\lambda_o{}^2 \vartheta^2 \mathbf{F}_{ef}{}^T \mathbf{F}_{ef} \end{aligned} \tag{9.31}$$

Equation (9.30) can be solved for $\delta\lambda$ so that the change of displacement given by (9.28) is defined. Solution of the quadratic equation (9.30) yields two roots, $\delta\lambda_1$ and $\delta\lambda_2$. We select the appropriate root by calculating both solutions and substituting them into (9.28). We now have:

$$\begin{aligned} \Delta\mathbf{q}_{n1} &= \Delta\mathbf{q}_o + \delta\bar{\mathbf{q}} + \delta\lambda_1 \delta\mathbf{q}_t \\ \Delta\mathbf{q}_{n2} &= \Delta\mathbf{q}_o + \delta\bar{\mathbf{q}} + \delta\lambda_2 \delta\mathbf{q}_t \end{aligned} \tag{9.32}$$

Of the two solutions above, we select the displacement that lies closest to the old incremental direction $\Delta\mathbf{q}_o$. This procedure can be implemented by finding the solution with the minimum angle between $\Delta\mathbf{q}_o$ and $\Delta\mathbf{q}_n$; hence, the maximum cosine of the angle, is expressed as:

$$\cos\theta = \frac{\Delta\mathbf{q}_o{}^T \Delta\mathbf{q}_n}{\Delta l^2} = \frac{\Delta\mathbf{q}_o{}^T \left(\Delta\mathbf{q}_o + \delta\bar{\mathbf{q}}\right)}{\Delta l^2} + \delta\lambda \frac{\Delta\mathbf{q}_o{}^T \delta\mathbf{q}_t}{\Delta l^2} = \frac{a_4 + a_5 \delta\lambda}{\Delta l^2} \tag{9.33}$$

The process of determining of the load increment using the arc-length method is shown schematically in Fig. 9.3. After convergence at the equilibrium point $\left(\mathbf{q}_0, \lambda_0 \mathbf{F}_{ef}\right)$, an incremental tangential predictor $(\Delta\mathbf{q}_1, \Delta\lambda_1)$ is calculated, leading to the point $\left(\mathbf{q}_1, \lambda_1 \mathbf{F}_{ef}\right)$. The first iteration uses (9.30) and (9.31) with the old value $\Delta\mathbf{q}_o$ as $\Delta\mathbf{q}_1$ and the old $\Delta\lambda_o$ as $\Delta\lambda_1$, to obtain $\delta\mathbf{q}_1$ and $\delta\lambda_1$, after which the updating procedure leads to:

$$\begin{aligned} \Delta\mathbf{q}_3 &= \Delta\mathbf{q}_2 + \delta\mathbf{q}_2 \\ \Delta\lambda_3 &= \Delta\lambda_2 + \delta\lambda_2 \end{aligned} \tag{9.34}$$

When added to the displacements $\mathbf{q}_o$ and load level λ_o at the end of the previous increment, the process leads to the point $\left(\mathbf{q}_2, \lambda_2 \mathbf{F}_{ef}\right)$ in Fig. 9.3. The next iteration again applies (9.30) and (9.31) with the old value $\Delta\mathbf{q}_o$ as $\Delta\mathbf{q}_2$ and the old $\Delta\lambda_o$ as $\Delta\lambda_2$, in order to obtain $\delta\mathbf{q}_2$ and $\delta\lambda_2$, after which the updating procedure leads to $\Delta\mathbf{q}_3 = \Delta\mathbf{q}_2 + \delta\mathbf{q}_2$ and $\Delta\lambda_3 = \Delta\lambda_2 + \delta\lambda_2$. The iterative process ends when convergence is reached. The flowchart for this procedure is given by Crisfield (1991).

For most practical problems, the scaling parameter ϑ introduced in (9.21) can be set to zero (Crisfield, 1981, 1991). This is the case here.

9.3.3 Integrating the Rate Equations – Return to the Yield Surface

The associated flow rules given by (6.43) are of incremental nature. The solution of the constitutive equations is based on the predictor/corrector approach. This method, however, leads to errors that are unrelated to the lack of equilibrium but are caused by the errors in the integration of the flow rules and their relation to the incremental/iterative solution procedure. Even if equilibrium is exactly satisfied at the beginning and end of the increment, the solution will not correspond exactly with a solution in which the increment itself was cut into a number of smaller increments, for each of which equilibrium was exactly ensured (Crisfield, 1991). If the stress and strain increments were very small, one could effectively proceed with the previous tangential stiffness with no significant loss of accuracy. The strains and subsequent stress resultant increments, however, are not infinitesimally small; consequently, the errors accumulate leading to a drift from the yield surface. If we follow the process described in Chaps. 5 and 6 to determine the plastic multiplier $\Delta\lambda_i$, we use (5.69), repeated here for convenience:

$$\Delta\boldsymbol{\lambda} = \left[\mathbf{a}^{\mathbf{T}}\left(\mathbf{K}+\mathbf{K_g}\right)\mathbf{a} + \left(\mathbf{H} - \mathbf{a_b}^{\mathbf{T}}\mathbf{A_b} - \mathbf{a_m}^{\mathbf{T}}\mathbf{A_m} - \mathbf{a_s}^{\mathbf{T}}\mathbf{A_s}\right)\right]^{-1}\mathbf{a}^{\mathbf{T}}\left(\mathbf{K}+\mathbf{K_g}\right)\Delta\mathbf{q} \tag{9.35}$$

with

$$\begin{aligned}
\mathbf{a_i}^{\mathbf{T}} &= \left\{ \frac{\partial F^*{}_i}{\partial N_{xi}} + p_u \frac{\partial F^*{}_i}{\partial N_{xyi}};\ \frac{\partial F^*{}_i}{\partial N_{yi}} + p_v \frac{\partial F^*{}_i}{\partial N_{xyi}};\ \frac{\partial F^*{}_i}{\partial Q_{xi}} + \frac{\partial F^*{}_i}{\partial Q_{yi}};\right. \\
&\quad \left. \frac{\partial F^*{}_i}{\partial M_{xi}} + p_{\phi x} \frac{\partial F^*{}_i}{\partial M_{xyi}};\ \frac{\partial F^*{}_i}{\partial M_{yi}} + p_{\phi y} \frac{\partial F^*{}_i}{\partial M_{xyi}} \right\} \\
p_u &= \frac{2\Delta u_i{}^2}{\Delta u_i{}^2 + \Delta v_i^2};\ p_v = \frac{2\Delta v_i{}^2}{\Delta u_i{}^2 + \Delta v_i{}^2}; \\
p_{\phi x} &= \frac{2\Delta\phi_{xi}{}^2}{\Delta\phi_{xi}{}^2 + \Delta\phi_{yi}{}^2};\ p_{\phi y} = \frac{2\Delta\phi_{yi}{}^2}{\Delta\phi_{xi}{}^2 + \Delta\phi_{yi}{}^2}
\end{aligned} \tag{9.36}$$

The meaning of all the functions and parameters in the above relations is explained in Chap. 5. In this case, we compute $\mathbf{a_i}$ at the beginning of the increment; we then obtain the stress resultants that lie outside of the yield surface at the end of an increment, as shown in Fig. (9.4), in which $\Delta\boldsymbol{\Sigma}$ is an increment of the stress resultants.

The situation shown in Fig. 9.4 requires that steps be taken to return the stress resultants to the yield surface, to prevent an accumulation of errors that would lead to overprediction of the collapse load. The procedure discussed by Crisfield (1991) is adopted here to overcome this shortcoming. We first determine the point of intersection of the elastic stress vector with the yield surface. In this case, we require that the stress resultants after application of the increment of loading remain on the yield surface. This can be written as:

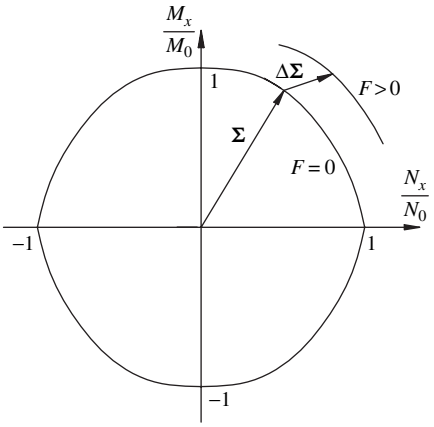

Fig. 9.4 Drift from the yield surface

$$F\left(\boldsymbol{\Sigma}+\beta\Delta\boldsymbol{\Sigma}\right)=0 \tag{9.37}$$

where $\boldsymbol{\Sigma}$ is a stress resultant vector (see Fig. 9.4), which is a function of both the bending moment M and normal force N; $\Delta\boldsymbol{\Sigma}$ is an increment of the stress resultants; and β is a scaling parameter. As the yield function is expressed in terms of the stress resultants, the function $\boldsymbol{\Sigma}+\beta\Delta\boldsymbol{\Sigma}$ is given by:

$$\boldsymbol{\Sigma}+\beta\Delta\boldsymbol{\Sigma}=\boldsymbol{\Sigma}+\beta\Delta\boldsymbol{\Sigma}\left(M+\beta\Delta M, N+\beta\Delta N\right) \tag{9.38}$$

To return to the yield surface, we use the yield surface of the form given by (5.1) rewritten here for convenience:

$$F\left(\boldsymbol{\Sigma}\right)=\left(\frac{M^*}{M_0}\right)^2+\left(\frac{N^*}{N_0}\right)^2-1=0 \tag{9.39}$$

where M_0, N_0 are the moment and normal force capacities of the cross section of the shell, respectively, given by:

$$M_0=\frac{\sigma_0 h^2}{4},\ N_0=\sigma_0 h \tag{9.40}$$

and σ_0 is a yield stress; h is the thickness of the shell; and M^*, N^* are the stress resultant intensities given by (6.33), (6.34).

Note that we did not consider the influence of the parameter α, responsible for representation of the progressive development of the plastic curvatures across the thickness of the shell, on the errors related to the integration of the rate equations (compare (5.8), (5.9)).

Multiplying both sides of (9.39) by σ_0^2 we obtain:

$$F\left(\boldsymbol{\Sigma}\right) = \left(\frac{M^*}{M_0}\right)^2 {\sigma_0}^2 + \left(\frac{N^*}{N_0}\right)^2 {\sigma_0}^2 - {\sigma_0}^2 = 0 \tag{9.41}$$

Substituting (9.40) into the above yields:

$$F\left(\boldsymbol{\Sigma}\right) = \frac{16M^2}{h^4} + \frac{N^2}{h^2} - {\sigma_0}^2 = 0 \tag{9.42}$$

with M^*, N^* replaced by M, N for brevity. Using (9.37), we write:

$$F\left(\boldsymbol{\Sigma} + \beta\Delta\boldsymbol{\Sigma}\right) = \frac{16\left(M + \beta\Delta M\right)^2}{h^4} + \frac{\left(N + \beta\Delta N\right)^2}{h^2} - {\sigma_0}^2 = 0 \tag{9.43}$$

simplifying (9.43), we obtain a quadratic expression for β:

$$\left(\frac{16\Delta M^2}{h^4} + \frac{\Delta N^2}{h^2}\right)\beta^2 + \left(\frac{32M\Delta M}{h^4} + \frac{2N\Delta N}{h^2}\right)\beta + \left(\frac{16M^2}{h^4} + \frac{N^2}{h^2}\right) - {\sigma_0}^2 = 0 \tag{9.44}$$

where we require a positive root of (9.44). Once a parameter β is found, we scale down the stress resultants until the yield surface F becomes zero (Ortiz and Popov, 1985).

References

Cook, R.D., Malkus, D.S., Plesha, M.E. (1989). Concepts and applications of finite element analysis. 3rd edition, John Wiley & Sons, New York.

Crisfield, M.A. (1981a). Finite element analysis for combined material and geometric nonlinearities. In W. Wunderlich et al. (eds.) Nonlinear Finite Element Analysis in Structural Mechanics, Springer-Verlag, New York, 325–338.

Crisfield, M.A. (1981b). A fast incremental/iterative solution procedure that handles 'snap-through'. Comp. Stuct., 13, 55–62.

Crisfield, M.A. (1983). An arc-length method including line searches and accelerations. Int. J. Num. Meth. Eng., 19, 1269–1289.

Crisfield, M.A. (1991). Non-linear Finite element Analysis of Solids and Structures. Vol. 1. John Wiley & Sons Ltd, New York.

Crisfield, M.A. (1997). Non-linear Finite element Analysis of Solids and Structures. Vol. 2. John Wiley & Sons Ltd, New York.

Ketter, R.L. and Prawel, S.P. (1969). Modern Methods of Engineering Computations. McGraw-Hill Book Company.

Ortiz, M. and Popov, E.P. (1985). Accuracy and stability of integration algorithms for elastoplastic constitutive relations. Int. J. Num. Meth. Eng., 21, 9, 1561–1576.

Owen, D.R.J. and Hinton, E. (1980). Finite Elements in Plasticity: Theory and Practice, Pineridge Press, Swansea, UK.

Riks, E. (1979). An incremental approach to the solution of snapping and buckling problems. Int. J. Solids Struct., 15, 529–551.

Voyiadjis, G.Z. and Shi, G. (1990). Finite Element Large Deformation Analysis for the Elasto-Plastic Behavior of Plates and Shells. Scientific Report No. 2, submitted to Martin Marietta Manned Space System, New Orleans, LA 70189, September 1990.

Wempner, G.A. (1971). Discrete approximations related to nonlinear theories of solids. Int. J. Solids Struct., 7, 1581–1599.

Zienkiewicz, O.C. (1978). The Finite Element Method, McGraw-Hill, NY.

Appendix

Interpolation Formulas for Displacement Field

The two-dimensional interpolation formulas for the displacement field, discussed in Sect. 3.2.3 are given below:

$$\begin{aligned}\phi_x(\xi,\eta) = &\frac{3}{4a}\lambda_x\left[\left(1-\xi^2\right)(1-\eta)\right]w_1 + \frac{3}{4a}\lambda_x\left[\left(1-\xi^2\right)(1+\eta)\right]w_2\\ &-\frac{3}{4a}\lambda_x\left[\left(1-\xi^2\right)(1+\eta)\right]w_3 - \frac{3}{4a}\lambda_x\left[\left(1-\xi^2\right)(1-\eta)\right]w_4\\ &+\frac{1}{8}\left[2+2\xi-3\lambda_x\left(1-\xi^2\right)\right](1-\eta)\,\phi_{x1}\\ &+\frac{1}{8}\left[2+2\xi-3\lambda_x\left(1-\xi^2\right)\right](1+\eta)\,\phi_{x2}\\ &+\frac{1}{8}\left[2-2\xi-3\lambda_x\left(1-\xi^2\right)\right](1+\eta)\,\phi_{x3}\\ &+\frac{1}{8}\left[2-2\xi-3\lambda_x\left(1-\xi^2\right)\right](1-\eta)\,\phi_{x4}\end{aligned} \tag{A.1}$$

$$\begin{aligned}\phi_y(\xi,\eta) = &-\frac{3}{4b}\lambda_y\left[\left(1-\eta^2\right)(1+\xi)\right]w_1 + \frac{3}{4b}\lambda_y\left[\left(1-\eta^2\right)(1+\xi)\right]w_2\\ &-\frac{3}{4b}\lambda_y\left[\left(1-\eta^2\right)(1-\xi)\right]w_3 - \frac{3}{4b}\lambda_y\left[\left(1-\eta^2\right)(1-\xi)\right]w_4\\ &+\frac{1}{8}\left[2-2\eta-3\lambda_y\left(1-\eta^2\right)\right](1+\xi)\,\phi_{y1}\\ &+\frac{1}{8}\left[2+2\eta-3\lambda_y\left(1-\eta^2\right)\right](1+\xi)\,\phi_{y2}\\ &+\frac{1}{8}\left[2+2\eta-3\lambda_y\left(1-\eta^2\right)\right](1-\xi)\,\phi_{y3}\\ &+\frac{1}{8}\left[2-2\eta-3\lambda_y\left(1-\eta^2\right)\right](1-\xi)\,\phi_{y4}\end{aligned} \tag{A.2}$$

$$u(\xi,\eta)=\frac{1}{8}[1+\xi][1-\eta]u_1+\frac{1}{8}[1+\xi][1+\eta]u_2 \\ +\frac{1}{8}[1-\xi][1+\eta]u_3+\frac{1}{8}[1-\xi][1-\eta]u_4 \tag{A.3}$$

$$v(\xi,\eta)=\frac{1}{8}[1+\xi][1-\eta]v_1+\frac{1}{8}[1+\xi][1+\eta]v_2 \\ +\frac{1}{8}[1-\xi][1+\eta]v_3+\frac{1}{8}[1-\xi][1-\eta]v_4 \tag{A.4}$$

$$\begin{aligned} w(\xi,\eta)=&\frac{1}{4}\left[1+\xi-\frac{\lambda_x}{2}\left(\xi^3-\xi\right)\right]\left[1-\eta+\frac{\lambda_y}{2}\left(\eta^3-\eta\right)\right]w_1 \\ &+\frac{1}{4}\left[1+\xi-\frac{\lambda_x}{2}\left(\xi^3-\xi\right)\right]\left[1+\eta-\frac{\lambda_y}{2}\left(\eta^3-\eta\right)\right]w_2 \\ &+\frac{1}{4}\left[1-\xi+\frac{\lambda_x}{2}\left(\xi^3-\xi\right)\right]\left[1+\eta-\frac{\lambda_y}{2}\left(\eta^3-\eta\right)\right]w_3 \\ &+\frac{1}{4}\left[1-\xi+\frac{\lambda_x}{2}\left(\xi^3-\xi\right)\right]\left[1-\eta+\frac{\lambda_y}{2}\left(\eta^3-\eta\right)\right]w_4 \\ &+\frac{1}{8}\left[-1+\xi^2+\lambda_x\left(\xi^3-\xi\right)\right](1-\eta)\frac{a}{2}\phi_{x1} \\ &+\frac{1}{8}\left[-1+\xi^2+\lambda_x\left(\xi^3-\xi\right)\right](1+\eta)\frac{a}{2}\phi_{x2} \\ &+\frac{1}{8}\left[1-\xi^2+\lambda_x\left(\xi^3-\xi\right)\right](1+\eta)\frac{a}{2}\phi_{x3} \\ &+\frac{1}{8}\left[1-\xi^2+\lambda_x\left(\xi^3-\xi\right)\right](1-\eta)\frac{a}{2}\phi_{x4} \\ &+\frac{1}{8}\left[1-\eta^2+\lambda_y\left(\eta^3-\eta\right)\right](1+\xi)\frac{b}{2}\phi_{y1} \\ &+\frac{1}{8}\left[-1+\eta^2+\lambda_y\left(\eta^3-\eta\right)\right](1+\xi)\frac{b}{2}\phi_{y2} \\ &+\frac{1}{8}\left[-1+\eta^2+\lambda_y\left(\eta^3-\eta\right)\right](1-\xi)\frac{b}{2}\phi_{y3} \\ &+\frac{1}{8}\left[1-\eta^2+\lambda_y\left(\eta^3-\eta\right)\right](1-\xi)\frac{b}{2}\phi_{y4} \end{aligned} \tag{A.5}$$

where:

$$\xi=\frac{2x}{a},\ \eta=\frac{2y}{b} \qquad -1\le\xi,\eta\le 1 \tag{A.6}$$

Index